CONDITION MONITORING OF ACTIVE MAGNETIC BEARING SYSTEMS

R. GOUWS M.Eng

Thesis submitted for the degree *Philosophiae Doctor Ingeneriae*
in Electrical and Electronic Engineering at the Potchefstroom
Campus of the North-West University

Promotor: Prof. Dr. G. van Schoor

May 2007
Potchefstroom

SUMMARY

In this thesis, the author contextualises condition monitoring of active magnetic bearing (AMB) systems and proposes the real-time condition monitoring of AMB systems. Three real-time fault detection, diagnosis, correction and identification schemes for vibration forces on the rotor of a rotational AMB system are proposed.

Two AMB systems were used to conduct this research. The one was a fully suspended 250 kW water cooling AMB pump from which historical fault data was obtained and the other was an experimental double radial AMB test rack on which the three real-time schemes were implemented. The historical fault data obtained from the AMB pump were categorised into subsynchronous, rotor synchronous and supersynchronous vibration forces. It was decided to use the historical fault data to induce the same fault conditions that occurred on the AMB pump on the AMB test rack.

Various fault detection techniques were implemented on the historical fault data. This was done to obtain the best technique for a specific fault condition. These techniques together with the historical fault data were used in the design of the three real-time schemes.

The focus of this research is on external faults, since the research of internal faults to the magnetic bearing control system is well established. Various schemes exist where off-line diagnosis and identification of internal and external faults are performed on AMB systems, but the area of real-time identification and correction of external faults still needs to be explored. This study proposes three real-time detection, diagnosis, correction and identification schemes for external faults to the magnetic bearing control system of rotational AMB systems. These schemes use the available AMB sensors and actuators to perform condition monitoring and correction, since machine components in industrial applications operate in harsh environments and are not always easily accessible to install condition monitoring equipment.

The last scheme focuses on real-time multiple frequency fault detection, diagnosis, correction and identification of external faults on rotational AMB systems, since more than one fault can occur simultaneously on the AMB system. Analysis of a multiple frequency fault by a single frequency fault scheme causes incorrect identification and correction of the fault. Four articles were submitted for publication on the three real-time schemes.

The three real-time schemes perform three main tasks: 1) fault detection, 2) fault diagnosis and error correction and 3) fault identification.

Displacement and current masking were performed during the fault detection stage. The vibratory amplitudes and frequencies were extracted by means of the Wigner-Ville distribution. Discrete sampling of the displacement and current signals of the physical AMB system was performed by the dSPACE® 1104 controller board.

Pattern recognition techniques, statistical diagnosis, cascaded fuzzy logic and pattern construction were used to calculate fault features during the fault diagnosis and error correction stages. Error correction algorithms were used to correct the fault during the error correction stage. During the fault identification stage, data fitting, fuzzy logic, ISO standards and pattern recognition were used to calculate the type, parameters, vibratory level and zone of the vibration force. A historical fault database was used during the identification process.

Correction factors were calculated to observe the improvement each scheme has over the optimised PID controller when vibration forces are applied. Scheme 3 provided the best result for improving subsynchronous vibration forces, scheme 1 the best for rotor synchronous vibration forces and scheme 2 the best for supersynchronous vibration forces. Scheme 3 provided the best overall result with the best average improvement. All three real-time schemes were able to correct and minimize vibration forces to a stable operating condition.

The three real-time schemes only stabilize the rotor with respect to the stator and do not remove the vibration force. When correction forces are applied to the AMB system, to correct the effect of the vibration forces, it may increases the stress of other critical components e.g. the power amplifiers and system base, which may cause components to be damaged or break down. These stressed components need to be identified by the user as critical or non-critical and the necessary steps must be taken to operate the AMB system under the fault condition or to shut down the system and repair the fault.

The maximum current capability and bandwidth of the power amplifiers, run-time of the DSP processors and bandwidth of the sensors were the main factors limiting the applicability of the real-time schemes. Since the power amplifiers and sensors were designed and specified for normal operational bandwidth, it was not possible to fully evaluate supersynchronous vibration forces.

OPSOMMING

In hierdie proefskrif ondersoek die outeur die stand van kondisiemonitering op aktiewe magnetiese laer (AML) stelsels en stel die intydse kondisiemonitering van AML stelsels voor. Drie intydse foutdeteksie, -diagnose, -korreksie en -identifikasie skemas vir vibrasiekragte op roterende AML stelsel word voorgestel.

Twee AML stelsels is gebruik vir hierdie navorsing. Die een was 'n ten volle gesuspendeerde 250 kW waterverkoelingspomp waarvan historiese foutdata bekom is en die ander is 'n eksperimentele dubbel radiale AML toetsstelsel waarop die drie intydse skemas geïmplementeer is. Die historiese foutdata van die AML pomp is gekategoriseer in subsinkrone, rotorsinkrone en supersinkrone vibrasiekragte. Daar is besluit om die historiese foutdata te gebruik om dieselfde foutkondisies wat op die AML pomp voorgekom het, op die AML toetsstelsel te induseer.

Verskeie foutdeteksietegnieke is geïmplementeer op die historiese foutdata. Dit is gedoen om die beste tegniek vir die spesifieke foutkondisie te vind. Hierdie tegnieke saam met die historiese foutdata is gebruik in die ontwerp van die drie intydse skemas.

Die fokus van die navorsing is op eksterne foute aangesien baie navorsing reeds bestaan oor die area van interne foute tot die magnetiese laer beheerstelsel. Verskeie skemas bestaan waar aflyn diagnose en identifikasie van interne en eksterne foute op AML stelsels gedoen is, maar 'n leemte in die area van intydse identifikasie en korreksie van eksterne foute bestaan. Hierdie studie stel drie intydse deteksie, diagnose, korreksie en identifikasie skemas vir eksterne foute tot die magnetiese laer beheerstelsel op roterende AML stelsels voor. Hierdie skemas gebruik die bestaande sensors en kragversterkers om kondisiemoniteering en korreksie te verrig aangesien masjienkomponente in industriële toepassings nie altyd toeganklik is om kondisiemoniteringstoerusting te installeer nie.

Die laaste skema fokus op intydse foutdeteksie, -diagnose, -korreksie en -identifikasie van eksterne foute met meer as een frekwensiekomponent op roterende AML stelsels, omdat meer as een fout gelyktyding kan voorkom op AML stelsels. Analise van 'n fout met meer as een frekwensiekomponent deur 'n enkel frekwensie foutdeteksiestelsel lei tot foutiewe identifikasie en korreksie van foute. Vier artikels is ingestuur vir publikasie oor die drie intydse skemas.

Die drie intydse skemas voer drie hooftake uit: 1) foutdeteksie, 2) foutdiagnose en -korreksie en 3) foutidentifikasie.

Posisie en stroom "masking" is uitgevoer gedurende die foutdeteksie stadium. Die vibrasie amplitudes en frekwensies is bepaal deur die Wigner-Ville distribusie. Diskrete ontrekking van die posisie- en stroomseine van die fisiese AML stelsel is uitgevoer deur die dSPACE® 1104 beheerbord.

Patroonherkenningstegnieke, statistiese diagnose, gekaskeerde wasige logika en patroonkonstruksie is gebruik om foutinligting te bekom gedurende die foutdiagnose en -korreksie stadiums. Foutkorreksie algoritmes is gebruik om die fout te korrigeer gedurende die foutkorreksie stadium. Gedurende die foutidentifikasiestadium is datapassing, wasige logika, ISO standaarde en patroonherkenning gebruik om die tipe, parameters, vibrasievlak en sone van die vibrasiekragte te bepaal. `n Historiese fout databasis is gebruik gedurende die foutidentifikasieproses.

Korreksiefaktore is bereken om die verbetering wat elke skema op die PID beheerder het, wanneer vibrasiekragte toegepas word, te bepaal. Skema 3 het die beste verbetering tot gevolg met subsinkrone vibrasiekragte, skema 1 die beste met rotorsinkrone en skema 2 die beste met supersinkrone vibrasiekragte. Al drie intydse skemas is in staat om vibrasiekragte tot `n stabiele werk toestand te minimaliseer.

Die drie intydse skemas stabiliseer slegs die rotor ten opsigte van die stator en verwyder nie die vibrasiekragte nie. Wanneer korreksiekragte toegepas word op die AML stelsel om die effek van die vibrasiekragte te kanselleer mag dit spanning op ander kritiese komponente soos die kragversterkers en stelselbasis plaas, wat kan veroorsaak dat hierdie komponente beskadig word. Hierdie komponente met verhoogde spanning moet vervolgens deur die gebruiker geïdentifiseer word as krities of nie krities en die nodige stappe moet geneem word om die AML stelsel met die fouttoestand te bedryf of om die stelsel te stop en die fout te herstel.

Die maksimum stroomvermoë en bandwydte van die kragversterkers, looptyd van die DSP prosesseerders en bandwydte van die sensors is die hooffaktore wat die toepassing van die intydse skemas beperk. Aangesien die kragversterkers en sensors gespesifiseer was vir normale operasionele bandwydte is dit nie moontlik om supersinkrone vibrasiekragte ten volle te evalueer nie.

The reverent and worshipful fear of the Lord is the beginning of Wisdom, and the knowledge of the Holy One is insight and understanding. For by me [Wisdom from God] your days shall be multiplied, and the years of your life shall be increased.

Proverbs 9:10-11

And behold, I am coming speedily. Blessed is he who observes and lays to heart and keeps the truths of the prophecy (the predictions, consolations and warnings) contained in this book.

Revelation 22:7

Wysheid begin met die dien van die Here, wie die Heilige ken, het werklik insig. As jy wysheid het, sal jy lank lewe, jou lewensjare sal vermeerder word.

Spreuke 9:10-11

Jesus sê toe: "Kyk, Ek kom gou! Geseënd is elkeen wat die woorde van hierdie profetiese boek ter harte neem."

Openbaring 22:7

ACHNOWLEDGEMENTS

This research was carried out in the laboratory of the McTronX research group at the North West University (Potchefstroom campus).

I would like to thank prof George van Schoor for all his time, patience and support during this study. Thanks to my best friend Markus Storm for support during this time. All my love to Chrisna van Heerden.

I would like to thank the Institute for Process Technology, Automation and Measurement Technology (IPM) at the University of Applied Sciences Zittau/Görlitz in Germany for making it possible to work on the 250 kW water cooling AMB pump.

Financial support by M Tech Industrial and the Deutscher Akademischer Austausch Dienst (DAAD) is greatly appreciated.

TABLE OF CONTENTS

APPENDIX SECTION

LIST OF FIGURES

LIST OF TABLES

NOMENCLATURE

ABBREVIATIONS	DEFINITION
ALE	Adaptive line enhancement
AM	Amplitude modulation
AMB	Active magnetic bearing
ANC	Adaptive noise cancelling
ANN	Artificial neural networks
AR	Autoregressive
ARMA	Autoregressive moving average techniques
CBM	Condition based maintenance
CSR	Current slew rate
DSP	Digital signal processors
ESDFT	Equi-sampled discrete Fourier transform
FFS	Forward feature selection
FFT	Fast Fourier transform
FLC	Fuzzy logic controller
FLNN	Fuzzy logic neural networks
FMECA	Failure modes, effects and criticality analysis
FSR	Force slew rate
GA	Genetic algorithm
GUI	Graphical user interface
HFD	Higher frequency domain
HFRT	High frequency resonance technique
LCEPS	Linear cepstrum
LPV	Linear parameter-varying
LTCEPS	Linear thresholded cepstrum
MLP	Multi layer perceptron
MMF	Magneto-motive force
NNR	Nearest neighbour rule
NNRC	Nearest neighbour rule with class membership
PWVD	Pseudo-Wigner-Ville distribution
RMS	Root mean square
SA	Synchronous average
SCD	Spectral correlation density
SNR	Signal-to-noise ratio
SOM	Self organising maps
STD	Standard deviation
STFT	Short time Fourier transform
SVM	Support vector machines
TCEPS	Thresholded cepstrum
THID	Total harmonic current distortion
THVD	Total harmonic voltage distortion
VAR	Variance
WT	Wavelet transform
WVD	Wigner-Ville distribution
1NNR	One nearest neighbour rule

SYMBOLS	**DEFINITION**
A	Amplitude of the vibration force
A_B	Amplitude of the boundary error
$A_{Correct}$	Amplitude of the correcting reference current
$A_{Measure}$	Amplitude of the measured displacement error
A_{System}	Fitting amplitude
Avg_{max_fault}	Average maximum fault dataset
A_e_1	Magnitude of the current fault
A_i_1	Current 1 amplitude
B	Frequency of the vibration force
$B_{Correct}$	Frequency of the correctional reference current
b_{eq}	Damping constant
B_{error}	Boundary error
$B_{Measure}$	Frequency of the measured displacement error
B_1, B_2 and B_3	Three frequencies during multiple frequency analysis
$B1_p$	Displacement boundary 1 (fault indicator)
$B2_p$	Displacement boundary 2 (system critical state)
$B3_p$	Displacement boundary 3 (system shutdown state)
B_e_1	Frequency of the current spectrum
C	Phase of the vibration force
cf	Correction factor
$C_{Measure}$	Phase of the measured displacement error
C_{min}	Minimum radial clearance
C_{system}	Fitting phase
C_e_1	Phase of vibration force
D	Offset of the vibration force
$D_{Correct}$	Offset of the correctional reference current
D_{max}	Maximum peak displacement
$D_{Measure}$	Offset of the measured displacement error
D_e_1	Offset of the fault
D_i_1	Current offset
e_B	Boundary error
e_d	Diagnosis output error
e_{fit}	Error fitting factor
e_{fuz1}, e_{fuz2}, e_{fuz3}	Fuzzy 1, 2 and 3 current error
e_{i1} and e_{i2}	Current 1 and 2 errors
e_{i1_ref} and e_{i2_ref}	Reference (historical) 1 and 2 current errors
e_p	Position correction error
e_{ref}	Reference (historical) database error
e_{r1_pat}, e_{r2_pat}, e_{r3_pat}	Displacement error pattern 1, 2 and 3
e_{1_c}, e_{2_c}, e_{3_c}	Constructed patterns for frequencies B_1, B_2 and B_3
e_{1_pat}, e_{2_pat}	Pattern 1 error and pattern 2 error
e_{1_ref}, e_{2_ref} and e_{3_ref}	Reference (historical) database errors
F	Load capacity
F_d	Vibration (disturbance) force
F_{data}	Type of historical fault data
F_{ec}	Correction force
fit	Accuracy of the fit
$Fit_{Boundary}$	Boundary fitting factor

SYMBOLS	DEFINITION
$FitB1_p, FitB2_p, FitB3_p$	Fitting factor for boundary 1, 2 and 3
$fit\_\%$	Percentage fitting factor
F_{max}	Maximum load capacity
f_s	Switching frequency
f_1, f_2	Force on top and bottom magnetic bearings
f_3, f_4	Carrier and vibration force of the rotor
i_0	Bias current
i_{ref}	Reference current
i_{ref_1} and i_{ref_2}	Reference current for top and bottom magnetic bearings
$i_{ref\_1\_add}$ and $i_{ref\_2\_add}$	Correction reference currents
i_{ref_1R}, i_{ref_2R}	Relation for reference current 1 and 2
i_1, i_2	Current in top and bottom electromagnets
i_{1_fault}	Fault current
i_{1_mask}	No fault current (masked current)
k_{eq}	Stiffness constant
K_m	Constant of the magnetic bearing
k_p, k_i and k_D	PID controller gains
L_{coil}	Inductance of the coil
$MAX\text{-}error$	Maximum displacement error
$MIN\text{-}error$	Minimum displacement error
m_{rotor}	Mass of rotor
$m_{unbalance}$	Unbalance mass of the rotor
N	Rotational speed
N_{fit}	Number of the dataset
No_fault_{water}	No fault displacement of the water cooling AMB pump
$PA1_{max}, PA2_{max}$	Maximum current output of power amplifier 1 and 2
P_f	Pattern fault
R_{coil}	Resistance of the coil
set	Number of the data set with closest fit
sub_{new}	Trained subsynchronous vibration force pattern
sub_1, sub_2 and sub_3	Subsynchronous vibration force correctional patterns
t_c, t_r	Cycle and running time
V_l	Fault vibratory level
x_{de}	Air-gap function for dynamic eccentricity
x_{mp}	No fault displacement
x_p	Actual displacement
x_{perror}	Displacement error
x_{p_fault}	Fault displacement
x_{pn}	Nominal air gap
x_{pmax}	Maximum positive displacement
x_{pmin}	Average of the maximum negative displacement
xpn_{double_radial}	Nominal air gap of the double radial AMB
xpn_{water}	Nominal air gap of the water cooling AMB pump
x_{se}	Air-gap function for static eccentricity
y_p	y-axis displacement
ζ	Damping ratio
φ	Phase shift of the unbalance force
ω	Rotational speed frequency
ω_n	Natural frequency

CHAPTER 1

INTRODUCTION

Condition monitoring and maintenance management is a holistic multidiscipline based on systems thinking [128]. The concept of condition monitoring is to select a measurable parameter on the machine which will change as the health or condition of the machine deteriorates [98]. Condition monitoring of critical machinery has many economic benefits. A number of conventional vibration analysis techniques exist by which certain faults in rotating machinery can be identified and repaired to prevent catastrophic failure of components [150].

One of the major aspects of condition monitoring and diagnosis of mechanical equipment is to determine what needs to be repaired and when it needs to be repaired. This decision is based on a combination of skill and experience. Both of these are used to interpret the available data and to determine what information should be made available.

It can take many years of training to interpret the available information, since so much of diagnosis relies on skill and experience. Some of the primary difficulties that arise when there is a need to perform diagnosis tasks are: 1) lack of experienced staff, 2) lack of time to perform the task and 3) lack of consistence in performing the diagnosis task [164].

Active magnetic bearings (AMBs) are non-containing, which means they have negligible friction loss, no wear and higher reliability. An advantage of performing condition monitoring on AMB systems is the inherent availability to displacement and actuator current values. Faults on AMB systems can be categorised into internal and external to the magnetic bearing control system. The research performed in this thesis focuses on external faults.

This study explores condition monitoring of systems with AMBs and techniques that can be implemented for specific system fault conditions. The study proposes three real-time detection, diagnosis, correction and identification schemes for vibration forces on the rotor of a rotational AMB system. These schemes use the available sensors and actuators to perform correction. The main advantage of the last scheme is its capability to detect, diagnose and identify multiple frequency vibration forces.

Various fault tolerant schemes exist for AMB systems, where additional sensors, power amplifiers, controllers and actuating coils are installed to increase the reliability of the system [1], [2], [16], [22], [29], [77], [90], [118], [167]. The research performed by the reference studies focus on diagnosis and correction of internal faults. The identification of these faults is performed off-line.

Other non-tolerant schemes (schemes which do not install additional sensors and power amplifiers) exist where diagnosis and evaluation of the internal components (I/O board channel, controller, sensors and power amplifiers) of the AMB system is performed [30], [47], [78]. Schemes focussing on the detection of bearing magnet coil failures and microprocessor hardware failure also exist [131], [35]. Various schemes exist where off-line diagnosis and identification of external faults (overhung rotor, rotor mass loss, rotor impact, etc.) are performed on AMB systems [7], [87], [94]. The area of real-time identification and correction of these faults still need to be explored.

Schemes capable of performing real-time displacement and current analysis, correction and identification of external faults (vibration forces) to the magnetic bearing control system therefore need to be explored and developed. Approaches focussing on real-time identification and correction of external faults (rotor deformations, misalignments, foundation looseness, etc.) on a rotational AMB system by means of displacement or current analysis (where the available sensors and actuators are used) could not be found in the literature.

In industrial applications more than one fault can occur at the same time. When a correction system only focuses on correcting one of these faults, the response of the system improves, but the optimum result is not obtained. When a single fault correction system evaluates the total vibration index (a collection of all the vibration forces acting on the system) incorrect identification and correction of the vibration index occurs. A third scheme capable of performing real-time multiple frequency fault detection, diagnosis, correction and identification of vibration forces on the rotor of a rotational AMB system therefore need to be explored and developed. Approaches focussing on real-time multiple frequency identification and correction of vibration forces on a rotational AMB system could not be found in the literature.

This chapter starts with an overview of condition monitoring and AMB systems. A problem statement followed by the aim and objectives of the research is then provided. The research methodology is provided followed by an overview of the thesis. The chapter ends with the publication status of the research.

1.1. CONDITION MONITORING

Complex rotating machinery can be maintained in a scheduled, time based fashion, routine inspections can be performed and potential faults identified. A disadvantage is that machinery in perfect operating condition can be disassembled unnecessarily which can induce faults, whereas small incipient faults may not be detected soon enough. In contrast with condition based maintenance (CBM), the maintenance schedule is based on the actual condition of the machine [125].

CBM can be used to prevent expensive downtime and damages due to unforeseen problems, if the condition of the machine is diagnosable via relevant measurements. Vibration monitoring, which is a technology often employed in the context of CBM, has been used successfully in a wide range of condition monitoring applications [128]. Vibration monitoring is useful for the identification of specific types of fault conditions that are commonly experienced in rotating machinery, e.g. imbalance, looseness, etc. Chapter 2 provides more detail on condition monitoring procedures, measurements and techniques.

System monitoring usually refers to monitoring of external faults to the magnetic bearing control system and component monitoring usually refers to monitoring of internal faults to the magnetic bearing control system. Section 1.2 provides more detail on external and internal faults on AMB systems.

Vibration monitoring allows for variation in speed [120] and load [150]. Dynamic loads can influence the interpretation of vibrations associated with a primary fault mechanism [57]. The application of advanced signal processing techniques can reduce or even eliminate some of the environmental disturbances related to vibration signals [19], [120], [150], such as external and internal noise in the form of vibration sources, speed and amplitude variations.

The application of such techniques aims to accentuate the signal while simultaneously reducing the noise or disturbance. The modified and enhanced signals can then be interpreted with pattern recognition techniques. The diagnosis of multiple fault conditions may require simultaneous interpretation of a number of variables that in combination reflect the true condition of the machine. The operator can be assisted in making consistent decisions regarding the status of the machine, by applying pattern recognition techniques [53]. More detail on pattern recognition is available in section 4.5.5.

Pattern recognition techniques have traditionally been used to make accurate classification decisions based on a number of extracted features [56]. However, the successful application of pattern recognition techniques relies on the availability of a sufficiently large data set of all fault conditions. In practice, it is often expensive or even impossible to compile such a data set from experimental data. Simulated models can then be used to expand the available experimental data set, using expert knowledge on the nature of expected faults [121].

Faults in rotating machinery can be detected using vibration (and current) analysis [89]. Chapter 4 provides detail on signal processing techniques that can be used for fault detection. Some guidelines on acceptable vibration standards are available, but are often too conservative for industrial use [13]. Acceptable vibration levels are therefore often adjusted for each individual case [64]-[69].

1.2. ACTIVE MAGNETIC BEARING SYSTEMS

The reliability of an AMB system can be improved by implementing a fault tolerant scheme, where additional sensors, power amplifiers, controllers and actuating coils are installed [1], [2], [16], [22], [29], [77], [90], [118], [167]. The research performed by the reference studies focuses on diagnosis and correction of internal faults. The identification of these faults is performed off-line.

Faults on AMB systems can be broadly classified as either *internal* or *external* to the magnetic bearing control system. This classification relates to the way in which the faults can be dealt with. Internal faults include: power amplifier malfunctions [70], transducer malfunctions [1], loss of I/O board channel [15], bearing magnet coil failures [131], computer software errors [167] and computer hardware errors [35]. External faults include: rotor impact [29], rotor mass loss [51], motion of system base [46], rotor deformation [62], sudden change in loading [10], rotor rub [139], bent rotor [38], misalignments [94] and rotor faults [30]. Section 3.7 provides more detail on faults on AMB systems.

The demand for highly reliable systems at any operating conditions caused an increase in the industrial application of AMBs. Industries expect reliable and safe operation of their machines, high efficiency and availability at all times [125]. Most industries cannot afford downtime and therefore operate machines until they break down. A shortage of skilled staff causes machines to operate under fault conditions which cause the machine to eventually break down.

Spending money on condition monitoring equipment and training staff is expensive and most companies prefer not to take this route. Installing condition monitoring equipment is sometimes not possible, since machines operate in harsh environments and is not easily accessible [86]. In order to satisfy these requirements and needs, failure detection and diagnosis in real-time becomes increasingly important.

Due to the shortage of skilled, on-site personnel, much effort has been focused on the automated analysis of vibration signals [128]. Although positive results have been reported in literature [100], [128], the analysis process depends on the type of machinery (similarity in electrical and mechanical construction of the new machine compared to the one tests were performed on), environmental influences (speed, static and dynamic load) and operational factors [14].

Some international standards on mechanical vibration of rotating AMB systems exist [70], [71]. These provide guidelines for acceptable vibration levels, but need to be adapted for the specific industrial application.

1.3. PROBLEM STATEMENT

The purpose of the research is to benchmark condition monitoring of AMB systems and explore the real-time condition monitoring of AMB systems. In industrial applications the connection of sensors for condition monitoring is not always possible, since the machinery is not easily accessible. It was therefore decided to use the available sensors and actuators of the AMB system, eliminating the installation of additional equipment for the monitoring and correction process.

Various faults occur on an AMB system as shown in figure 1.1. Faults can occur on: 1) components connected to the rotor of the AMB system, 2) the coupling connecting machinery and components with the AMB system, 3) machinery connected to the rotor of the AMB system and 4) free standing machinery causing motion of the base of the AMB system. These faults are categorised as external faults and form the main focus of this research. Research of internal faults to the magnetic bearing control system is well established and not included in this study.

Various schemes exist where off-line diagnosis and identification of internal and external faults are performed on AMB systems, but the area of real-time identification and correction of external faults still needs to be explored. Approaches focussing on real-time identification and correction of external faults (misalignments, rotor deformations, foundation looseness, etc.) on a rotational AMB system by means of displacement or current analysis (where the available sensors and actuators are used) could not be found in the literature. Schemes capable of performing real-time displacement and current analysis, correction and identification of external faults to the magnetic bearing control system therefore need to be explored and developed.

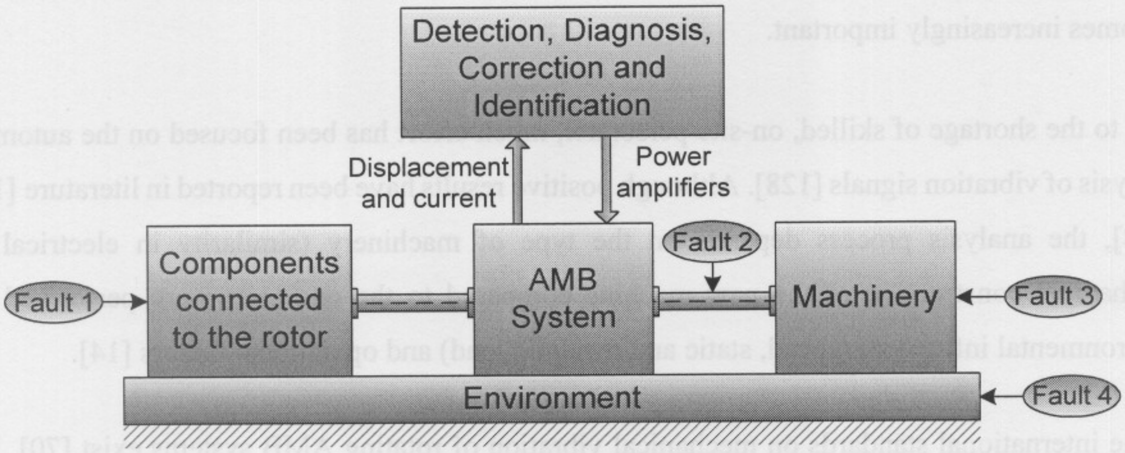

Figure 1.1: AMB system operating under fault conditions.

More than one fault can occur at the same time in industrial applications. When a correction system only focuses on single frequency fault correction, the system response improves, but the optimum result is not obtained. Incorrect identification and correction of the fault can therefore occur. Approaches focussing on real-time multiple frequency identification and correction of vibration forces on a rotational AMB system could not be found in the literature. A third scheme capable of performing real-time multiple frequency fault detection, diagnosis, correction and identification of vibration forces on the rotor of a rotational AMB system therefore need to be explored and developed.

The real-time detection, diagnosis and correction schemes only stabilises the rotor with respect to the stator and do not remove the fault from the system. When correction forces are applied to the AMB system, to cancel (correct) the effect of the vibration forces, it may increase the stresses in other critical components e.g. the power amplifiers and system base, which may cause components to be damaged or break down. These stressed components need to be identified by the user as critical or non-critical and the necessary steps must be taken to operate the AMB system under the fault condition or to shut down the system and repair the fault.

The research presented in this thesis attempts to identify and compensate harmonic sources, which are not necessarily synchronous with the rotor spin rate. Some of the work presented in this thesis can be described as compensation of asynchronous vibration with periodic excitation.

1.4. RESEARCH AIMS AND OBJECTIVES

This thesis proposes three real-time detection, diagnosis, correction and identification schemes for vibration forces on the rotor of a rotational AMB system. The three real-time detection, diagnosis, correction and identification schemes are divided into the following major subsystems: 1) detection and data collection, 2) signal processing and feature extraction, 3) monitoring and diagnosis, 4) identification and 5) correction.

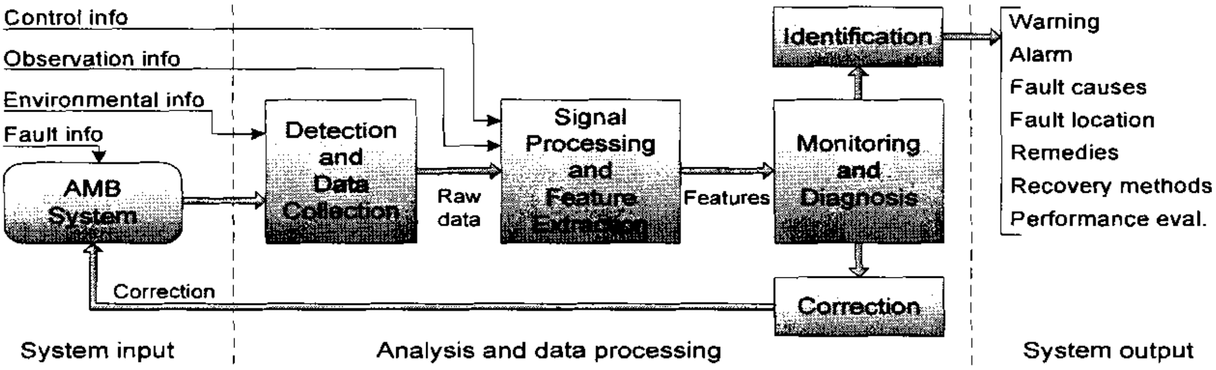

Figure 1.2: Real-time schemes configuration (adapted from [164]).

Figure 1.2 provides the configuration of the real-time schemes, which is divided into the following three sections: 1) system input, 2) analysis and data processing and 3) system output. The system input section contains all the information needed by the analysis and data processing section to provide a diagnosis output. The analysis and data processing section uses the control information, observation information, environmental information and AMB system output to perform data collection, signal processing and feature extraction. The monitoring, diagnosis and identification subsystems use the extracted features to provide a system output. The system output is divided into warning, alarm, fault causes, fault location, remedies, recovery methods and performance evaluation. The correction subsystem uses the extracted features to apply correction forces on the AMB system. The rest of this section details each of the subsystems of the real-time detection, diagnosis, correction and identification schemes as research objectives.

1.4.1. DETECTION AND DATA COLLECTION

A sensor array converts non-electrical quantities into electrical quantities for the purpose of computerized post-processing. The selection of the correct sensors is the key to effective condition monitoring and diagnosis, because without the ability to acquire accurate information the quantitative monitoring and accurate diagnosis of the AMB system would be impossible. Faults occurring on the system can be stored to a historical fault database in real-time, which can be used for identification and correctional purposes. More detail on the detection subsystems is available in sections 5.3.3, 6.2.1 and 7.2.1.

Data collection can be employed in one of two types of measurements:

- Direct measurement

This method uses displacement sensors to measure the actual displacement that directly reflects the condition of the rotor. Direct sensing is usually more prone to noise interference, since the sensors are closely located to the power amplifiers. Filtering is therefore essential, but care must be taken not to filter frequencies necessary for diagnosis.

- Indirect measurement

In this method sensors are not used for directly measuring physical quantities; they are used to reflect changes in other parameters (e.g. vibration, temperature and current) that are sensitive to the problem concerned. This is the usual way of employing sensors in real-time monitoring and diagnosis applications [164]. Section 4.2.1 provides more detail on data collection.

1.4.2. SIGNAL PROCESSING AND FEATURE EXTRACTION

The signal processing and feature extraction subsystem receives measurements and operating parameters from the controller and processes them on the basis of the signal nature and requirements from the monitoring and diagnosis subsystem. Noise reduction is performed to provide useful features. More detail on noise filtering is available in section 2.6.

Feature extraction is a procedure that maps incoming signals into useable features. This task can be processed in the time or frequency domain. In the time domain, basic characteristics of a time-varied signal are usually extracted as features. In the frequency domain, various signal processing techniques exist. Frequency domain analysis is especially useful for vibration monitoring and diagnosis applications of rotational machinery [123]. More detail on feature extraction is available in section 4.5.2.

1.4.3. MONITORING AND DIAGNOSIS

The functions of the monitoring and diagnosis subsystem are as follows:

- Detecting any form of deviation from the normal situation

A threshold test of a feature is the most simple and straightforward method of detecting deviation. If the deviation value exceeds this threshold then it is considered that a degradation of the AMB system is possibly occurring. When an abnormal situation is detected the severity and the potential problem needs to be determined. Some problems develop rapidly such as a situation where the operation of the AMB system exceeds the maximum limits by a very large amount in a short period of time, which will require fast response to avoid catastrophic failure [104]. More detail on monitoring measurements and techniques is available is section 2.5.

- Diagnosing potential problems

The functions of diagnosis and identification are to test the truthfulness of the alarming and warning signals generated from the detection stage, to diagnose prior to failure the causes of degenerative trends in the AMB system and to provide corrective actions to be taken so that breakdowns do not take place [123]. Thus, for diagnosis and identification to operate successfully, the selection of an accurate data interpretation scheme is vital. Knowledge-based diagnosis (rule-based, case-based and model-based diagnosis) and fuzzy logic diagnosis are the two diagnosis techniques that can be applied. More detail on the diagnosis subsystems for the three real-time schemes are available in sections 5.3, 6.2.2 and 7.2.2.

1.4.4. IDENTIFICATION

The warning indications usually correspond to slowly developed problems that will not immediately cause serious damages to the AMB system, but needs to be analysed in detail. The AMB system can still run for a while in order to complete the current costly task, but the causes of these problems usually need to be identified in order to prevent them from causing secondary problems. The alarming indications usually correspond to quickly developed problems related to critical operating units or critical operating conditions. These alarms are needed for immediate attention and usually requires machine shutdown [131]. More detail on the identification subsystems is available in sections 5.5, 6.2.3 and 7.2.3.

1.4.5. CORRECTION

When a vibration (disturbance) force occurs on the rotor of the AMB system, correction forces are applied to cancel the effect of the vibration forces. This correction can cause an increase in the stress of critical components, which can cause components to be damaged. It is therefore crucial to identify these components. Free-body diagrams and mass-spring-damper systems explaining different fault conditions and different stress points (stressed components) on the AMB system is provided in appendix B. More detail on the correction subsystems is available in sections 5.3, 6.2.2 and 7.2.2.

1.5. RESEARCH METHODOLOGY

The research is divided into two main phases. The first phase focuses on performing condition monitoring and implementing fault detection techniques on the historical fault data obtained from the 250 kW water cooling AMB pump (SM400/400), which is situated at the Boxberg power plant in Germany. More detail on the 250 kW water cooling AMB pump is provided in section 5.1 and appendix A. This phase was completed as part of an exchange program to the University of Applied Sciences Zittau/Görlitz in Germany.

The second phase focuses on the design process of three real-time detection, diagnosis, correction and identification schemes. The schemes were tested on a simulation model, before practically implementing them on the double radial AMB test rack. More detail on the double radial AMB test rack is provided in section 5.1 and appendix A. This phase was completed at the North-West University (Potchefstroom campus) in South Africa. Figure 1.3 shows a block diagram of the different phases of the research. The rest of this section provides more detail on the phases.

1.5.1. PHASE 1: CONDITION MONITORING AND FAULT DETECTION

A first approach to obtain fault measurements was to dismantle the AMB system to introduce a specific fault condition on the healthy rotor and bearings. Yet, this approach was undesirable, as the dismantling of the AMB system changes environmental conditions (the vibration signals), impeding direct comparison of before and after measurements. Furthermore it was not possible to make any changes to the 250 kW water cooling AMB pump since the pump was in use.

During phase 1 (shown in figure 1.3) condition monitoring was performed on the 250 kW water cooling AMB pump to obtain historical fault data. The vibration forces that occurred on the rotor of the AMB pump were categorised into the following three historical fault datasets: 1) subsynchronous vibration forces, 2) rotor synchronous vibration forces and 3) supersynchronous vibration forces. The vibration forces occurring on the AMB pump were stored to a historical fault database. Section 5.2 provides more detail on the vibration forces on the rotor of the AMB system.

A simulation model was created in MATLAB®, which provided the ideal no fault displacement and current. The discrepancy of the displacement and current was obtained by subtracting the no fault displacement and current (expected output of the simulation model) from the fault displacement and current (observed output of the practical AMB system). The pump pressure, pump values and temperature were also available, but were only used to evaluate the fault data. More detail on this process is provided in section 5.3.2.

Features were extracted by implementing advanced fault detection techniques on the discrepancy signals. An expert system used the extracted features to provide a result on the specific fault condition. Different fault detection techniques were implemented to determine which techniques provide the best output for a specific fault condition. More detail on the fault detection techniques is provided in chapter 4. Appendix E provides results on fault detection techniques that were implemented on the 250 kW water cooling AMB pump.

1.5.2. PHASE 2: DETECTION, DIAGNOSIS, CORRECTION AND IDENTIFICATION

Phase 2 (shown in figure 1.3) focuses on the design of three real-time fault detection, diagnosis, correction and identification schemes and implementation of the vibration forces on the double radial AMB test rack.

It was decided to use the historical fault data (obtained over a period of three years) to induce the same fault conditions that occurred on the 250 kW water cooling AMB pump on the double radial AMB test rack. From this setup a good comparison was obtained on how the schemes respond before a fault and after a fault is induced.

The historical fault data were induced on a simulation model of the double radial AMB test rack. This was done to observe how the practical system will respond to the induced faults and to optimise the performance of the real-time schemes. A detection, diagnosis and correction subsystem uses the displacement and current to detect and correct the induced fault. An identification subsystem use the technical variables obtained from the detection, diagnosis and correction subsystem to identify the fault.

The same process is repeated for the practical AMB system and the simulated results are compared with the experimental results. Chapters 5, 6 and 7 provide more detail on the design of the three proposed real-time fault detection, diagnosis, correction and identification schemes. Chapter 8 provides a comparison between the three proposed schemes.

Discrete sampling of the displacement and current signals of the physical AMB system was done by means of the dSPACE® 1104 controller board, equipped with a DSP TMS320F240 from Texas Instruments. More detail on the real-time implementation and hardware setup of the dSPACE® controllers is provided in section 5.4 and appendix C.

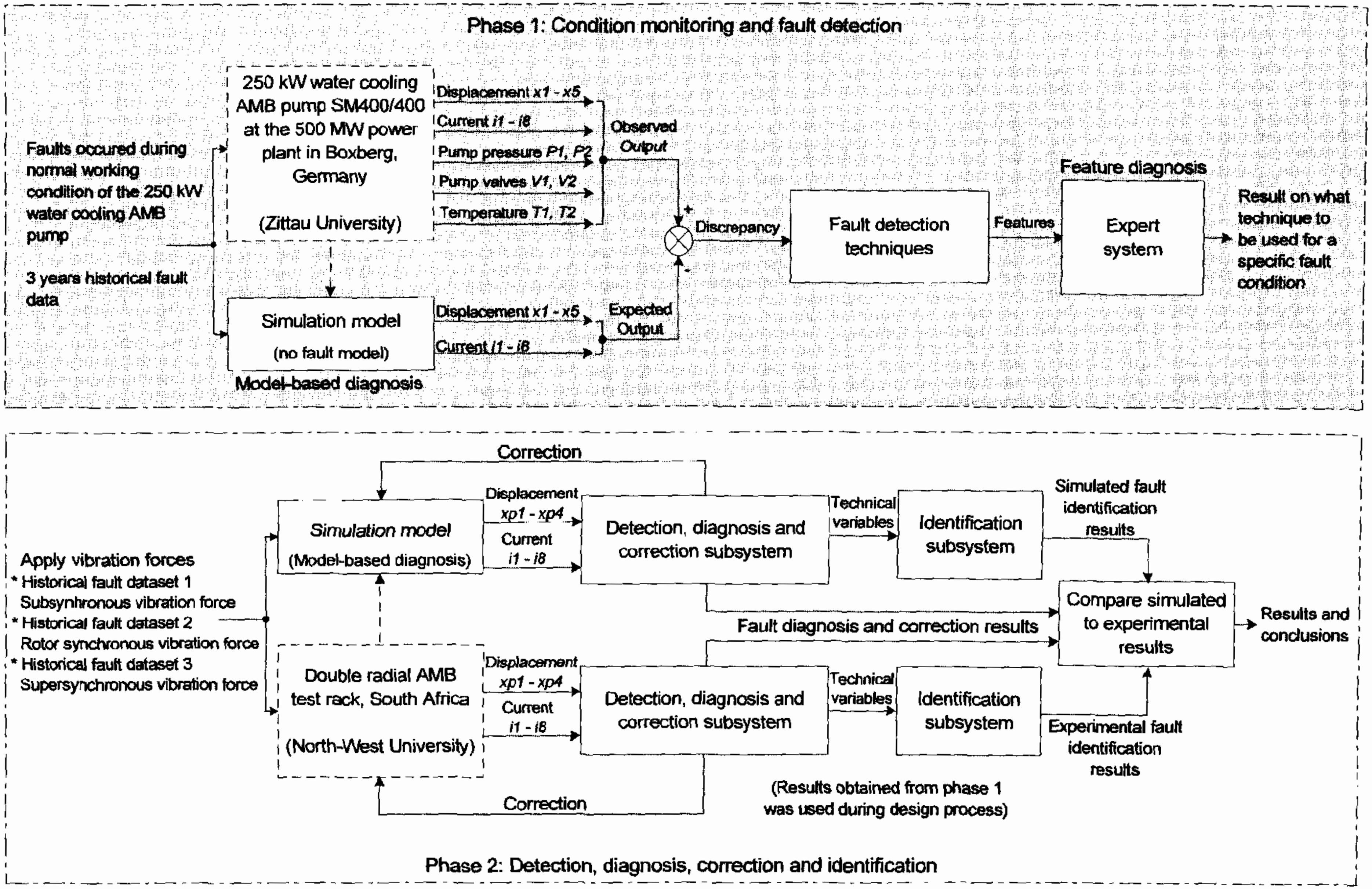

Figure 1.3: Block diagram of the different phases of the research.

1.6. THESIS OVERVIEW

This section provides a brief outline of the thesis. Chapter 2 outlines a brief literature study on condition monitoring and vibration monitoring. The benefits and disadvantages of condition monitoring and condition based maintenance are discussed. An overview on the evaluation standards of vibration monitoring and the effect of machine speed and load on the vibration level is provided. The chapter ends with the effect of temperature and spurious low frequency 'ski-slope' effects in vibration monitoring.

Chapter 3 outlines a brief literature study on AMB systems. The operation of AMBs and background information on bearings and sensors are discussed. Sections 3.5 and 3.6 focus on the benefits and limitations of AMBs, respectively. Section 3.7 focuses on faults on AMB systems.

Chapter 4 is dedicated to fault detection and signal processing techniques. Standard fault detection techniques are discussed followed by time and frequency domain features and advanced signal processing techniques. The aim is to provide the reader with background information on fault detection techniques.

Chapter 5 proposes a real-time displacement analysis, correction and identification scheme. This scheme uses the available displacement to detect, correct and identify vibration (disturbance) forces on the rotor of a rotational AMB system. Chapter 6 proposes a real-time current analysis, correction and identification scheme. This scheme uses the available current to detect, correct and identify vibration forces on the rotor of a rotational AMB system. Chapter 7 proposes a real-time multiple frequency fault detection, correction and identification scheme. This scheme analyses, correct and identify multiple frequency vibration forces on the rotor of a rotational AMB system. In chapters 5, 6 and 7 simulation and real-time results of the correctional and identification subsystems are provided. Results are discussed and the schemes are evaluated.

Chapter 8 provides the final conclusions of the thesis. In this chapter the three real-time detection, diagnosis, correction and identification schemes are evaluated. Section 8.4 focuses on improvements and aspects left for future research.

Several appendixes provide detailed information that has been removed from the main body for ease of reading and comprehension. Appendix A provides photos of the 250 kW water cooling AMB pump and double radial AMB test rack. Appendix B provides screenshots of the simulation GUI, the Simulink® simulation model. Appendix C provides the real-time Simulink® model and screenshots of the Controldesk® interface.

Appendix D provides the mass-spring-damper constants used in the simulation and real-time models. Appendix E provides the results obtained from the different fault detection techniques. The displacement and current data used in this section was obtained from the 250 kW water cooling AMB pump. Appendix F provides a list of suppliers on condition monitoring. Appendix G provides a list of datasheets, catalogs, photos and movie clips found on the available CD.

1.7. PUBLICATION STATUS OF RESEARCH

The work presented in this thesis has been documented in four articles that are in different stages of publication or evaluation for publication. The publication status of these articles together with the relevant abstracts is provided:

- Gouws R. and van Schoor G., "Real-time detection and correction of vibration forces on the rotor of a rotational active magnetic bearing system," *Mechanical Systems and Signal Processing*, Revision 1, Nov. 2006.

  Article abstract:

  In this article real-time detection and correction of vibration forces on the rotor of an AMB system is performed. The real-time scheme performs three main tasks: 1) fault detection, 2) fault diagnosis and 3) error correction. Historical fault data from a fully suspended 250 kW water cooling AMB pump was used in the design process of the fault detection subsystem. Signal masking and error calculation were performed during the fault detection process on the displacement signals of the AMB system. Fault detection techniques, statistical diagnosis and fuzzy logic were used to calculate fault features during the fault diagnosis stage. The error correction subsystem was divided into subsynchronous and supersynchronous vibration error correction. Subsynchronous vibration error correction forces the controller to overcompensate for vibration forces and reduces the vibration force on the rotor. Supersynchronous vibration error correction corrects vibration forces by inducing correction forces onto the rotor of the AMB. The reference current of the corresponding amplifiers are manipulated to create these correction forces. Experiments were performed on a double radial AMB test rack to demonstrate the effectiveness of the proposed method in the real-time detection, diagnosis and correction of vibration forces on the rotor of an AMB system. The detection, diagnosis and correction subsystem corrected and minimised the vibration forces to a stably operating condition. The last phase of this article focuses on the identification of the vibration forces. An identification subsystem performs this task and displays the type and parameters of the vibration forces.

  The design of the real-time displacement analysis, correction and identification scheme is provided in chapter 5.

- Gouws R. and van Schoor G., "A current analysis and correction system for vibration forces on the rotor of a rotating active magnetic bearing system," *SAIEE Africa Research Journal (Journal of the South African Institute of Electrical and Electronic Engineers)*, Accepted for Publication, April 2007.

  Article abstract:

  In this article, a real-time detection, correction and identification scheme for vibration forces on the rotor of a rotating AMB is proposed. Current analysis was performed during the real-time detection subsystem by comparing ideal no fault currents with fault currents. Pattern recognition was performed by using an input feature obtained from the Wigner-Ville distribution and by comparing fault current patterns with historical fault database patterns obtained from a fully suspended 250 kW water cooling AMB pump. A fuzzy logic controller used the output of the pattern recognition process to perform error correction on the AMB system. A fault identification subsystem provides the type of fault, where the fault occurred in the AMB system, the current state of the rotor and the parameters of the fault. Experiments were performed on a double radial AMB test rack to demonstrate the effectiveness of the proposed scheme in the detection, correction and identification of vibration forces on the rotor of an AMB system. The detection, diagnosis and correction scheme corrected and minimised vibration forces to a stable operating condition.

  The design of the real-time current analysis, correction and identification scheme is provided in chapter 6.

- Gouws R. and van Schoor G., "Multiple frequency fault detection, correction and identification of vibration forces on the rotor of a rotational active magnetic bearing system," *IEEE/ASME Transactions on Mechatronics*, Submitted for Publication, April 2007.

  Article abstract:

  In this article a real-time fault detection, correction and identification scheme for vibration forces on the rotor of a rotational AMB system is proposed. Condition monitoring was performed on the displacement signals of a fully suspended 250 kW water cooling AMB pump, to obtain historical fault data. A pattern recognition subsystem compared the real-time displacement error patterns with the displacement error patterns from the historical fault database. A fuzzy logic controller used the patterns from the pattern recognition subsystem to perform error correction. The Wigner-Ville distribution extracted the vibratory amplitudes and frequencies, which was used as input features to the pattern construction and pattern recognition subsystems. Experiments were performed on a double radial AMB test rack to demonstrate the effectiveness of the proposed scheme in the detection, correction and identification of vibration forces on the rotor of an AMB system. The detection and correction subsystem was able to correct and minimize multiple frequency vibration forces to a stable operating condition. The identification subsystem calculated the type, parameters, vibratory level and zone of the vibration forces. The main advantage of this scheme is its capability to detect, correct and identify multiple frequency vibration forces.

  The design of the real-time multiple frequency fault detection, correction and identification scheme is provided in chapter 7.

- Gouws R. and van Schoor G., “A comparative study on fault detection and correction techniques on AMB systems,” *Proceedings of the IEEE Africon 2007 conference*, Namibia, Accepted for Presentation, Sep. 2007.

Article abstract:

In this article a distinction between three real-time fault detection, correction and identification schemes for vibration forces on the rotor of a rotational AMB system is made. Historical fault data obtained from a fully suspended 250 kW water cooling AMB pump was used in the design process of the three schemes. The real-time schemes perform three main tasks: 1) fault detection, 2) fault diagnosis and error correction and 3) fault identification. Displacement and current masking were performed during the fault detection stage and the vibratory amplitudes and frequencies were extracted by means of the Wigner-Ville distribution. Pattern recognition techniques, statistical diagnosis and fuzzy logic were used to calculate fault features during the fault diagnosis and error correction stages. During the fault identification stage, data fitting, fuzzy logic and ISO standards were used to calculate the type, parameters, vibratory level and zone of the vibration force. A comparison between the experimental results obtained from a double radial AMB test rack was performed to demonstrate the effectiveness of the proposed schemes in the real-time detection, correction and identification of vibration forces on the rotor of a rotational AMB system. The three real-time schemes were able to correct and minimize vibration forces to a stable operating condition.

A comparison between the fault detection and correction techniques on AMB systems is provided in chapter 8.

CHAPTER 2
CONDITION MONITORING

2.1. INTRODUCTION

This chapter focuses on providing the reader with background information on condition monitoring. The chapter starts with an overview of condition monitoring, followed by a discussion on vibration monitoring. The chapter concludes with condition monitoring analysis methods, condition monitoring measurements and noise filtering during condition monitoring. Appendix F provides a list of suppliers of condition monitoring equipment.

Condition monitoring and maintenance management are holistic and multidisciplinary in nature and are based on systems thinking. The concept of condition monitoring is to select a measurable parameter in the machine which will change as the health or condition of the machine deteriorates. Rao [128] provides an overview of condition monitoring and methodologies for fault detection. In condition monitoring, machines are regularly subjected to 'health checks' or vibration inspections. Advantages of condition monitoring include [50]: 1) lower levels of vibration which result in less mechanical wear, 2) less energy usage and 3) longer machine running time which result in less repair overheads.

Vibration monitoring is one of a number of online techniques which fall in the category of condition monitoring. This thesis focuses mainly on vibration monitoring therefore it was decided to include a vibration monitoring section (section 2.3). In this section an overview of vibration monitoring is provided, followed by the effect of machine speed and load on the vibration level. The section ends with a discussion on the evaluation standards for vibration monitoring. Various international vibration monitoring standards are available [64]-[68].

There are three distinct forms of maintenance [125]: 1) breakdown maintenance, 2) periodic shutdown maintenance and 3) condition based maintenance. Breakdown maintenance is simply "run to failure" and allows no intervention in operation. The plant is maintained only when forced by a breakdown. Breakdown maintenance has low short-term capital expense, but high long-term capital expense. Periodic shutdown maintenance was once the industry norm. During periodic shutdown machines are overhauled and new components fitted irrespective of the operating condition. Condition based maintenance is the most cost effective form of plant maintenance. The plant is monitored or repaired only according to the diagnosed condition [125].

2.2. CONDITION MONITORING

Condition monitoring is divided into offline and online monitoring as shown in figure 2.1. In the case of offline monitoring the monitored object is not in a running state while monitored. Online monitoring is applied to running machinery. Condition monitoring is further divided into periodical and continuous. Periodical condition monitoring can be performed offline or online, but continuous monitoring is usually performed online.

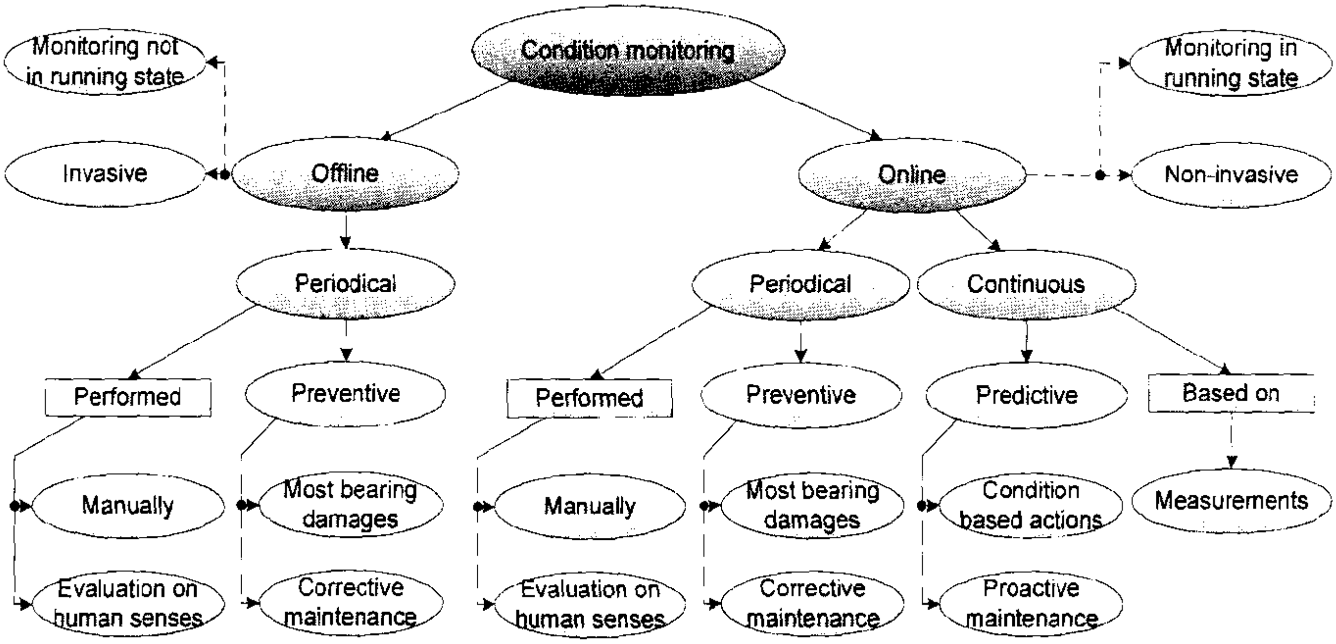

Figure 2.1: Overview of condition monitoring.

Offline monitoring can be invasive, which means that the machine structure must be disassembled for monitoring. On the contrary, online monitoring is almost always non-invasive. Continuous online monitoring is based on measurements. Periodical monitoring is performed manually and can include evaluation based on human senses [46].

The advantages of continuous condition monitoring include [83]: 1) damages can be detected as soon as they appear, 2) trends can be formed automatically, 3) minimum need for labour, 4) detection of sudden changes is possible and 5) motors that are difficult to reach can easily be monitored. The advantages of periodical condition monitoring include [88]: 1) machines can be cleaned from dust or other particles when measurements are done, 2) investment for condition monitoring is smaller than in continuous condition monitoring schemes and 3) humans can discover changes in appearance such as mechanical damages, loose blots, etc.

There are continuous online systems designed mainly for condition monitoring of electric machines. These systems usually consist of measuring and data processing devices, which can be permanently connected to a data bus supplying information to the analysing computer or data can be collected from the device occasionally. The decision on continuous data transfer or manually performed data collection is made mainly on the cost of instrumentation and labour [81].

Preventive maintenance with scheduled service procedures can prevent typical damages. For example, if the majority of bearings exceed their expected lifetime, the preventive maintenance can prevent most of the bearing damages by changing bearings before the expected lifetime expires [147]. On the other hand, if the expected lifetime cannot be determined (deterioration expectations are not known e.g. in the case of rotor faults) the scheduled maintenance is relatively inefficient [125].

Maintenance can be corrective which means that broken components are replaced or repaired. Unplanned downtime and possible breakdown of machinery can make corrective maintenance very expensive [46]. Predictive maintenance means condition based actions. These require condition monitoring in order to detect deterioration. Proactive maintenance aims to improve the object (process) so that the probability of the damage is decreased in the future [58].

2.3. VIBRATION MONITORING

Vibration monitoring is one of a number of online techniques, complementary to such measures as performance checking using non-dimensional flow, measurement of pressure, temperature, axial movement, etc. All of these techniques, collectively called condition monitoring, have the common objective of showing malfunction or deterioration in machine operation in a numerative manner. They can be used to assess the need, if any, for corrective action [88].

Vibrations on machines are in general periodic in nature, although some unsteadiness in the signal is to be expected. This means that the signal repeats itself after a definite time interval (usually the time taken for one revolution). Periodic vibration may be considered as the oscillation of a particle about a fixed datum position [147]. The smallest form is where the displacement varies sinusoidally with time. More complex vibrations may be considered as being the addition of many different sine waves (usually in the form of one or more harmonic series).

The acceleration component in a vibration signal depends on the square of the frequency, which means that if significant high frequency content is present in a signal, the acceleration level will be high and conversely, if the high frequency content is of interest, the acceleration should be measured [130].

Mechanical and magnetic forces cause vibrations in electric machines. The principal source of vibration in electrical machines are: 1) the attractive magnetic force between the rotor and stator [34], 2) the slot harmonics [88], 3) the saturation harmonics, 4) the response of the stator end windings to the electromagnetic forces on the conductors [151], 5) the rotor eccentricity and the flexibility of the rotor [156].

In addition, mechanical load can have eccentricity or it can induce vibration due to its mechanical structure or the load can process materials that give shocks to the motor axle or to the stator frame (crushers, pumps, etc.) The vibration components caused by normal operation should be considered and separated from the machine fault induced vibration [34].

Overall vibration level monitoring is quite commonly used [151]. The overall limits for vibration are given by the international standard ISO 10816-1 [67], which define the RMS velocity limits for the good, allowable, just tolerable and not permissible classes. Overall level monitoring offers quite limited means for condition monitoring, because it cannot reveal incipient faults. On the other hand, many non-cyclic bearing faults increase the overall vibration level and the vibration is spread over a wide frequency range so that frequency analysis alone cannot reveal the fault [156].

2.3.1. BACKGROUND VIBRATIONS

Background vibration or vibration originating outside the machine is the first possible cause of non-repeatability. Some machine bedplates, for example pumps mounted on a thin cover sheet, are notoriously responsive for the running condition of nearby machines. Vibration can easily be transmitted through interconnecting pipework, which respond to pulsating forces [152].

On some machines the vibration level is quite high even with the machine shut-down. One way to overcome this problem of variable measurement is to ensure that the vibration levels are obtained with the machine both offline and online. Another method is to provide isolation between the two machines in the form of anti-vibration mounts [168].

For meaningful trend results the background vibration should be small compared to that experienced when running. A beat occasionally occurs in the vibration level due to interaction between machines running at slightly different speeds [130].

2.3.2. EFFECT OF MACHINE SPEED, LOAD, ETC.

The measurement of consistent results on variable speed and load machines are very difficult. The machine should be brought back to the same condition, before the measurements are taken, otherwise the effect of changes in speed and load on the measurements must be taken into account.

Speed can affect overall level results, when running in the proximity of the resonant or critical speed of the machine or its support. On high speed turbines, even changing the temperature of the lubricating oil can have a dramatic effect, especially when the machine is prone to instability originating in the bearings [130]. Similarly some machines are prone to changes in load. For example process pumps running well away from their maximum efficiency point, can generate a significant frequency component at Vane passage frequency, which can vary from reading to reading [64].

2.3.3. VARIATION OF SIGNAL AT CONSTANT OPERATING CONDITIONS

Most signals in the real world consist of a combination of two types of signals, namely a 'deterministic' portion, which is usually the signal of interest and a 'random' portion, which is generally considered as noise. Time domain averaging and process domain averaging can be used to enhance the two different parts of the signal [64].

2.3.3.1. TIME DOMAIN AVERAGING

Time domain averaging means the data is averaged as it is acquired by the instrument, before processing commences. It should only be used when the signal is repetitive and a consistent trigger point is available. The signal-to-noise ratio (SNR) can be improved. Time averaging is particularly useful in the analysis of signals from faulty gearboxes. It cannot be used with success on rolling bearings, since there is not a purely rolling action and there is a small amount of slip of the roller on the track [28].

2.3.3.2. PROCESS DOMAIN AVERAGING

A statistically more accurate estimate of the signal can be obtained through process domain averaging. The SNR will not be improved. Each time a process is executed, the individual values of the output can vary to some degree. For example, the values in each line of a spectral output can show some variation in amplitude although tending towards a mean value. Averaging will provide a better estimate of this mean value.

The time taken to acquire one memory period in spectrum analysis depends on the number of lines chosen for the spectrum (i.e. resolution), and the frequency range taken [99]:

$$t = \frac{\text{Number of lines}}{\text{Frequency range}} \tag{2.1}$$

The number of averages (or memory periods), which should be taken depends on the variability of the data, and obviously affects the time taken to complete the measurements. In practice, it is found that on most machines a number of averages, corresponding to a 30 second measuring period, is adequate to provide consistent data [130].

2.3.4. TEMPERATURE EFFECTS

A high impedance accelerometer can be used up to a temperature of 250 °C. A normally used low-impedance accelerometer with built-in electronics is not recommended for use as a roving pick-up on hot surfaces (more than 100 °C) [130].

It is recommended that an accelerometer with a good thermal stability is used if machines with hot surfaces are to be measured. Normally accelerometers which use the piezo-electric crystal in a shear configuration have better thermal stability than those using the crystal in compression. The bearings of an AMB system are designed to withstand certain temperatures. High temperature sensors are recommended for AMB systems operating under high temperature conditions [145].

2.3.5. SPURIOUS LOW FREQUENCY 'SKI-SLOPE' EFFECT

A problem which is quite often encountered in taking measurements is the generation of low frequency noise. It is particularly noticeable, when the acceleration signal is integrated and with low frequency ranges (e.g. 0 – 200 Hz). For a decrease in frequency by a factor of 10, the noise floor will increase by 10 for acceleration, but by 100 for velocity. Typical noise are the following: 1) base strain effects (affected by ambient conditions and thermal transients), 2) power supply effects (i.e. transient caused by switching on the power supply) and 3) cable noise [86].

2.3.6. EVALUATION STANDARD FOR VIBRATION MONITORING

The machine condition can be determined by using the effective value of the vibration velocity. This value can be determined by almost all conventional vibration measurement devices. The international standard for mechanical vibration on non-rotating machines (ISO 10816-3) separates machines into the following groups that take the type of installation into account [68]: A) the vibration values from machines are put into operation, B) machines can run in continuous operation without any restrictions, C) vibration values indicate that for a limited period of time the machine condition is not suitable for continuous operation and corrective measures should be taken at the next opportunity and D) dangerous vibration values and damage could occur to the machine [66], [67].

2.4. CONDITION MONITORING ANALYSIS METHODS

Various analysis methods exist for the condition monitoring of machines. These methods can be divided into deterministic and non-deterministic methods [120]. Deterministic means that the physical parameters of the object determine the condition estimate with the aid of heuristics and calculations directly. Deterministic methods include parameter estimation, rule-based methods, fuzzy-logic and mathematical modelling. A diagram showing the different condition monitoring analysis methods is provided in figure 2.2.

Non-deterministic means that a significant degree of contingency or unknown determining factors exist. The measured quantity does therefore not determine the condition directly. Non-deterministic methods include probability distributions and artificial neural networks. Non-deterministic methods often use statistical pattern classification for decision-making [36].

Condition analysis procedure often includes both types of analyses. Often, based on some deterministic model, the values describing the condition are formed. These values are then post processed with non-deterministic methods (e.g. in the article of Kyusung [84]).

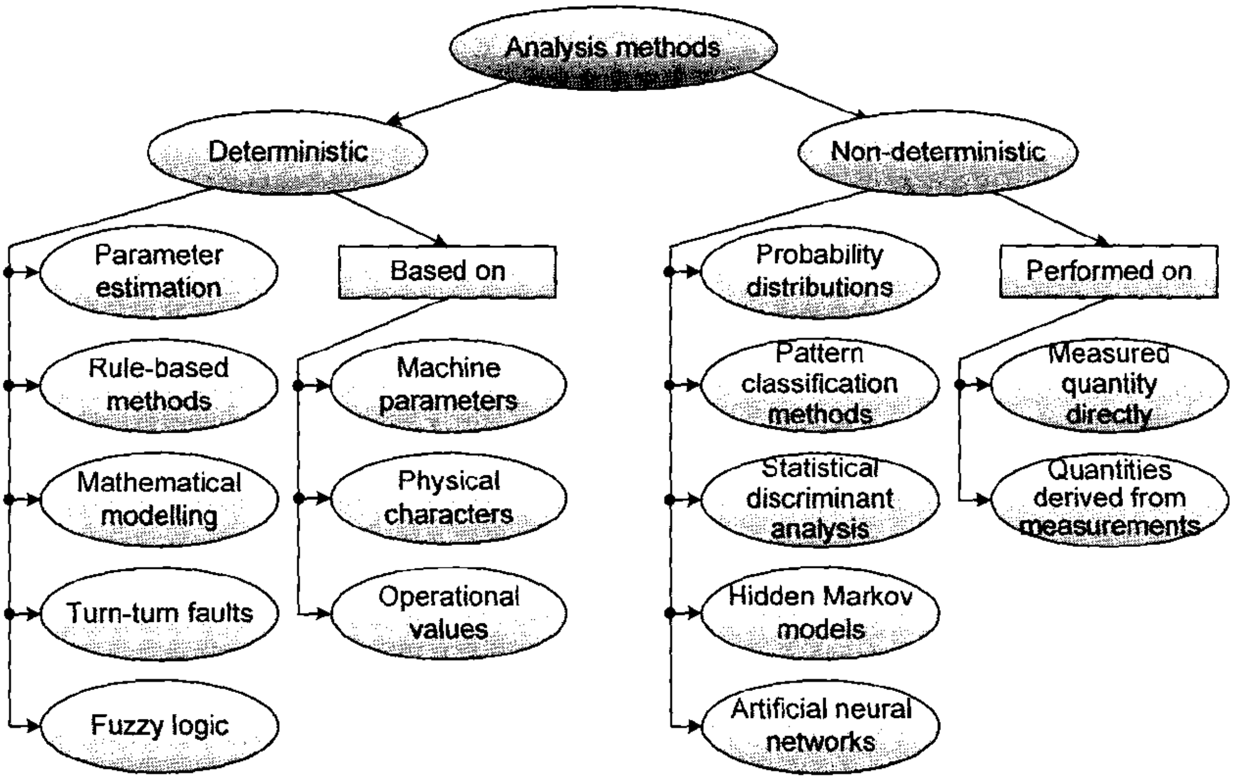

Figure 2.2: Condition monitoring analysis methods.

2.4.1. DETERMINISTIC APPROACH

A deterministic approach (shown in figure 2.2) based on known machine parameters, parameter estimation, physical characters and operational values is suitable for indication of faults that have a definite limit to distinguish faulty and healthy conditions. This is possible especially in cases, where the measurement is closely connected to a physical phenomenon or an indication is based on estimated values and a mathematical model [10].

A purely deterministic approach becomes difficult if indication of incipient faults has to be automated. A visual inspection of spectrum components can reveal a fault that cannot be given by deterministic limits or equations [45].

Turn-to-turn faults are an example of faults that can be indicated by a purely deterministic approach. Symmetrical components of current can be calculated when at least two phase currents are measured (and no earth fault is present). A negative sequence current can indicate turn-to-turn faults or asymmetric supply [61]. It is necessary to recognise the characteristic negative sequence impedance offline to avoid a false positive fault indication. In the article by Kliman [79], this is done with the calculation of the characteristic negative sequence impedance in a healthy condition.

Fuzzy logic has been used in the condition monitoring analyses by Mechefske [101] and Benbouzid [11]. Mechefske used fuzzy logic in order to classify frequency spectra derived from a vibration signal from a low speed bearing. Fuzzy memberships were formed using the average and standard deviation of each useful frequency component from healthy and different faulty case measurements.

2.4.2. STATISTICAL ANALYSIS APPROACH

Statistical methods (shown in figure 2.1) are often used in order to indicate faults. Statistical analysis is performed on the measured quantity directly or to the quantity derived from measures. The use of statistical analysis using an artificial neural network (ANN) has been demonstrated (e.g. in the article of Chow [25]) in which a neural network indication of a bearing fault is presented. Schoen [143] has used ANN and the stator current measurement in order to indicate rotor eccentricity.

Paya and Esat [121] have used ANNs in fault diagnostics using Wavelets in order to pre-process the vibration signal. The main difficulties of ANNs are that educational data are case specific and other factors than faults can cause conditions that indicate faults.

A comparison between the deterministic autoregressive modelling technique and the ANN technique is made in research of Baillie [9]. Other statistical methods that are used in condition monitoring include clustering of data [124], statistical discriminant analysis and Hidden Markov models [117].

A time-frequency analysis can be used when the changes in measured quantities are small and time variant. This is a normal situation in the case of very incipient faults or when the measured quantity is weakly linked to faults. Time-frequency transformation is most often performed by the short time Fourier transform (STFT) or by Wavelet transform (WT). The indication of faults in time-frequency analysis can be automated by using, multi layer perceptron (MLP) neural network or statistical pattern recognition methods such as discriminant analysis or self-organising maps (SOM) [122], [168]. More detail on statistical analysis methods is available in chapter 4.

2.5. CONDITION MONITORING MEASUREMENTS

If the condition monitoring of an electric machine is based on measurements there are two ways to indicate an alarm level for deterioration. The first one is the use of alarm limits on a measured or analysed quantity and the other is the change in the long-term trend of measurements, which indicates change in the motor or drive. Measurements can be analysed in time- or frequency domain or in combination of these (time-frequency analysis) [119].

The following are some of the quantities that indicate the condition of an electrical motor: 1) stator current, 2) power, 3) axial, stray and air gap flux, 4) electrical and mechanical torque, 5) vibration, 6) temperature and 7) rotational velocity. Some of the techniques that indicate the condition of an electrical motor are: 1) electrical and magnetic techniques, 2) measurement of the rotor displacement, 4) temperature images, 5) chemical analysis and 6) visual inspection [50].

Online condition monitoring can utilise all of the listed techniques. However, some of these techniques require expensive devices and are therefore used mostly for the monitoring of big generators (partial discharge, gas analysis, etc.). In addition, some methods require installation that can be made only when the motor is disassembled. For example, an air gap flux measurement requires a sensor in the air gap, but the axial flux can be measured outside the motor frame [81].

2.6. NOISE FILTERING DURING CONDITION MONITORING

When analysing the complicated vibration produced by several machines, the measurement of periodic components embedded in noise becomes a problem. If the frequencies and amplitudes of any periodic components in the vibration can be measured, then this is the first step towards tracing their origins [25].

A problem that may arise is that associated with the round-off error through calculation. In situations where the detection of weak components is required, it may be more appropriate to separate and classify all possible sought waveforms, before performing any kind of filtering or smoothing operation on the signal [31].

If this is not carried out beforehand, the weak components of the signal that need to be identified may be eliminated, particularly when applying an average to a signal with very weak components, embedded in high-level noise. This would be likely to occur, because the quantization and round-off errors, through the averaging process, may eliminate the little difference there is between those signals which have weak components and those which do not [31].

A basic technique used for noise filtering is based on a time-averaging procedure. It is important to point out that with this technique, if the correct phase synchronisation is not carried out, the specific component that is being sought will be eliminated. Furthermore, when one attempts to analyse the whole spectrum signature, it is necessary to perform a phase synchronisation for each component present in the signal, and this may be rather impractical [12].

According to Bendat and Piersol [12], this procedure is also problematic when applied to signals which have non-stationary components present, as they can generate severely distorted results. This is the case of the petroleum wellhead vibration (described by Bendat and Piersol), which includes components caused by fluid slug vibration. In these situations, Bendat and Piersol argue that there may be a strong temptation in analysing non-stationary data to treat it as if the data were a sample record from a stationary random process.

2.7. CONCLUSION

This chapter provided the reader with background information on condition monitoring and discussed the effect of machine speed and load on the vibration level. The low frequency 'ski-slope' effect was also discussed.

Condition monitoring is divided into offline and online monitoring. Periodical condition monitoring can be performed offline or online, but continuous monitoring is performed online. As mentioned in the research methodology section (section 1.5) of chapter 1, condition monitoring was performed over a period of three years on the 250 kW water cooling AMB pump. This monitoring can be categorised as online continuous.

Predictive maintenance detects deterioration and proactive maintenance aims to improve the object (process) so that the probability of the damage is decreased in the future. The three online fault schemes performed predictive maintenance which is proactive in nature, since the schemes detected and corrected the fault.

The research performed in this thesis mainly focuses on vibration monitoring. Vibration monitoring is one of a number of online condition monitoring techniques. Various international standards for the mechanical vibration of non-rotating and rotating machines exist, which can be used to categorise the vibration level of a machine.

Condition monitoring analysis methods can be broadly divided into deterministic and non-deterministic methods. More detail on these methods is available in chapter 4.

CHAPTER 3

ACTIVE MAGNETIC BEARINGS

3.1. INTRODUCTION

This chapter provides an overview of the operation and benefits of active magnetic bearing (AMB) systems. Faults on AMB systems are classified into internal and external. Detailed explanations on each of these classifications are provided. The limitations of AMB systems and measures for reducing risks of failure are also discussed.

An AMB is a mechatronical system and contains information processing components, software and feedback loops [144]. AMBs have become established in bearing technology over the past few years. Radial loads or thrust loads are acquired by utilising a magnetic field to support the shaft rather than a mechanical force as in fluid film or rolling element bearings [4].

An AMB system constitutes four basic components [70]: (1) magnetic actuator, (2) electronic control, (3) power amplifier and (4) rotor displacement sensor. In many ways, magnetic bearing components resemble electric motors with the basic magnetic actuator being constructed of soft ferromagnetic material which is electromagnetically activated by a coil of wire [48]. An AMB typically consists of three or more electromagnets, each of which exerts an attractive force on the ferromagnetic rotor, levitating it without contact.

In particular, AMBs need extensive improvements in reliability for wide and safe field application. This requirement can be met by improving the individual reliability of each component or by introducing an intelligent system capable of fault detection and diagnosis [73].

Magnetic bearings are non-containing, which means they have negligible friction loss, no wear, and higher reliability. Magnetic bearings enable previously unachievable surface speeds to be attained. Lubrication is eliminated, meaning that these bearings can be incorporated into processes that are sensitive to contamination, such as the vacuum chambers in which many semiconductor manufacturing processes take place [48].

Magnetic bearings are inherently unstable and require active control to ensure proper levitation. Compared to conventional bearings, magnetic bearings have relatively low stiffness.

Magnetic bearings are more expensive and bulkier than conventional bearings, mainly due to the size of the magnets needed [77].

Stiffness, damping and force characteristics of the bearing can be adapted to actual machine operating conditions by adaptive control strategies, easily implemented into the feedback control device [85].

The condition monitoring system is normally not an integral part of conventional systems, such as motors and turbomachinery, but AMB systems are ideally suited for diagnosis and correction, since the bearing system is already equipped with sensors and actuators, which provide the exact displacement and current values during machine operation [2].

The sensor signals (which are usually used for control purposes) can be analyzed to obtain information on the system's operating condition. Furthermore the bearing magnets can be used to apply test signals to the system, the response which can again be analyzed, yielding detailed information about the system that allows for identification of complete system dynamics and detection of changes in system behaviour [47].

The growth in the area of industrial applications of AMB systems caused an increase in the demand of highly reliable systems at any operating conditions. AMBs are currently applied to high-speed rotating machinery, like turbo pumps [54], flywheels for energy storage [3] and turbo compressors [96].

3.2. FIRST PRACTICAL MAGNETIC BEARING

Beams [159] developed the first practical magnetic suspension for high speed rotating devices. These devices include high speed rotating mirrors, ultracentrifuges and high speed centrifugal field rotors.

Beams further employed magnetic suspension as a means to carry out extensive experiments on physical properties in areas of isotope separation, biophysics, materials science and gravitational physics. He typically thought of ways to modify and improve experimental equipment. The improved equipment then provided much better experimental results [6].

3.3. OPERATION OF AN AMB

Figure 3.1 provides a layout of the operation of an AMB, where the stator, rotor and flux path can be seen. AMBs operate on the principle that ferromagnetic particles are attracted by an electromagnet [132].

This property of the rotor makes it ideal for a rotor to be supported by an electromagnet in the stator of a motor. The purpose of the electromagnet is to apply a force on the rotor to maintain a constant air gap between the rotor and the stator [97].

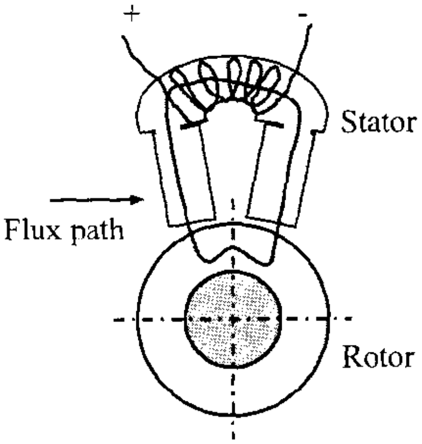

Figure 3.1: Operation of an AMB [132]

As the air gap between these two parts decreases, the attractive force increases, therefore, electromagnets are inherently unstable. A control system is needed to regulate the current and provide stability of the forces and position of the rotor [73].

The control process begins by measurement of the rotor position by means of a position sensor. The signal from this device is received by control electronics, which compares it to the desired position during machine start-up. Any differences between these two signals result in calculation of the force necessary to pull the rotor back to the desired position [85].

The position error is translated into two commands to the power amplifiers connected to the magnetic bearing stator. The current is increased in the one power amplifier, causing an increase in magnetic flux, an increase in the forces between the rotating and stationary components, and finally, movement of the rotor toward the stator along the axis of control. While the current in the one power amplifier increases, the current in the other power amplifier decreases with the inverse effect [59].

Since the natural tendency of the stator is to attract the rotor until it makes contact, some control action is required to modulate the magnetic field and maintain the rotor in the desired position. The most common type of control involves the feedback of shaft position. This information is then used by the control system to modulate the magnetic field through power amplifiers, so that the desired rotor position is maintained even under changing shaft load conditions [87].

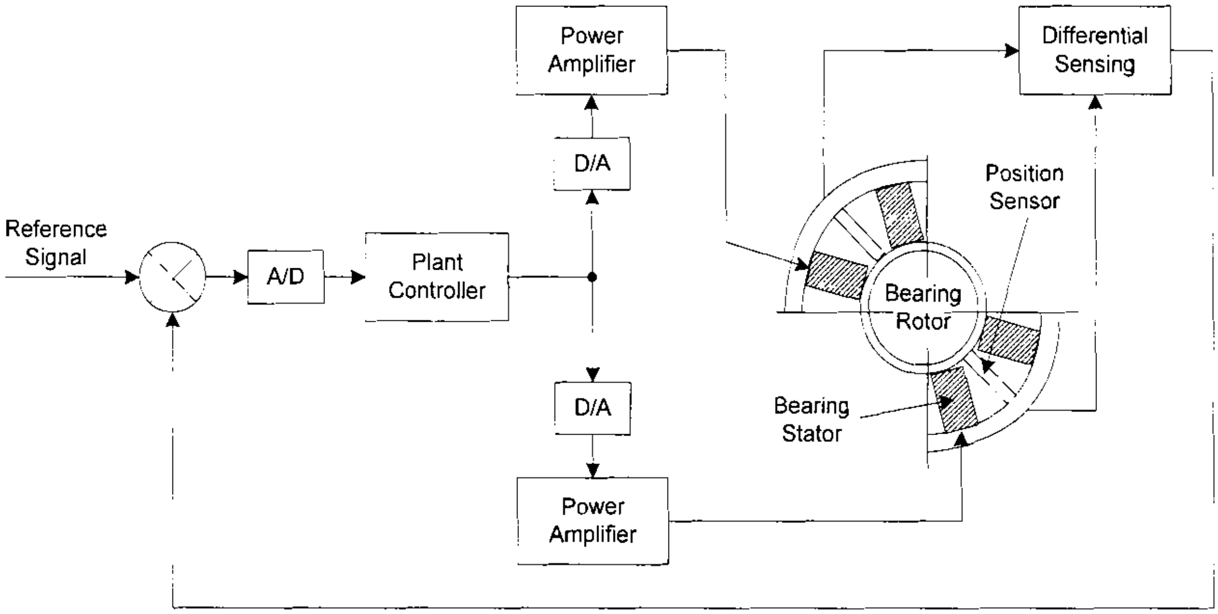

Figure 3.2: An active magnetic bearing system [130]

An AMB system constitutes magnetic actuators, position sensors, a control system and power amplifiers, as shown in the figure 3.2. The bearing actuators and sensors are located in the machine, while the control system and amplifiers are generally located remotely [130].

3.4. BACKGROUND ON BEARINGS AND SENSORS

To provide support in more than one direction, magnetic poles are oriented about the periphery of a radial bearing as shown in figure 3.3.

Radial bearing construction is very similar to that of an electric motor, involving the use of stacked steel laminations, around which power coils are wound. Stacked laminations are also used in the rotor to minimize eddy current losses, which are a small source of drag in a magnetic bearing and cause localized heating on the rotor [90].

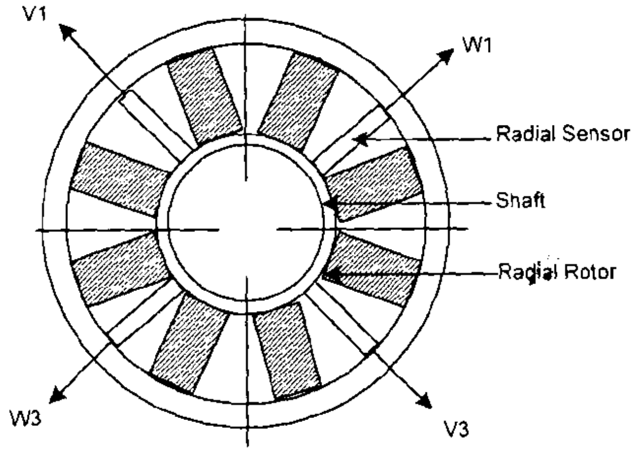

Figure 3.3: Magnetic poles for support [7]

The sensors are also oriented about the periphery of the stator, usually inside a ring or individual tubes mounted adjacent to the actuator poles. Position sensors are used, that measure the distance of the air gap between the sensor and the rotor laminations. Two measurements are taken for each radial axis and the rotor center position is calculated by means of a bridge circuit [5].

A typical rotating machine will experience forces in both the radial and axial directions. Typically, a 5-axis orientation of bearings is used, incorporating 2 radial bearings of 2 axes each, and 1 thrust bearing. The orientation of these axes is shown in figure 3.4.

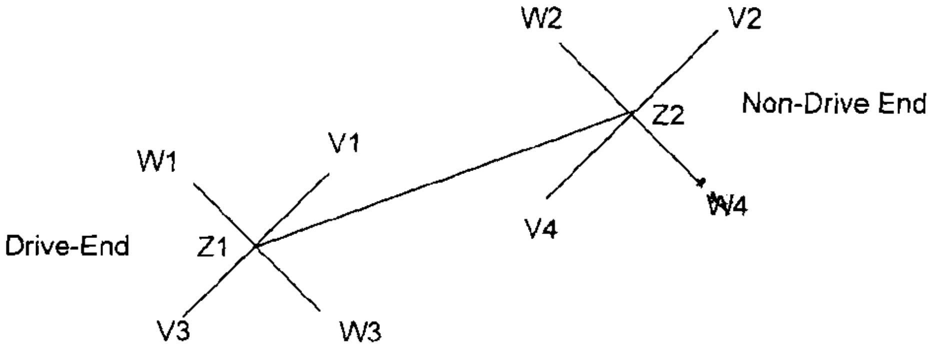

Figure 3.4: 5-axis orientation of a magnetic bearing [153]

Thrust bearings provide a magnetic flux path in the axial direction, between 2 stators oriented on either side of a thrust rotor (or disc). This is then mounted on the rotating shaft as shown in figure 3.5. An axial sensor measures the position of the shaft [77].

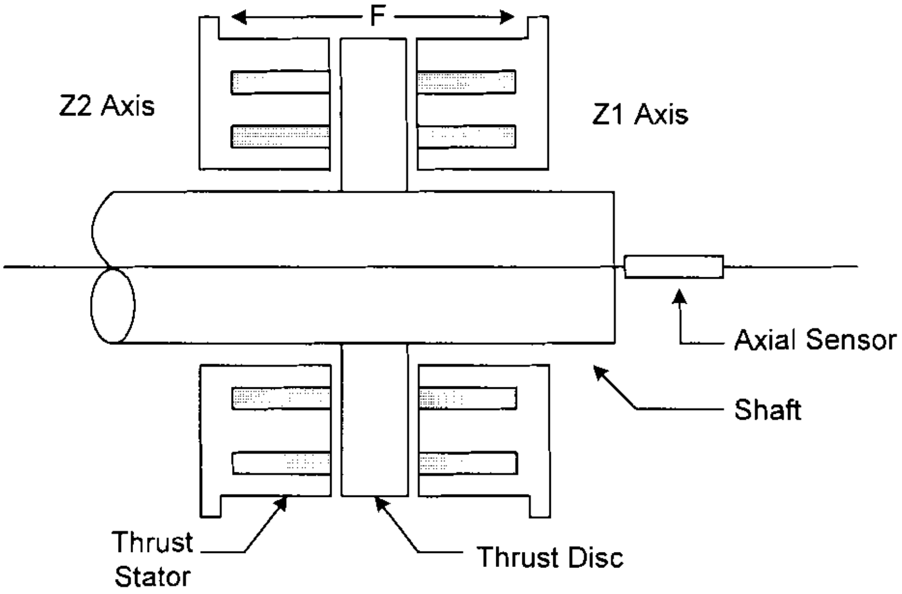

Figure 3.5: Thrust bearing [132]

3.5. BENEFITS OF ACTIVE MAGNETIC BEARINGS

The following section provides some benefits of AMB systems.

3.5.1. HIGH RELIABILITY

With magnetic bearings there is no contact between the rotating and stationary parts, meaning there is no wear. In most cases failure modes are limited to control electronics, power electronics, and electrical windings. These components have design lives far greater than that of conventional bearings [148].

Magnetic bearings are fitted with protective retainer (backup) bearings and have built-in overload protection. Magnetic bearings can signal process control equipment to stop the machine instantaneously in the case of excessive load [29].

Magnetic bearings provide high reliability and long service intervals in time critical applications for semiconductor manufacturing, vacuum pumps, and natural gas pipeline compression equipment [165].

Users are aware that, beyond function, the aspects of safety and related areas become increasingly important. Safety is more than a mere technical issue. It contains a strong component of psychological interpretation, and expectations as to safety are running very high.

Reliability on the other hand appears to be more amenable to engineering calculations and to economic considerations [23].

Mathematical tools for assessing reliability of classical technical systems, and performance numbers for comparing them, such as mean time between failures, are readily available. The reliability analysis of given technical structures and systems, consisting of a more or less large number of classical components, is rather well developed [76].

3.5.2. CLEAN ENVIRONMENTS

In a magnetic bearing system, particle generation due to wear and the need for lubrication are eliminated. There is therefore no chance of contaminating a clean process with oil, grease or solid particles [137].

Magnetic bearings offer a dry, clean and economic solution for semiconductor fabrication equipment, vacuum pumps, gas and air compressors, and various other turbo machines that require submersion in process fluid, even under pressure [33].

3.5.3. HIGH SPEED APPLICATIONS

The fact that a rotor spins in space without contact with the stator means drag on the rotor is minimal. That opens up the opportunity for the bearing to run at exceptionally high speeds, where the only limitation becomes the yield strength of the rotor material [137]. Please note windage losses under limitations of magnetic bearings (section 3.6.4).

3.5.4. POSITION AND VIBRATION CONTROL

Magnetic bearings use advanced control algorithms to influence the motion of the shaft and therefore have inherent capability to precisely control the position of the shaft within microns and to virtually eliminate vibrations [78].

3.5.5. EQUIPMENT DESIGN, DEVELOPMENT AND TESTING

A magnetic bearing system can be used as an exciter, where the bearing force is modulated for deliberately exciting vibrations. The excitation force is applied to the rotor without contact and can be measured precisely. This makes magnetic bearings a valuable tool in equipment design, development and testing as well as in rotor dynamic research [155].

3.5.6. MACHINE DIAGNOSTICS

In order to function, a magnetic bearing must determine rotor position, rotor vibration and bearing load. This information is processed into an electronic database which provides an output to the end users, such that there is a constant knowledge of the operating state of the machine. This allows the user to detect incipient faults, plan maintenance and optimise performance [137].

3.5.7. ELIMINATION OF OIL SUPPLY

Magnetic bearings do not require oil lubrication so they are well suited to applications such as canned pumps, turbo-molecular vacuum pumps, turbo-expanders and centrifuges where oil cannot be employed [4].

3.5.8. LOW POWER CONSUMPTION AND LONG LIFE

There is no contact between the rotor and stator, this means no wear. Where fluid film bearings have high friction losses due to the oil shearing effects, magnetic bearing losses are due to low level air drag, eddy currents and hysteresis [78].

Also the losses associated with oil pumps, filters and piping are much greater than the power associated with controls and power amplifiers. Overall, magnetic bearings normally have an order of magnitude lower power consumption than oil film bearings [4].

3.5.9. LOW WEIGHT

A recent study of aircraft gas turbine engines indicates that the elimination of oil supply and associated components with magnetic bearings could reduce the engine weight by approximately 25 % [4].

3.5.10. EXTREME CONDITIONS

The following section provides some extreme conditions of AMB systems.

3.5.10.1. TEMPERATURE

The magnetic bearing system is capable of operating through an extremely wide temperature range. Magnetic bearings can operate as low as -256 °C and as high as 220 °C, thus allowing operation where traditional bearings will not function [3].

3.5.10.2. CORROSIVE FLUIDS

Magnetic bearings can operate in corrosive environments by means of canning both the stationary and rotating parts [169].

3.5.10.3. PRESSURE

Magnetic bearings are virtually insensitive to pressure. They can be submerged in process fluid under pressure without the need for seals, as is the case with conventional bearings. Magnetic bearings can also operate in vacuum where their operation is even more efficient due to lack of windage [4].

3.6. LIMITATIONS OF ACTIVE MAGNETIC BEARINGS

3.6.1. LARGER BEARINGS

Magnetic bearings have a specific load capacity (maximum load per unit of area of application) lower than most conventional bearing systems which results in bearings that are physically larger than other similarly specified bearings. Magnetic bearings therefore have a lower load capacity [4], [149].

3.6.2. HIGHER COMPLEXITY AND COST

The higher complexity of magnetic bearings often means the initial purchase price is higher than competing technologies. However, magnetic bearings' life cycle cost can often be less than traditional bearings. This is particularly true where the alternatives are exotic bearings [4], [7].

3.6.3. REQUIRES ELECTRICAL POWER

Magnetic bearings require power to drive the control systems, sensors and electromagnets [165].

3.6.4. WINDAGE LOSSES

At high rotating speed, windage (friction between moving parts and air) becomes a problem. For inline electric motors the circumferential speed needs to be limited not due to the material strength but due to high windage losses at the motor surface. These windage losses increase linearly with pressure [103].

Modern flywheel uninterruptible power supplies has a useful power delivery for 10 to 50 seconds, a maximum surface speed of 122 m/s and windage losses over 1 kW for systems not operating in a vacuum [109].

3.7. FAULTS ON ACTIVE MAGNETIC BEARINGS

System faults can be broadly classified as either *internal* or *external* to the magnetic bearing control system. This classification then relates to the way in which the faults can be dealt with following occurrence.

3.7.1. EXTERNAL FAULTS

Faults that are external to the magnetic bearing/control system do not generally require any reconfiguration of the control system itself although some adjustment or adaptation of the control algorithm may improve operation. Consideration of abnormal, or fault related, system disturbances in the controller design will also improve robustness to certain aberrations from normal operating conditions [83].

Faults are considered to be external when either the fault manifests itself as, or the effect of the fault can be replicated by, some external vibration (disturbance) acting on the system. These disturbances will always have a transient component and possibly a steady state component. Typical faults that can be classified in this way include the following:

3.7.1.1. ROTOR IMPACT

A direct impact of the rotor with a foreign body could occur in a number of applications. For example, a pump or turbine fluid/air intake could be contaminated with solid matter. This type of fault would result in an impulsive force acting directly on the rotor, the magnitude of which would depend on velocity, mass and material hardness [29].

3.7.1.2. ROTOR MASS LOSS (LOAD UNBALANCE)

This type of fault is well documented for high-speed turbines where loss of compressor or turbine blades, though uncommon, can occur. Typically, sudden loss of a blade occurs due to a fracture at the blade root. This can be modelled by a step change in amplitude of the synchronous forces acting on the rotor [51].

3.7.1.3. MOTION OF SYSTEM BASE (FOUNDATION LOOSENESS)

Motion of the system base, on which the bearings are mounted, can occur in various applications and environments [148]. In transport applications, motion of the vehicle will be transmitted to internally mounted machines. Base motion may also arise from external vibration sources (e.g. other machines), seismic events and accidental impacts or explosions [46].

3.7.1.4. ROTOR DEFORMATION

Deformation of the rotor while in operation could occur for a number of reasons. For example, a plastic deformation of the rotor or ancillary component may occur due to excessive loading/wear. Another possibility is thermal deformation, for example, due to rotor rub. This effect can be modelled by synchronous forces acting directly on the rotor, but for control purposes should not be treated the same as unbalance [62].

3.7.1.5. SUDDEN CHANGES IN LOADING (OVERHUNG ROTOR)

A change in the steady state load could occur due to some fault conditions. For example, in compressor or pump applications, a sudden change in fluid pressures due to an external fault or error will result in a step-change in the axial rotor loading. Rotor mass loss events will also cause a step change in mean loading due to a change in the total weight of the rotor [10].

3.7.1.6. ROTOR RUB

Contact of the rotor with stationary components causes vibration both of the rotor and the surrounding ancillaries. This may occur for a variety of reasons e.g. rotor deformation, unbalance changes or component damage. It will generally be characterised by directly forced rotor vibration, mainly at the synchronous frequency, although sub-harmonics and higher frequencies will also be present. Rotor rub can significantly alter the closed loop dynamics of the system and if so, treatment as an external fault may be inappropriate [139].

3.7.1.7. BENT ROTOR

In the case of a bent rotor, the excitation is proportional to the magnitude of the bow along the rotor [38], [50]. A bent rotor gives rise to synchronous excitation, as with mass unbalance, and the relative phase between the bend and the unbalance causes different changes of phase angle through resonance than would be seen in the pure unbalance case, as described in [111], [112].

3.7.1.8. MISALIGNMENT

Misalignment occurs when there are geometry changes due to assembly procedures. Misalignment is typically caused by the following conditions [94]:

- Inaccurate assembly of components, such as motors, pumps, etc.
- Relative position of components shifting after assembly
- Distortion due to forces exerted by piping
- Distortion of flexible supports due to torque
- Temperature induced growth of machine structure
- Coupling face not perpendicular to the shaft axis
- Soft foot, where the machine shifts when hold down bolts are torqued.

If the machine speed is varied, the vibration due to imbalance will vary as the square of the speed. If the speed is doubled, the imbalance component will rise by a factor of four, while misalignment-induced vibration will not change in level [49].

3.7.1.9. ROTOR FAULTS

Mechanical faults in the system could be catastrophic if the system cannot retain adequate control. Possible faults of this nature include fatigue, cracking, deformation of the rotor or detachment of part of the rotor. Also, problems not directly attributable to the rotor can occur, such as external rubbing, ancillary parts becoming loose or unexpected impacts or loading. Mechanical abnormalities in the rotor can be considered as a variation in system parameters. As such, there is a realistic chance that these types of faults can be included in robustness specifications during the controller design stage [30].

3.7.2. INTERNAL FAULTS

3.7.2.1. POWER AMPLIFIER FAILURE OR MALFUNCTION

To power each magnet coil, a solid state amplifier is commonly used. Although, these units are inherently reliable, their dynamic performance depends on a number of variables (e.g. ambient temperature and power demand). The amplifiers are usually configured for either voltage or current control. When amplifiers and magnet poles are configured in opposing pairs, loss of a single amplifier and pole will result in an attractive force from the remaining opposite pole. Unless this can be turned off quickly the rotor will collide with the backup bearings [70].

Actuator faults in AMB systems may have a number of causes. Problems may arise in any point in the series connection of amplifier, wiring, and coil. Connectors or cables may fail, amplifiers and fuses may burn. For experimental purposes actuator faults can be restricted to open circuit failures that can be tolerated by the system, i.e. failures of a lower sensor coil such that the current suddenly goes to zero [30].

Without correction, such a failure can be modelled as a decrease in bearing stiffness combined with the disability to exert downward forces onto the rotor, as a consequence of the changes in the actuator. The system may become unstable in one channel (axis). As the case with uncorrected sensor faults, unstable behaviour with violent crashes of the rotor against the retainer (backup) bearings is the consequence [90].

3.7.2.2. TRANSDUCER MALFUNCTIONS (SENSOR FAILURE)

The malfunction of a transducer could produce a variety of erroneous signals. However, a short circuit or an open circuit is likely to produce a dc signal. Other than an electrical fault, physical damage or deterioration is a likely cause of sensor malfunction. For example, damage to the shaft at the measurement surface will affect proximity detectors [1].

Without correction, failure of a sensor leads to the controller being provided with incorrect position information. As a consequence, the controller sets up inappropriate reference currents, which inevitably entails a destabilization of the system. Violent crashes of the rotor against the retainer (backup) bearings are the consequence [77].

The electronics may fail or the signals may be disturbed, most often by excessive noise from electromagnetic sources, which are mistaken as sensor signals.

3.7.2.3. LOSS OF I/O BOARD CHANNEL

The complete loss of a channel on the computer input/output board would produce an undefined control input or output signal. A possible cause of this type of fault would be a circuit break or short in the connection cable [15].

3.7.2.4. BEARING MAGNET COIL FAILURES

The failure of a magnet coil usually occurs due to a breakdown in winding insulation, resulting in a short circuit. Depending on where the short occurs, there will be a reduction in the number of effective coil windings [131].

3.7.2.5. COMPUTER SOFTWARE ERRORS (CONTROLLER FAILURE)

Real-time control software can be susceptible to latent programming errors that may arise unexpectedly and may be difficult to pre-detect. These types of errors will result, at best, in unpredictable behaviour or, at worst, in program termination. The key to avoiding this type of situation is well structured programming and thorough program testing. Code can be written with a certain degree of built in tolerance to run-time errors [22].

However, a complete program execution failure would require a redundant microprocessor to take over control [167]. The alternative is to rapidly restart the processor, which would require reloading of the control program, initialising and restarting. It is doubtful whether this could be achieved in the necessary time-scale [145].

Examples of software failures are a system breakdown, run-time exceptions, i.e. address errors and bus time-out, or incompatible program versions. The software area is least covered by systematic approaches to improve its reliability [29].

3.7.2.6. COMPUTER HARDWARE FAILURES

A failure of microprocessor hardware is relatively uncommon, but would probably have similar consequences to a program termination. Again the only alternative for dealing with this type of problem would be if back-up hardware were available to take over the control operation [35].

3.8. MEASURES FOR REDUCING RISKS OF FAILURE

The following section provides measures for reducing risks of failure.

3.8.1. QUALITY CONTROL AND STANDARDS

An overall approach for systematically introducing quality aspects into the design, production and operation of products and systems, are standardized procedures as described in the ISO 9000 series [66]. A company or an establishment following the procedures of ISO 9000 can be recognized as a certified institution with a defined quality level. In addition the ISO 14839 provides information and standards on mechanical vibration of rotating machinery equipped with active magnetic bearings [70].

3.8.2. SYSTEMATIC CHECK OF THE DESIGN

A classical method to ensure best practice of the state of the art is to use the FMECA approach for checking the design, i.e., to do a Failure Modes, Effects, and Criticality Analysis. In this approach a group of experts with different background, from design, production, test, repair, and potential users, are evaluating the design or the product [153].

They have to identify potential failure modes, determine the effects and consequences of such failures and their criticality, and suggest modifications of the design to improve it. There are various standards and specifications on how to proceed in detail, depending on the application areas (see for example the military standard procedures MIL-STD-1629A [66]). FMECA is an integral part of any QS 9000 compliant quality system [126].

3.8.3. SOFTWARE DEVELOPMENT SYSTEM

In a mechatronic system, software is an integral part of the system and has to be developed and implemented. The software has to be logically correct, and the operating system should take care of the syntax. In addition to that, the correct time sequence of the computational tasks is most essential in real time applications [107].

For industrial AMB applications most often proprietary software is running on single chip digital signal processors (DSP) giving an efficient and economic solution, which is dedicated to specific tasks with well-defined constraints. For experimental application the tasks usually are much more diverse, sometimes complex and require a versatile solution [94].

For complex tasks it may not be sufficient to just use a high-speed computer with high sampling frequency and assume that this is adequate for real time operation. It might be better to use a real time operating system (RTOS) from the onset in order to develop and finally operate the software. Such RTOS are available in various versions, such as dSPACE®, RTLinux®, XO/2® and VxWorks® [108].

3.8.4. REDUNDANCY

One way of improving reliability is to use redundant components and redundant information. There are two different kinds of redundancy. If the failure of a single component cannot be corrected and is critical for the system's safety, the function of this component should be guaranteed by redundant hardware. Two or more of these same components have to be arranged in parallel, in order to replace any failed component [33].

Appropriate failure detection and switchover schemes are crucial, and the increase in the number of components actually counteracts the overall reliability to some extent. If the function of a component is at least partially performed by another component as well, then the functional relation between these components can be used as an analytical redundancy to replace the failed component partially, or to reduce the extent and cost of a hardware redundancy [44].

If the rotor is driven by a motor drive, switching the motor from its drive mode to generator mode can supply sufficient electrical power to the system again, until the rotor can coast down safely in its retainer bearings [87].

Diagnostics and identification tools are being used for fault detection of various kinds of fault-tolerant control systems. A general introduction is given in [16] and [22]. In magnetic bearings, faults on redundant sensors and actuators and other redundant machine components have been detected and corrected, see [29], [90], [107] and [140].

3.9. FUTURE AMB CONTROL TECHNOLOGIES

Future AMB control technologies are likely to be driven by [87]: (1) higher operating speeds, (2) lower power loss, (3) greater use of available clearance, (4) generalised actuation, sensing and control and (5) control of unbalance response.

3.9.1. HIGHER OPERATING SPEEDS

Magnetic bearings already permit higher operating speeds than conventional bearings. However, the demand for even greater speed is strong, e.g., for energy storage flywheel systems for electric vehicles. Higher rotational speed implies a greater rotor gyroscopic effect which results in the plant being linear parameter-varying (LPV) [118].

3.9.2. LOWER POWER LOSS

Lower power loss is especially important for high-speed applications, since rotation of the rotor in a supporting magnetic field can cause significant losses which result in reduced machine efficiency and excessive rotor heating [109].

A common approach to improve the force slew rate is to introduce a bias current (or flux ϕ). With a bias, the actuator may also be accurately modelled as linear. The disadvantage of operation with a bias is the associated ohmic loss in the coil ($I^2 R \propto \phi^2$), rotating hysteresis loss ($\propto \phi$), alternating hysteresis loss ($\propto \phi^{1.6}$), and eddy current loss ($\propto \phi^2$) [166].

For high speed rotating machinery, the eddy current loss is dominant; herein we refer to it as the rotating loss. This rotating loss may result in excessive rotor heating. Moreover, it results in decreased machine efficiency. Thus, operation without bias is appealing in applications where efficiency is critical, for example energy storage flywheels [166].

3.9.3. GREATER USE OF AVAILABLE AIR GAP

Most industrial magnetic bearing systems use a large air gap during operation. A larger air gap (e.g. 1 mm) results in greater actuator linearity near the centered position and thus simplifies control design and tuning. However to reduce bearing size, weight and power consumption, it is desirable to use a smaller air gap during operation. For some applications, such as precision positioning platforms the required motion may be large and a reduction of the bearing size may not be possible [142].

3.9.4. GENERALISED ACTUATION, SENSING AND CONTROL

For every axis of motion there has been a devoted sensor, actuator and control system, each performing a single operation. Recently there has been a shift away from this approach. For example, magnetic actuators are used to inductively sense position as well as apply forces [90].

Motor and bearing functions are achieved with a single actuator. Direct digital control of amplifier switching is used to eliminate the separate amplifier servo-control loop, thus combining the amplifier and rotor controllers. The advantages of these generalised actuation, sensing and control methods are reduced cost and increased design flexibility [80].

3.9.5. CONTROL OF UNBALANCED RESPONSE

Control of unbalanced response has been an area of intense research over the last few years, which requires substantial laboratory and industrial experience to provide a good outcome. Herzog *et al.* [54] propose a generalized notch filter to be used in a redundant multivariable feedback loop to reduce the response of the control system to rotor imbalance so as to avoid actuator saturation.

3.10. CONCLUSION

Magnetic bearings have structured themselves in bearing technology over the past few years. Industries, small companies and even the everyday man can benefit from the advantages of magnetic bearings.

High reliability, clean environments, high speed applications together with advantages in position and vibration control are only a few of the advantages of magnetic bearings. Like any other bearing, magnetic bearings also have limitations. Larger bearings, higher complexity and higher cost are a few of the limitations of magnetic bearings.

The quality and performance of an AMB system can be greatly improved by implementing the steps outlined in the measures for reducing risks of failure.

Faults on AMB systems were classified into internal and external, with internal focussing on faults occurring within the hardware and software of the AMB system and external focussing on faults caused by some external vibration (disturbance) force acting on the system. These faults can be detected, corrected and identified by using fault detection techniques and intelligent control systems. The next chapter provides information on these fault detection techniques.

CHAPTER 4

FAULT DETECTION TECHNIQUES

4.1. INTRODUCTION

This chapter focuses on providing the reader with background information on fault detection techniques. An overview of the techniques currently available and an explanation of the techniques used in this research are provided.

As mentioned in the research methodology section (section 1.5) of chapter 1, the research is divided into two phases. Phase 1 focuses on performing condition monitoring and implementing fault detection techniques on the historical fault data obtained from the 250 kW water cooling AMB pump (SM400/400). An expert system then uses the extracted features from the different fault detection techniques to provide a result on which techniques provide the best output (best feature) for specific fault conditions. In phase 2 these techniques are incorporated in the design of the three real-time detection, diagnosis, correction and identification schemes.

Figure 4.1 provides a tree diagram of the different fault detection techniques. Fault detection techniques can be broadly categorised into linear and non-linear processing techniques. The benefits of non-linear processing techniques versus standard linear processing techniques depend on the complexity of the problem. The area of linear processing techniques is not discussed in this thesis. Non-linear processing techniques can be categorised into: 1) time domain analysis, 2) frequency domain analysis, 3) time-frequency analysis and 4) feature analysis.

The fault detection techniques in the shaded blocks were studied in depth and were implemented on the historical fault data of the 250 kW water cooling AMB pump. Results on the implementation of these techniques are available in appendix E. The conclusion section of this chapter provides more detail on the techniques incorporated in the design of the three real-time schemes (phase 2).

The fault detection techniques in the clear blocks were not implemented on the historical fault data. Shock pulse analysis and spike energy analysis are used to detect impacts on bearings. This approach was not chosen for AMB systems, since the correction system must prevent any impacts to the bearings.

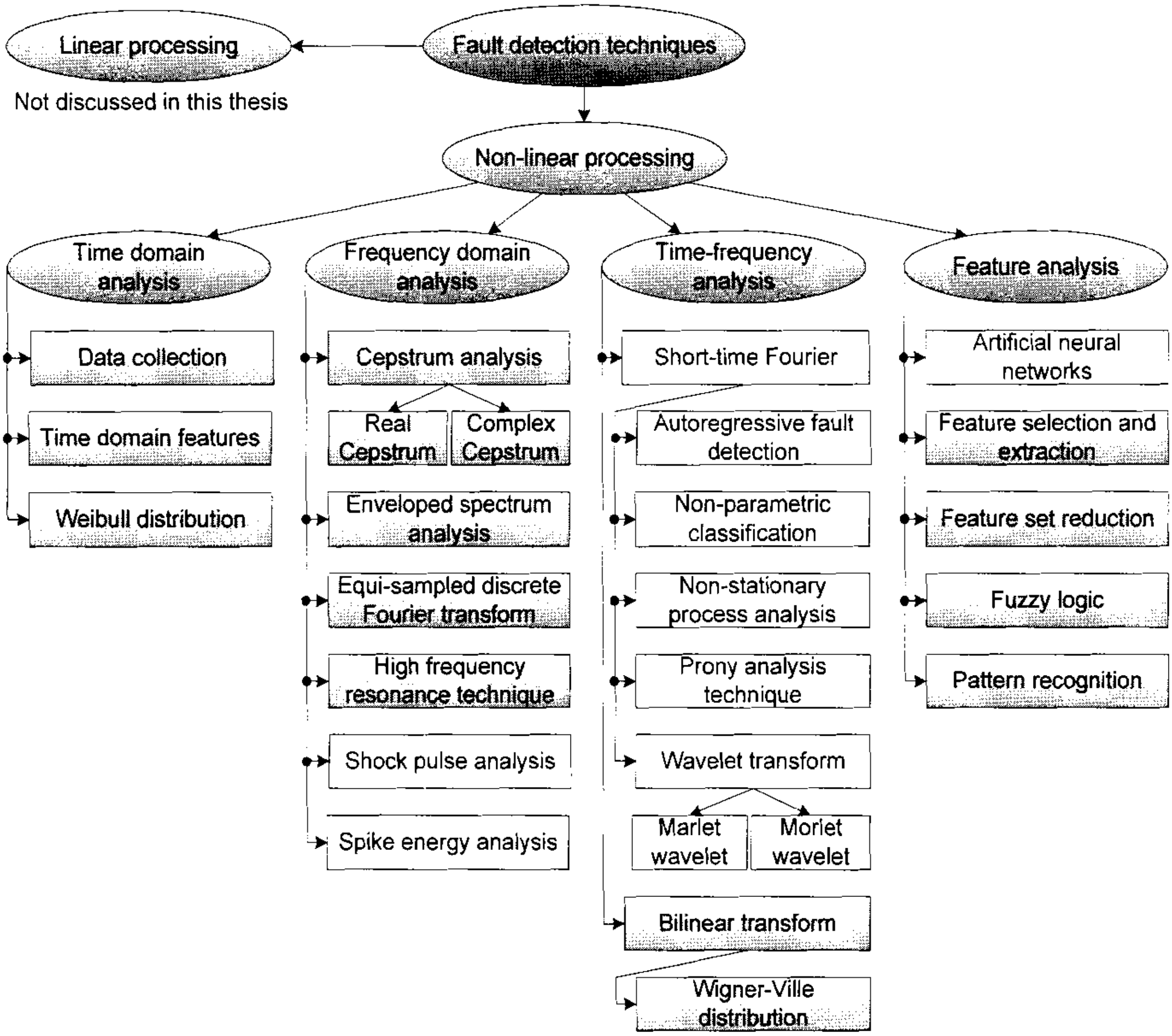

Figure 4.1: Tree diagram of the different fault detection techniques.

The area of bilinear transforms was chosen above short-time Fourier transforms (STFTs), since STFTs segment the data into overlapping time-windows. Bilinear transforms uses the instantaneous frequency for analysis, which provides a more direct type of analysis. More detail is provided in section 4.4

Fuzzy logic was chosen above artificial neural networks (ANNs), since ANNs focus on a black box approach and fuzzy logic on a grey box approach. A fuzzy logic controller has the ability to incorporate experience, intuition and heuristics instead of relying on a mathematical model.

The rest of this chapter provides a short explanation on each of the fault detection techniques mentioned in figure 4.1.

4.2. TIME DOMAIN ANALYSIS

4.2.1. DATA COLLECTION

The collection of a consistent and reliable set of measurements, covering the physical and electrical properties of the machinery, is vital for reliable diagnosis of faults [56]. A-priori knowledge regarding the factors influencing vibration measurements is important to define a meaningful and compact feature set. Statistical considerations indicate that increasing the sample size may reduce the variance of results. The sample size is especially important to discover the potential non-linear relationships inherent in the data [56]. RMS acceleration has been successfully used for years using a magnet-mounted accelerometer feeding into a vibration meter.

4.2.2. TIME DOMAIN FEATURE

The following time domain features can be extracted from data [18], [75], [100]: mean, root mean square (RMS), crest factor, variance, skewness and kurtosis. A brief description of each follows: The mean value of a function $x(t)$ over an interval T is:

$$\bar{x} = \frac{\int_0^T x(t)dt}{T} \tag{4.1}$$

The RMS value of a function $x(t)$ over an interval of T is:

$$x_{rms} = \sqrt{\frac{\int_0^T x(t)^2\,dt}{T}} \tag{4.2}$$

The crest factor is the ratio of the peak level to the RMS level:

$$CF = \frac{x_{max}}{x_{rms}} \tag{4.3}$$

The variance is the mean square value relative to the mean:

$$\sigma^2 = \frac{1}{T}\int_0^T [x(t) - \bar{x}]^2\,dt \tag{4.4}$$

The skewness is the third statistical moment of a distribution:

$$S = \frac{1}{\sigma^3 T}\int_0^T x^3 dt \tag{4.5}$$

The kurtosis is the fourth statistical moment of a distribution:

$$K = \frac{1}{\sigma^4 T}\int_0^T x^4 dt \tag{4.6}$$

4.2.3. WEIBULL DISTRIBUTION

The Weibull distribution is useful in the statistical analysis of vibration signals, especially with skewed distributions [115]. The Weibull distribution was invented in 1937 by Waloddi Weibull when comparing mortality rates of different population groups. He invented a formula that could describe the different shaped graphs in each of the three zones [58].

$$R(T) = e^{-\left(\frac{T}{\eta}\right)^{\beta}} \qquad \text{(2 Parameter Weibull)} \qquad (4.7)$$

where $R(T)$ represent the reliability at time T, T is the time considered, η is the characteristic life, β is the shape parameter and e is the base for natural logs (2.71828).

Information on the advantages and disadvantages of Weibull analysis are available in [76].

4.3. FREQUENCY DOMAIN ANALYSIS

It is well known that defects in rotating machinery may be monitored using vibration frequency domain analysis. Certain features from frequency domain analysis can be generated to predict multiple faults [86]. These features can be determined by using common condition-monitoring techniques. The following features can be extracted from frequency domain analysis: 1) amplitude of the vibration spectrum at rotational frequency and 2) higher frequency domain components.

According to Taylor [152], force imbalance in a rotor may be detected using vibration frequency domain analyses. A peak in the spectrum at the running speed frequency of the shaft will indicate imbalance. The amplitude of acceleration at the running speed frequency may be related to the amount of imbalance in the rotor.

4.3.1. CEPSTRUM ANALYSIS

Cepstrum analysis is used to detect periodicities in the spectral analysis of a signal, as well as to separate the effect of varying transfer functions [127]. It is well suited as a tool for the detection of families of harmonics with equal spacing. It is defined as the inverse Fourier transform of the logarithm of the Fourier transform of a time signal $x(t)$ and is given by [115]:

$$C_{cxx}(\tau) = \Im^{-1}\left\{\log_{10}\Im\{x(t)\}\right\} \qquad (4.8)$$

The real Cepstrum is defined as

$$RCEPS(x) = \mathrm{real}\left(\Im^{-1}\left(\log\left|\Im(x)\right|\right)\right) \qquad (4.9)$$

where $\Im$ is the Fourier transform and $\Im^{-1}$ is the inverse Fourier transform of the input signal.

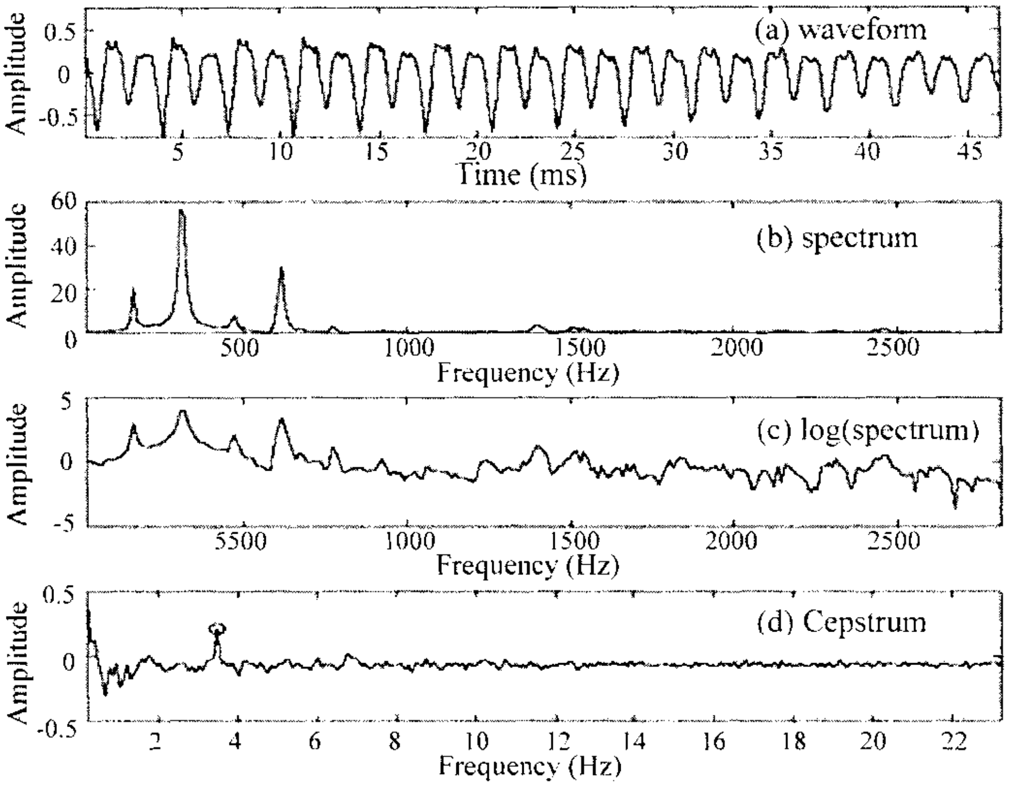

Figure 4.2: Cepstrum calculation [102].

The name Cepstrum comes from reversing the first four letters in the word "spectrum". Figure 4.2 (a) shows an input waveform. The waveform is spectrum analysed (shown in figure 4.2 (b)) and the log of the magnitude spectrum (shown in figure 4.2 (c)) is then obtained. The Cepstrum analysis (shown in figure 4.2 (d)) is obtained by the inverse Fourier of the log of the magnitude spectrum. From the Cepstrum analysis the defect frequency is clearly visible. The nonlinear (inharmonic) system can be made more linear by using the log spectrum [102].

4.3.2. ENVELOPE SPECTRUM ANALYSIS

Envelope spectrum analysis is a technique especially suitable for early detection of damage [55]. The technique consists of a bandpass filter that reduces frequency components not related to the bearing. The signal is then enveloped by fullwave rectification and lowpass filtered before an analysis of the spectrum is performed [115].

Stewart Hughes [130] demonstrated that the bearing condition is best indicated by looking at the demodulated signal in a narrow frequency band, centred around the natural frequency of the bearing housing. The bearing defect frequencies, dependent only on bearing geometry and speed, show up clearly in the demodulated signal, whereas in the normal frequency spectrum they could lie buried in low frequency background noise.

The block diagram shown in figure 4.3 summarises the steps of the envelope analysis process. The frequency analysis of the envelope provides a diagnosis of the vibration, i.e. the defect frequencies become evident. A defect frequency, which exceeds the background level in the spectrum by 20 dB, indicates a fault condition, which needs to be rectified. With regular monitoring the machine can still be run [158].

Unlike other methods that depend on measuring an overall bearing damage level, the envelope spectrum provides a positive diagnostic tool, that points conclusively to the bearing, without any interference of high frequency noise [130].

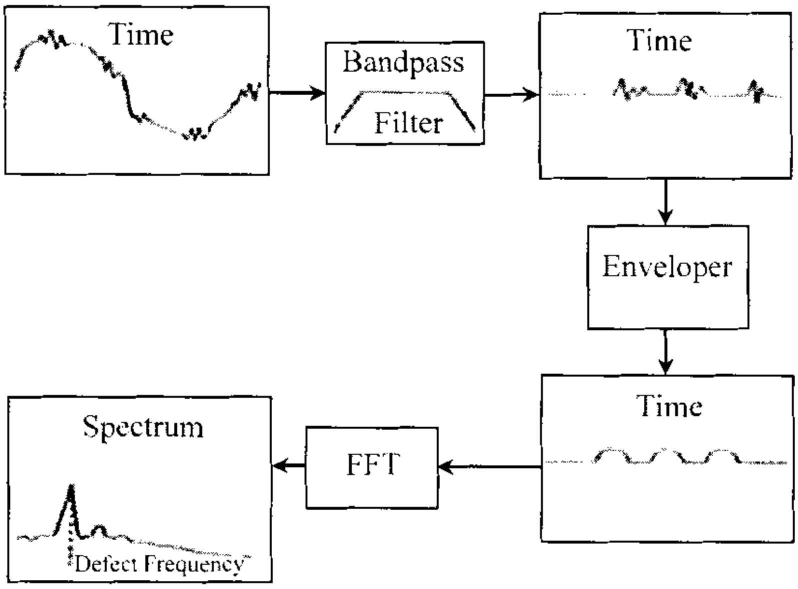

Figure 4.3: Block diagram of envelope process [158].

4.3.3. EQUI-SAMPLED DISCRETE FOURIER TRANSFORM (ESDFT)

Figure 4.4 provides a block diagram of the enveloped equi-sampled discrete Fourier transform (ESDFT). Low frequency large amplitude AMB vibration components can be separated from higher frequency response signals by means of a band pass filter. In the envelope spectrum method, the resulting signal is rectified and low-pass filtered in order to detect the envelope of the signal [116].

The low frequency information is extracted from the carrying resonance frequency band. After these operations the resulting signal is transformed to the frequency domain by means of the ESDFT. An absolute maximum plot is obtained and the data is analysed for increases in defect frequencies.

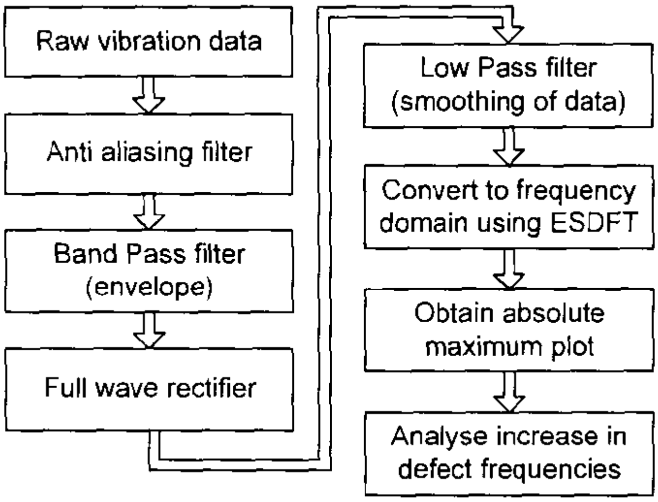

Figure 4.4: Block diagram of the enveloped ESDFT.

The ESDFT is defined as [161]:

$$ESDFT(k,m) = FFT(k * m,n), \qquad k = 0,\dots,N/m-1 \;, n = 1,\dots,N \tag{4.10}$$

where N is the number of samples in the FFT and m is the width of the comb filter in the frequency domain.

The DFT of the k^{th} entry of the n^{th} channel, $y(k,n)$ is given by (4.11) [99]

$$y(k,n) = \sum_{p=1}^{M} u(p,n)e^{-j2\pi(p-1)(k-1)/M}, \qquad k = 1,\dots,M \;, n = 1,\dots,M \tag{4.11}$$

and the convolution of k and m is obtained by using

$$w(l) = \sum_{j} k(j)m(l+1-j), \qquad l = 1,\dots M \tag{4.12}$$

where w is the convolution vector.

The ESDFT is inversely related to the period (in samples) over which the synchronous average (SA) is taken in the time domain. Hence long periods in the time domain give a small value of m in the frequency domain (the combs of the comb filter spaced close together) and vice versa [17].

It is well known that the SA may reduce noise by a factor of $1/\sqrt{N}$ [105] (where N is the number of samples in the buffer). In particular, any vibration not synchronous with the trigger period T will be filtered out if a sufficient number of averages are taken. As the ESDFT, actually computes an SA it should also reduce the noise by a factor of $1/\sqrt{N}$. Hence the good performance of the SA in reducing non-synchronous noise is also apparent in the ESDFT.

More specifically, it is shown that the frequency components at the characteristic defect frequency (and harmonics) actually correspond to the spectral information of the signal average. The ESDFT retains the frequency components only corresponding to integer multiples of the trigger frequency T_f. The ESDFT keeps the prototype filters corresponding to an integer multiple of the sampling frequency, which corresponds to the trigger frequency [12].

The frequency domain transfer function of the ESDFT is given by

$$ESDFT(j\omega) = \left|H_o(e^{j\omega})\right| + \ldots + \left|H_{mL}(e^{j\omega})\right| \tag{4.13}$$

where $m = 1, 2, 3\ldots$ and L is an integer corresponding to $L = F_s/F_t$ (F_s is the sampling frequency and F_t is the trigger frequency) and $J = 1/L = F_t/F_s$.

The prototype DFT filter bank [160] is a shifted version of the prototype filter $H_0(e^{j\omega})$

$$\begin{aligned} \left|H_{mL}(e^{j\omega})\right| &= \left|H_o(e^{j\omega-(2\pi k/M)})\right| \qquad , k = mL \\ &= \left|H_o(e^{j\omega})\right| + \cdots + \left|H_0(e^{j\omega-2\pi mL/M})\right| \\ &= \sin(M\omega/2)/\sin(\omega/2) + \cdots + \sin\left(m\left(\omega - 2\pi mL/M\right)\right) \end{aligned} \tag{4.14}$$

where $k = mM/L$ and $(M/L)/M = J = 1/L = F_t/F_s$.

4.3.4. HIGH FREQUENCY RESONANCE TECHNIQUE (HFRT)

The high frequency resonance technique (HFRT) of envelope detection is described by McFadden and McFadden [99]. A bearing defect excites a high frequency resonance at the characteristic defect frequency in the same way that a bell rings when struck by a hammer.

Thus the envelope of the high frequency resonance provides information about the (low frequency) modulating function. The signal from the accelerometer is amplified and bandpass filtered around a resonance. An envelope detector consisting of a non-linear element (a half- or fullwave rectifier, or raising the signal to a power such as with a squarer) is subsequently applied to extract the envelope of the signal. The frequency component is then analysed at the characteristic defect frequency [113].

The HFRT utilizes the fact that much of the energy resulting from a defect impact manifests itself in the higher resonant frequencies of a system. Demodulation of these frequency bands through use of the envelope technique is then employed to gain further insight into the nature of the defect while further increasing the signal to noise ratio. If periodic, the defect frequency is then present in the spectra of the enveloped signal [57].

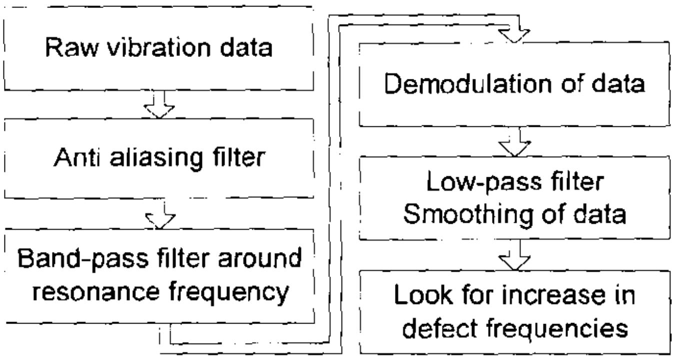

Figure 4.5: High frequency resonance technique process.

Figure 4.5 shows a process diagram for the HFRT. Raw vibration data is passed through an anti-aliasing filter. The signal is then bandpass filtered around a selected high frequency band. The bandpassed signal is then demodulated with a non-linear rectifier and low pass filtered to cancel high frequency components and retain the low frequency information associated with the fault [99]. The HFRT takes advantage of the large amplitudes of a defect signal in the range of a high frequency system resonance, and provides a demodulated signal with a high defect signal-to-noise ratio in the absence of low frequency mechanical noise.

The HFRT filters the signal around a suitable demodulation frequency, followed by rectification and lowpass filtering (envelope detection) [127]. The normalized ratio of the demodulation peak in the demodulation spectrum relative to the carpet level provides a measure of the defect growth and is regarded as the best feature of bearing defect evolution [147].

In Shiroshi [146] the effect of non-linear transfer functions on the amplitude density function and power spectrum of band limited 'white noise' is derived. On p. 222 of Akansu [8] the result of $y = bx^2$ is given as:

$$S\eta(\omega) = S_1(\omega) + S_2(\omega) + S_3(\omega)$$

where

$$\begin{aligned} &S_1(\omega) = 4b^2A^2(\Delta\omega)^2\delta(\omega) \text{ for } \omega = 0 \\ &S_2(\omega) = 4b^2A^2(\Delta\omega - |\omega|) \text{ for } |\omega| \le \Delta\omega \\ &S_3(\mathrm{w}) = 2b^2A^2(\Delta\omega - |(|\omega| - 2\omega_0)|) \text{ for } 2\omega_0 - \Delta\omega < |\omega| < 2\omega_0 + \Delta\omega \end{aligned} \tag{4.15}$$

where the power spectrum has a constant value A, centred at ω_0 and bandwidth of $\Delta\omega$. It should be noted that the above expressions are based on the assumption of continuous signals [99].

4.3.5. SHOCK PULSE ANALYSIS

This type of analysis is used to detect impacts on the bearings. Information on shock pulse analysis is available in [23].

4.3.6. SPIKE ENERGY ANALYSIS

This type of analysis measures the intensity of the energy spikes. Spike energy analysis is similar in theory to shock pulse analysis. Information on spike energy analysis is available in [165].

4.4. TIME-FREQUENCY ANALYSIS

Frequency spectrum monitoring has become common in fault detection besides overall level monitoring. In most cases the ordinary Fourier transform is used to obtain frequency information. The main disadvantages of the Fourier transform are that every short duration interference in the signal is spread over the whole frequency band, the frequency components represent the whole time series and that even a slight frequency change in the signal makes it hard to analyse the frequency content. Frequencies that are close together cannot be separated if the frequency resolution is low [28].

Recently, the time-frequency analysis has been introduced as a condition monitoring tool by many researches [18], [32], [119], [121]. An advantage of time-frequency distributions is that they can reveal details of non-stationary signals and signals that evolve with time. In general, time-frequency analysis requires a lot of calculation power and the interpretation of the results require a lot of effort [36].

4.4.1. SHORT-TIME FOURIER TRANSFORM

The short-time Fourier transform (STFT) is used to analyse the frequency spectra of signals that evolve with time. Information on the STFT is available in [32], [43] and [141].

4.4.1.1. AUTOREGRESSIVE FAULT DETECTION

There exists much written material about autoregressive fault detection, but less empirical experimentation. This method has the capability to obtain high spectral resolution with short datasets [101]. Information on autoregressive fault detection is available in [91], [92], [93] and [135].

4.4.1.2. PRONY ANALYSIS TECHNIQUE

This analysis technique analyses transient component [135]. The technique is useful to determine complex natural resonances and complex amplitudes associated with exponential representations of waveforms [124]. Information on the Prony analysis technique is available in [21], [26], [39], [40], [75], [86], [92], [93] and [134].

4.4.1.3. WAVELET TRANSFORM

Wavelet transform are used to reduce the dimensionality of a vibration signal [39]. Wavelet transform operate on the principle that all signals can be reconstructed from sets of local signals of varying scale and amplitude, but constant shape [116]. Information on wavelet transform is available in [8], [17], [84], [110], [113], [121] and [168].

4.4.2. BILINEAR TRANSFORMS

Another class of time-frequency distributions is the so called bilinear transforms. Unlike spectrograms, they do not segment the data [141]. The WVD is the basic transform of bilinear transforms. The WVD is based on the instantaneous frequency, which is the derivative of the phase of the signal [18].

Bilinear transforms and STFT are used in similar applications and the selection between these transforms is often done experimentally. Further, the success of analysis depends on proper tuning of the parameters [43]. The WVD is widely utilised in a wide area of fault detection of mechanical structures, such as gear transmission or machine tool wear [74], [119].

Amplitude modulated signals that are not found in spectrograms can be revealed by the WVD, because the frequency components or time domain transients are too close together. On the other hand, the bilinear nature of the WVD leads to interference between components in the time-frequency domain [32]. In addition, the cross terms between noise and signal makes WVD noisy. WVD even places the noise at times where the signal is pure from noise. The unambiguity is poor, because of the fact that WVD gives negative values unlike the spectrogram [28], [39].

4.4.2.1. WIGNER-VILLE DISTRIBUTION

The Wigner-Ville distribution (WVD) was first defined for quantum mechanics by E. P. Wigner in 1932 and later by J. Ville [163] in 1948 who derived a joint representation from a mathematical foundation to utilise it in signal representation. This distribution approximates a specified time-frequency description in the minimum mean-square error sense [106].

The technique was developed to overcome a limitation of the STFT, where high-resolution cannot be obtained simultaneously in both the time and the frequency domains [110]. Due to similarities the WVD has been interpreted by Flandrin and Escudié [42] as a modified version of the STFT.

In the WVD, no reduction of the number of data points in the time-shifting operation is necessary [146]. The starting point for this distribution is the Fourier transform of the ensemble-average instantaneous correlation as shown in (4.16) [24]:

$$FT(x(t)) = \int_{\infty}^{+\infty} E\left(x(t+\frac{\tau}{2})x^*(t-\frac{\tau}{2}) \right) e^{-j2\pi v\tau} d\tau \tag{4.16}$$

where x^* is the conjugate of x for complex signals or Hilbert transform of x for real signals which, in theory, is a measure of the frequency content of a non-stationary random process $x(t)$.

However, in practice, it is never possible to compute the ensemble-average function accurately, because an infinite number of data are necessary [24]. One solution to deal with the non-stationary case is to omit the ensemble-average in (4.17):

$$WVD(x(t,v)) = \int_{\infty}^{+\infty} x(t+\frac{\tau}{2})x^*(t-\frac{\tau}{2}) e^{-j2\pi v\tau} d\tau \tag{4.17}$$

Equation (4.17) represents the WVD, which belongs to the class of bilinear frequency distributions defined by Cohen [28] and given by the equation below [106]:

$$C(t,v;\phi) = \frac{1}{2\pi} \int_{-\infty}^{+\infty}\int_{-\infty}^{+\infty}\int_{-\infty}^{+\infty} e^{j(\xi u - \tau v - \xi\tau)} \phi(\xi,\tau;t,v) x(u+\frac{\tau}{2}) x^*(u-\frac{\tau}{2}) du\, d\tau\, d\xi \tag{4.18}$$

where ø(ξ, τ; t, v) is the kernel function, u is time and ξ and τ are the bilinear distribution time delays [41].

The discrete representation of (4.17) is [146]:

$$WVD(x(T_s,v)) = \frac{T_s}{\pi} \sum_{k=-\infty}^{+\infty} x^*(t-kT_s)x(t+kT_s)e^{-2ivkT_s} \tag{4.19}$$

where T_s is the sampling period and must be chosen so that $T_s \leq (\pi/2\omega_{max})$ and ω_{max} is the highest frequency in a random signal [28].

4.5. FEATURE ANALYSIS

4.5.1. ARTIFICIAL NEURAL NETWORKS

The area of artificial neural networks is well known and much written material exists, some of these are [11], [121], [122], [136] and [141].

4.5.2. FEATURE SELECTION AND EXTRACTION

The vibration signals form a multivariate feature space. The required number of training samples for a classifier generally increases exponentially as a function of the number of features, assuming uncorrelated data [56]. Furthermore, the performance of the classifier is closely linked to the quality of the features.

The extraction of a compact feature set, which may still capture most of the correlation inherent in the original sample space, is thus crucial in a multivariate setting. Suitable feature extraction methods highlight the important discriminating characteristics of the data, while simultaneously ignoring the irrelevant attributes (i.e. noise) [56].

The frequency domain provides a useful feature set for machine diagnostics [115]. Machine defects are related to specific frequency domain features [115], [128]. The frequency domain is well suited to the detection of periodic machine vibrations. Impulsive vibrations are better analysed in the time domain than in the frequency domain. The wavelet transform analyses a signal jointly in the time-frequency domain, subject to the uncertainty principle. The uncertainty principle states that an increase in time resolution results in a decrease in frequency resolution and vice versa [114].

4.5.3. FEATURE SET REDUCTION

The reduction of the feature set to the minimum required for acceptable modelling is important in the design of structured experiments. The influence of a set of experimental variables on the response variable(s) is determined by conducting a series of experiments. The resulting response surface may be used in a simulation to augment the existing data set [114].

Since the required number of experiments is exponentially proportional to the number of experimental variables to be considered, the smallest possible number of features should be used. An exhaustive evaluation of all possible experiments would be prohibitive. More sophisticated experimental design techniques would therefore be required to minimize the required number of hypercubes to cover the multivariate space [168].

4.5.4. FUZZY LOGIC

Fuzzy logic controllers have the ability to cope with knowledge presented in a linguistic form instead of a conventional mathematical framework [27]. Much written material exist on fuzzy logic, some of these are [11], [52], [101], [133], [141] and [162].

4.5.5. PATTERN RECOGNITION

The performance of a non-linear classifier, such as a neural network, is directly dependent on the number of training examples relative to the degrees of freedom (complexity) of the classifier [53], [56]. As a rule of thumb, the number of samples should be 10 to 100 for each independent feature [162].

Jack and Nandi [72] examine the use of support vector machines (SVM), a pattern recognition technique, in the detection of bearing faults in a test rig. The aim of the SVM technique is to find the largest separating hyperplane (support vectors). The kernel function maps the data, using a non-linear transfer function, into another dimension in which the classes could be linearly separable with an appropriate choice of parameters.

Jack and Nandi [72] also examine the important question of feature selection using a genetic algorithm (GA). Their [72] results indicate that the SVM comes close to the ANN without GA feature selection [72]. Using GA feature selection the SVM and ANN have comparable performance [45], [154].

A pattern recognition system consisting of sensing, pre-processing, feature extraction, classification and post processing is shown in figure 4.6. Pre-processing of data includes filtering, domain transforms or segmentation of data. Segmentation of data is done in order to isolate one period of a signal or different operation modes from each other. The feature extraction converts the pre-processed data to sets of numerical values namely feature vectors that describe the different classes [14].

The features should be selected such that for patterns of one class (such as healthy system) the sets of values are as similar as possible and that the sets differ as much as possible from the sets of other classes (such as a faulty system). In the classification phase, the feature vectors are placed in one or several classes using template matching, distance calculations or neural networks.

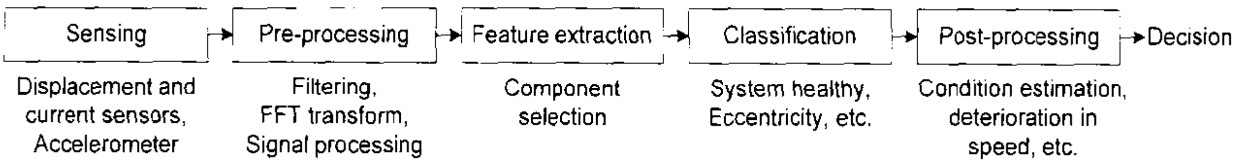

Figure 4.6: Phases of the pattern recognition system.

4.6. CONCLUSION

This chapter provided background information on fault detection techniques. An overview of the techniques currently available and an explanation of the techniques used in this research were provided.

In appendix E the three historical fault datasets (subsynchronous vibration force, rotor synchronous vibration force and supersynchronous vibration force) are compared with the fault detection techniques. The features obtained from the fault detection techniques are divided into good features, better features and measurable features. Measurable features are features which provided the best results for the specific fault condition.

For the subsynchronous vibration force data the measurable frequency features were obtained from the ESDFT, WVD and autocorrelation function. For the rotor synchronous vibration force data the measurable frequency features were obtained from the WVD, autocorrelation function and spectral correlation density function. For the supersynchronous vibration force data the measurable frequency features were obtained from the Cepstrum analysis, HFRT and WVD.

Measurable amplitude features for the subsynchronous, rotor synchronous and supersynchronous vibration force data were obtained from the RMS, mean, minimum, maximum, standard deviation and variance. More detail on the results of the fault detection techniques on the historical fault data of the 250 kW water cooling AMB pump is available in appendix E.

It was therefore decided to incorporate the WVD as a measurable frequency feature and the minimum and maximum as measurable amplitude features in the design of the three real-time schemes. Data collection, pattern recognition, pattern construction and fuzzy logic were used as additional techniques in the design process. More detail on the design of the three real-time schemes is available in chapters 5, 6 and 7.

CHAPTER 5

DESIGN OF THE REAL-TIME DISPLACEMENT ANALYSIS, CORRECTION AND IDENTIFICATION SCHEME

5.1. INTRODUCTION

This chapter focuses on the design of the real-time displacement analysis, correction and identification scheme. As mentioned in chapter 1, the design of the real-time scheme in this chapter is the first of three real-time detection, diagnosis, correction and identification schemes.

The process in which the machine components are regularly checked and the condition i.e., whether it is healthy or faulty, is checked on the basis of vibration signals obtained from the machine components, is called vibration based condition monitoring. Vibration monitoring on AMB systems can be broadly carried out at three levels [95]: 1) Overall vibration level measurement, to detect that a problem exists, 2) spectral or frequency analysis, to locate where the problem exists in the machine and 3) special techniques, which indicate what the problem is at a more detailed level.

There are many different vibration analysis based methods which are used to detect faults. An overview of the most important classical time-invariant techniques is given in [129]. Vibration data from a faulty system exhibits different non-linear and transient events and the analysis of such events requires specific techniques which go beyond the classical Fourier approach. For the application of this study the Wigner-Ville distribution (WVD) was used for diagnosis purposes.

AMB systems are ideally suited for condition monitoring, diagnosis and correction purposes, since the bearing system is already equipped with sensors and actuators. These sensors and actuators provide the exact displacement and current during machine operation.

Two AMB systems have been used in the design process of the on-line AMB fault detection and correction scheme. The one was a fully suspended 250 kW water cooling AMB pump from which historical fault data was captured and the other was an experimental double radial AMB test rack. The test rack was used for verification purposes, since it was not possible to implement the detection and correction scheme on the water cooling AMB pump. A diagram of the double radial AMB system can be seen in *figure 5.1*. The physical AMB system comprises a standard 8 pole heteropolar bearing geometry. Table 5.1 provides the specifications of the double radial AMB.

A photo of the double radial AMB test rack can be seen in appendix A. The fault diagnosis and correction scheme was implemented on this AMB system.

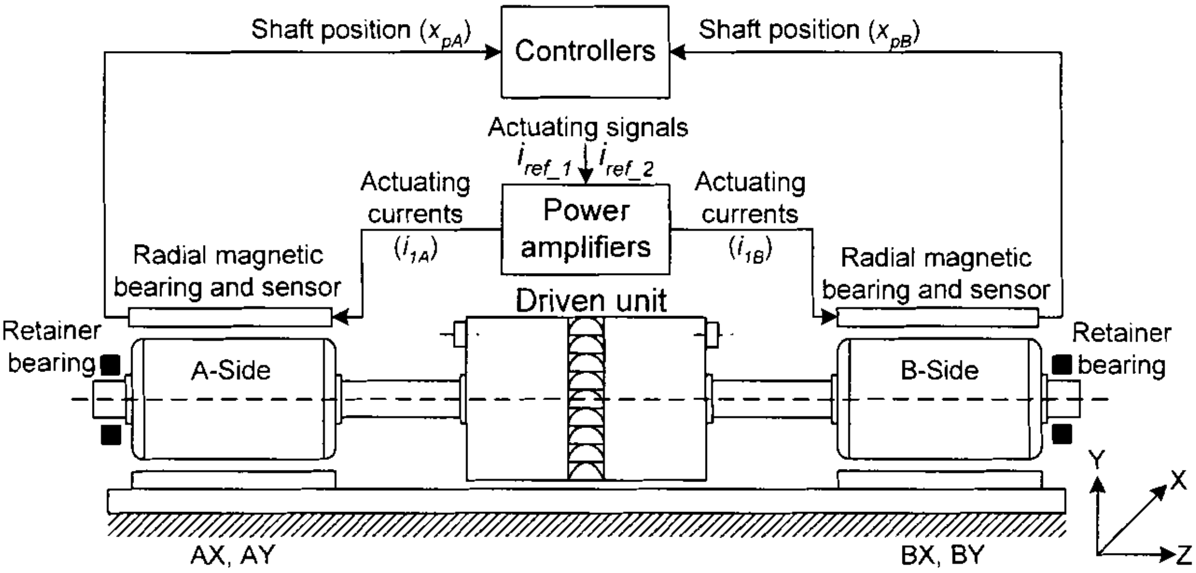

Figure 5.1: Double radial AMB system

Condition monitoring was performed on the water cooling AMB pump for a period of 3 years, in order to obtain historical fault data. With the historical fault data of the water cooling AMB pump it was possible to calculate the exact vibration force and induce it on the double radial AMB test rack. Various fault detection techniques have been implemented on the data to obtain features for fault detection. These features are used as inputs to the on-line correction scheme.

There are two ways to perform diagnosis on AMB systems. The first is a signal-based approach, which relies on the analysis of the displacement and current signals and the last is a model-based approach which utilizes a mathematical model of the AMB system [37], [44], [63]. In order to develop the on-line diagnosis and correction scheme, a combination of signal-based analysis and model-based analysis was performed.

Table 5.1: Specifications of the double radial AMB system

PARAMETER	SPECIFICATION	UNIT	DESCRIPTION
F_{max}	500	N	Maximum load capacity
x_{pn}	0.6	mm	Nominal air gap
i_0	3	A	Bias current
i_1	10	A	Peak current
k_{eq}	500	N/mm	Equivalent stiffness
b_{eq}	2.5	N.s/mm	Equivalent damping
m_{rotor}	14	kg	Mass of rotor
$m_{unbalance}$	7.643×10^{-3}	kg	Unbalance mass of the rotor
ω_n	188.98	rad/sec	Natural frequency

The first step in the design process of the on-line diagnosis and correction scheme was to evaluate the vibration forces that occurred in the 250 kW water cooling AMB pump and develop a scheme capable of detecting these vibration forces. The second step was to diagnose the vibration forces and extract features. The last step was to use the features to correct the AMB system. This process is detailed in section 5.3.

Discrete sampling of the displacement and current signals of the physical AMB system was done by means of the dSPACE® 1104 controller board, equipped with a DSP TMS320F240 from Texas Instruments.

A diagram of the fully suspended 250 kW water cooling AMB pump can be seen in figure 5.2 and a photo of the practical AMB system in appendix A. Due to technical aspects it was not possible to make any changes to this AMB system. Table 5.2 provides the specifications of the water cooling AMB pump.

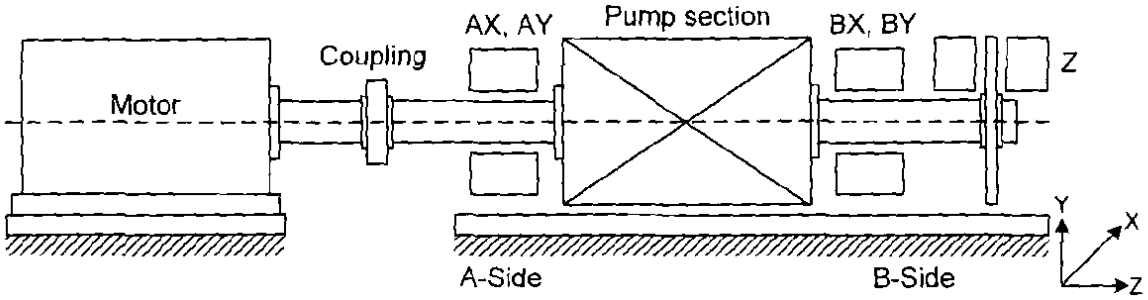

Figure 5.2: Water cooling AMB pump

Table 5.2: Specifications of the water cooling AMB pump

PARAMETER	SPECIFICATION AXIAL	 RADIAL	UNIT	DESCRIPTION
F	12000	7500	N	Load capacity
x_{pn}	0.8	0.4	mm	Nominal air gap
i_0	6	6	A	Bias current
i_1	15	15	A	Peak current

The scheme presented in this chapter attempts to identify and compensate harmonic sources, which are not necessarily synchronous with the rotor spin rate. The identification and compensation subsystems focus on persistent harmonic excitations on the rotor of the AMB system. The compensation subsystem was designed to compensate for vibration forces occurring on the rotor of the AMB system in real-time. Detail on the classification of the vibration forces on the rotor of the AMB system can be found in section 5.2.

The identification subsystem was designed to provide the following output: 1) type of vibration force (unbalance, misalignment, foundation looseness or as otherwise specified in the historical fault database), 2) vibration force fit to a specific dataset, 3) vibration force side (A-side or B-side), 4) vibration force axes (x or y), 5) current state of the rotor (good condition, fault in system or system critical), 6) vibration force parameters (A, B, C and D) and 7) day and time of the vibration force. Detail on the identification subsystem can be found in section 5.5.

This chapter begins with identifying and categorising the vibration forces that occur on the rotor of the AMB system. The identification of the fault detection techniques is discussed in chapter 4. An overview of the diagnosis and correction subsystem is then provided, followed by the design of the simulation and practical AMB models. Under the diagnosis and correction subsystem heading, the design of the fault (vibration force) detection subsystem, subsynchronous vibration force diagnosis subsystem, rotor synchronous and supersynchronous vibration force diagnosis subsystem and error correction subsystem are provided. An overview of the hardware setup is then provided, followed by the design of the identification subsystem. The chapter concludes with a comparison between the simulation and experimental results.

5.2. VIBRATION FORCES ON THE ROTOR OF THE AMB SYSTEM

The following section provides an overview of the vibration forces on the rotor of the 250 kW water cooling AMB pump. Historical fault data have been captured by performing condition monitoring on the displacement signals of the water cooling AMB pump over a period of 3 years. Error signals were then calculated for each of the historical data sets and the signals were used as input to the simulation and practical AMB models (see section 5.3.2) to induce the same faults that occurred on the water cooling AMB pump on the double radial AMB test rack.

It became evident from the historical fault data of the 250 kW water cooling AMB pump that vibration forces can be categorised into the following three vibration force categories: 1) subsynchronous, 2) rotor synchronous and 3) supersynchronous. Subsynchronous refers to vibration forces with frequencies lower than the rotational speed frequency of the rotor, rotor synchronous refers to frequencies very close to the rotational speed frequency and supersynchronous refers to frequencies higher than the rotational speed frequency (ω) of the rotor. Normal vibration level refer to a vibration level where the vibration forces are within the safety specifications of the AMB system and faults on the AMB system refer to vibration forces that cause an alarm to trip or cause damage to the AMB system.

5.2.1 HISTORICAL FAULT DATASET 1: SUBSYNCHRONOUS VIBRATION FORCES

Subsynchronous vibration induced in the 250 kW water cooling AMB pump by motion of nearby machinery cannot be described as a fault, if the vibration doesn't cause an alarm to trip or actual failure of the AMB system. All the subsynchronous vibration data from the historical fault database of the 250 kW water cooling AMB pump caused an alarm to trip and in some cases caused damage to the AMB system. When therefore referring to subsynchronous vibration of nearby machinery, the author refers to subsynchronous vibration that will cause an alarm to trip or has caused an alarm to trip. Vibration forces causing subsynchronous vibrations on the rotor of the 250 kW water cooling AMB pump occurred due to external vibrations from machines running at low rotational speeds in the vicinity.

5.2.2 HISTORICAL FAULT DATASET 2: ROTOR SYNCHRONOUS VIBRATION FORCES

Rotor synchronous vibration forces on the rotor of the 250 kW water cooling AMB pump occurred due to temperature growth of the machine structure, shifting of the relative position of components after assembly and the coupling face not being perpendicular to the shaft axis. Further vibrations in this dataset occurred due to excessive force of the water against the pump blades, during extreme valve opening and closing. The faults (vibration forces) in this dataset were either characterised as coupling misalignments or as rotor unbalances. When referring to faults, the author refers to vibration forces that will cause damage to the AMB system or have caused damage to the AMB system.

5.2.3 HISTORICAL FAULT DATASET 3: SUPERSYNCHRONOUS VIBRATION FORCES

Supersynchronous vibration forces on the rotor of the 250 kW water cooling AMB pump occurred due to loose bolts on the motor side, which caused vibration forces in the motor that were carried onto the shaft of the AMB pump. A diagram of the water cooling AMB pump and pump specifications can be seen in figure 5.2 and table 5.2, respectively.

Further vibrations on the rotor of the water cooling AMB pump occurred due to external vibrations from machines running at high rotational speeds in the vicinity. The faults (vibration forces) in this dataset were characterised as foundation looseness faults. When referring to foundation looseness faults the author refer to vibration forces that caused an alarm to trip or caused damage to the AMB system. Foundation looseness or motion of the system base can occur in various applications and environments. External vibration sources (e.g. other machines) and accidental impacts or explosions may cause base motion [94].

5.3. DIAGNOSIS AND CORRECTION SCHEME

5.3.1. OVERVIEW

Figure 5.3 shows an illustration of the vibration force detection process. At start up the AMB system is suspended with only PID controllers and rotated at the desired speed of 1000 rpm. Displacement masking and boundaries calculation are performed during this initial period when no vibration forces are occurring on the AMB system. The masked displacement and boundaries are stored to memory.

When a vibration force occurs on the rotor, the scheme detects the fault (vibration force), calculates the vibration error and calculates the frequency. The stored no fault (no vibration) displacement is used to calculate the vibration error. When the frequency of the vibration force is lower than the rotational speed of the rotor, then the subsynchronous diagnosis and correction subsystem forces the PID controller to overcompensate for the vibration error. When the vibration force frequency is higher than the rotational speed frequency of the rotor, the rotor synchronous and supersynchronous diagnosis and correction subsystem induces correction currents onto the rotor.

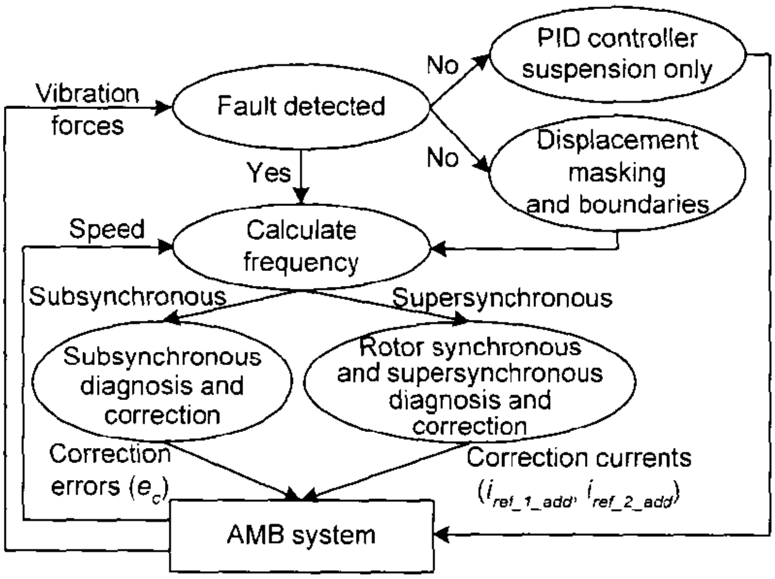

Figure 5.3: Illustration of the vibration force detection process.

Figure 5.4 shows the rotor view of the vibration and correction forces where the PID controller fails to correct the vibration force on the rotating rotor. The vibration force causes the rotor to move downward on the A-side and without immediate correction the rotor will crash against the retainer bearings. This chapter focuses on the real-time detection and correction of these vibration forces.

Correction forces are applied on the rotor by increasing or decreasing the reference currents i_{ref_1} and i_{ref_2} according to the direction of the vibration force. The exact magnitude, frequency, phase and offset in the vibration force need to be calculated before a correction force can be applied. The historical fault data (detailed in section 5.2) from the water cooling AMB pump are used to induce vibration forces on the double radial AMB test rack. This process is explained in detail in section 5.3.2.

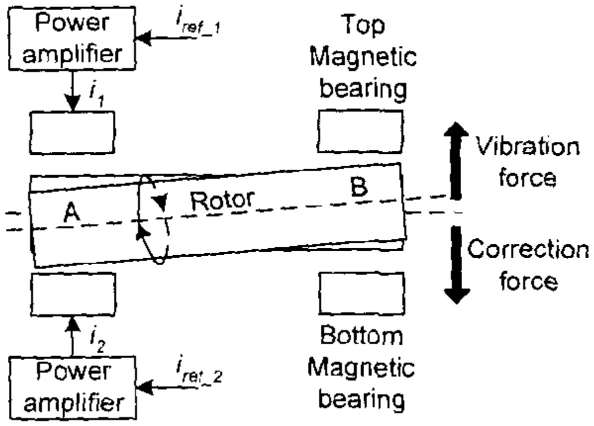

Figure 5.4: Illustration of the vibration and correction forces of the rotor of the AMB system.

Figure 5.5 provides an overview of the detection, diagnosis and correction scheme that was implemented on the double radial AMB test rack. The fault detection subsystem detects the induced vibration forces on the AMB system and calculates the displacement error (e). The fault detection subsystem is explained in detail in section 5.3.3.

The magnitude, frequency, phase and offset of the vibration force on the rotor is contained in both the displacement (x_p) and currents (i_1 and i_2) of the AMB system. For this scheme the displacement was used to calculate the error. After a fault has been detected, the error signal (e) is sent to the fault diagnosis and feature extraction subsystems. The fault diagnosis subsystems are explained in detail in sections 5.3.5 and 5.3.6.

The error correction subsystem uses these features to force the PID controller to overcompensate for the displacement error (during subsynchronous vibration forces) and stabilises the rotor by inducing correction forces on the rotor (during supersynchronous vibration forces).

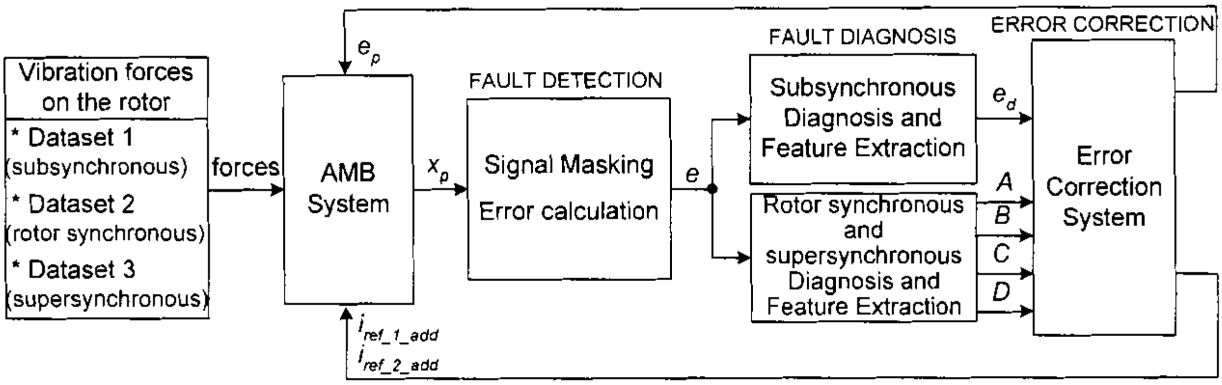

Figure 5.5: Overview of the detection, diagnosis and correction scheme

The displacement error (e_d) is used for subsynchronous vibration force correction and the extracted fault features: Amplitude (A), frequency (B), phase (C) and offset (D) are used for supersynchronous vibration force correction. The error correction subsystem is explained in detail in section 5.3.7. The parameter e_p represents the position correction error and $i_{ref\_1\_add}$ and $i_{ref\_2\_add}$ the correction reference currents for the top and bottom magnetic bearings, respectively.

The fault diagnosis section is divided into subsynchronous and rotor synchronous and supersynchronous vibration force diagnosis, since the error made on the fault feature B was too great during the subsynchronous vibration force diagnosis test. The reason for this was that too much time was needed to complete one cycle of the fault, during subsynchronous vibration forces.

The fault detection techniques need at least one cycle of the fault signal to calculate the exact frequency. The time necessary to calculate the exact frequency during supersynchronous vibration forces was sufficient. A different method of analysing the subsynchronous vibration forces therefore had to be developed, and it was decided to correct subsynchronous vibration forces by forcing the PID controller to overcompensate for the faults (vibration forces) occurring. The rest of this section details the function of each of the blocks in figure 5.5.

5.3.2. SIMULATION AND PRACTICAL AMB MODELS

A simulation model of the AMB system was necessary to observe how the practical system will respond to faults (vibration forces), when the diagnosis and correction subsystem is implemented. The simulation (dashed and solid lines) and practical (solid lines) models of the double radial AMB system with rotational rotor faults are shown in figure 5.6.

The actual position (x_p) is subtracted from the reference position to provide the position error (e_p). This is fed to a PID controller which together with the bias current (i_0) provides the reference currents (i_{ref_1} and i_{ref_2}) for the power amplifiers. The forces (f_1 and f_2) are calculated with $(K_m \cdot i_1^2)/x_p^2$ and $(K_m \cdot i_2^2)/(g_t)^2$, where K_m is the constant of the magnetic bearing and g_t is the total air gap. The position (x_p) is obtained by double integrating the forces and dividing the answer with the mass of the rotor (m).

For the simulation model, the vibration force (f_4) on the rotor was induced by subtracting the position error (e_p) from the reference error index ($e_{ref} sin(\omega_2 t)$) and feeding this to a controller. The reference error (e_{ref}) represents the error calculated from the historical fault data (detailed in section 2) of the water cooling AMB pump and the index ($sin(\omega_2 t)$) represents the carrier of the AMB pump.

The output of the controller is then added as a reference force (f_4) and the connection to add a reference current fault (i_f) to the reference current (i_{ref}) is disconnected. The carrier force ($f_3(\omega_1 t)$) of the double radial AMB was kept constant and the vibration force (f_4) was stored to file. The stored file now contains both the carriers of the water cooling AMB pump and the double radial AMB test rack. The file was then demodulated to subtract the carrier of the water cooling AMB pump and the remainder was used to simulate vibration forces on the rotor. These vibration forces (f_4) are synchronously placed on the carrier of the double radial AMB test rack.

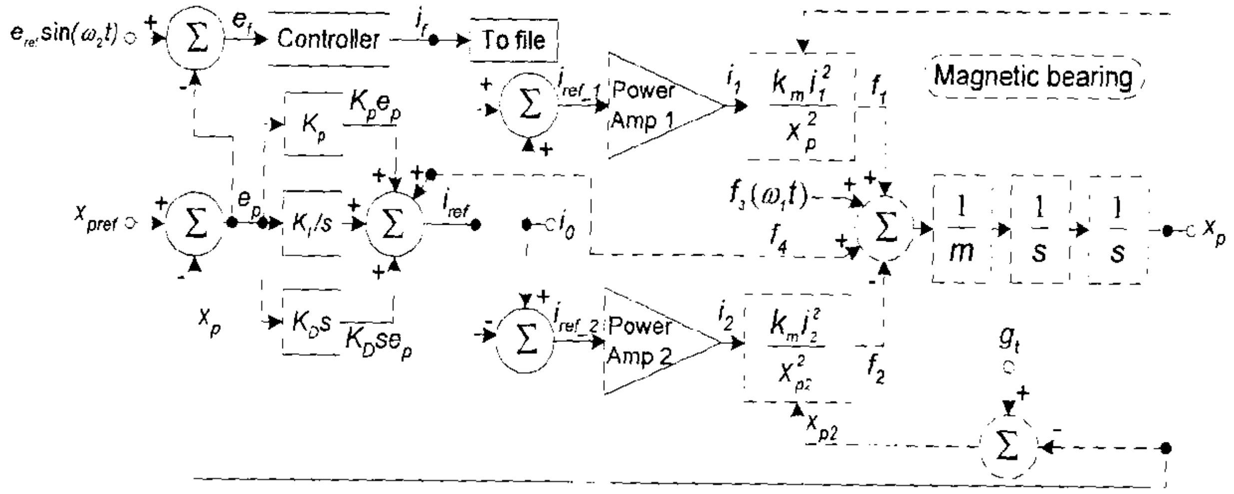

Figure 5.6: Simulation (dashed and solid lines) and practical (solid lines) AMB models with rotational rotor faults

For the practical AMB system the connection to add a reference current fault (i_f) to the reference current (i_{ref}) is restored and the vibration force (f_4) is disconnected. The reference current fault (i_f) is then stored to file, during the controlling process of the rotating double radial AMB test rack. The file is demodulated to subtract the carrier of the water cooling AMB pump and the remainder is used as reference current faults to induce vibration forces on the rotor. These reference current faults (i_f) are synchronously placed on the carrier of the double radial AMB test rack. The calculation of the spring-mass-damper constants can be found in appendix D.

5.3.3. FAULT DETECTION SUBSYSTEM

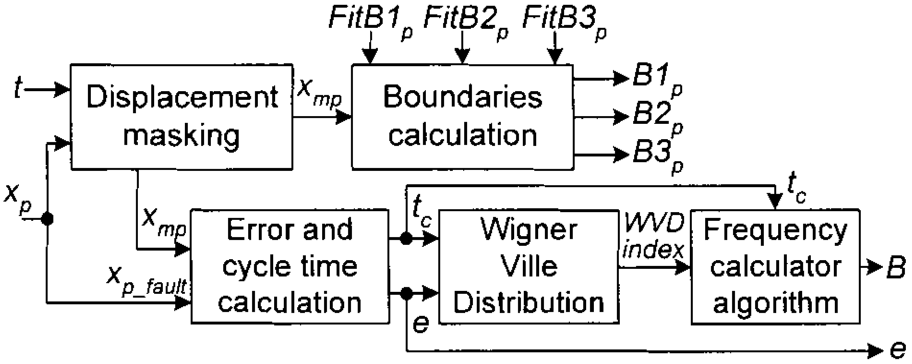

Figure 5.7: Fault detection subsystem

The fault detection subsystem constitutes displacement masking, error calculation, boundary calculation and frequency calculation, as shown in figure 5.7. Displacement masking is performed by capturing one cycle of the displacement signal under no fault (no vibration) condition and fitting a sine wave to it.

The sine wave representation of the no fault displacement (x_{mp}) is stored to memory. When a fault occurs in the AMB system, the displacement (x_p) is called the fault displacement (x_{p_fault}). The no fault displacement (x_{mp}) is subtracted from the fault displacement (x_{p_fault}) to provide the error (e).

The frequency (B) is calculated by using the WVD and a frequency calculator algorithm. The accuracy of the frequency was improved by sampling the WVD at twice the cycle time (t_c) of the error signal (e). The WVD is calculated from the displacement error (e) and the peaks P_1 and P_2 are calculated from the positive peaks of the WVD as shown in figure 5.8.

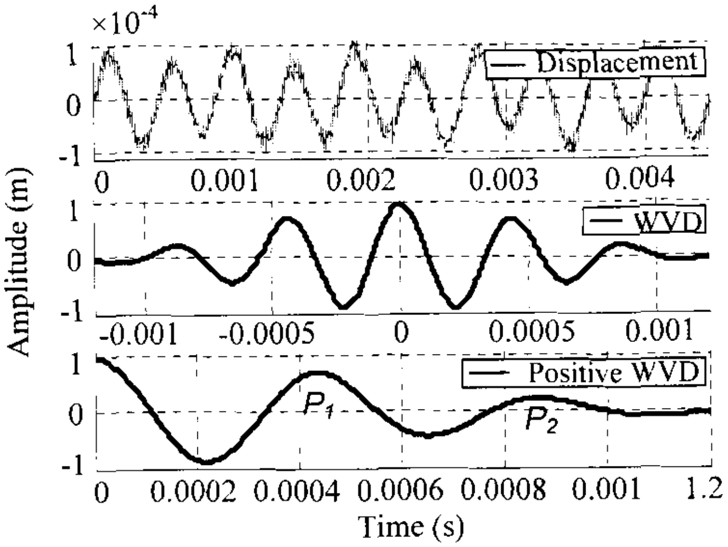

Figure 5.8: Frequency calculation with the WVD

From peak P_1 the frequency of the fault was calculated at 2277.9 Hz. This frequency calculation is only to illustrate the WVD process and is not a representation of the data obtained from the 250 kW water cooling AMB pump. It can be seen from (5.1) that the second peak (P_2) is a multiple of the first peak. The value calculated in this equation provides an estimate of the error factor on the first peak (P_1). In this case the frequency calculated has 99.77 % accuracy.

$$\frac{P_2}{P_1} = \frac{8.8\times10^{-4}}{4.39\times10^{-4}} = 2.0046 \tag{5.1}$$

The WVD provides only an estimate of the frequency during subsynchronous vibration force analysis, but the precise frequency during supersynchronous vibration force analysis.

Three boundaries $B1_p$ to $B3_p$ was chosen for the double radial AMB system. Boundary $B1_p$ operates as a fault indicator, $B2_p$ operates as the system critical state and $B3_p$ operates as the system shutdown state. An orbital representation of the displacements (x_p and y_p) with the three boundaries ($B1_p$, $B2_p$ and $B3_p$) can be seen in figure 5.9.

Table 5.3 provides the calculations for the displacement boundaries ($B1_p$, $B2_p$ and $B3_p$). In this table the three boundaries of the double radial AMB are calculated by fitting the no fault displacements of the double radial AMB with fitting factors ($FitB1_p$, $FitB2p$ and $FitB3_p$). The fitting factors are calculated by (5.3).

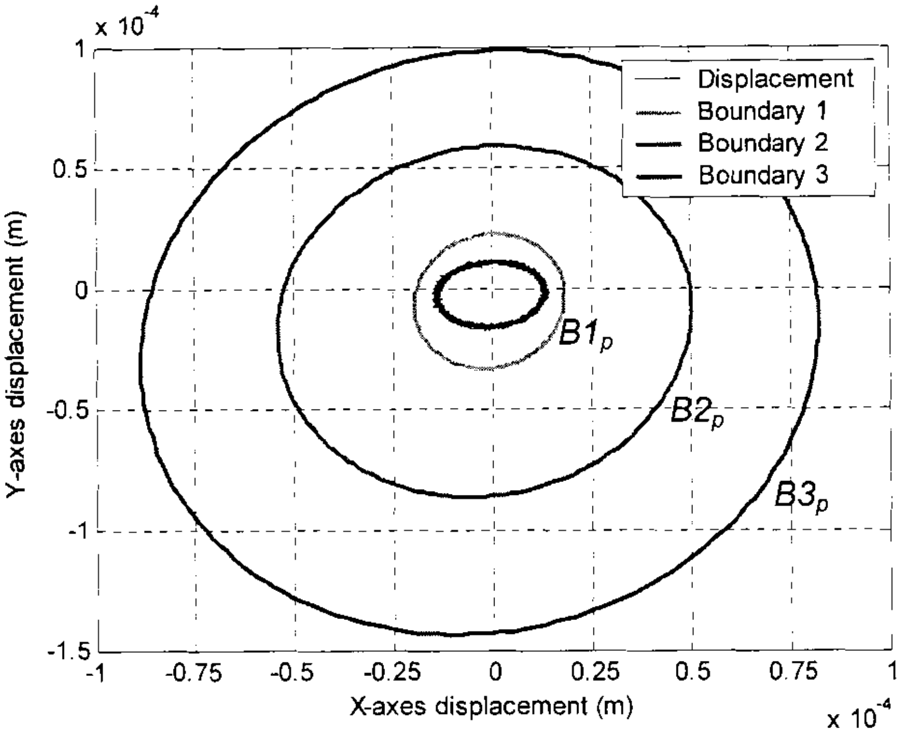

Figure 5.9: Orbital representation of the displacement boundaries

The average maximum fault (obtained from the maximums of the subsynchronous, rotor synchronous and supersynchronous vibration force datasets) is calculated as follows:

$$Avg_{max\_fault} = \frac{Max_{low\_freq} + Max_{medium\_freq} + Max_{high\_freq}}{3} \tag{5.2}$$

where Avg_{max_fault} refers to the average maximum fault dataset, Max_{low_freq} to the maximum displacement of all the faults in the subsynchronous vibration force dataset, Max_{medium_freq} to the maximum displacement of all the faults in the rotor synchronous vibration force dataset and Max_{high_freq} to the maximum displacement of all the faults in the supersynchronous vibration force dataset.

The fitting factor for $FitB1_p$, $FitB2p$ and $FitB3_p$ are calculated as follows:

$$Fit_{Boundary} = \frac{Avg_{max\_fault} \cdot xpn_{double\_radial} \cdot fit\_\%}{No\_fault_{water} \cdot xpn_{water}} \tag{5.3}$$

where $Fit_{Boundary}$ refers to the boundary fitting factor, No_fault_{water} to the no fault displacement of the water cooling AMB pump, xpn_{water} to the nominal air gap of the water cooling AMB pump, xpn_{double_radial} to the nominal air gap of the double radial AMB and $fit\_\%$ to the percentage fitting factor.

The boundaries $B1_p$, $B2_p$ and $B3_p$ are calculated as follows:

$$Boundary = Fit_{Boundary} \cdot No\_fault_{double\_radial} \tag{5.4}$$

where $Boundary$ refers to the boundary of the double radial AMB and $No\_fault_{double\_radial}$ to the no fault displacement of the double radial AMB.

The actual x-axis displacement (x_p) is calculated from the average of the maximum negative displacement (x_{pmin}) and the maximum positive displacement (x_{pmax}). The same rule applies for the y-axis displacement (y_p).

Table 5.3: Calculation of the displacement boundaries

	x_{pmax} (μm)	x_{pmin} (μm)	x_p (μm)	y_{pmax} (μm)	y_{pmin} (μm)	y_p (μm)
NO FAULT (WATER COOLING AMB PUMP)	35	-38	36.5	38	-41	39.5
NO FAULT (1000 rpm – DOUBLE RADIAL AMB)	13	-14	13.5	12	-15	13.5
MAX SUBSYNCHRONOUS VIBRATION FORCE DATASET	84.80	-101.00	92.9	259.13	-252.63	255.88
MAX ROTOR SYNCHRONOUS VIBRATION FORCE DATASET	91.95	-71.91	81.53	238.25	-224.07	231.16
MAX SUPERSYNCHRONOUS VIBRATION FORCE DATASET	78.05	-85.12	81.59	225.75	-212.19	218.97
AVERAGE MAXIMUM FAULT	84.93	-86.01	85.47	235.75	-229.63	232.69
FITTING FACTOR: $FitB1_p$ (20 %)	1.456	1.358	1.407	1.861	1.680	1.771
FITTING FACTOR: $FitB2_p$ (55 %)	4.004	3.735	3.870	5.118	4.621	4.870
FITTING FACTOR: $FitB3_p$ (90 %)	6.552	6.111	6.332	8.375	7.561	7.968
BOUNDARY $B1_p$ (1000 rpm – DOUBLE RADIAL AMB)	18.928	-19.010	18.969	22.334	-25.203	23.769
BOUNDARY $B2_p$ (1000 rpm – DOUBLE RADIAL AMB)	52.052	-52.290	52.171	61.419	-69.309	65.364
BOUNDARY $B3_p$ (1000 rpm – DOUBLE RADIAL AMB)	85.176	-85.554	85.365	100.504	-113.415	106.960

The fitting factors ($FitB1_p$, $FitB2p$ and $FitB3_p$) are calculated at 20 % for $B1_p$, 55 % for $B2_p$ and 90 % for $B3_p$ of the average maximum fault. Tables 5.1 and 5.2 provide the specifications on each of the AMB systems. The boundaries $B2_p$ and $B3_p$ are discussed in detail in section 5.5. The results on the techniques for fault detection can be found in appendix E.

5.3.4. RESPONSE CALCULATIONS FOR THE DIAGNOSIS SUBSYSTEMS

From table 5.3 it can be seen that boundary $B1_p$ is calculated only for the ideal condition where the rotor is rotating at 1000 rpm. Since the rotor speed (N) may vary, the actual speed is used as parameter in the calculation of boundary $B1_p$. For this purpose the spring, mass and damper system of figure 5.10 (a) will be used. The parameters in this section are defined in table 5.1.

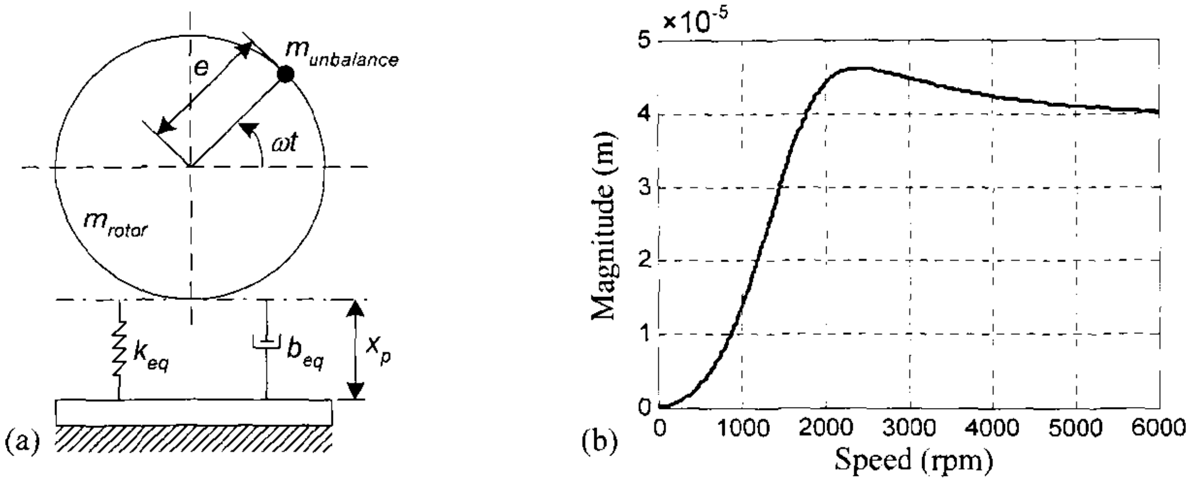

Figure 5.10: (a) Spring, mass and damper system (b) response with speed (N) variation

The equation of motion for the system in figure 5.10 (a) is given by:

$$-k_{eq}x_p - b_{eq}\dot{x}_p = (m_{rotor} - m_{unbalance})\frac{d^2x_p}{dt^2} + m_{unbalance}\frac{d^2}{dt^2}(x_p + e\sin\omega t)$$

$$-k_{eq}x_p - b_{eq}\dot{x}_p = m_{rotor}\ddot{x}_p - m_{unbalance}\ddot{x}_p + m_{unbalance}\ddot{x}_p + m_{unbalance}\left(-\omega^2 e\sin\omega t\right)$$

$$m_{rotor}\ddot{x}_p + b_{eq}\dot{x}_p + k_{eq}x_p = m_{unbalance}\omega^2 e\sin\omega t \tag{5.5}$$

The response of the system is given by $x_p = X_0\sin(\omega t - \phi)$, where

$$X_0 = \frac{\omega_n^2 m_{unbalance}\omega^2 e/k_{eq}}{\sqrt{(\omega_n^2 - \omega^2)^2 + (2\zeta\omega_n\omega)^2}} = \frac{m_{unbalance}\cdot e\cdot r^2}{m_{rotor}\cdot\sqrt{(1-r^2)^2 + (2\cdot\zeta\cdot r)^2}} \tag{5.6}$$

and

$$\zeta = \frac{b_{eq}}{2\cdot\sqrt{k_{eq}\cdot m_{rotor}}},\ r = \frac{\omega}{\omega_n}\ \text{and}\ \omega = \frac{2\pi\cdot N}{60} \tag{5.7}$$

When the rotational speed (N) of the rotor increases the magnitude (X_0) also increases, which causes an increase in the amplitude of the boundary ($B1_p$). The response of the system with variation in speed can be seen in figure 5.10 (b). For the calculations of this section, the eccentricity (e) was taken as the radius of the rotor (shown in figure 5.10 (a)) and the unbalance mass ($m_{unbalance}$) was calculated by reverse engineering (5.5) and using practical measurements of the displacement (x_p) at various rotational speed (N).

5.3.5. SUBSYNCHRONOUS VIBRATION FORCE DIAGNOSIS SUBSYSTEM

Figure 5.11 provides a diagram of the subsynchronous vibration force diagnosis subsystem, which focuses on the diagnosis of vibration forces with frequencies lower than the rotational speed frequency of the rotor. The boundary error (e_B) is calculated by subtracting the actual displacement (x_p) of the rotor from displacement boundary 1 ($B1_p$). The amplitude of the first boundary displacement ($B1_p$) is a function of the rotational speed of the rotor and follows the response shown in figure 5.10 (b).

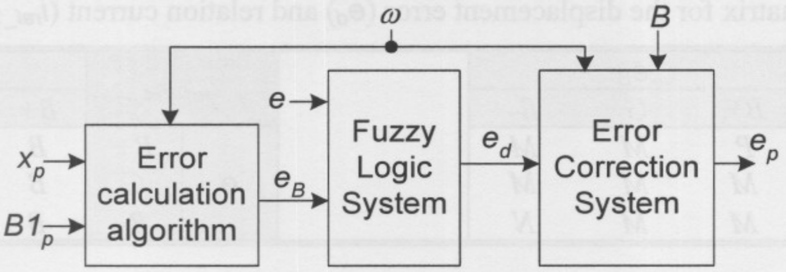

Figure 5.11: Subsynchronous vibration force diagnosis subsystem

The displacement error (e_d) is obtained from a fuzzy logic system with displacement error (e) and boundary error (e_B) as inputs. The fuzzy surface plot used to calculate e_d is shown in figure 5.13. The displacement error (e_d) is passed onto the error correction subsystem. The error correction subsystem uses the frequency (B) to distinguish the fault (vibration force) as a subsynchronous or supersynchronous vibration force. The correction is performed when the vibration force frequency is lower than the rotational speed frequency (ω) of the rotor.

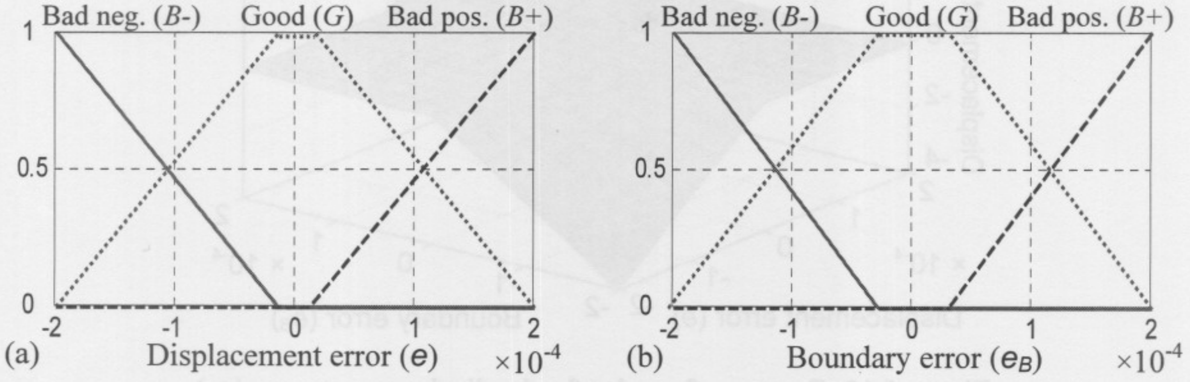

Figure 5.12: Fuzzy membership functions for the (a) displacement error and (b) boundary error

Figure 5.12 provides the fuzzy membership functions for the displacement error (e) and the boundary error (e_B). Fuzzification is performed by using the overlapping fuzzy sets bad negative (*B*-), good (*G*) and bad positive (*B*+).

The detection, diagnosis a correction scheme is an extremely complex scheme which is inherently fuzzy. A fuzzy logic controller was used, because it has the ability to incorporate experience, intuition and heuristics to the scheme instead of relying on a mathematical model. The fuzzy control strategies are further embodies by sets of IF-THEN rules. Using a different controlling method could result in a complex mathematical model which might be less effective during real-time implementation.

Table 5.4: Rule matrix for the displacement error (e_d) and relation current (i_{ref_1R})

e_d		e_B		
		B+	*G*	*B-*
e	*B+*	*P*	*M*	*M*
	G	*M*	*M*	*M*
	B-	*M*	*M*	*N*

i_{ref_1R}		e_B		
		B+	*G*	*B-*
e	*B+*	*B*	*B*	*B*
	G	*B*	*M*	*B*
	B-	*B*	*B*	*T*

The basic rule for using the features (e_B and e) is: IF e_B AND e THEN e_d. The same rule applies for the workforce relation current 1 (i_{ref_1R}), which is explained in section 5.3.6. Table 5.4 provides the rule matrix for the displacement error (e) and the relation current (i_{ref_1R}). Defuzzification of the fuzzy membership functions e_d and i_{ref_1R} are performed by using overlapping fuzzy sets negative (*N*), middle (*M*) and positive (*P*) and bottom (*B*), middle (*M*) and top (*T*), respectively.

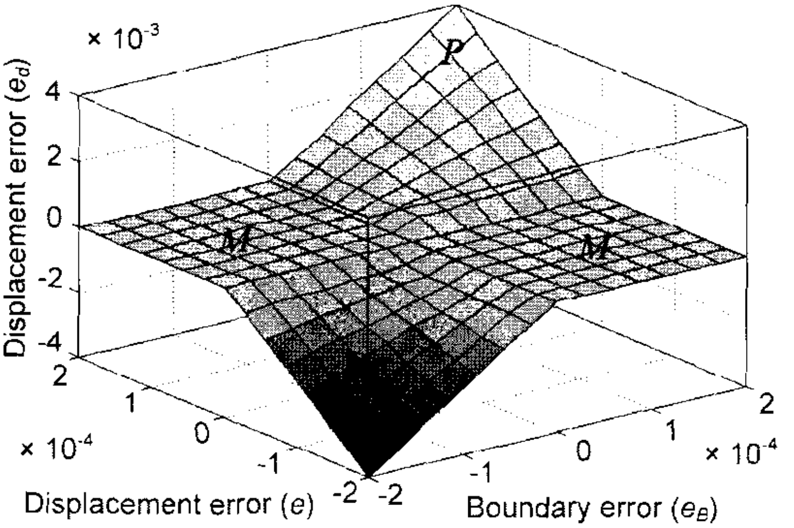

Figure 5.13: Fuzzy surface plot for the displacement error (e_d).

From figure 5.13 it can be seen that the displacement error reaches a maximum when both the displacement error (e) and boundary error (e_B) reach maxima.

5.3.6. ROTOR SYNCHRONOUS AND SUPERSYNCHRONOUS DIAGNOSIS SUBSYSTEM

The features (A, C and D) are calculated with the supersynchronous vibration force diagnosis subsystem, shown in figure 5.14. This subsystem focuses on the diagnosis of vibration forces with frequencies higher than the rotational speed frequency of the rotor. The amplitude (A) and offset (D) are calculated with a fuzzy logic system with minimum and maximum as inputs. The fuzzy surface plots of A and D are shown in figure 5.17 and figure 5.18, respectively. The phase (C) is calculated by trigonometrical functions and a phase calculator algorithm.

When a vibration (disturbance) force causes the rotor to move downward on the A-side as shown in figure 5.4, the current i_1 (and i_{ref_1}) need to be more than the current i_2 (and i_{ref_2}) to stabilise the rotor to the centre position.

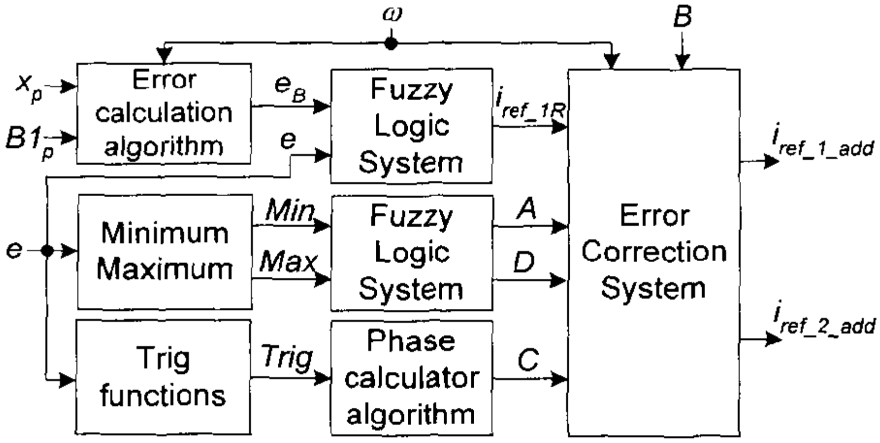

Figure 5.14: Rotor synchronous and supersynchronous vibration force diagnosis subsystem

This relation between the amplitude of the vibration force and amount of current required by each amplifier, are called the workforce relation current and is defined by i_{ref_1R} and i_{ref_2R}. i_{ref_1R} refers to the workforce relation current for the top power amplifier and i_{ref_2R} refer to the workforce relation current for the bottom power amplifier.

The workforce relation current serves as an amplifier (booster) and increases or decreases the amplitude of the correction force according to the error made on the displacement. These increases and decreases at the correct amplifiers, causes faster correction force response times.

Figure 5.15 provides the fuzzy surface plot for the workforce relation current 1 (i_{ref_1R}), with displacement error (e) and boundary error (e_B) as inputs.

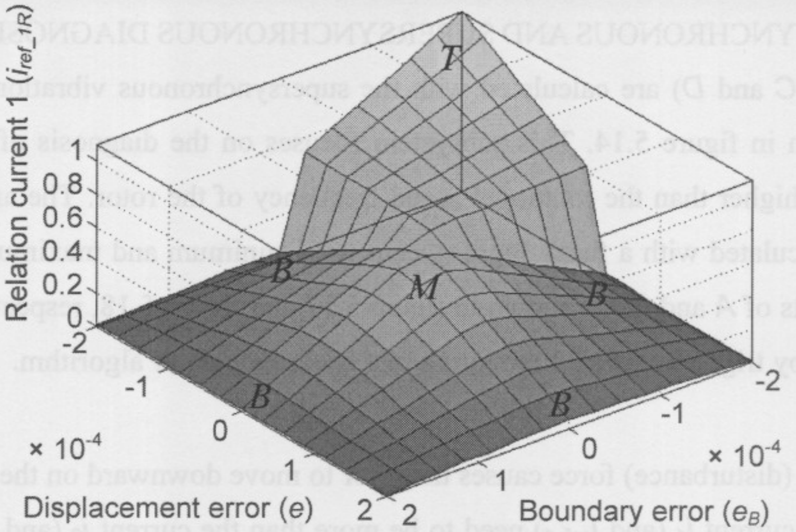

Figure 5.15: Fuzzy surface plot for workforce relation current 1 (i_{ref_1R}).

The workforce relation current 1 (i_{ref_1R}) reaches maximum, when both the displacement error and boundary error reaches maxima. The workforce relation current 2 is calculated as follows:

$$i_{ref\_2R} = 1.0 - i_{ref\_1R} \tag{5.8}$$

The error correction subsystem uses the features *A, B, C, D* and i_{ref_1R} to calculate the correction reference currents $i_{ref\_1\_add}$ and $i_{ref\_2\_add}$ that will be used to induce correction forces on the rotor. The correction reference currents will be added to the AMB controller reference currents. The error correction subsystem uses the frequency (*B*) to distinguish the fault (vibration force) as a subsynchronous or supersynchronous vibration force. The correction is performed when the vibration force frequency is higher than the rotational speed frequency (ω) of the rotor.

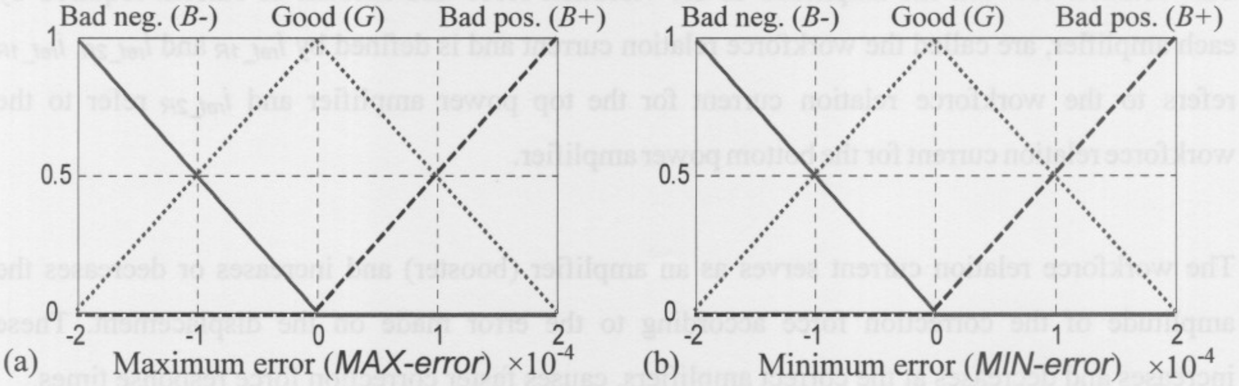

Figure 5.16: Fuzzy membership functions for the (a) maximum error and (b) minimum error

Figure 5.16 provides the fuzzy membership functions for the maximum error (*MAX-error*) and the minimum error (*MIN-error*). *MAX-error* refers to the maximum error over a period of time.

The maximum block identifies the position of the largest element in each column of the displacement error (*e*) over a period of time. *MIN-error* refers to the minimum error over a period of time. The minimum block identifies the position of the smallest element in each column of the displacement error (*e*) over a period of time. Fuzzification is performed by using the overlapping fuzzy sets bad negative (*B-*), good (*G*) and bad positive (*B+*).

Table 5.5: Rule matrix for the amplitude (*A*) and offset (*D*)

A		*MAX-error*		
		B+	*G*	*B-*
MIN-error	*B+*	*S*	*S*	*S*
	G	*VB*	*S*	*S*
	B-	*B*	*VB*	*S*

D		*MAX-error*		
		B+	*G*	*B-*
MIN-error	*B+*	*P*	*M*	*M*
	G	*P*	*M*	*M*
	B-	*M*	*N*	*N*

The basic rule for using the features (*MAX-error* and *MIN-error*) is: IF *MAX-error* AND *MIN-error* THEN *A*. The same rule counts for variable *D*. Table 5.5 provides the rule matrix for the amplitude (*A*) and the offset (*D*). Defuzzification of the fuzzy membership functions *A* and *D* are performed by using overlapping fuzzy sets small (*S*), big (*B*) and very big (*VB*) and negative (*N*), middle (*M*) and positive (*P*), respectively.

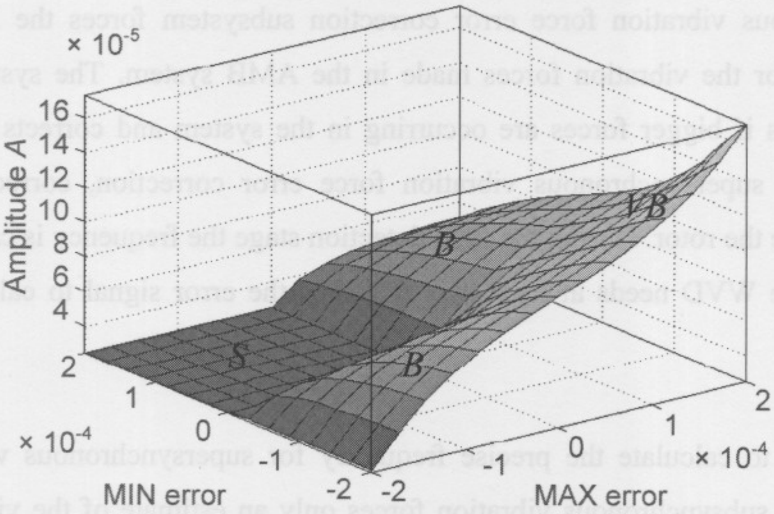

Figure 5.17: Fuzzy surface plot for amplitude *A*

Figure 5.17 shows the fuzzy surface plot for amplitude *A*, with minimum error and maximum error as inputs. Amplitude *A* reaches a maximum, when the maximum error reaches a maximum and the minimum error reaches a minimum.

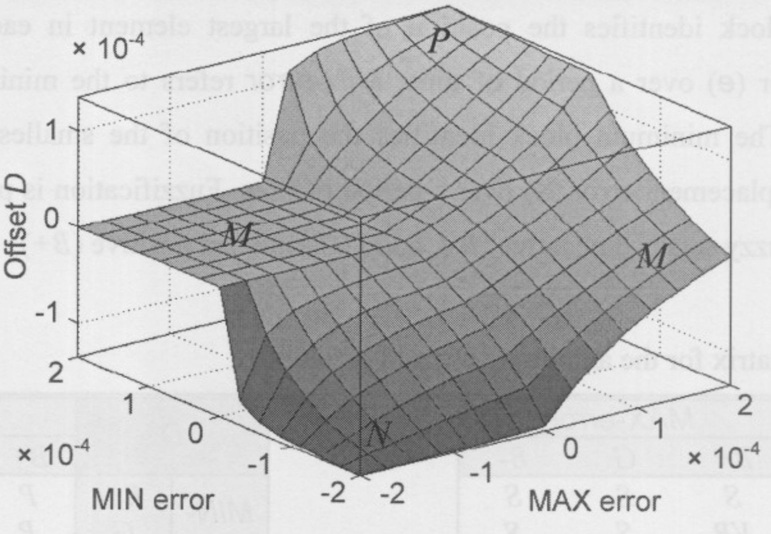

Figure 5.18: Fuzzy surface plot for offset *D*

Figure 5.18 shows the fuzzy surface plot for offset *D*, with minimum error and maximum error as inputs. The offset *D* reaches a maximum when the maximum error and minimum error reach maxima.

5.3.7. ERROR CORRECTION SUBSYSTEM

The subsynchronous vibration force error correction subsystem forces the PID controller to overcompensate for the vibration forces made in the AMB system. The system reacts on the vibration forces as if bigger forces are occurring in the system and corrects or minimises the vibration. During supersynchronous vibration force error correction, correctional forces are applied to stabilise the rotor. During the fault detection stage the frequency is calculated by using the WVD, but the WVD needs at least two cycles of the error signal to calculate the precise frequency.

The time needed to calculate the precise frequency for supersynchronous vibration forces is sufficient, but for subsynchronous vibration forces only an estimate of the vibration frequency can be obtained. The WVD therefore serves as en excellent decision maker between subsynchronous and supersynchronous vibration forces and provides the precise frequency during supersynchronous vibration forces.

During supersynchronous vibration force diagnosis, the fault features (*A*, *B*, *C*, *D*) extracted from the AMB system are subject to system parameters. The measured features therefore need to be fitted with the following equations for them to represent the correcting features:

$$\begin{gathered} A_{Correct} = A_{Measure} \times A_{system} \\ \text{with} \quad A_{system} = 1.667 \times 10^5 \text{ A/m} \end{gathered} \tag{5.9}$$

where $A_{Correct}$ represents the amplitude of the correcting reference current, $A_{Measure}$ represents the amplitude of the measured displacement error obtained from the fuzzy controller and A_{System} represents the fitting amplitude.

A_{system} has a large value, due to the large difference between the measured amplitude of the displacement error and the needed amplitude of the correctional reference current. A_{system} was calculated by adding all the gain components between the displacement (x_p) and the reference currents (i_{ref_1} and i_{ref_2}).

$$B_{Correct} = B_{Measure} \tag{5.10}$$

The frequency of the correctional reference current ($B_{Correct}$) is the same as the frequency of the measured displacement error ($B_{Measure}$).

$$\begin{gathered} C_{Correct} = C_{Measure} + C_{system} \\ \text{with} \quad C_{system} = 2.5 \text{ rad} \end{gathered} \tag{5.11}$$

The phase of the measured displacement error ($C_{Measure}$) need to be shifted, due to phase shifts caused by the integral and derivative components of the PID controller and integration of the AMB model on the measured displacement error. The fitting phase (C_{system}) was calculated by adding the phase shifts caused by the integral and derivative components of the PID controller and phase shift caused by integration of the AMB model.

$$D_{Correct} = D_{Measure} \tag{5.12}$$

The offset of the correctional reference current ($D_{Correct}$) is the same as the offset of the measured displacement error ($D_{Measure}$).

The error correction equation for the top magnetic bearing is given by (5.13) and added to i_{ref_1}.

$$\begin{aligned} i_{ref\_1\_add} &= -i_{ref\_1R} \cdot A_{correct} \sin\left(B_{correct} t + C_{correct}\right) + D_{correct} \\ &= -i_{ref\_1R} \left(1.667 \times 10^5\right) \cdot A_{Measure} \sin\left(B_{Measure} t + \left(C_{Measure} + 2.5\right)\right) + D_{Measure} \end{aligned} \tag{5.13}$$

The error correction equation for the bottom magnetic bearing is given by (5.14) and added to i_{ref_2}.

$$i_{ref\_2\_add} = i_{ref\_2R} \cdot \left(1.667 \times 10^5\right) \cdot A_{Measure} \sin\left(B_{Measure} t + \left(C_{Measure} + 2.5\right)\right) + D_{Measure} \tag{5.14}$$

5.4. HARDWARE SETUP

Discrete sampling of the displacement signals of the physical AMB system was done by means of the dSPACE® 1104 controller board, equipped with a DSP TMS320F240 from Texas Instruments. A user-interface was created in Controldesk® to perform data acquisition on the physical system. The real-time implementation process and hardware setup is detailed in appendix C.

Due to the complexity of the control, detection and correction, the dSPACE® controller was not able to handle all the instructions and real-time errors occurred. This problem was solved by implementing two dSPACE® 1104 controller boards, one for each axis of the magnetic bearing. A roller bearing was installed on the right side of the rotor. This lead to an increase in the sampling time of the DSP, since only one side has to be suspended.

The vibration forces and speed sensor calculations were performed by the left dSPACE® controller and communicated to the other dSPACE® controller by means of D/A and A/D channels. Diagnosis and correction were performed by the right dSPACE® controller. Figure 5.19 shows the hardware setup with the dSPACE® controllers.

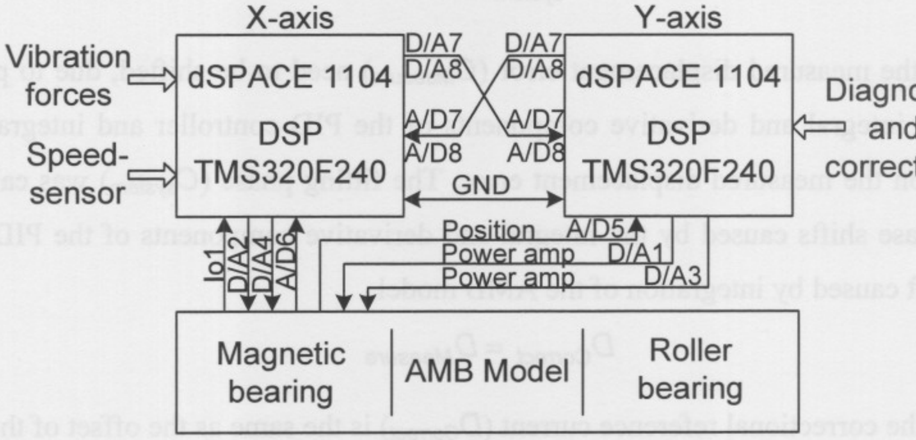

Figure 5.19: Hardware setup with the dSPACE® controllers

During the investigation of the displacement signals of the double radial AMB system, it became evident that synchronous vibrations were introduced by the roller bearing when the rotor was rotating. These vibrations were incorporated in the displacement masking and boundary calculation process of the fault detection subsystem (detailed in section 5.3.3).

Figure 5.20 shows the masked (x_{mp}) and actual displacement (x_p) during the practical implementation phase. The no fault displacement (x_{mp}) is subtracted from the fault displacement (x_{p_fault}) to provide the displacement error (e).

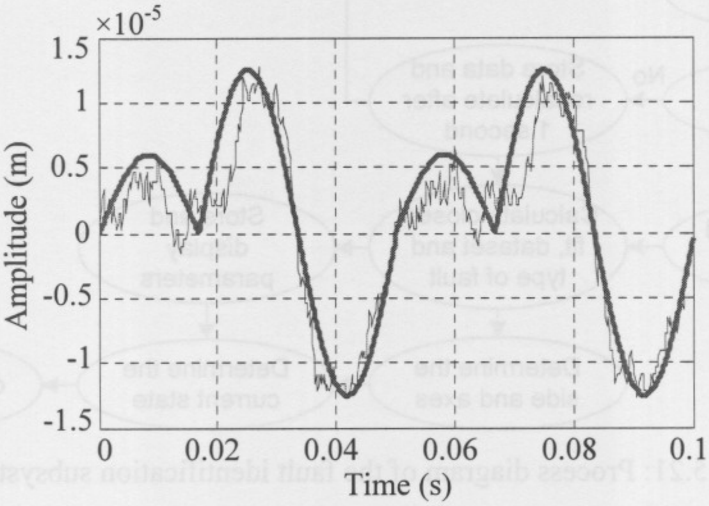

Figure 5.20: Displacement masking during the practical implementation phase

The amplitude (A) and frequency (ω) were used as scaling factors on the masked displacement. When the amplitude (A) of the displacement increased, the amplitudes of the individual signals in the masked displacement also increased and when the frequency (ω) increased (i.e. when the rotor is turning faster) the frequency of the individual signals in the masked displacement also increased.

5.5. FAULT IDENTIFICATION SUBSYSTEM

Figure 5.21 provides the process diagram of the fault identification subsystem. When no fault (no vibration force) is detected (i.e. when the parameters A, B, C and D are zero), the identification subsystem provides no output. When a fault (vibration force) is detected, the subsystem uses the frequency to determine to which dataset (subsynchronous, rotor synchronous or supersynchronous) the fault belongs. The subsystem calculates the best possible fit of the historical fault data in the specific dataset with the data obtained from the practical AMB system.

If the frequency rapidly changes from one dataset to another, the subsystem saves the output, predicts the closest type of fault (unbalance, misalignment, foundation looseness or as specified in the historical fault database) and recalculates the fault in the new dataset. When the frequency stays within a certain dataset, the subsystem is set to repeatedly calculate the average error over a time period of 1 second. The time period was calculated at five times the period of the masked displacement at 1000 rpm. The type of fault is allocated to the fault in the dataset with the smallest error over the available time period.

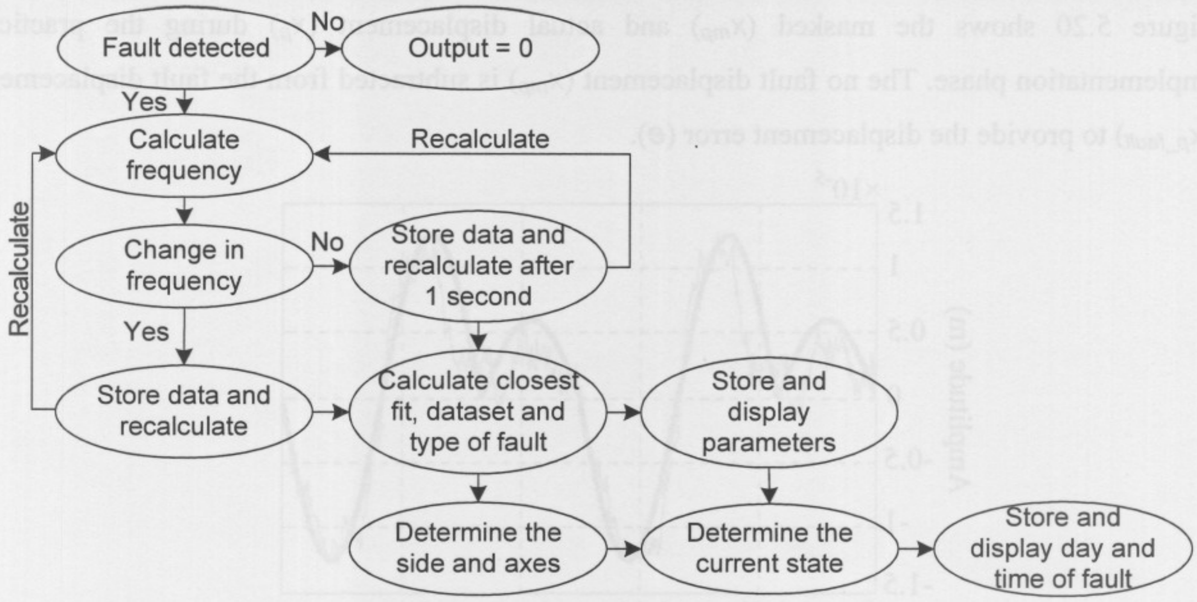

Figure 5.21: Process diagram of the fault identification subsystem

After the type of fault is stored, the subsystem displays the parameters of the fault and determines the current state of the fault. The current state of the fault is calculated from the boundaries ($B1_p$, $B2_p$ and $B3_p$). The subsystem determines the side and axes where the fault occurs from the displacement error signals. The identification subsystem was limited to the A-side and the y-axes, due to the installation of the roller bearing on the B-side and the limitation in the sampling time of the dSPACE® controller. The day and time when the fault first occurred is saved and displayed.

Figure 5.22 shows the parameter diagram of the fault identification subsystem used to calculate the type of fault, parameters of the fault, where the fault occurs, critical state of the fault and time when the fault occurred. The data fitting system calculates and compares the best possible fit of the parameters A, B, C and D of the running AMB system with the parameters (A_{base}, B_{base}, C_{base} and D_{base}) of the historical fault database. The parameters A_{base}, B_{base}, C_{base} and D_{base} were calculated separately from the historical database error (e_{ref}) and forms part of the database. The parameter calculator system uses the same building blocks of the diagnosis system in section 5.3.6 to calculate the parameters A_{base}, B_{base}, C_{base} and D_{base}. The data fitting system has access to all the datasets in the historical fault database and calls the number of the dataset (*set*) when a fit has been completed. The data fitting system sends the number of the dataset (*set*) with the closest fit and the accuracy of the fit (*fit*) to the diagnostic system. The historical fault database provides the diagnostic system with the type of fault (F_{data}).

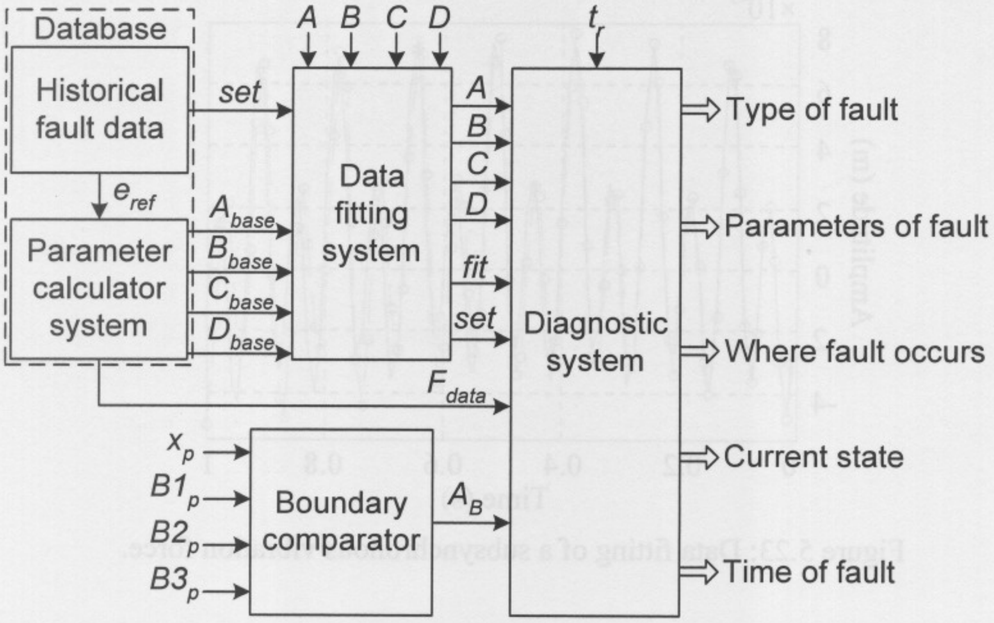

Figure 5.22: Parameter diagram of the fault identification subsystem

The output is displayed as a percentage fit to a specific dataset and the corresponding fault in the dataset. Each time the identification subsystem recalculates the frequency the parameters A, B, C and D are saved as the output parameters of the fault.

The amplitude of the boundary error (A_B) is obtained by comparing the actual displacement (x_p) with the displacement boundaries ($B1_p$, $B2_p$ and $B3_p$). This index provides the diagnostic system with the current state of the rotor. The current state of the rotor is divided into four sections: 1) good operating condition where $x_p < B1_p$, 2) fault in system where $B1_p \leq x_p < B2_p$, 3) critical state where $B2_p \leq x_p \leq B3_p$ and 4) system shutdown where $x_p > B3_p$.

Faults are allocated to the A-side and B-side and can occur in the x and y axes. The side and axes with the largest displacement error indicates where the fault causes the most damage. The exact time when the fault first occurred is saved and displayed. The running time (t_r) parameter is used to calculate the exact time.

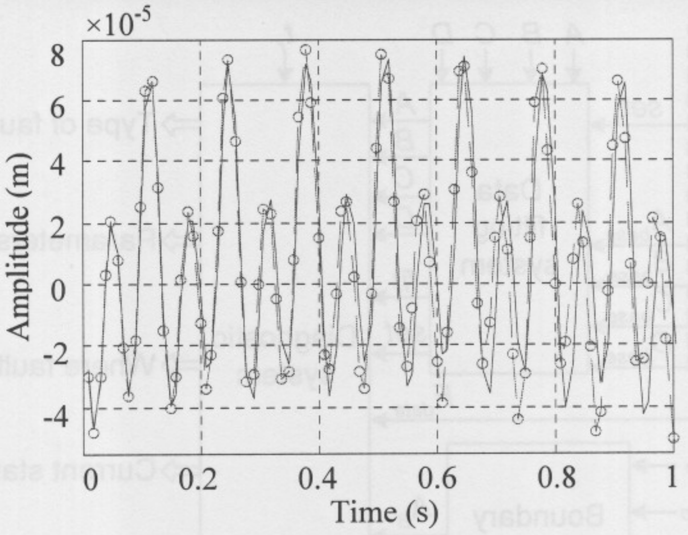

Figure 5.23: Data fitting of a subsynchronous vibration force.

Figure 5.23 displays data fitting of a subsynchronous historical fault (calculated from the parameters A_{base}, B_{base}, C_{base} and D_{base}) with the fault calculated from the parameters A, B, C and D obtained from the practical AMB system. The solid lines in figure 5.23 represent the historical fault from the water cooling AMB pump and the dashed lines with the circle markers represent the fault from the double radial AMB system. In figure 5.23 the frequency of the fault stayed constant within the subsynchronous vibration force area, therefore the sampling time of the parameters was kept constant.

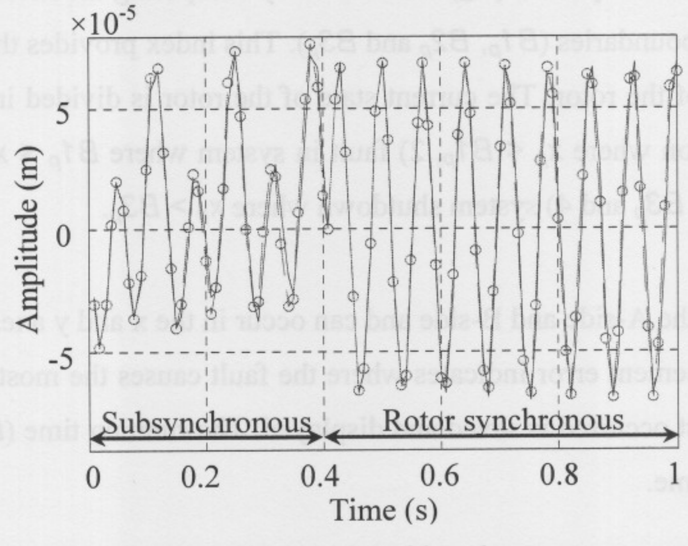

Figure 5.24: Data fitting of subsynchronous with sudden change to rotor synchronous vibration force

Figure 5.24 displays data fitting where the frequency of the fault changed from the subsynchronous vibration force area to the rotor synchronous vibration force area. The sampling time of the parameters was increased when the frequency entered the rotor synchronous vibration force area. The sampling of the parameters is performed by the data fitting system.

Figure 5.25 shows a screenshot of the fault identification program written in MATLAB®. This program calculates and displays the type of vibration force (unbalance, misalignment, foundation looseness or as otherwise specified in the historical fault database), vibration force fit to a specific dataset, side of the vibration force (A-side or B-side), vibration force axes (x or y), rotor state (good condition, fault in system or system critical), vibration force parameters (*A*, *B*, *C* and *D*), day and time when the vibration force occurred.

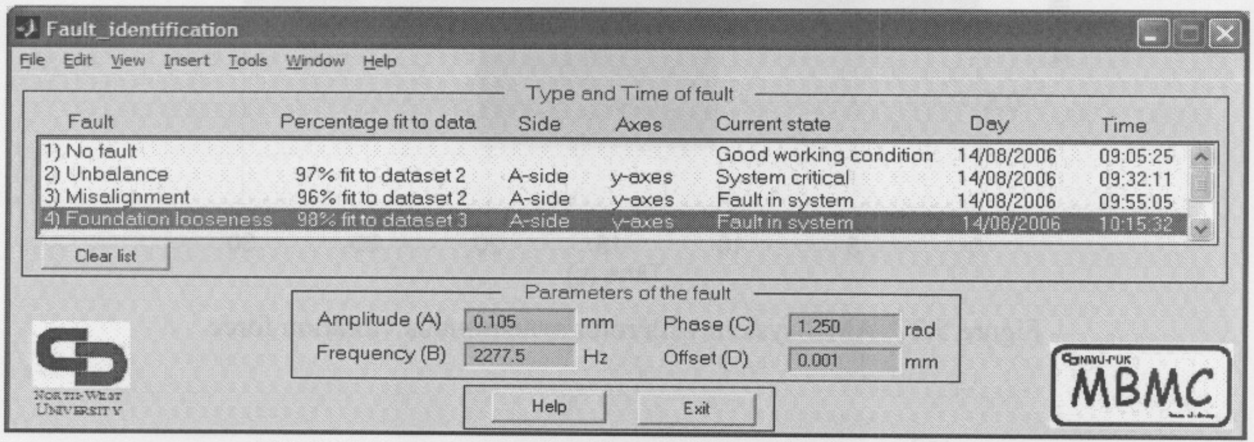

Type and Time of fault

Fault	Percentage fit to data	Side	Axes	Current state	Day	Time
1) No fault				Good working condition	14/08/2006	09:05:25
2) Unbalance	97% fit to dataset 2	A-side	y-axes	System critical	14/08/2006	09:32:11
3) Misalignment	96% fit to dataset 2	A-side	y-axes	Fault in system	14/08/2006	09:55:05
4) Foundation looseness	98% fit to dataset 3	A-side	y-axes	Fault in system	14/08/2006	10:15:32

Parameters of the fault

Amplitude (A) 0.105 mm
Frequency (B) 2277.5 Hz
Phase (C) 1.250 rad
Offset (D) 0.001 mm

Figure 5.25: Screenshot of the fault identification program

5.6. SIMULATION VERIFICATION

5.6.1. SIMULATION RESULTS

During the simulation phase of this scheme the rotational speed frequency was chosen at 1000 rpm and faults (vibration forces) were induced by applying the vibration force (f_4) files onto the AMB system to see how the diagnosis and correction scheme reacts. The displacement (x_p) of the AMB system with subsynchronous and rotor synchronous vibration forces can be seen in figure 5.26 and figure 5.27, respectively.

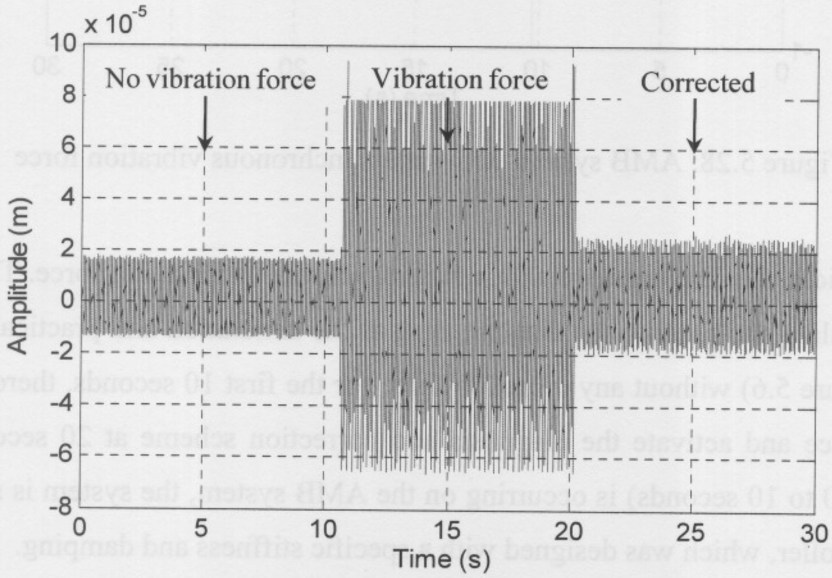

Figure 5.26: AMB system with subsynchronous vibration force

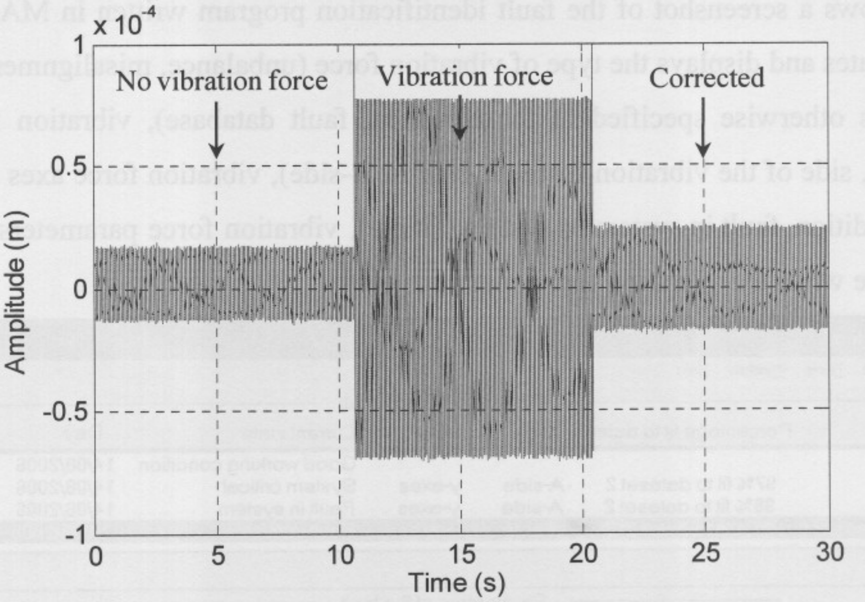

Figure 5.27: AMB system with rotor synchronous vibration force

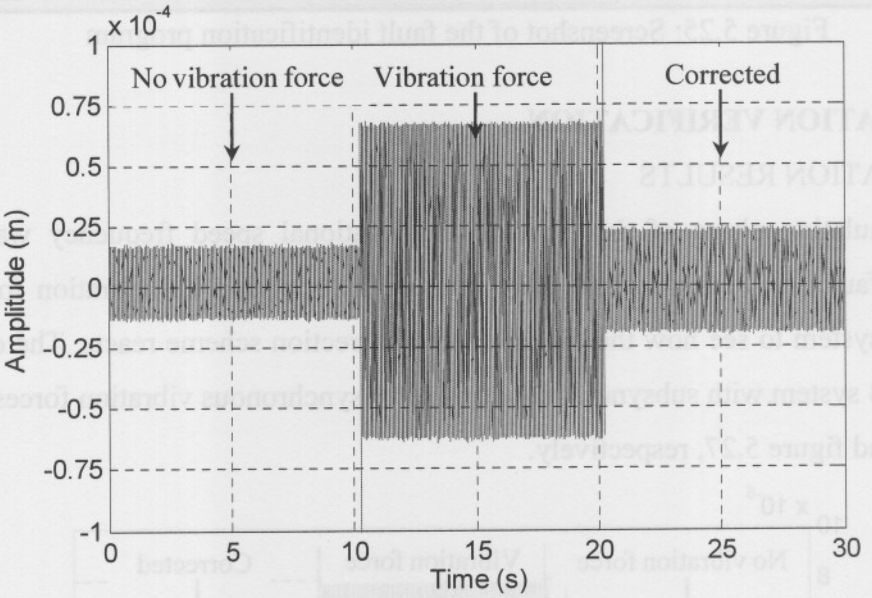

Figure 5.28: AMB system with supersynchronous vibration force

Figure 5.28 provides the displacement with a supersynchronous vibration force. The scheme was designed to simulate and capture the displacement of the simulation and practical AMB models (as shown in figure 5.6) without any vibration force for the first 10 seconds, thereafter to induce the vibration force and activate the diagnosis and correction scheme at 20 seconds. When no vibration force (0 to 10 seconds) is occurring on the AMB system, the system is suspended only by the PID controller, which was designed with a specific stiffness and damping.

The induced vibration forces were scaled to smaller amplitude. This was done to prevent the rotor from crashing against the retainer bearings and causing damage to the AMB system. When the non-scaled vibration forces were induced the optimised PID controller became unstable. The figures in this section show the scaled vibration forces (10 to 20 seconds) and how the diagnosis and correction scheme reacts on them (after 20 seconds).

A good comparison can therefore be made between the optimised PID controller (10 to 20 seconds) and the proposed diagnosis and correction scheme (activated after 20 seconds). The diagnosis and correction scheme was able to minimise the vibration forces. The simulation GUI and base code used to obtain results in this section can be found in appendix B.

5.6.2. EXPERIMENTAL RESULTS

During the practical implementation phase of this scheme the rotor speed was held constant at 1000 rpm and vibration forces were induced by implementing the reference current fault (i_f) files onto the AMB system to see how the diagnosis and correction scheme reacts. The implementing of the reference current fault (i_f) files are described in section 5.3.2 and appendix C.

The displacement (x_p) of the AMB system with subsynchronous and rotor synchronous vibration forces can be seen in figure 5.29 and figure 5.30, respectively. Figure 5.31 provides the displacement with a supersynchronous vibration force.

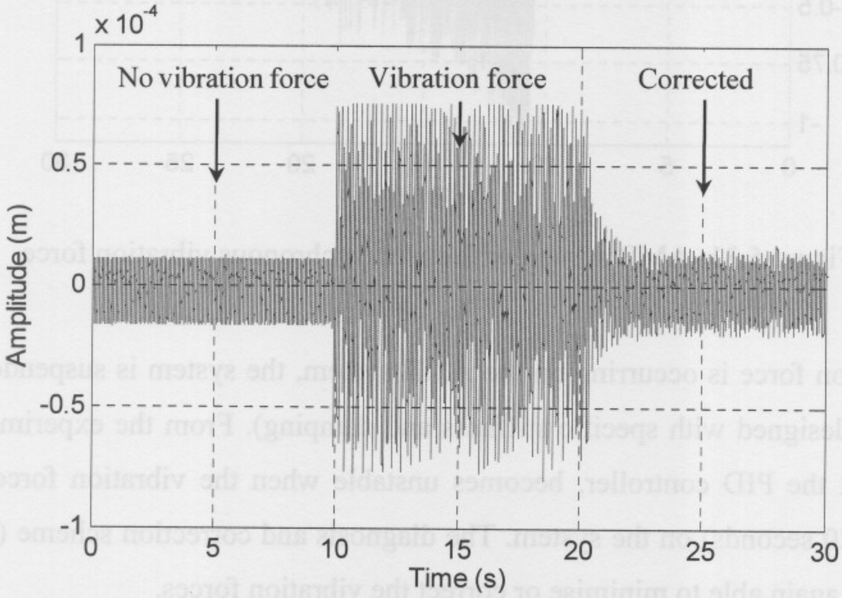

Figure 5.29: AMB system with subsynchronous vibration force

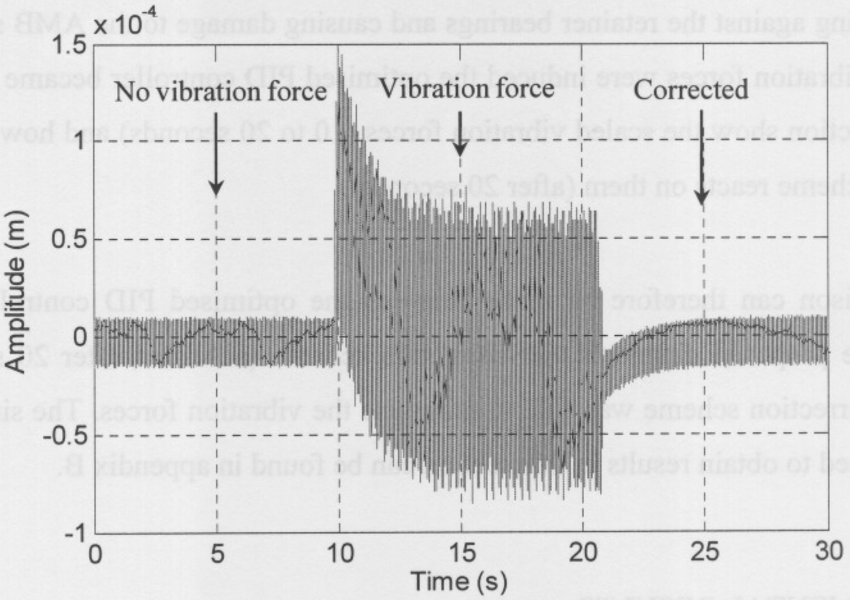

Figure 5.30: AMB system with rotor synchronous vibration force

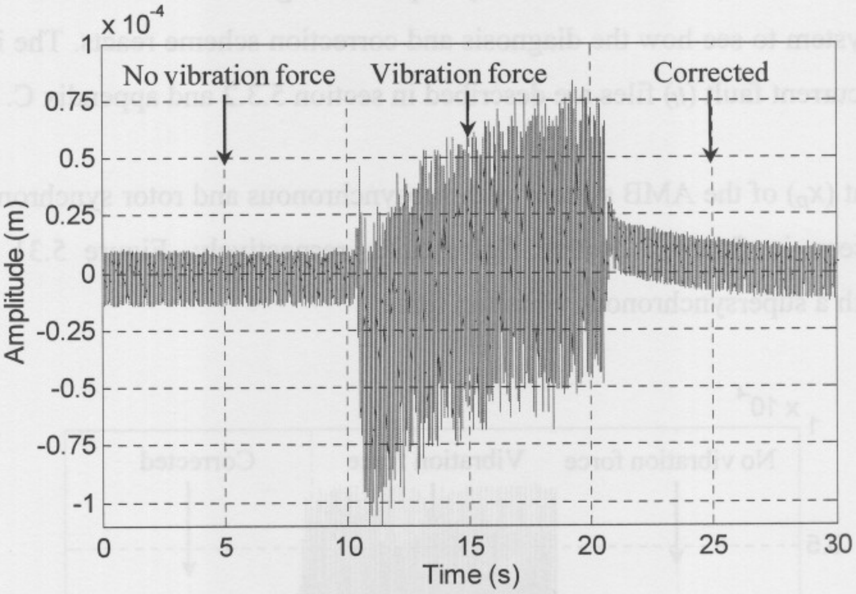

Figure 5.31: AMB system with supersynchronous vibration force

When no vibration force is occurring on the AMB system, the system is suspended only by the PID controller (designed with specific stiffness and damping). From the experimental results it can be seen that the PID controller, becomes unstable when the vibration forces are induced (between 10 to 20 seconds) on the system. The diagnosis and correction scheme (activated after 20 seconds) was again able to minimise or correct the vibration forces.

The author would like to refer the reader's attention to results obtained in a study by Britcher [20]. His study provides a comparison between different digital controllers used in magnetic bearing systems. From these results the reader can make a comparison between different optimised digital controllers and the proposed correction scheme mentioned in this chapter.

5.7. CONCLUSION

The scheme presented in this chapter concentrated on the detection and correction of vibration forces on the rotor of an AMB system. The fault diagnosis and error correction stages were divided into subsynchronous, rotor synchronous and supersynchronous vibration force subsystems, with the subsynchronous vibration force subsystem forcing the controller to overcompensate for vibration forces and the rotor synchronous and supersynchronous vibration force subsystem correcting the vibration forces by inducing correction forces onto the rotor of the AMB system.

The detection and correction scheme corrected and minimised faults (vibration forces) to a stable operating condition. The experimental results obtained from the double radial AMB test rack correlated with the simulated results. The methods and implementation of predictive simulation, model validation and test implementation were shown here to be useful for detection, diagnosis and correction of faults on AMB systems.

During the fault identification section the precise fault was calculated by performing data fitting on the historical fault data of the water cooling AMB pump and the parameters A, B, C and D obtained from the double radial AMB test rack.

The current limit of the power amplifiers and the run-time of the processors were the two main limitations of this scheme, during the practical implementation phase. During normal operation of the double radial AMB, the power amplifiers require 4 to 5 ampere, which only leaves 5 to 6 ampere for fault inducement and correctional purposes. Due to the complexity of the diagnosis and correctional subsystems, a lot of processing time was required, which caused run-time errors during real-time implementation on the dSPACE® controller. This problem was solved by implementing an additional dSPACE® controller.

The overall performance of the error correction subsystem is determined by the integrated performance of the individual subsystems. The method of performing detection, diagnosis and correction must be seen as a whole and the performance of the complete scheme, rather than a single component must be evaluated. The method of real-time frequency extraction with the WVD and real-time feature extraction by means of the fuzzy logic controller are the most crucial components in the design of the detection, diagnosis and correction scheme.

At startup the AMB system is suspended only by the PID controller. When a vibration (disturbance) force occurs on the system, the detection, diagnosis and correction scheme measures the exact error and applies correction forces. At this stage the measured error decreases and causes the correction subsystem to apply correction forces with smaller amplitudes. At the next stage the measured error increases (due to smaller correction forces) and the correction subsystem applies correction forces with larger amplitudes. This controlling process is repeated until the no vibration force is detected.

Appendix G provides a list of additional information applicable to this chapter.

CHAPTER 6

DESIGN OF THE REAL-TIME CURRENT ANALYSIS, CORRECTION AND IDENTIFICATION SCHEME

6.1. INTRODUCTION

This chapter provides the design of the real-time current analysis, correction and identification scheme. As mentioned in chapter 1, the design of the real-time scheme in this chapter is the second of three real-time detection, correction and identification schemes.

This scheme focuses on using the available sensors and actuators to perform current analysis. A real-time detection, diagnosis and correction scheme was developed that performed the current analysis process and induced correctional forces on the rotor of the rotating AMB system. The detection scheme constitutes current masking and feature extraction performed by the Wigner-Ville distribution (WVD). The diagnosis and correction scheme constitutes pattern recognition and fuzzy logic.

The same two AMB systems used in chapter 5 were used in this scheme. The historical fault datasets and vibration forces on the rotor of the AMB systems are the same as defined in chapter 5.

6.2. SCHEME DEVELOPMENT

This section explains the scheme development process of the real-time current analysis, correction and identification scheme. A process diagram of the vibration and correction forces is shown in figure 6.1. At start up the AMB system is suspended only with PID controllers and rotated at the desired speed of 1000 rpm.

Current masking is performed during this initial period when no vibration forces are occurring on the AMB system. The rotational speed of the rotor is used as input to the current masking process. The masked current is stored to memory.

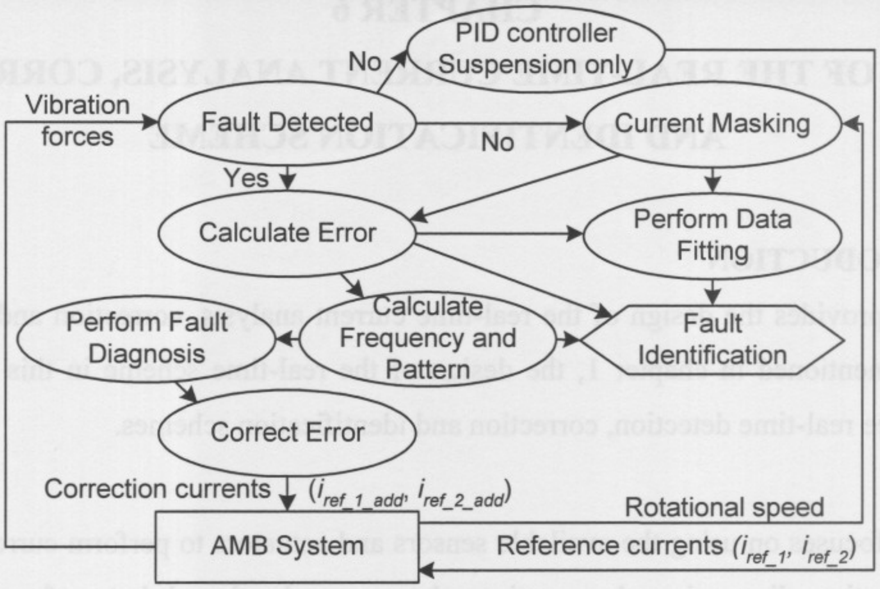

Figure 6.1: Illustration of the vibration force detection process.

When a vibration force occurs on the rotor, the scheme detects the fault (vibration force) and calculates the vibration error, frequency and pattern. The stored no fault current is used to calculate the vibration error. Data fitting is then performed on the vibration error and the masked current.

The fault identification subsystem identifies the fault according to results obtained from the data fitting, vibration error, frequency and pattern. The frequency and pattern are sent to the fault diagnosis and error correction subsystems, which calculate the correction currents needed to stabilise the rotor.

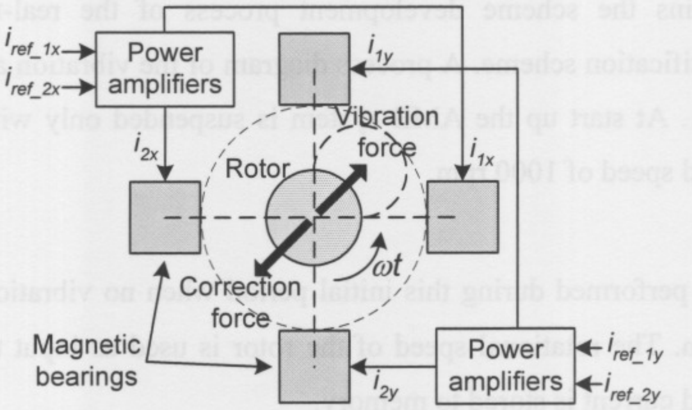

Figure 6.2: Illustration of the vibration and correction forces on the rotor of the AMB system.

The rotor view of the vibration and correctional forces, where the PID controller fails to correct the vibrations is shown in figure 6.2. In this diagram a vibration force causes the rotor to suddenly move to the upward right corner. Without immediate correction the rotor will crash against the retainer bearings and cause damage to the AMB system.

Correction forces are applied on the rotor by increasing or decreasing the reference currents i_{ref_1} and i_{ref_2} according to the direction of the vibration force. The real-time detection, diagnosis and correction scheme performs the calculations for the correction forces.

Figure 6.3 provides an overview of the detection, diagnosis and correction scheme that was implemented on the double radial AMB test rack. The fault detection subsystem uses the currents i_1 and i_2 to detect the vibration forces on the AMB system and calculates the current errors e_{i1} and e_{i2}, through a process of current masking and error calculation. The fault detection subsystem is explained in section 6.2.1.

After a fault has been detected, the error signals (e_{i1} and e_{i2}) are sent to the fault diagnosis subsystem where feature extraction is performed. The fault diagnosis subsystem is explained in section 6.2.2. The error correction subsystem uses the diagnosis output error (e_{d1}) and the workforce relation current (i_{ref_1R}) as features to stabilise the rotor by inducing correction forces on the rotor. The error correction subsystem is explained in section 6.2.2.

The parameters $i_{ref\_1\_add}$ and $i_{ref\_2\_add}$ represent the correction reference currents for the top and bottom magnetic bearings, respectively.

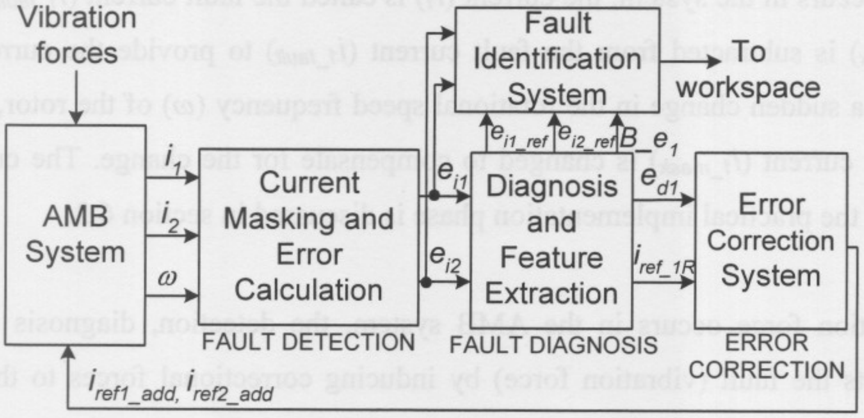

Figure 6.3: Overview of the detection, diagnosis and correction scheme.

The fault identification subsystem uses the current errors (e_{i1} and e_{i2}), historical database errors (e_{i1_ref} and e_{i2_ref}) and the frequency (B_e_1) to identify the type of vibration force. The fault identification subsystem is explained in section 6.2.3.

The same simulation and practical AMB models (for inducement of vibration forces on the rotor of the AMB systems) described in section 5.3.2 were used during the design of the real-time current analysis, correction and identification scheme of this chapter.

6.2.1 FAULT DETECTION SUBSYSTEM

The fault detection subsystem (shown in figure 6.4) constitutes current masking, error calculation and frequency calculation. Current masking is performed by capturing one cycle of the current (i_1) during a no fault condition of the AMB system. A sine wave representation of the no fault current (i_{1_mask}) is obtained and stored to memory. This process is done only once and when no vibration force is occurring on the AMB system.

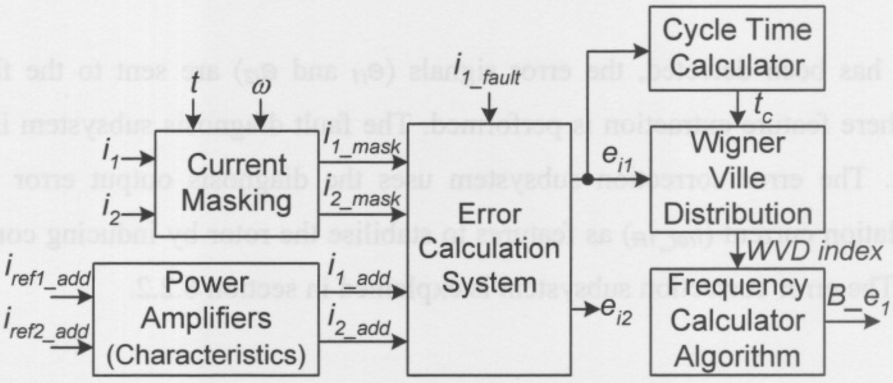

Figure 6.4: Fault detection subsystem.

When a fault occurs in the system, the current (i_1) is called the fault current (i_{1_fault}). The no fault current (i_{1_mask}) is subtracted from the fault current (i_{1_fault}) to provide the current error (e_{i1}). When there is a sudden change in the rotational speed frequency (ω) of the rotor, the frequency of the no fault current (i_{1_mask}) is changed to compensate for the change. The current masking process during the practical implementation phase is discussed in section 6.3.

When a vibration force occurs in the AMB system, the detection, diagnosis and correction scheme corrects the fault (vibration force) by inducing correctional forces to the shaft. These correctional forces are applied by adding correctional reference currents (i_{ref1_add} and i_{ref2_add}) to the existing reference currents (i_{ref_1} and i_{ref_2}).

When the correctional reference currents are applied the actual currents (i_1 and i_2) change. To retain the initial error information prior to the error correction the error correction currents need to be subtracted from the resulting currents of the corrected system. In this manner a change in error conditions will be sensed and appropriately corrected by a change in the error correction currents.

The WVD was calculated by using (4.48) and the frequency (B_e_1) was calculated from the WVD and a frequency calculator algorithm. The accuracy of the frequency was improved by sampling the WVD at twice the cycle time (t_c) of the error signal (e_{i1}).

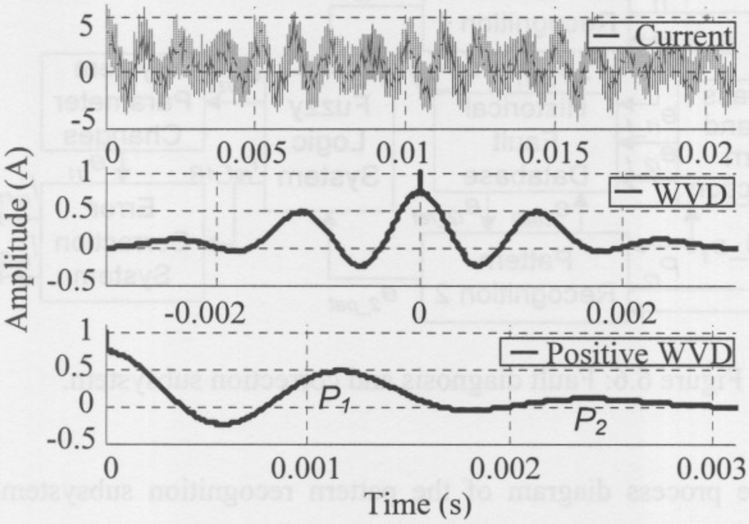

Figure 6.5: Frequency calculation with the WVD.

The WVD is calculated from the current error (e_{i1}) and the peaks P_1 and P_2 are calculated from the positive peaks of the WVD as shown in figure 6.5. From peak P_1 the frequency of the fault was calculated at 854.7 Hz. This frequency calculation is only to illustrate the WVD process and is not a representation of the data obtained from the 250 kW water cooling AMB pump.

It can be seen from (6.1) that the second peak (P_2) is a multiple of the first peak. The value calculated in this equation provides an estimate of the error factor on the first peak (P_1). In this case the frequency calculated has 99.15 % accuracy.

$$\frac{P_2}{P_1} = \frac{2.36 \times 10^{-3}}{1.17 \times 10^{-3}} = 2.017 \tag{6.1}$$

6.2.2 FAULT DIAGNOSIS AND CORRECTION SUBSYSTEM

This section discusses the fault diagnosis and correction subsystem, shown in figure 6.6. The pattern recognition 1 and 2 subsystems compare the current errors (e_{i1} and e_{i2}) of the real-time AMB system with the reference current errors (e_{i1_ref} and e_{i2_ref}) of the historical fault database. The pattern recognition 1 and 2 subsystems call (e_{call1} and e_{call2}) the reference current errors from the database at a specific frequency (B_e_1). When a fault occurs without a recognisable pattern, the pattern is band-pass filtered (centre frequency being the error frequency (B_e_1)) and stored to the historical fault database.

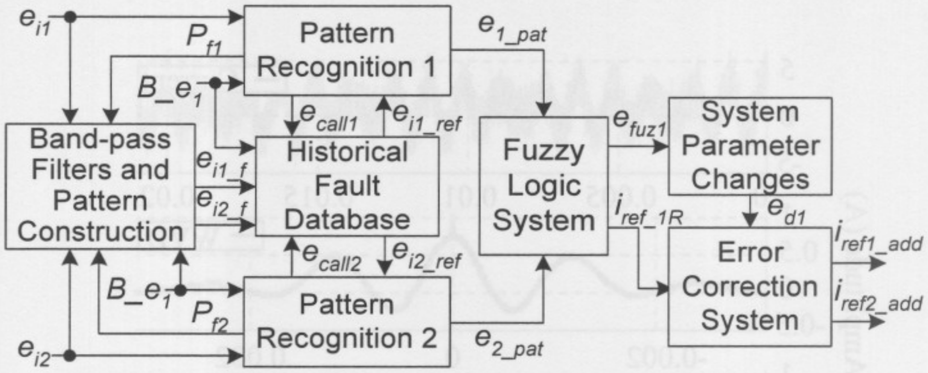

Figure 6.6: Fault diagnosis and correction subsystem.

Figure 6.7 shows the process diagram of the pattern recognition subsystem. The subsystem measures the difference between the real-time current errors (e_{i1} and e_{i2}) and the reference current errors (e_{i1_ref} and e_{i2_ref}) from the historical fault database. If the error difference is big, the error obtained from the real-time AMB system is used for correctional purposes. At this stage no recognisable pattern exists and the pattern construction subsystem constructs and stores a new pattern.

When the error difference is small (close to zero), the subsystem calculates the frequency and closest pattern to the available real-time data. If the frequency stays constant, the subsystem uses the closest pattern to correct the fault. If the frequency changes the subsystem tests the data in the historical fault database for a possible combination pattern.

When no combination of the available data is found, the subsystem uses the real-time error to correct the fault. A new pattern is constructed and stored to the database and the pattern calculation process is repeated. If the subsystem finds a combination pattern, the subsystem uses the pattern and stores the pattern as a combination pattern.

The construction subsystem constructs and stores new patterns (e_{i1_f} and e_{i2_f}) according to the fault signals (e_{i1} and e_{i2}), when it receives pattern faults (P_{f1} and P_{f2}) from the pattern recognition subsystems.

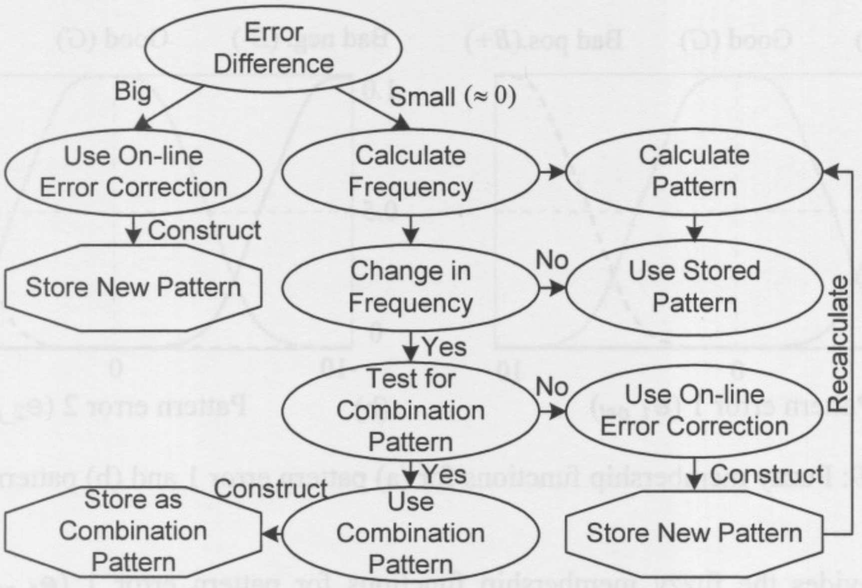

Figure 6.7: Process diagram of the pattern recognition subsystem.

The more faults occur in the AMB system the more new correctional data become available. The subsystem is able to switch between different patterns and train itself to react on faults that are a combination of the available fault data. An orbital representation of the currents (i_{1x} and i_{1y}) and three subsynchronous vibration force correctional patterns can be seen in figure 6.8. Pattern sub_{new} is a trained pattern which consists of pieces of three subsynchronous vibration force correctional patterns sub_1, sub_2 and sub_3.

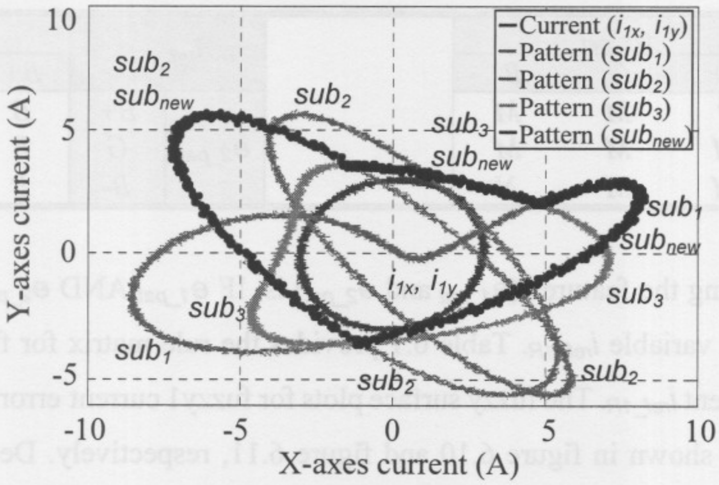

Figure 6.8: Orbital representation of the subsynchronous vibration force pattern errors.

The pattern (sub_{new}) was stored as a combination pattern and decreased the vibration forces on the rotor of the AMB system. For each of the patterns in the historical fault database there exist a frequency and description.

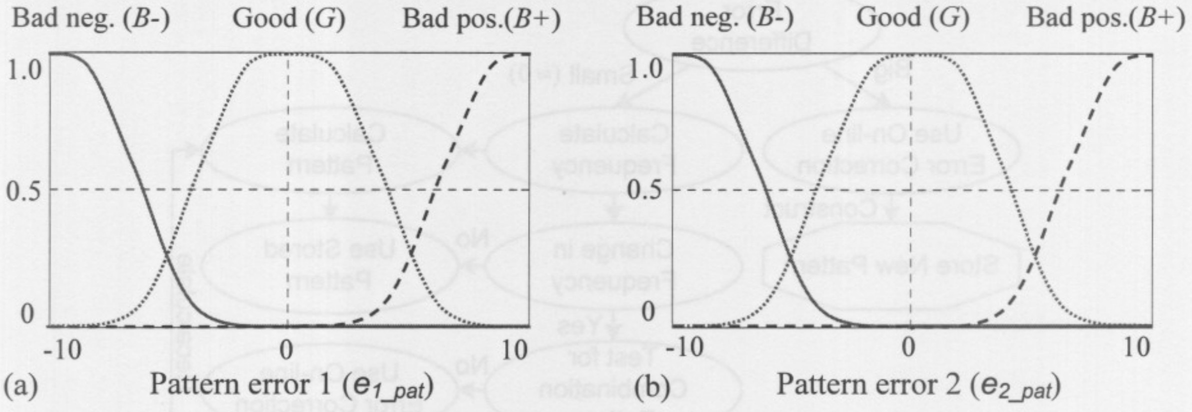

Figure 6.9: Fuzzy membership functions for (a) pattern error 1 and (b) pattern error 2.

Figure 6.9 provides the fuzzy membership functions for pattern error 1 (e_{1_pat}) and pattern error 2 (e_{2_pat}). Fuzzification is performed by using the overlapping fuzzy sets bad negative (*B-*), good (*G*) and bad positive (*B+*).

The fuzzy logic controller has the ability to cope with knowledge represented in a linguistic form instead of a conventional mathematical form. The mathematical model of the diagnosis and correction subsystem is complex and implementation of the model as a real-time controller would be less effective than using the proposed fuzzy controller.

Table 6.1: Rule matrix for fuzzy current error (e_{fuz1}) and relation current (i_{ref_1R})

e_{fuz1}		e_{1_pat}		
		B+	*G*	*B-*
e_{2_pat}	*B+*	*P*	*M*	*M*
	G	*M*	*M*	*M*
	B-	*M*	*M*	*N*

i_{ref_1R}		e_{1_pat}		
		B+	*G*	*B-*
e_{2_pat}	*B+*	*B*	*B*	*B*
	G	*B*	*M*	*B*
	B-	*B*	*B*	*T*

The basic rule for using the features (e_{1_pat} and e_{2_pat}) is: IF e_{1_pat} AND e_{2_pat} THEN e_{fuz1}. The same rule applies for variable i_{ref_1R}. Table 6.1 provides the rule matrix for fuzzy1 current error e_{fuz1} and relation current i_{ref_1R}. The fuzzy surface plots for fuzzy1 current error (e_{fuz1}) and relation current 1 (i_{ref_1R}) are shown in figure 6.10 and figure 6.11, respectively. Defuzzification of the fuzzy membership functions e_{fuz1} and i_{ref_1R} are performed by using overlapping fuzzy sets negative (*N*), middle (*M*) and positive (*P*) and bottom (*B*), middle (*M*) and top (*T*), respectively.

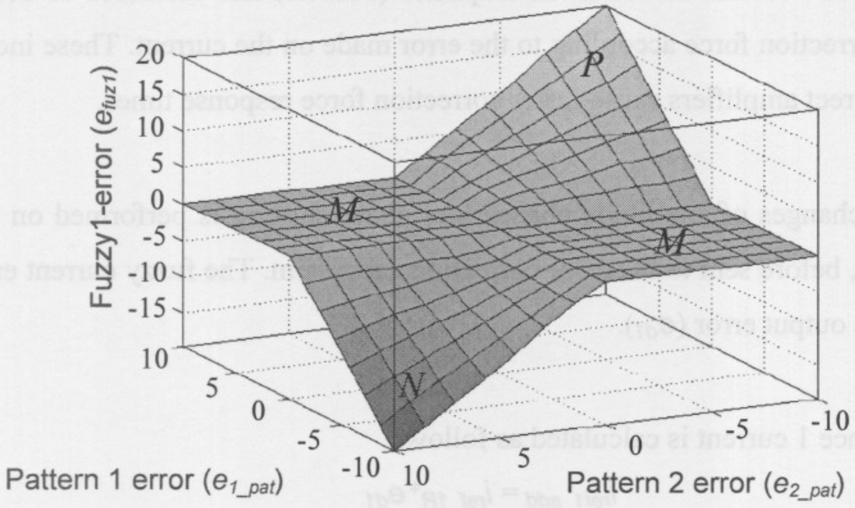

Figure 6.10: Fuzzy surface plot for fuzzy1 current error (e_{fuz1}).

When a vibration force causes the rotor to move downward, the reference current 1 (i_{ref_1}) needs to be more than reference current 2 (i_{ref_2}) to stabilise the rotor to the centre position.

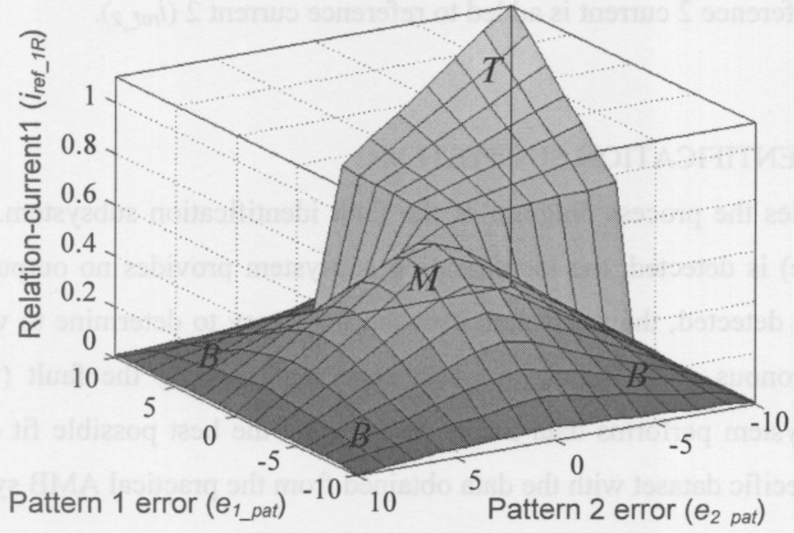

Figure 6.11: Fuzzy surface plot for relation current 1 (i_{ref_1R}).

This relation between the amplitude of the vibration force and amount of current required by each amplifier is called the workforce relation current and is defined by i_{ref_1R} and i_{ref_2R}. i_{ref_1R} refer to the workforce relation current for the top power amplifier and i_{ref_2R} refer to the workforce relation current for the bottom power amplifier.

Workforce relation current 2 (i_{ref_2R}) is calculated as follows:

$$i_{ref\_2R} = 1.0 - i_{ref\_1R} \tag{6.2}$$

The workforce relation current serves as an amplifier (booster) and increases or decreases the amplitude of the correction force according to the error made on the current. These increases and decreases of the correct amplifiers cause faster correction force response times.

System parameter changes of amplitude change and phase shifting is performed on the fuzzy1 current error (e_{fuz1}), before sent to the error correction subsystem. The fuzzy current error is then called the diagnosis output error (e_{d1}).

Correctional reference 1 current is calculated as follows:

$$i_{ref1\_add} = i_{ref\_1R} * e_{d1} \tag{6.3}$$

The correctional reference 1 current is added to reference current 1 (i_{ref_1}). Correctional reference 2 current is calculated as follows:

$$i_{ref2\_add} = -i_{ref\_2R} * e_{d1} \tag{6.4}$$

The correctional reference 2 current is added to reference current 2 (i_{ref_2}).

6.2.3 FAULT IDENTIFICATION SUBSYSTEM

Figure 6.12 provides the process diagram of the fault identification subsystem. When no fault (no vibration force) is detected, the identification subsystem provides no output. When a fault (vibration force) is detected, the subsystem uses the frequency to determine to which frequency dataset (subsynchronous, rotor synchronous or supersynchronous) the fault (vibration force) belongs. The subsystem performs data fitting to calculate the best possible fit of the historical fault data in the specific dataset with the data obtained from the practical AMB system.

If the frequency rapidly changes from one dataset to another, the subsystem saves the output, predicts the closest type of fault (unbalance, misalignment, foundation looseness or as otherwise specified in the historical fault database) and recalculates the fault in the new dataset.

When the frequency stays within a certain dataset, the subsystem is set to repeatedly calculate the average error over a time period of 1 second. The time period was calculated at five times the period of the masked current at 1000 rpm. The type of fault is given to the fault in the dataset with the smallest error over the available time period.

After the type of fault is stored, the subsystem displays the parameters of the fault and determines the current state of the fault. The current state of the fault is calculated from the maximum current output of the power amplifiers. The subsystem determines the side and axis where the fault occurs from the current error signals.

Faults are allocated to the A-side and B-side and can occur in the x, y and z axes. The identification subsystem was limited to the A-side and the y-axes, due to the installation of the roller bearing on the B-side and the limitation in the sampling time of the dSPACE® controller. The day and time when the fault first occurred is saved and displayed.

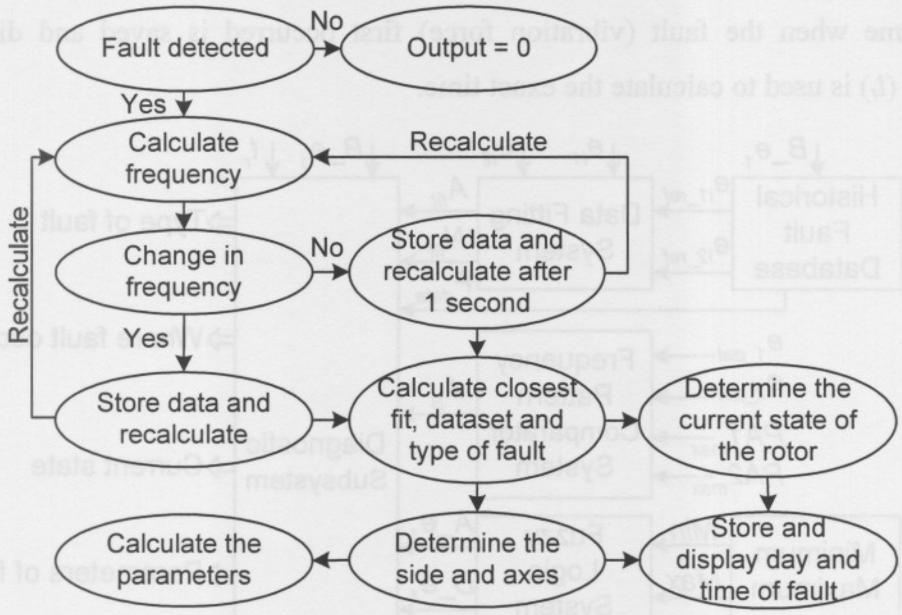

Figure 6.12: Process diagram of the identification subsystem.

Figure 6.13 shows the parameter diagram of the fault identification subsystem used to calculate the type of fault, where the fault occurs, current state of the fault, parameters of the fault and the day and time when the fault first occurred. The data fitting system calculates and compares the best possible fit of current 1 error (e_{i1}) and current 2 error (e_{i2}) of the real-time AMB system with the reference current 1 (e_{i1_ref}) and reference current 2 (e_{i2_ref}) of the historical fault database. The data fitting system sends the number of the dataset (N_{fit}) with the closest fit and the accuracy of the fit (A_{fit}) to the diagnostic subsystem.

The historical fault database provides the diagnostic subsystem with the type of fault (F_{data}). The output is displayed as a percentage fit to a specific dataset and the corresponding fault in the dataset. Each time the identification subsystem recalculates the frequency the parameters A_e_1, B_e_1, C_e_1 and D_e_1 are saved as the output parameters of the fault.

The amplitude of the frequency pattern error (A_B) is obtained by comparing pattern 1 error (e_{1_pat}) and pattern 2 error (e_{2_pat}) with the maximum current output of the power amplifiers ($PA1_{max}$ and $PA2_{max}$). This index provides the diagnostic subsystem with the current state of the rotor. The current state of the rotor is divided into four sections: 1) good operating condition, where $e_{1\_pat} < (0.2) \cdot PA1_{max}$; 2) fault in system, where $(0.2) \cdot PA1_{max} \leq e_{1\_pat} < (0.45) \cdot PA1_{max}$; 3) critical state, where $(0.45) \cdot PA1_{max} \leq e_{1\_pat} \leq (0.7) \cdot PA1_{max}$ and 4) system shutdown where $e_{1\_pat} > (0.7) \cdot PA1_{max}$. The same rules apply for e_{2_pat} and $PA2_{max}$.

The side and axis with the largest current error indicates where the fault causes the most damage. The exact time when the fault (vibration force) first occurred is saved and displayed. The running time (t_r) is used to calculate the exact time.

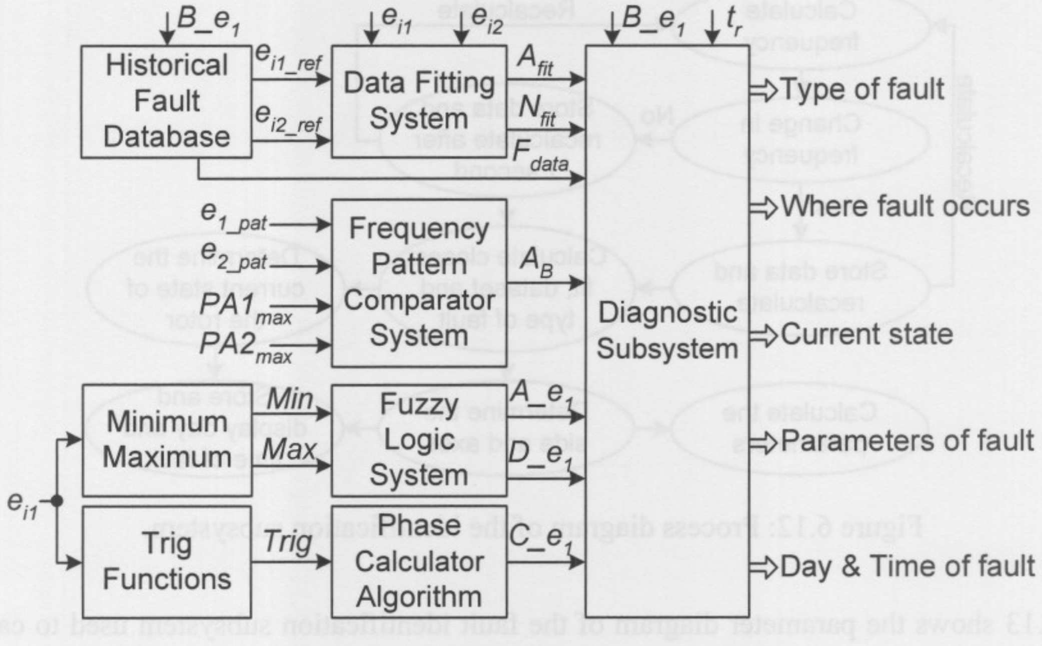

Figure 6.13: Fault identification subsystem.

Figure 6.14 displays data fitting where the frequency of the fault changed from the subsynchronous vibration force area to the supersynchronous vibration force area. The solid lines represent the historical database error (e_{i1_ref}) from the water cooling AMB pump and the dashed lines represent the real-time error (e_{i1}) from the double radial AMB system.

The sampling time of the parameters was increased when the frequency entered the supersynchronous vibration force area. Sampling (shown by the markers) of the parameters is performed by the data fitting system.

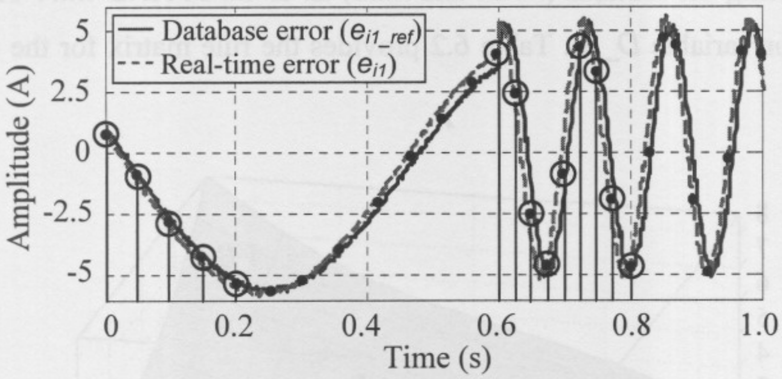

Figure 6.14: Data fitting of a subsynchronous with change to a supersynchronous vibration force.

Figure 6.15 provides the fuzzy membership functions for the maximum error (*MAX*) and minimum error (*MIN*). *MAX* refers to the maximum error over a period of time. The maximum block identifies the position of the largest element in each column of the current error (e_{i1}) over a period of time.

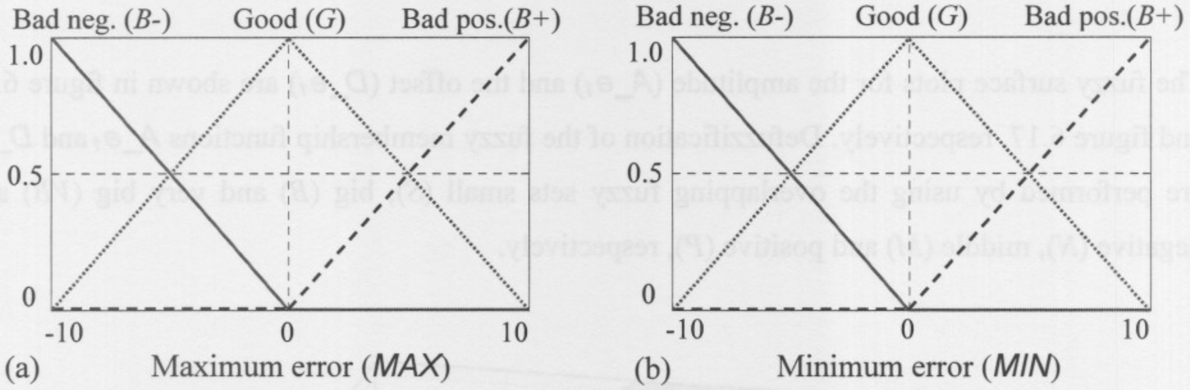

Figure 6.15: Fuzzy membership functions for the (a) maximum error and (b) minimum error.

MIN refers to the minimum error over a period of time. The minimum block identifies the position of the smallest element in each column of the current error over a period of time. Fuzzification is performed by using the overlapping fuzzy sets bad negative (*B*-), good (*G*) and bad positive (*B*+).

Table 6.2: Rule matrix for the amplitude (A_e_1) and offset (D_e_1)

A_e_1		*MAX*		
		B+	*G*	*B-*
MIN	*B+*	*S*	*S*	*S*
	G	*VB*	*S*	*S*
	B-	*B*	*VB*	*S*

D_e_1		*MAX*		
		B+	*G*	*B-*
MIN	*B+*	*P*	*M*	*M*
	G	*P*	*M*	*M*
	B-	*M*	*N*	*N*

The basic rule for using the features (*MAX* and *MIN*) is: IF *MAX* AND *MIN* THEN *A_e₁*. The same rule applies for variable *D_e₁*. Table 6.2 provides the rule matrix for the amplitude *A_e₁* and offset *D_e₁*.

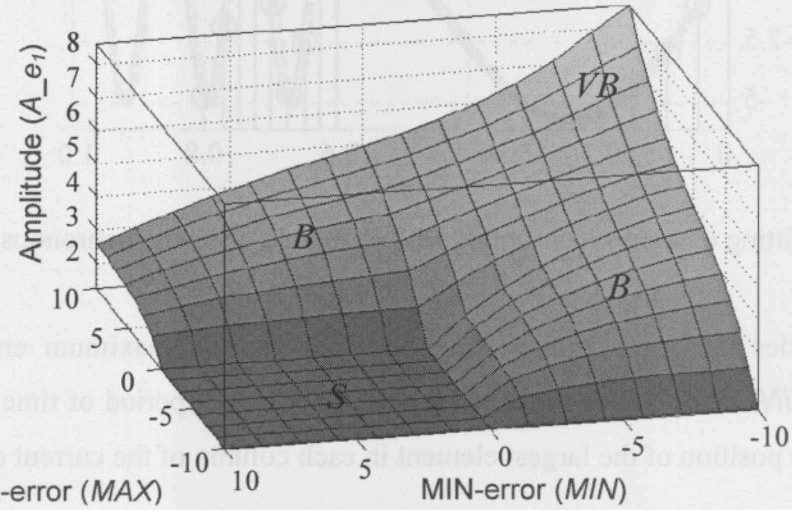

Figure 6.16: Fuzzy surface plot for amplitude *A_e₁*.

The fuzzy surface plots for the amplitude (*A_e₁*) and the offset (*D_e₁*) are shown in figure 6.16 and figure 6.17, respectively. Defuzzification of the fuzzy membership functions *A_e₁* and *D_e₁* are performed by using the overlapping fuzzy sets small (*S*), big (*B*) and very big (*VB*) and negative (*N*), middle (*M*) and positive (*P*), respectively.

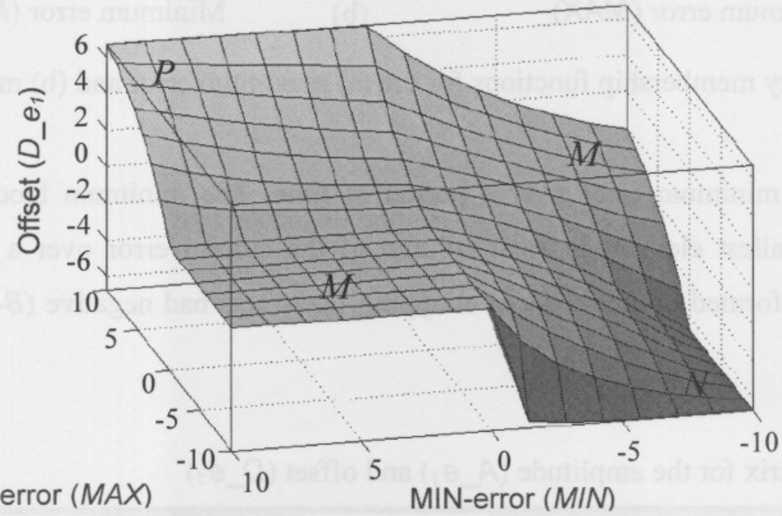

Figure 6.17: Fuzzy surface plot for offset *D_e₁*.

Figure 6.18 shows a screenshot of the fault identification program written in MATLAB®. This program calculates and displays the parameters of the fault identification subsystem of figure 6.13. Faults (vibration forces) are calculated and displayed as a specific type of fault (misalignment, foundation looseness, unbalance or as otherwise specified in the historical fault database), fault fit to a specific dataset, side where the fault occurs (A-side or B-side), axes where the fault occurs (x, y or z-axes), current state of the fault (good, fault, critical or shutdown) as well as the actual error percentage of the fault and day and time when the fault first occurred. The parameters (amplitude, frequency, phase and offset) of the fault are also shown.

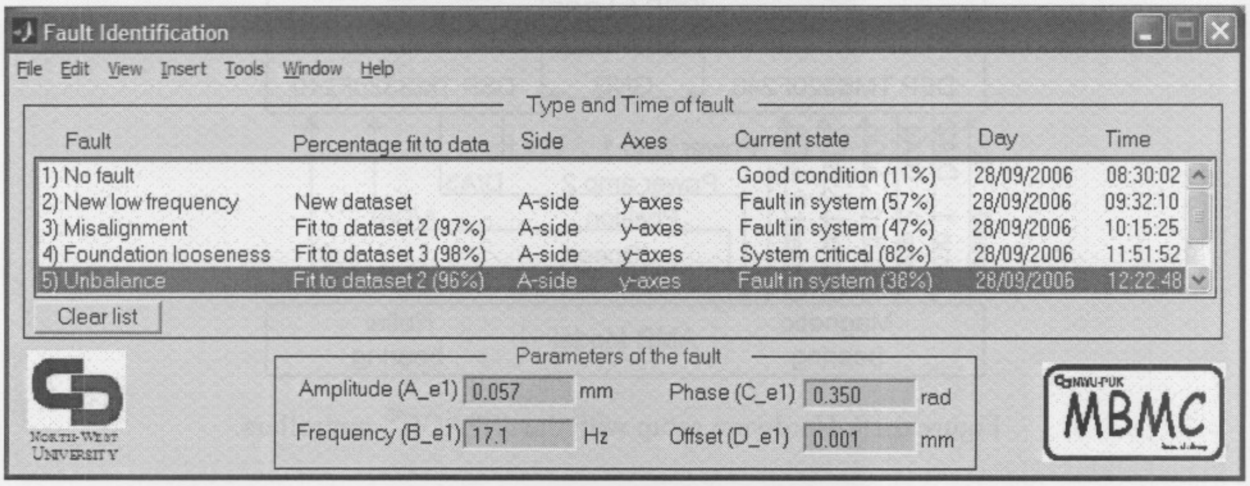

Fault	Percentage fit to data	Side	Axes	Current state	Day	Time
1) No fault				Good condition (11%)	28/09/2006	08:30:02
2) New low frequency	New dataset	A-side	y-axes	Fault in system (57%)	28/09/2006	09:32:10
3) Misalignment	Fit to dataset 2 (97%)	A-side	y-axes	Fault in system (47%)	28/09/2006	10:15:25
4) Foundation looseness	Fit to dataset 3 (98%)	A-side	y-axes	System critical (82%)	28/09/2006	11:51:52
5) Unbalance	Fit to dataset 2 (96%)	A-side	y-axes	Fault in system (38%)	28/09/2006	12:22:48

Amplitude (A_e1) 0.057 mm
Frequency (B_e1) 17.1 Hz
Phase (C_e1) 0.350 rad
Offset (D_e1) 0.001 mm

Figure 6.18: Screenshot of the fault identification program.

6.3. HARDWARE SETUP

Discrete sampling of the displacement and current signals of the physical AMB system was done by means of the dSPACE® 1104 controller board, equipped with a DSP TMS320F240 from Texas Instruments. A user-interface was created in Controldesk® to perform data acquisition on the physical AMB system. The real-time implementation process and hardware setup is detailed in appendix C.

Due to the complexity of the control, detection and correction, the dSPACE® controller was not able to handle all the instructions and real-time errors occurred. This problem was solved by implementing two dSPACE® 1104 controller boards, one for each axis of the magnetic bearing. A roller bearing was installed on the right side of the rotor, which increased the sampling time of the DSP, since only one side has to be suspended.

The vibration force calculations, speed sensor calculations and current masking process were performed by the left dSPACE® controller and communicated to the other dSPACE® controller via serial communication. The application of the vibration forces and diagnosis and correction scheme calculations were performed by the right dSPACE® controller. Figure 6.19 shows the hardware setup with the dSPACE® controllers.

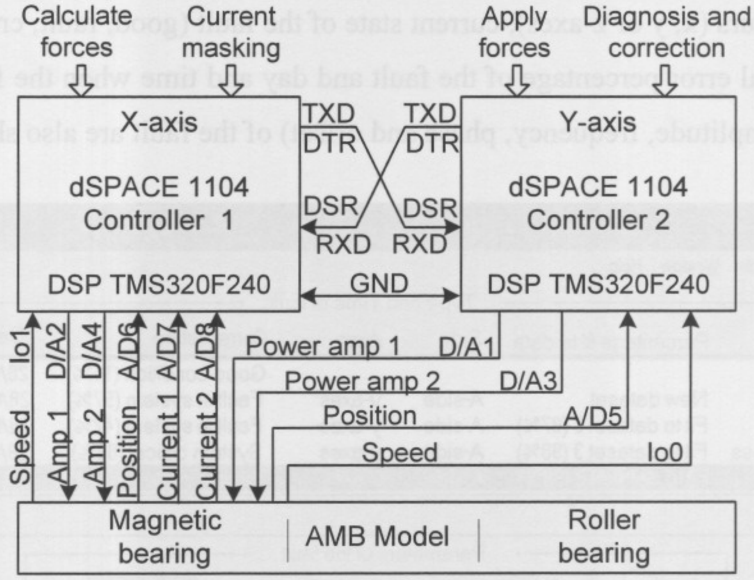

Figure 6.19: Hardware setup with the dSPACE® controllers.

During the investigation of the current signals of the double radial AMB system, it became evident that synchronous vibrations were introduced by the roller bearing when the rotor was rotating. These vibrations were therefore integrated into the current masking and correctional pattern calculation process of the fault detection and diagnosis subsystems (discussed in sections 6.2.1 and 6.2.2).

Figure 6.20 shows the masked current (i_{1_mask}) and the actual current (i_1) during the practical implementation phase. The no fault current (i_{1_mask}) is subtracted from the fault current (i_{1_fault}) to provide the current error (e_{i1}). The amplitude of the current (i_1) and the frequency (ω) obtained from the rotational speed of the rotor were used as scaling factors for the masked current. When the amplitude (i_1) and frequency (ω) increased, the amplitudes and frequencies of the individual signals in the masked current were also increased.

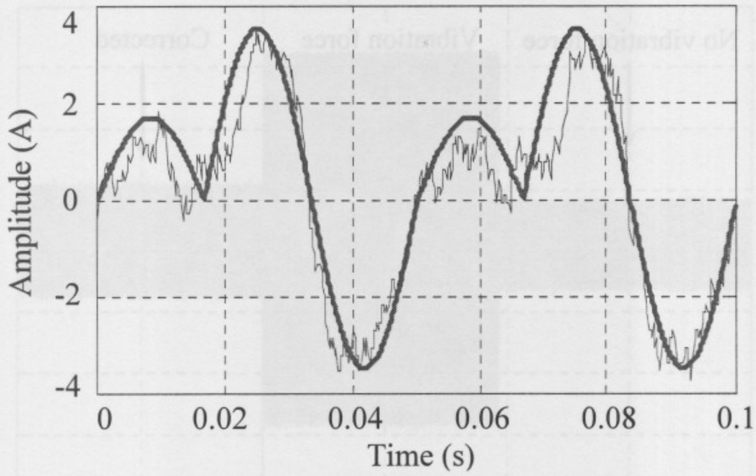

Figure 6.20: Current masking during the practical implementation phase.

6.4. SIMULATION VERIFICATION

This section provides the simulated and experimental results of the double radial AMB test rack, with subsynchronous, rotor synchronous and supersynchronous vibration forces.

6.4.1. SIMULATION RESULTS

During the simulation phase of this scheme the rotational speed frequency was chosen at 104.7 rad/sec (1000 rpm) and vibration forces were simulated by applying the vibration force (*f_4*) files to the AMB system to see how the diagnosis and correction scheme reacts.

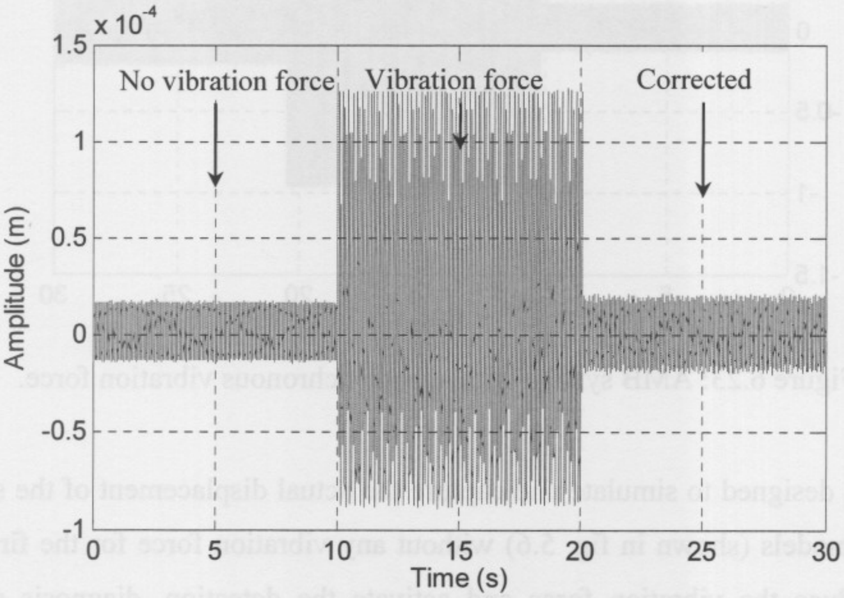

Figure 6.21: AMB system with subsynchronous vibration force.

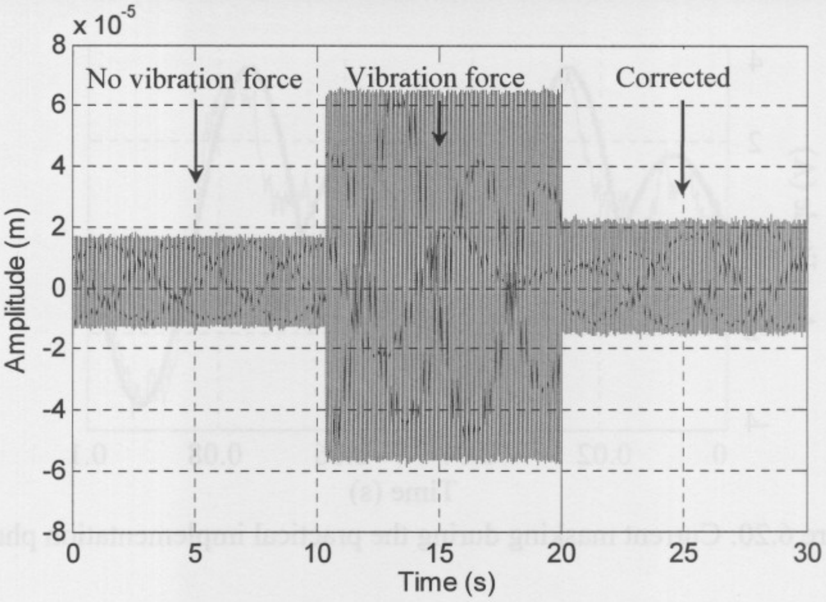

Figure 6.22: AMB system with rotor synchronous vibration force.

The displacement (x_p) of the AMB system with subsynchronous and rotor synchronous vibration forces can be seen in figure 6.22 and figure 6.21, respectively. Figure 6.23 provides the displacement with a supersynchronous vibration force.

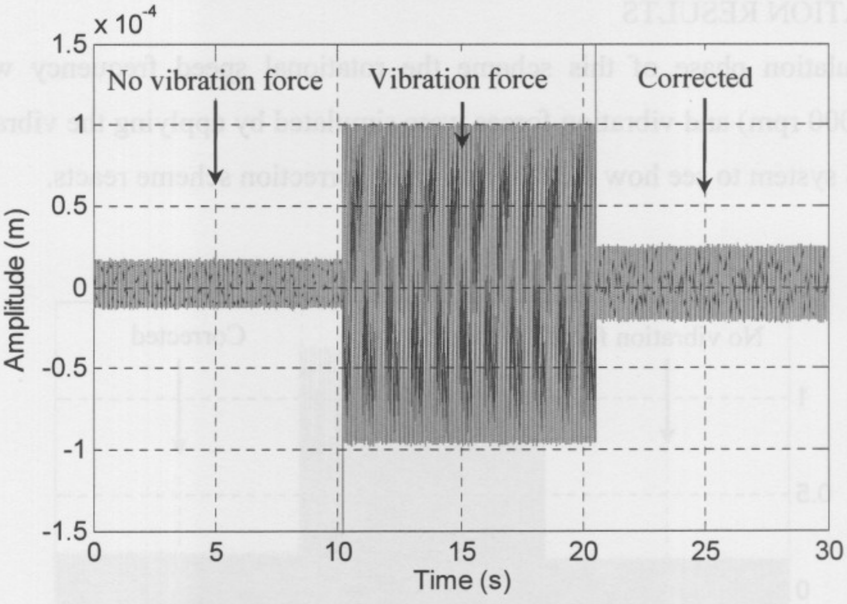

Figure 6.23: AMB system with supersynchronous vibration force.

The scheme was designed to simulate and capture the actual displacement of the simulation and practical AMB models (shown in fig. 5.6) without any vibration force for the first 10 seconds, thereafter to induce the vibration force and activate the detection, diagnosis and correction scheme after 20 seconds.

6.4.2. EXPERIMENTAL RESULTS

During the practical implementation phase of this scheme, the rotor speed was held constant at 1000 rpm and vibration forces were applied by implementing the reference current fault (I_f) files to the AMB system to see how the diagnosis and correction reacts.

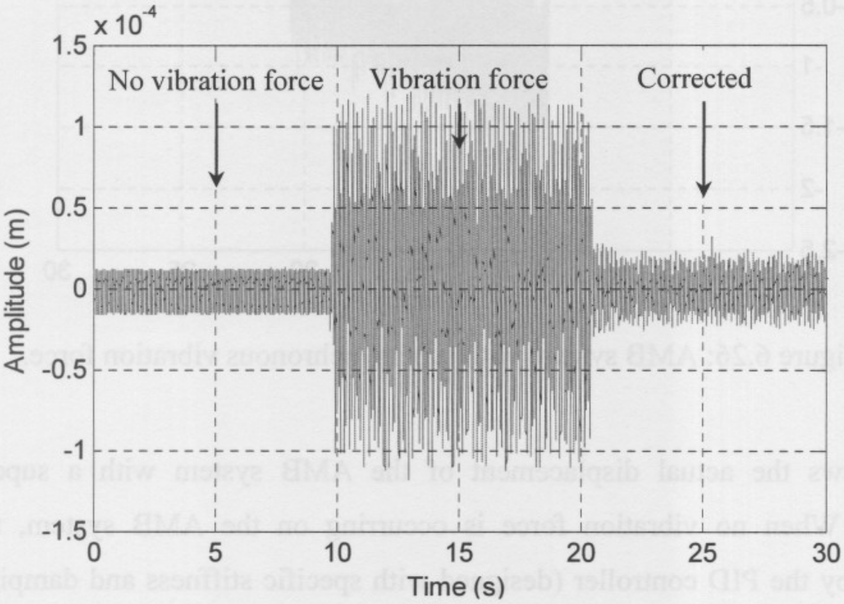

Figure 6.24: AMB system with subsynchronous vibration force.

Figure 6.24 and figure 6.25 show the actual displacement (x_p) of the AMB system with subsynchronous and rotor synchronous vibration forces, respectively.

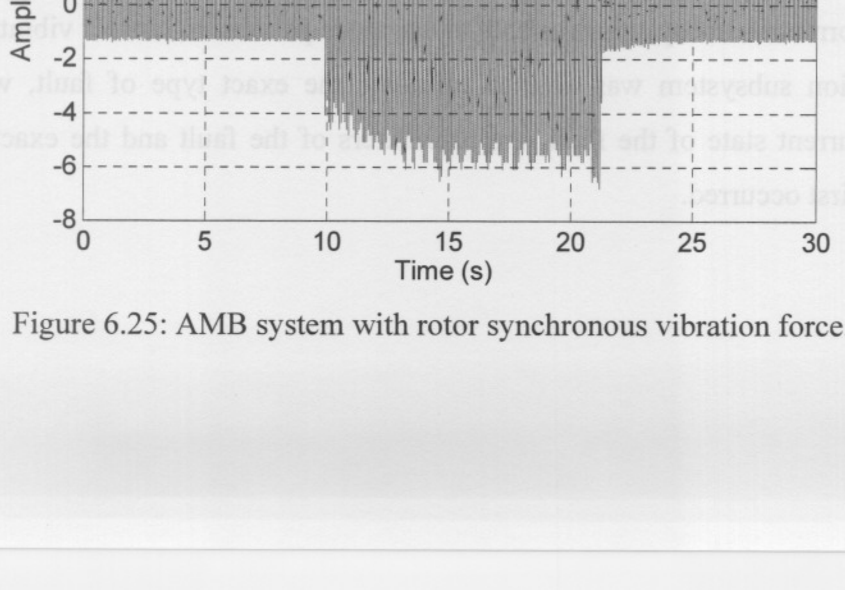

Figure 6.25: AMB system with rotor synchronous vibration force.

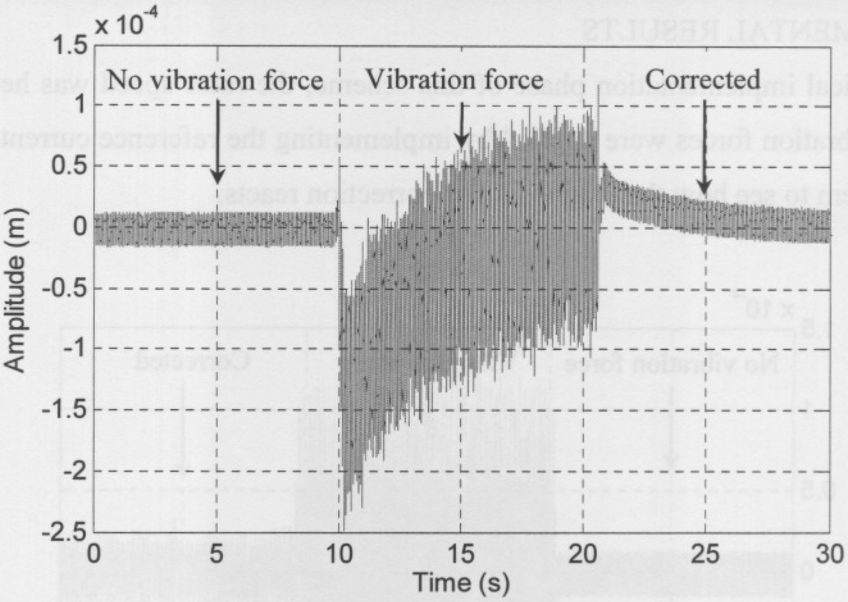

Figure 6.26: AMB system with supersynchronous vibration force.

Figure 6.26 shows the actual displacement of the AMB system with a supersynchronous vibration force. When no vibration force is occurring on the AMB system, the system is suspended only by the PID controller (designed with specific stiffness and damping). From the above figures it can be seen that the practical AMB system provides even better results than the simulation AMB model.

6.5. CONCLUSION

The scheme presented in this chapter focussed on current analysis, correction and identification of vibration forces on the rotor of an AMB system. The experimental results of the double radial AMB test rack correlated with the simulated results and vibration forces were corrected or minimised to a stable operating condition.

The pattern construction subsystem was able to construct new and combination patterns and the diagnosis and correction subsystem was able to use these patterns to correct vibration forces. The fault identification subsystem was able to calculate the exact type of fault, where the fault occurred, the current state of the fault, the parameters of the fault and the exact day and time when the fault first occurred.

The current limit of the power amplifiers and the run-time of the DSP processors were the two main limitations of this scheme. During normal operation of the double radial AMB, the power amplifiers require 4 ampere, which only leaves 6 ampere for fault application and correctional purposes.

Due to the complexity of the detection, diagnosis and correctional scheme, a lot of processing time was required, which caused run-time errors during real-time implementation on the dSPACE® controller. This problem was solved by implementing an additional dSPACE® controller.

The methods and implementation of predictive simulation, model validation and test implementation were shown here to be useful for detection, diagnosis and correction of vibration forces on the rotor of the AMB system. A list of additional information applicable to this chapter can be found in appendix G.

CHAPTER 7

DESIGN OF THE REAL-TIME MULTIPLE FREQUENCY FAULT DETECTION, CORRECTION AND IDENTIFICATION SCHEME

7.1. INTRODUCTION

This chapter provides the design of the real-time multiple frequency fault detection, correction and identification scheme. As mentioned in chapter 1, the design of the real-time scheme in this chapter is the third of the three real-time detection, correction and identification schemes.

This scheme uses the available sensors and actuators to perform multiple frequency fault detection and correction of vibration forces on the rotor of a rotational AMB. The detection subsystem constitutes displacement masking and feature extraction performed by the Wigner-Ville distribution (WVD). The diagnosis and correction subsystem constitutes pattern recognition and fuzzy logic.

The same two AMB systems used in chapters 5 and 6 were used in this scheme. The historical fault datasets and vibration forces on the rotor of the AMB systems are the same as defined in chapter 5.

7.2. SCHEME DEVELOPMENT

The following section explains the scheme development process of the real-time multiple frequency fault detection, diagnosis and correction scheme. The vibration force detection process is the same as used in chapter 6 (figure 6.1), except current masking is replaced with displacement masking. At start up the AMB system is suspended only with PID controllers and rotated at the desired speed of 1000 rpm.

Displacement masking is performed during the initial period when no vibration forces are occurring on the AMB system. The rotational speed of the rotor is used as input to the displacement masking process. The masked displacement is stored to memory.

When a vibration force occurs on the rotor (and when the PID controller fails to correct the vibration), the scheme detects the fault (vibration force) and calculates the vibration error, frequency and pattern. The stored no fault displacement is used to calculate the vibration error. Data fitting is then performed on the vibration error and masked displacement.

The fault identification subsystem identifies the fault according to the result obtained from the data fitting, vibration error, frequency and pattern. The frequency and pattern are sent to the fault diagnosis and error correction subsystems, which calculate the correction currents needed to stabilize the rotor. Correction forces are applied on the rotor by increasing or decreasing the reference currents i_{ref_1} and i_{ref_2} according to the direction of the vibration force.

Figure 7.1 provides an overview of the detection, diagnosis, correction and identification scheme that was implemented on the double radial AMB test rack. The fault detection subsystem uses the displacement (x_p) to detect the vibration forces on the AMB system and calculates the displacement error (e) and frequencies (B_1, B_2 and B_3) through a process of displacement masking.

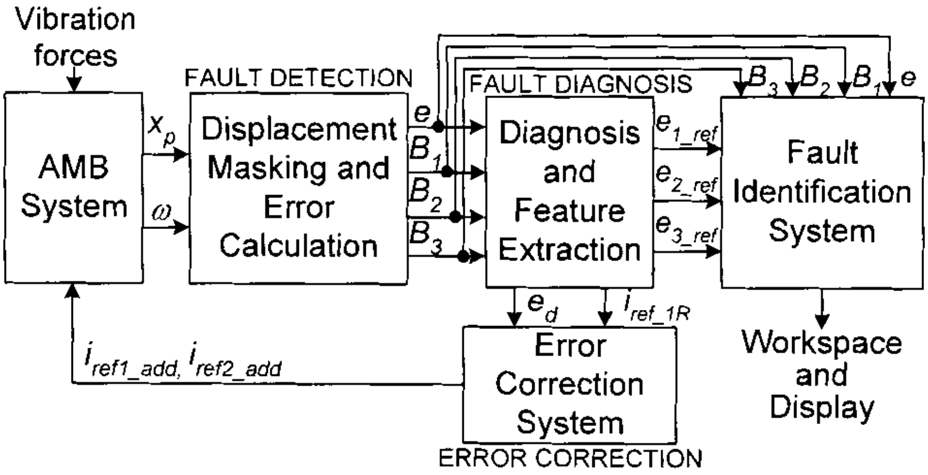

Figure 7.1: Detection, diagnosis, correction and identification scheme.

The parameters B_1, B_2 and B_3 represent three different frequencies obtained from the displacement error. This scheme focus on the analysis of only three frequencies, since a maximum of three frequencies were obtained simultaneously in the historical fault data of the water cooling AMB pump. The fault detection subsystem is explained in section 7.2.1.

After a fault has been detected, the error (e) and frequencies (B_1, B_2 and B_3) are sent to the fault diagnosis subsystem, where feature extraction is performed. The fault diagnosis subsystem is explained in section 7.2.2.

The error correction subsystem uses the diagnosis output error (e_d) and the workforce relation current (i_{ref_1R}) as features to stabilize the rotor by inducing correction forces on the rotor. The error correction subsystem is explained in section 7.2.2.

The parameters $i_{ref\_1\_add}$ and $i_{ref\_2\_add}$ represents the correction reference currents for the top and bottom magnetic bearings, respectively. The fault identification subsystem uses the displacement error (e), historical database errors (e_{1_ref}, e_{2_ref} and e_{3_ref}) and the frequencies (B_1, B_2 and B_3) to identify the vibration force. The fault identification subsystem is explained in section 7.2.3.

The same simulation and practical AMB models (for application of vibration forces on the rotor of the AMB systems) described in section 5.3.2 were used during the design of the real-time multiple frequency fault detection, correction and identification scheme of this chapter.

7.2.1 FAULT DETECTION SUBSYSTEM

The fault detection subsystem (shown in figure 7.2) constitutes displacement masking, error calculation and parameter calculation. Displacement masking is performed by capturing one cycle of the displacement (x_p) during a no fault condition of the AMB system. A sine wave representation of the no fault displacement (x_{mp}) is obtained and stored to memory. This process is done only once and when no vibration force is occurring on the AMB system.

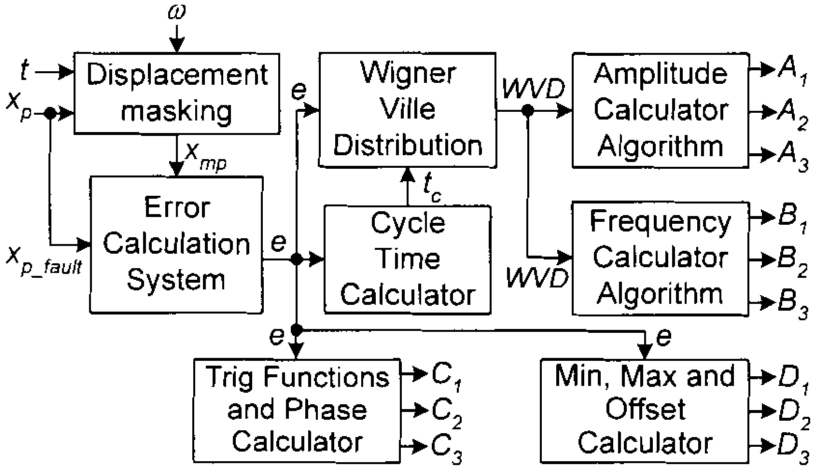

Figure 7.2: Fault detection subsystem.

When a fault occurs in the AMB system, the displacement (x_p) is called the fault displacement (x_{p_fault}). The no fault displacement (x_{mp}) is subtracted from the fault displacement (x_{p_fault}) to provide the displacement error (e).

When there is a sudden change in the rotational speed frequency (ω) of the rotor, the frequency of the no fault displacement (x_{mp}) is changed to compensate for the change. The displacement masking process during the practical implementation process is discussed in section 7.3.

The phase of the displacement error (e) was calculated by using trigonometrical functions and a phase calculator algorithm and divided the phase equally between C_1, C_2 and C_3. The offset was calculated from the maximum and minimum values of the displacement error (e) and an offset calculator algorithm and divided the offset equally between D_1, D_2 and D_3. The same process was used to calculate the phases and offsets of the reference displacement errors in the historical fault database.

The WVD was calculated by using (4.48) and the frequencies (B_1, B_2 and B_3) were calculated from the WVD and a frequency calculator algorithm. The accuracy of the frequency was improved by increasing the sampling time of the WVD to twice the cycle time (t_c) of the error signal (e).

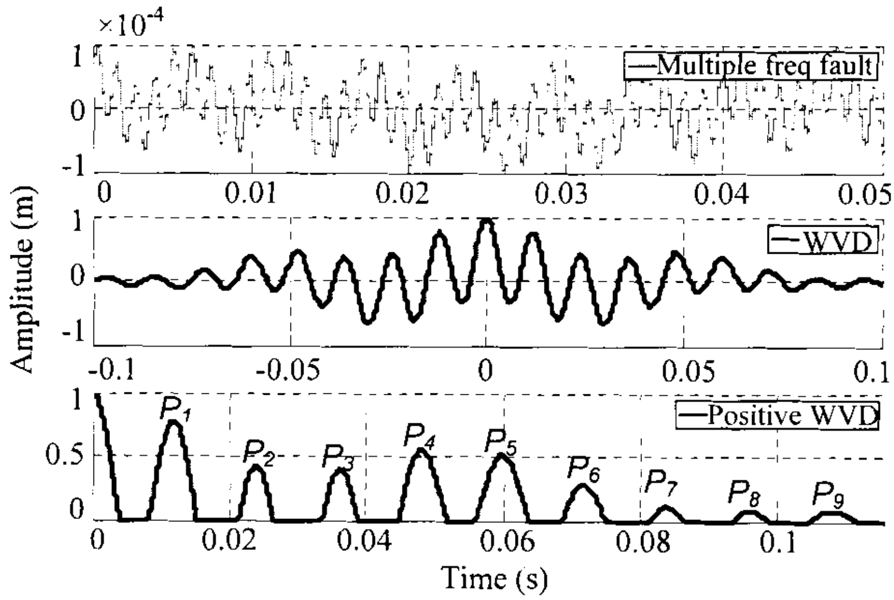

Figure 7.3: Multiple frequency fault calculation with the WVD.

Figure 7.3 provides the WVD spectrum of a multiple frequency fault. The historical fault data obtained from the 250 kW water cooling AMB pump was used during the WVD calculation. The WVD was calculated from the displacement error (e) and the peaks P_1 to P_9 was obtained from the positive peaks of the WVD as shown in figure 7.3.

Table 7.1 provides the values of the peaks shown in figure 7.3. The historical fault data of the 250 kW water cooling AMB pump was used during the frequency calculation process.

Table 7.1: Peak calculation with the WVD

PARAMETER	AMPLITUDE (m)	PERIOD (s)	DESCRIPTION
P_1	7.781×10^{-1}	1.200×10^{-2}	1st freq. comp. (highest)
P_2	4.338×10^{-1}	2.410×10^{-2}	2nd freq. comp.
P_3	3.921×10^{-1}	3.680×10^{-2}	3rd freq. comp. (lowest)
P_4	5.553×10^{-1}	4.811×10^{-2}	Same period as 2nd comp.
P_5	5.154×10^{-1}	5.980×10^{-2}	Multiple added freq.
P_6	2.792×10^{-1}	7.292×10^{-2}	Same period as 3rd comp.
P_7	1.067×10^{-1}	8.353×10^{-2}	Multiple added freq.
P_8	7.705×10^{-2}	9.631×10^{-2}	Same period as 2nd comp.
P_9	7.903×10^{-2}	1.098×10^{-1}	Same period as 3rd comp.

The amplitudes (A_1, A_2 and A_3) are calculated from peaks P_1, P_2 and P_3 at 0.098 mm, 0.055 mm and 0.049 mm, respectively. The amplitude values were calculated by multiplying the corresponding peak with the amplitude of the multiple frequency displacement error (e). From peak P_1 the frequency B_1 was calculated at 83.3 Hz.

Frequency B_2 was calculated from P_2, P_5 and P_7 as follows:

$$B_2 = \left| 2^{(1/2)}\frac{1}{P_2} - 2^{(3/5)}\frac{1}{P_5} - 2^{(3/7)}\frac{1}{P_7} \right| = 17.2\,\text{Hz} \tag{7.1}$$

Frequency B_3 was calculated from P_3, P_5 and P_7 as follows:

$$B_3 = \left| 2^{(1/3)}\frac{1}{P_3} - 2^{(2/5)}\frac{1}{P_5} - 2^{(2/7)}\frac{1}{P_7} \right| = 2.4\,\text{Hz} \tag{7.2}$$

The accuracy of frequency B_2 was calculated as follows:

$$B_{2\_accuracy} = \frac{16\cdot P_2}{4\cdot P_4 + 2\cdot P_8} = 1.001 \tag{7.3}$$

The accuracy of frequency B_3 was calculated as follows:

$$B_{3\_accuracy} = \frac{12\cdot P_3}{3\cdot P_6 + 2\cdot P_9} = 1.007 \tag{7.4}$$

From table 7.1 it can be seen that P_4 and P_8 are multiples of the second peak (P_2) and P_6 and P_9 are multiples of the third peak (P_3). These peaks provide an estimate of the error on peaks P_2 and P_3, respectively. From (7.3) the accuracy of B_2 is 99.9 % and from (7.4) the accuracy of B_3 is 99.3 %.

7.2.2 FAULT DIAGNOSIS AND CORRECTION SUBSYSTEM

This section discusses the fault diagnosis and correction subsystem, shown in figure 7.4. An error pattern component calculator subsystem uses the parameters (A, B, C and D) obtained from the fault detection subsystem to construct displacement error patterns e_{r1_pat}, e_{r2_pat} and e_{r3_pat}.

The pattern recognition subsystem calls (e_{call1}) the reference displacement errors from the database at specific frequencies (B_1, B_2 and B_3). The pattern recognition subsystem then compares the displacement error patterns (e_{r1_pat}, e_{r2_pat} and e_{r3_pat}) of the real-time AMB system with the reference displacement error patterns (e_{1_ref}, e_{2_ref} and e_{3_ref}) of the historical fault database. The same process used to calculate the displacement error patterns e_{r1_pat}, e_{r2_pat} and e_{r3_pat} was used to calculate the reference displacement error patterns e_{1_ref}, e_{2_ref} and e_{3_ref}.

When a fault occurs without a recognizable pattern, the pattern is band-pass filtered (centre frequency being the error frequencies B_1, B_2 and B_3) and stored to the historical fault database. The parameters e_{1_c}, e_{2_c} and e_{3_c} refer to the constructed patterns for frequencies B_1, B_2 and B_3, respectively.

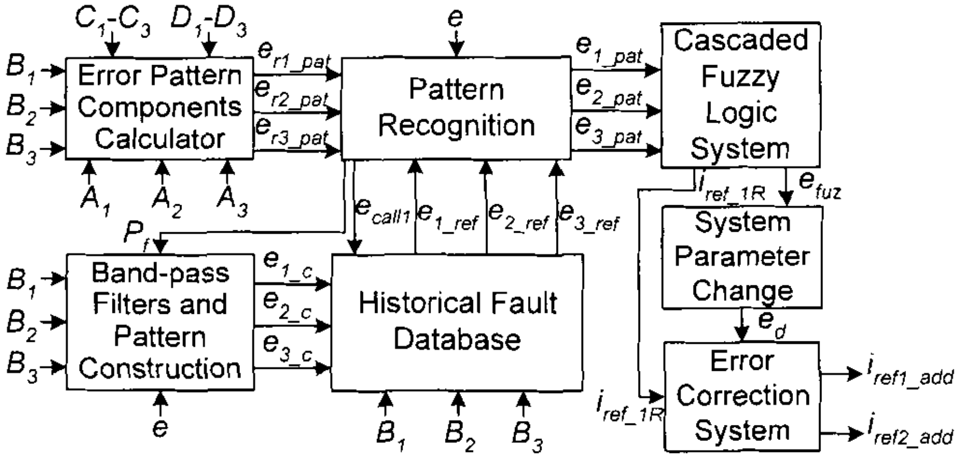

Figure 7.4: Fault diagnosis and correction subsystem.

Figure 7.5 shows the process diagram of the pattern recognition subsystem. The subsystem tests the difference between the real-time displacement error patterns (e_{r1_pat}, e_{r2_pat} and e_{r3_pat}) and the reference displacement error patterns (e_{1_ref}, e_{2_ref} and e_{3_ref}) from the historical fault database.

If the error difference is big, the error obtained from the real-time AMB system is used for correctional purposes. At this stage no recognizable pattern exists and the pattern construction subsystem constructs and stores a new pattern.

When the error difference is small (close to zero), the subsystem calculates the frequency and closest pattern to the available real-time data. If the frequency stays constant, the subsystem uses the closest pattern to correct the fault. If the frequency changes the subsystem tests the data in the historical fault database for a possible combination pattern.

When no combination of the available data is found, the subsystem uses the real-time error to correct the fault. A new pattern is constructed and stored to the database and the pattern calculation process is repeated. If the subsystem finds a combination pattern, the subsystem uses the pattern and stores the pattern as a combination pattern.

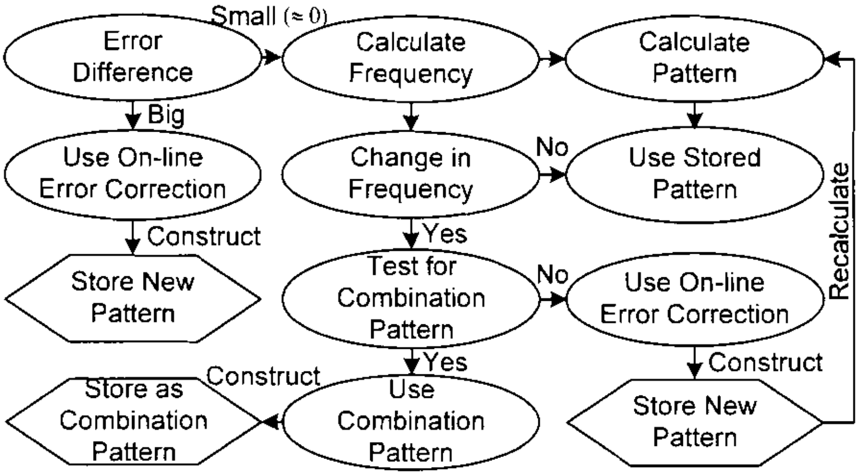

Figure 7.5: Process diagram of the pattern recognition subsystem.

The construction subsystem constructs and stores new patterns (e_{1_c}, e_{2_c} and e_{3_c}) according to the displacement error (e), when it receives a pattern fault (P_f) from the pattern recognition subsystems. The more faults occur in the AMB system, the more new correctional data becomes available. The subsystem is able to switch between different patterns and train itself to react on faults that are a combination of the available fault data.

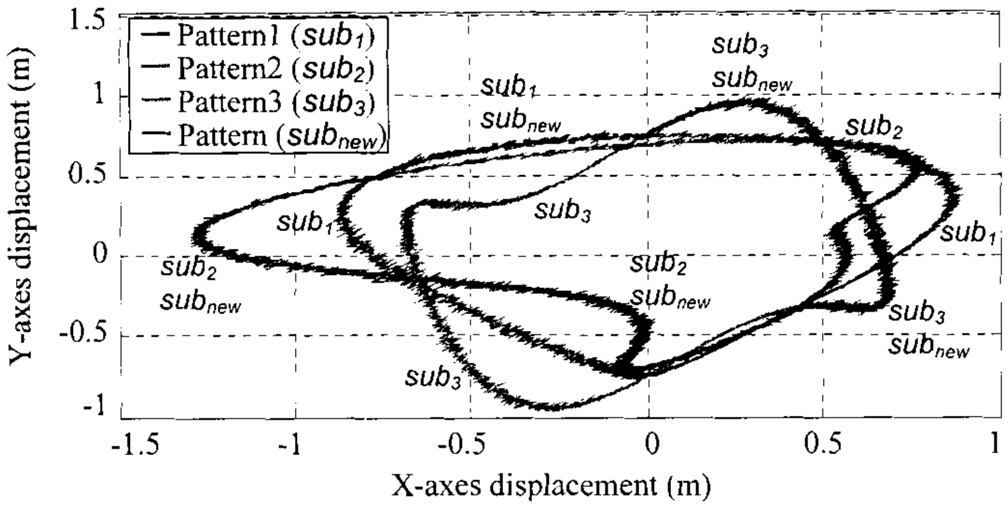

Figure 7.6: Orbital representation of the subsynchronous vibration force correctional pattern errors.

A displacement orbital representation of three subsynchronous vibration force correctional patterns is shown in figure 7.6. Pattern sub_{new} is a trained pattern which consists of pieces of three subsynchronous vibration force correctional patterns sub_1, sub_2 and sub_3. The pattern sub_{new} was stored as a combination pattern and decreased the vibration forces on the rotor of the AMB system. For each of the patterns in the historical fault database there exist a frequency and description.

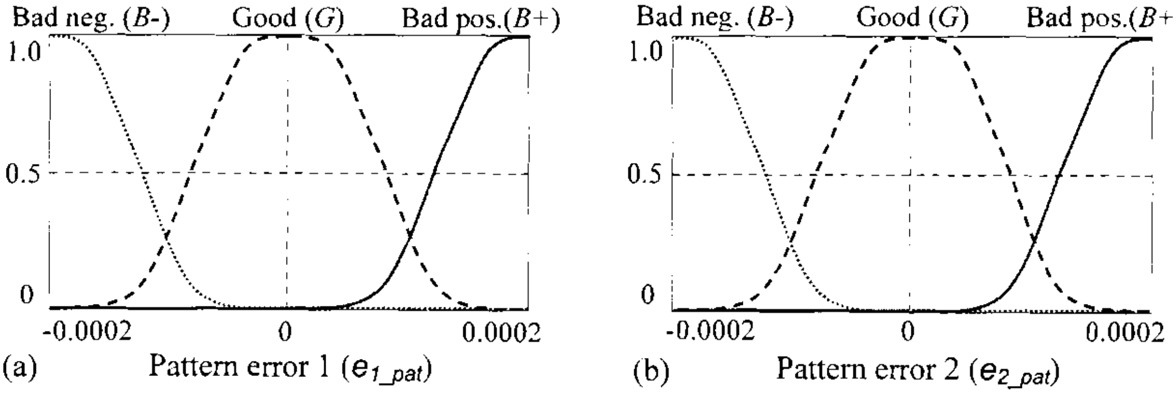

Figure 7.7: Fuzzy membership functions for (a) pattern error 1 and (b) pattern error 2

Figure 7.7 provides the fuzzy membership functions for pattern error 1 (e_{1_pat}) and pattern error 2 (e_{2_pat}). Fuzzification is performed by using the overlapping fuzzy sets bad negative (B-), good (G) and bad positive (B+). The membership function for pattern error 3 is the same as for pattern error 1.

Table 7.2: Rule matrix for fuzzy1 error (e_{fuz1}) and relation current1 (i_{ref_1R1})

e_{fuz1}		e_{1_pat}		
		B+	*G*	*B-*
e_{2_pat}	*B+*	*P*	*M*	*M*
	G.	*M*	*M*	*M*
	B-	*M*	*M*	*N*

i_{ref_1R1}		e_{1_pat}		
		B+	*G*	*B-*
e_{2_pat}	*B+*	*B*	*B*	*B*
	G	*B*	*M*	*B*
	B-	*B*	*B*	*T*

The basic rule for using the features (e_{1_pat} and e_{2_pat}) is: IF e_{1_pat} AND e_{2_pat} THEN e_{fuz1}. The same rule applies for variable i_{ref_1R1}. Table 7.2 provides the rule matrix for fuzzy1 error e_{fuz1} and relation current1 i_{ref_1R1}.

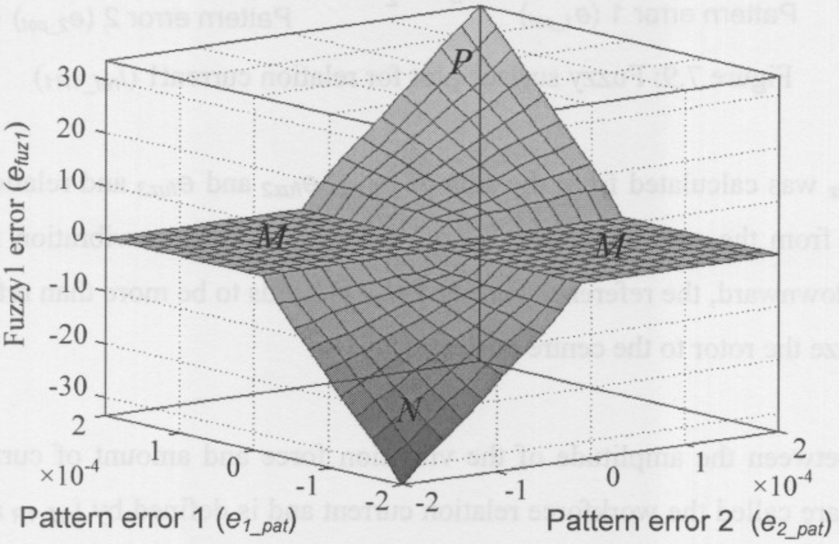

Figure 7.8: Fuzzy surface plot for fuzzy1 error (e_{fuz1})

The fuzzy surface plots for fuzzy1 error (e_{fuz1}) and relation current1 (i_{ref_1R1}) are shown in figure 7.8 and figure 7.9, respectively. Defuzzification of the fuzzy membership functions e_{fuz1} and i_{ref_1R1} are performed by using overlapping fuzzy sets negative (*N*), middle (*M*) and positive (*P*) and bottom (*B*), middle (*M*) and top (*T*), respectively.

Diagnosis of the whole system results in a complex set of rule bases, which was simplified by using a cascaded fuzzy logic module [52]. The displacement pattern errors (e_{1_pat}, e_{2_pat} and e_{3_pat}) are the inputs of the cascaded fuzzy logic module and fuzzy error (e_{fuz}) and relation current (i_{ref_1R}) are the outputs. The fuzzy surface plots for fuzzy2 error (e_{fuz2}) and fuzzy3 error (e_{fuz3}) are the same as shown in figure 7.8 and the fuzzy surface plots for relation current2 (i_{ref_1R2}) and relation current3 (i_{ref_1R3}) are the same as shown in figure 7.9.

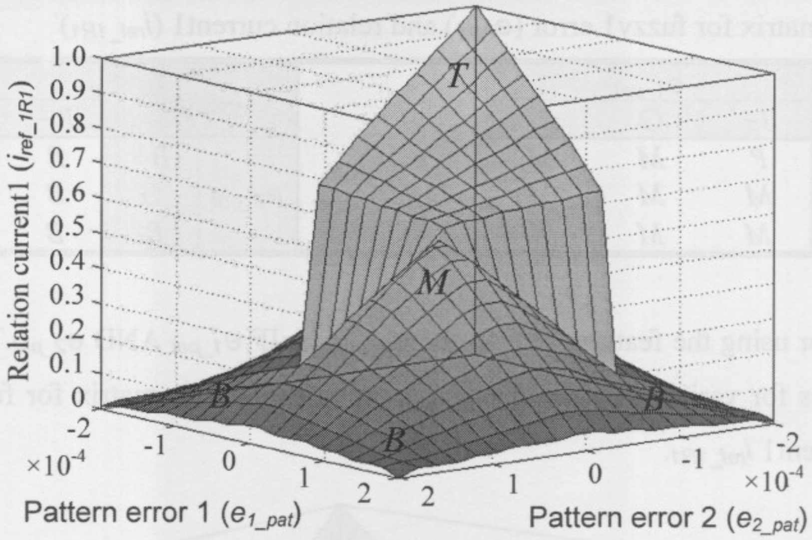

Figure 7.9: Fuzzy surface plot for relation current1 (i_{ref_1R1})

Fuzzy error e_{fuz} was calculated from the sum of e_{fuz1}, e_{fuz2} and e_{fuz3} and relation current i_{ref_1R} was calculated from the sum of i_{ref_1R1}, i_{ref_1R2} and i_{ref_1R3}. When a vibration force causes the rotor to move downward, the reference current 1 (i_{ref_1}) needs to be more than reference current 2 (i_{ref_2}) to stabilize the rotor to the centre position.

This relation between the amplitude of the vibration force and amount of current required by each amplifier are called the workforce relation current and is defined by i_{ref_1R} and i_{ref_2R}. i_{ref_1R} refer to the workforce relation current for the top power amplifier and i_{ref_2R} refer to the workforce relation current for the bottom power amplifier.

Workforce relation current 2 was calculated as follows:

$$i_{ref\_2R} = 1.0 - i_{ref\_1R} \tag{7.5}$$

The workforce relation current serves as an amplifier (booster) and increases or decreases the amplitude of the correction force according to the error made on the current. These increases and decreases of the correct amplifiers, causes faster correction force response times.

System parameter change of phase shifting was performed on the fuzzy current error (e_{fuz}), before send to the error correction subsystem. The fuzzy current error is then called the diagnosis output error (e_d).

Correctional reference current 1 was calculated as follows:

$$i_{ref1\_add} = i_{ref\_1R} {}^{*} e_d \tag{7.6}$$

The correctional reference current 1 is added to reference current 1 (i_{ref_1}). Correctional reference current 2 was calculated as follows:

$$i_{ref2\_add} = -i_{ref\_2R}{}^{*}e_d \tag{7.7}$$

The correctional reference current 2 is added to reference current 2 (i_{ref_2}).

7.2.3 FAULT IDENTIFICATION SUBSYSTEM

A process diagram of the fault identification subsystem is shown in figure 7.10. When no fault (no vibration) is detected, the identification subsystem provides no output. When a fault (vibration) is detected, the subsystem uses the frequency to determine to which frequency dataset (subsynchronous, rotor synchronous or supersynchronous) the fault (vibration force) belongs. This process was performed on all the displacement error patterns received from the real-time AMB system.

The subsystem performs data fitting to calculate the best possible fit of the historical fault data in the specific dataset with the data obtained from the practical AMB system. If the frequency rapidly changes from one dataset to another, the subsystem saves the output, predicts the closest type of fault (unbalance, misalignment, foundation looseness or as otherwise specified in the historical fault database) and recalculates the fault in the new dataset.

When the frequency stays within a certain dataset, the subsystem is set to repeatedly calculate the average error over a time period of 1 second. The time period was calculated at five times the period of the masked displacement at 1000 rpm. The type of fault is allocated the fault in the dataset with the smallest error over the available time period.

After the type of fault is stored, the subsystem displays the parameters of the fault and determines the vibratory level and zone of the fault. The subsystem determines the side and axes where the fault occurs from the displacement error signals.

Faults are allocated to the A-side and B-side and can occur in the x, y and z axes. The identification subsystem was limited to the A-side and the y-axes, due to the installation of the roller bearing on the B-side and the limitation in the sampling time of the dSPACE® controller. The day and time when the fault first occurred is saved and displayed.

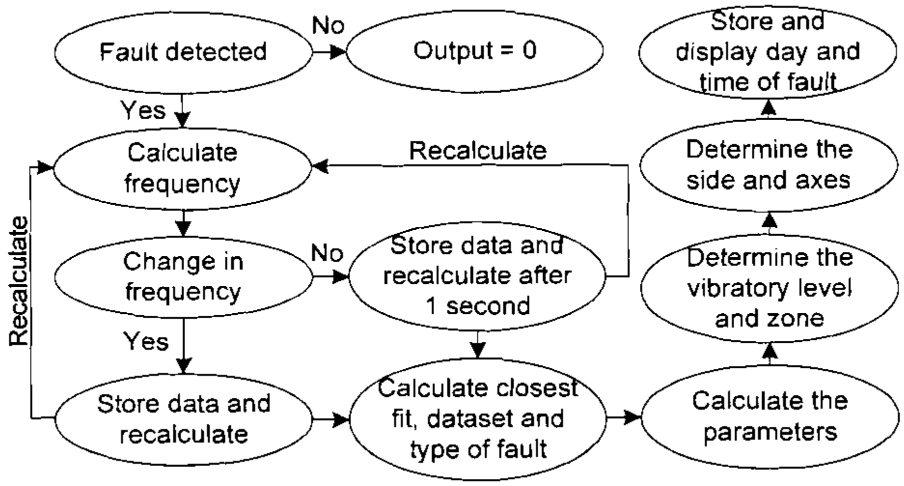

Figure 7.10: Process diagram of the fault identification subsystem.

Figure 7.11 shows the parameter diagram of the fault identification subsystem used to calculate the type of fault, parameters of the fault, the vibratory level of the fault, zone of the fault, where the fault occurs and the day and time when the fault first occurred.

The data fitting system calculates and compares the best possible fit of the displacement error patterns (e_{r1_pat}, e_{r2_pat} and e_{r3_pat}) of the real-time AMB system with the reference displacement error patterns (e_{1_ref}, e_{2_ref} and e_{3_ref}) of the historical fault database. The data fitting system sends the number of the dataset (N_{fit}) with the closest fit and the accuracy of the fit (A_{fit}) to the diagnostic subsystem.

The historical fault database provides the diagnostic subsystem with the type of fault (F_{data}). The output is displayed as a percentage fit to a specific dataset and the corresponding fault in the dataset. Each time the identification subsystem recalculates the fault the parameters A, B, C and D are saved as the output parameters of the fault.

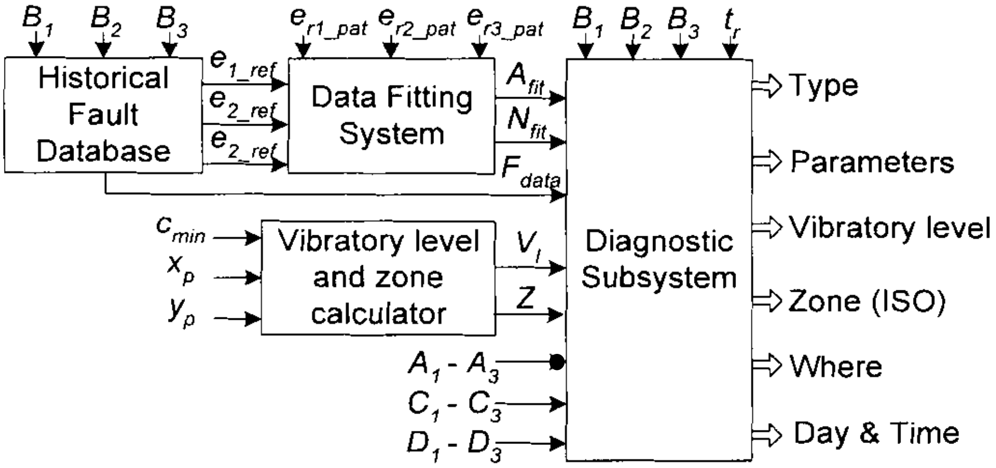

Figure 7.11: Fault identification subsystem.

The signals from the displacement transducers indicate the rotor journal position including the d.c. component (eccentricity) and a.c. component (vibration orbit) as shown in figure 7.12. Eccentricities from the clearance centre of the AMB (designated O-O_j) in the x and y directions are designated ε_x, ε_y, while the vibration orbit amplitudes in the x and y directions are designated α_x, α_y. The maximum peak displacement (D_{max}) of the rotor from the clearance centre of the radial AMB, is calculated as follows [69], [71]:

$$D_{max} = \max\left[\sqrt{x_p^2 + y_p^2}\right] \tag{7.8}$$

or approximated by (7.9), based on the orbit observation:

$$D_{max} \approx \sqrt{x_{max}^2 + y_{max}^2} \tag{7.9}$$

where $x_{max} = \varepsilon_x + \alpha_x$ and $y_{max} = \varepsilon_y + \alpha_y$

This formula to estimate the maximum displacement in a certain direction will generally overestimate the exact value with a maximum error of approximately 40 %. As a simpler procedure, the maximum value of the displacement values measured in two orthogonal directions is recommended as shown in figure 7.12, based on the waveform observation [64]:

$$D_{max} \geq \max\left[x_{max}, y_{max}\right] \tag{7.10}$$

In order to avoid contact problems between the rotor and stators, the following formula should be satisfied with a certain margin against the minimum radial clearance $C_{min\text{-}radial}$:

$$D_{max} < C_{min-radial} \tag{7.11}$$

The ratio between the minimum radial clearance (C_{min}) and the maximum peak displacement (D_{max}) as defined in accordance with ISO 14839-2 was used to determine the vibratory zone [71].

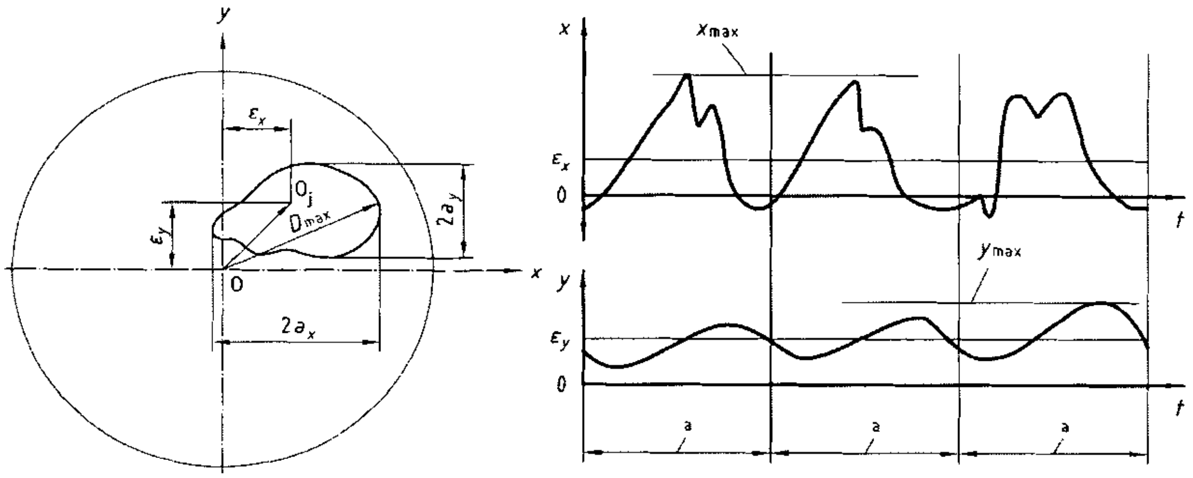

a) Orbit b) Vibration time history

Figure 7.12: Unfiltered shaft orbit and vibration time history [71].

The international standard for mechanical vibration of rotating machinery defines four zones [71]: A) vibratory displacement of newly commissioned machines, B) where the vibratory displacement is acceptable for unrestricted long-term operation, C) where the vibratory displacement is unsatisfactory for long-term continuous operation and D) the vibratory displacement causes severe damage to the machine. These zones (Z) were used to identify the vibratory level (V_l) of faults, during the identification process.

Table 7.3: Recommended criteria of zone limits [71]

ZONE LIMIT	DISPLACEMENT (D_{max})
A/B	$< 0.3\ C_{min}$
B/C	$< 0.4\ C_{min}$
C/D	$< 0.5\ C_{min}$

C_{min} is the minimum value of radial or axial clearance between the rotor and stator.

The zone table for magnetic bearings, established from international experience, is given in table 7.3 and the graphical descriptions are provided in figure 7.13. The parameter X represent the minimum radial clearance (C_{min}) in micrometers, the parameter Y represent the peak displacement (D_{max}) in micrometers and the parameter a represent to the ratio D_{max}/C_{min}.

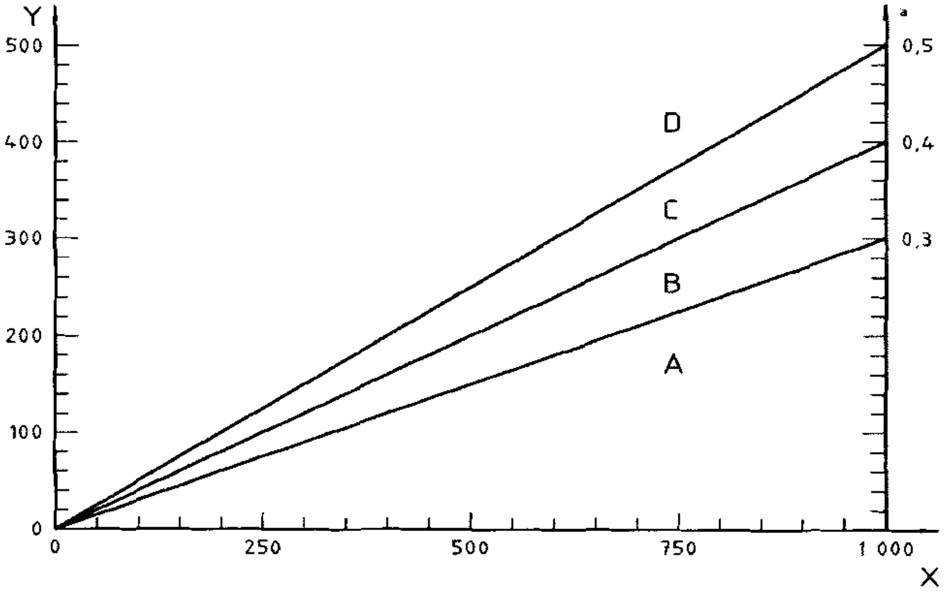

Figure 7.13: Zone limits for vibration criteria [71]

The minimum radial clearance (C_{min}) is defined as the minimum gap when statically moving the rotor in any radial direction. The retainer bearing gap is generally set to be C_{min} by design [65]. The side and axes with the largest displacement error indicates where the fault (vibration force) causes the most damage. The exact time when the fault first occurred was saved and displayed and was calculated from the running time (t_r).

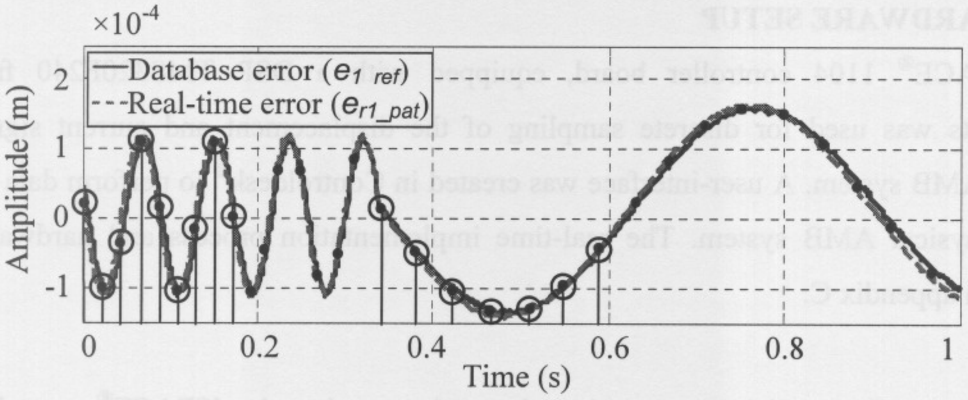

Figure 7.14: Supersynchronous with sudden change to subsynchronous vibration force data fitting.

Figure 7.14 displays data fitting where the frequency of the fault changed from the supersynchronous vibration force area to the subsynchronous vibration force area. The solid lines represent the reference displacement error pattern (e_{1_ref}) from the historical fault database of the water cooling AMB pump and the dashed lines represent the real-time displacement error pattern (e_{r1_pat}) from the double radial AMB test rack. Sampling (shown by the markers) was decreased when the frequency entered the subsynchronous vibration force area.

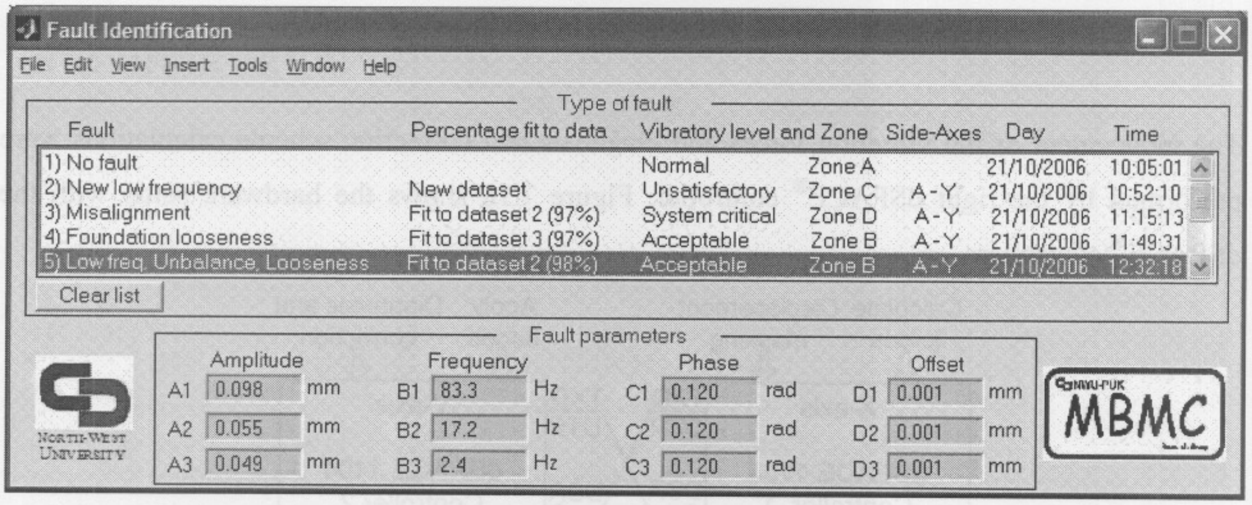

Type of fault

Fault	Percentage fit to data	Vibratory level and Zone		Side-Axes	Day	Time
1) No fault		Normal	Zone A		21/10/2006	10:05:01
2) New low frequency	New dataset	Unsatisfactory	Zone C	A-Y	21/10/2006	10:52:10
3) Misalignment	Fit to dataset 2 (97%)	System critical	Zone D	A-Y	21/10/2006	11:15:13
4) Foundation looseness	Fit to dataset 3 (97%)	Acceptable	Zone B	A-Y	21/10/2006	11:49:31
5) Low freq. Unbalance, Looseness	Fit to dataset 2 (98%)	Acceptable	Zone B	A-Y	21/10/2006	12:32:18

Fault parameters

Amplitude	Frequency	Phase	Offset
A1 0.098 mm	B1 83.3 Hz	C1 0.120 rad	D1 0.001 mm
A2 0.055 mm	B2 17.2 Hz	C2 0.120 rad	D2 0.001 mm
A3 0.049 mm	B3 2.4 Hz	C3 0.120 rad	D3 0.001 mm

Figure 7.15: Screenshot of the fault identification program.

Figure 7.15 shows a screenshot of the fault identification program written in MATLAB®. This program calculates and displays the parameters of the fault identification subsystem of figure 7.11. Faults (vibration forces) are calculated and displayed as a specific type of fault (misalignment, foundation looseness, unbalance or as otherwise specified in the historical fault database), fault fit to a specific dataset, vibratory level (normal, acceptable, system critical or unsatisfactory), vibratory zone (A-D), side where the fault occurs (A-side or B-side), axes where the fault occurs (x, y or z-axes) and day and time when the fault first occurred. The parameters (amplitude, frequency, phase and offset) of the different faults (vibration forces) are also shown.

7.3. HARDWARE SETUP

The dSPACE® 1104 controller board, equipped with a DSP TMS320F240 from Texas Instruments was used for discrete sampling of the displacement and current signals of the physical AMB system. A user-interface was created in Controldesk® to perform data acquisition on the physical AMB system. The real-time implementation process and hardware setup is detailed in appendix C.

Due to the complexity of the control, detection and correction, the dSPACE® controller was not able to handle all the instructions and real-time errors occurred. This problem was solved by implementing two dSPACE® 1104 controller boards, one for each axis of the magnetic bearing. A roller bearing was installed on the right side of the rotor. This lead to an increase in the sampling time of the DSP, since only one side has to be suspended.

The vibration force calculations, displacement masking process and speed sensor calculations were performed by the left dSPACE® controller and communicated to the other dSPACE® controller via serial communication.

The inducement of the vibration forces and diagnosis and correction scheme calculations were performed by the right dSPACE® controller. Figure 7.16 shows the hardware setup with the dSPACE® controllers.

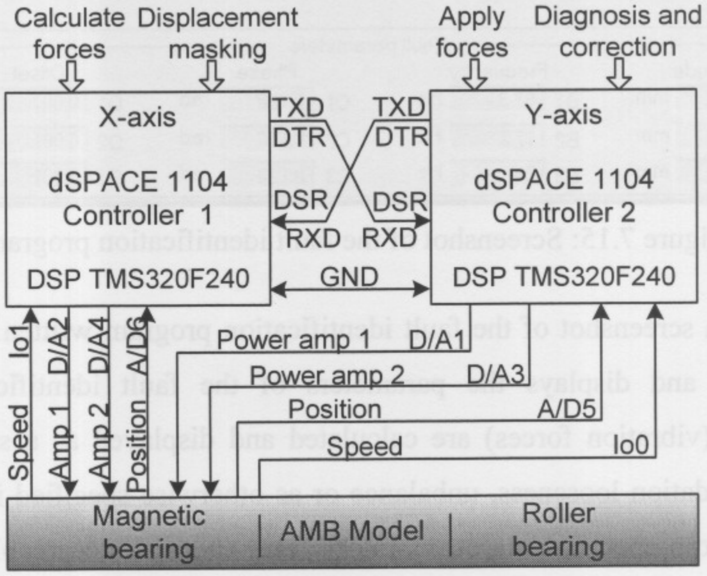

Figure 7.16: Hardware setup with the dSPACE® controllers.

During the investigation of the displacement signals of the double radial AMB system, it became evident that synchronous vibrations were introduced by the roller bearing when the rotor was rotating. These vibrations were therefore incorporated in the displacement masking and correctional patterns calculation process of the fault detection and diagnosis subsystems (discussed in sections 7.2.1 and 7.2.2).

Figure 7.17 shows the masked displacement (x_{mp}) and the actual displacement (x_p) during the practical implementation phase. The no fault displacement (x_{mp}) was subtracted from the fault displacement (x_{p_fault}) to provide the displacement error (e). The amplitude of the displacement (x_p) and the frequency (ω) obtained from the rotational speed of the rotor was used as scaling factors for the masked displacement. When the amplitude and frequency increased, the amplitudes and frequencies of the individual signals in the masked displacement were also increased.

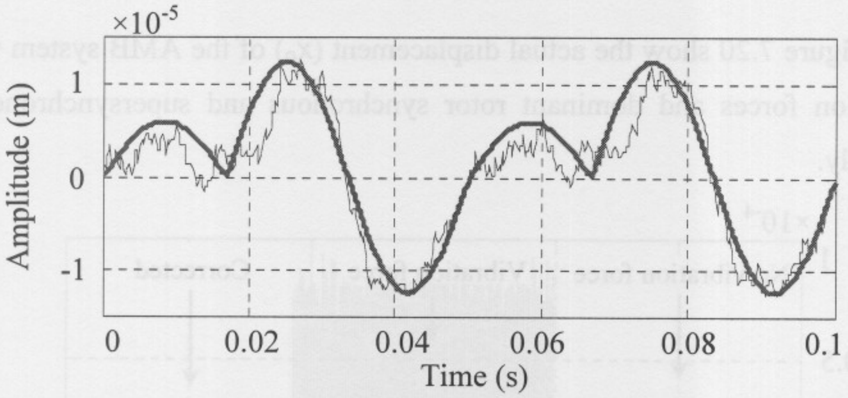

Figure 7.17: Displacement masking during the practical implementation phase.

7.4. SIMULATION VERIFICATION

7.4.1. SIMULATION RESULTS

This section provides the simulated and experimental results of the double radial AMB test rack, with multiple frequency vibration forces and dominant subsynchronous, rotor synchronous and supersynchronous vibration forces. During the simulation phase of this scheme the rotational speed frequency was chosen at 104.7 rad/sec (1000 rpm) and faults were induced by applying the vibration force (f_4) files onto the AMB system to see how the diagnosis and correction scheme reacts.

Figure 7.18 shows the actual displacement of the AMB system with multiple frequency vibration forces and dominant subsynchronous vibration force.

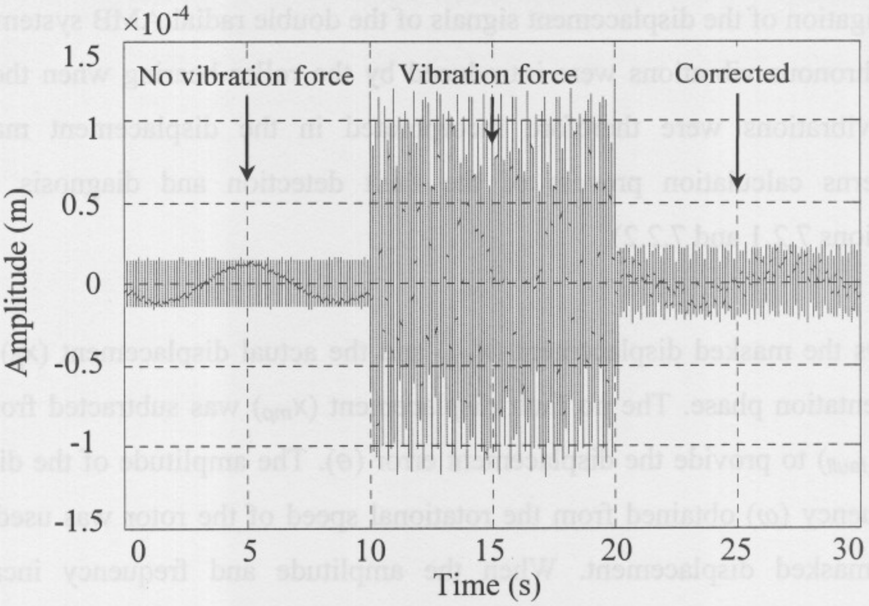

Figure 7.18: Multiple frequency vibration forces with dominant subsynchronous vibration forces.

Figure 7.19 and figure 7.20 show the actual displacement (x_p) of the AMB system with multiple frequency vibration forces and dominant rotor synchronous and supersynchronous vibration forces, respectively.

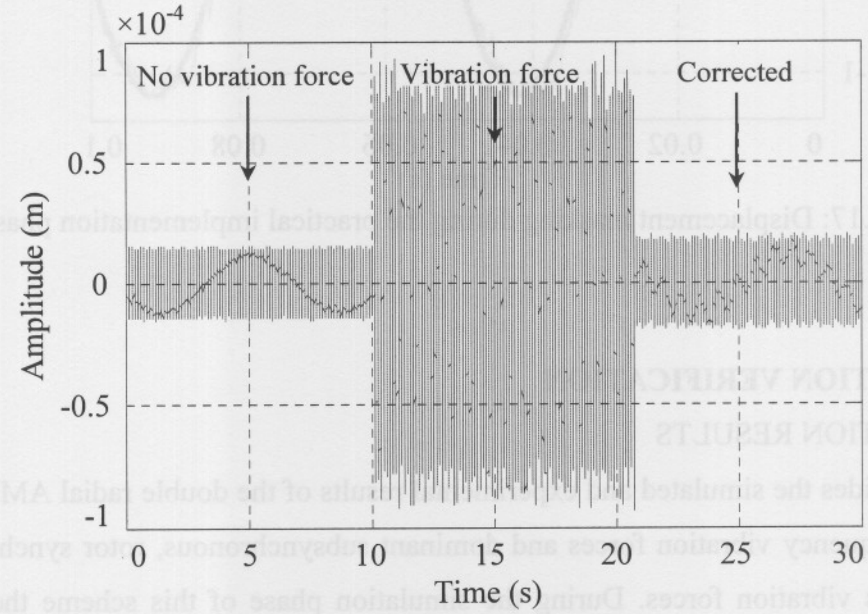

Figure 7.19: Multiple frequency vibration forces with dominant rotor synchronous vibration force.

The scheme was designed to simulate and capture the actual displacement of the simulation and practical AMB models (shown in fig. 5.6) without any vibration force for the first 10 seconds, thereafter to induce the vibration force and activate the detection, diagnosis and correction scheme after 20 seconds.

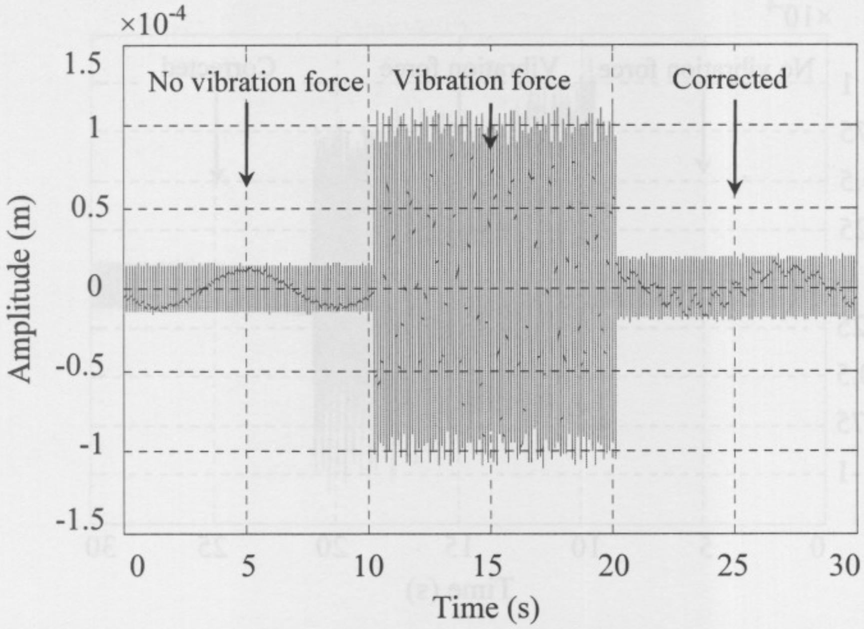

Figure 7.20: Multiple frequency vibration forces with dominant supersynchronous vibration force.

7.4.2. EXPERIMENTAL RESULTS

During the practical implementation phase of this scheme the rotor speed was held constant at 1000 rpm and vibration forces were applied by implementing the reference current fault (i_f) files onto the AMB system to see how the diagnosis and correction scheme reacts.

The displacement (x_p) of the AMB system with subsynchronous and rotor synchronous vibration forces can be seen in figure 7.21 and figure 7.22, respectively. Figure 7.23 provides the displacement with a supersynchronous vibration force.

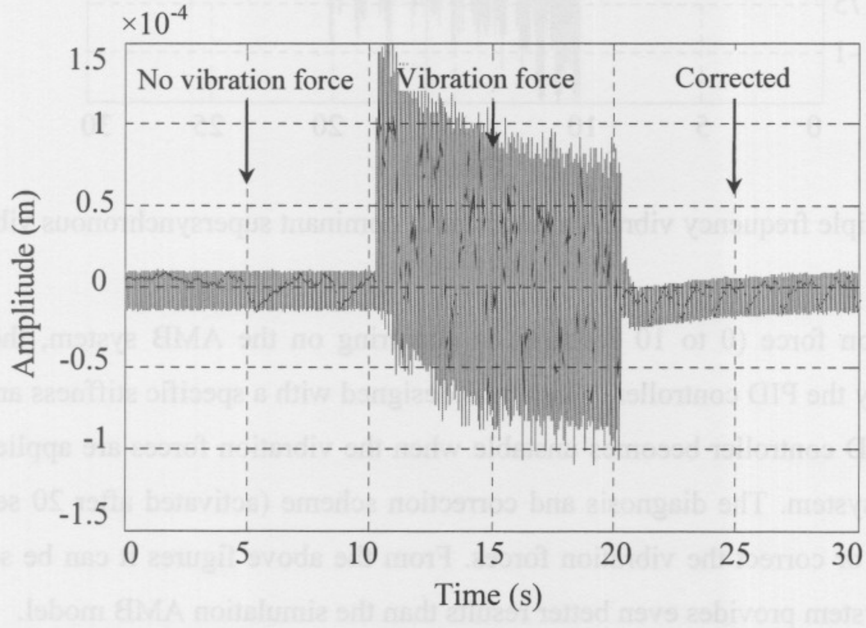

Figure 7.21: Multiple frequency vibration forces with dominant subsynchronous vibration force.

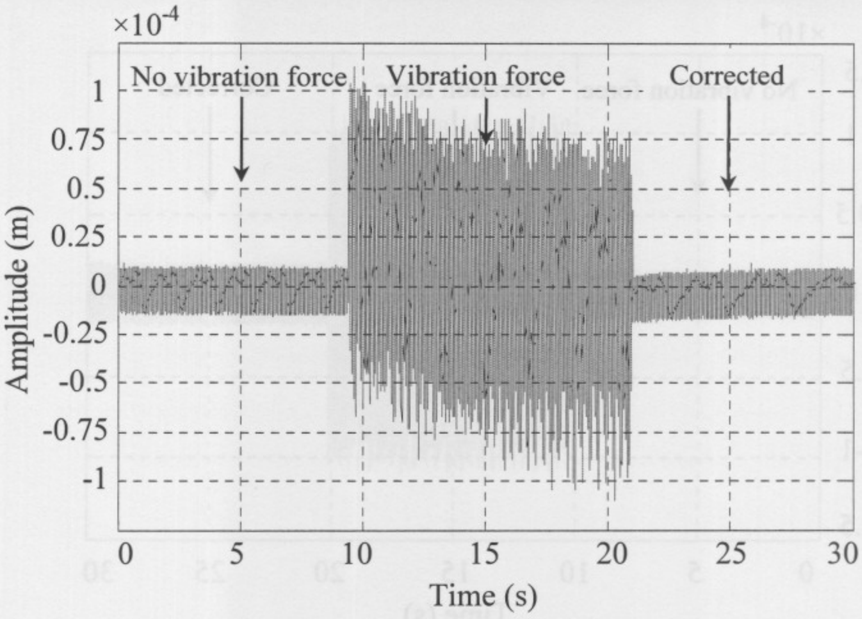

Figure 7.22: Multiple frequency vibration forces with dominant rotor synchronous vibration force.

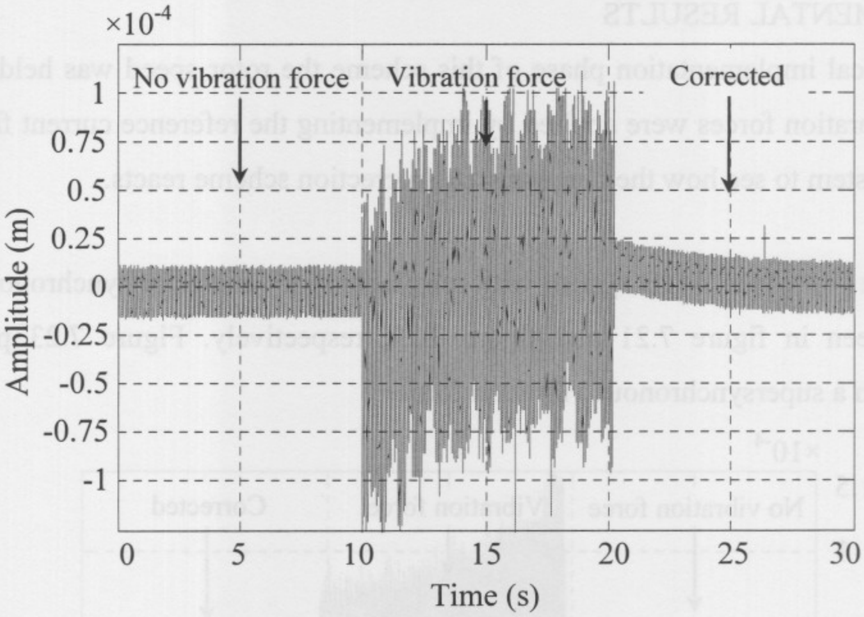

Figure 7.23: Multiple frequency vibration forces with dominant supersynchronous vibration force.

When no vibration force (0 to 10 seconds) is occurring on the AMB system, the system is suspended only by the PID controller, which was designed with a specific stiffness and damping. The optimised PID controller becomes unstable when the vibration forces are applied (10 to 20 seconds) on the system. The diagnosis and correction scheme (activated after 20 seconds) was able to minimise or correct the vibration forces. From the above figures it can be seen that the practical AMB system provides even better results than the simulation AMB model.

7.5. CONCLUSION

The scheme presented in this chapter focused on the detection, correction and identification of multiple frequency vibration forces on the rotor of an AMB system. The pattern construction subsystem was able to construct new and combination patterns and the diagnosis and correction scheme was able to use these patterns to correct vibration (disturbance) forces.

The fault identification subsystem was able to calculate the type of fault, the parameters of the fault, the vibratory level of the fault, the fault zone, where the fault occurred and the exact day and time when the fault first occurred. The implementation of the cascaded fuzzy logic module simplified the fault diagnosis and correction scheme and decreased the calculation time.
The experimental results of the double radial AMB test rack correlated with the simulated results and vibration forces was corrected or minimized to a stable operating condition.

The complexity of the detection, diagnosis and correctional scheme required a lot of processing time, which caused run-time errors during real-time implementation. This problem was solved by implementing an additional dSPACE® controller.

The current limit of the power amplifiers and the run-time of the DSP processors were the two main limitations of this scheme. During normal operation of the double radial AMB, the power amplifiers require 4 ampere, which only leaves 6 ampere for fault inducement and correctional purposes.

The methods and implementation of predictive simulation, model validation and test implementation were shown here to be useful in the detection, diagnosis, correction and identification of vibration forces on the rotor of the AMB system. A list of additional information applicable to this chapter is available in appendix G.

CHAPTER 8

CONCLUSIONS

8.1. INTRODUCTION

This chapter provides a comparative evaluation of the three real-time schemes, closure on the contribution of this thesis and detail on future research. The purpose of the research is to benchmark condition monitoring of AMB systems and present the reader with an illustration of real-time condition monitoring of AMB systems.

Various fault detection techniques were implemented on the historical fault data of the 250 kW water cooling AMB pump. This was done to obtain the best technique for a specific fault condition. These techniques were used in the design of the three real-time detection, diagnosis, correction and identification schemes for vibration forces on the rotor of a rotational AMB system. More detail on the contribution of the three real-time schemes is available in section 8.3.

8.2. COMPARATIVE EVALUATION OF THE REAL-TIME SCHEMES

In this section the three real-time schemes are compared. The results provided in the simulation verification sections (sections 5.6, 6.4 and 7.4) of chapters 5, 6 and 7 are used to calculate the improvement each scheme has over the optimised PID controller when vibration forces are applied. Table 8.1 provides the calculations for the displacement improvement of the three schemes. In this table the simulation and experimental results of the different schemes are compared. The designations V1, V2 and V3 represent the subsynchronous, rotor synchronous and supersynchronous vibration forces, respectively.

The measures 'no vibration (peak-peak)' and 'vibration force (peak-peak)' refer to the peak-to-peak displacement of the rotor without and with vibration forces applied, respectively. During this time the PID controller is active in the system, but fails to correct the vibration force. The measure 'corrected (peak-peak)' refers to the peak-to-peak displacement of the rotor when a real-time scheme is implemented.

Table 8.1: Comparison of the three real-time schemes.

		Scheme 1		Scheme 2		Scheme 3	
		Simulated	Experimental	Simulated	Experimental	Simulated	Experimental
No vibration (peak-peak) (µm)	V1	26.541	28.037	26.541	29.475	26.541	24.238
	V2	26.541	25.191	26.541	27.281	26.541	25.670
	V3	26.541	23.185	26.541	27.607	26.541	26.478
Vibration force (peak-peak) (µm)	V1	206.846	187.429	206.846	225.586	232.973	218.018
	V2	173.297	184.033	173.297	166.774	179.127	187.957
	V3	213.431	181.148	213.431	226.978	219.938	218.150
Corrected (peak-peak) (µm)	V1	43.241	34.579	41.287	40.895	39.885	34.358
	V2	31.631	29.573	38.010	27.558	38.616	34.775
	V3	39.234	24.551	31.099	31.951	43.109	34.854
Vibration relation	V1	7.793	6.685	7.793	7.653	8.778	8.995
	V2	6.529	7.305	6.529	6.113	6.749	7.322
	V3	8.042	7.813	8.042	8.222	8.287	8.239
Correction relation	V1	1.629	1.233	1.556	1.387	1.503	1.417
	V2	1.192	1.174	1.432	1.010	1.455	1.355
	V3	1.478	1.059	1.172	1.157	1.624	1.316
Improvement (%)	V1	616.4	545.2	632.7	626.6	727.5	757.8
	V2	533.7	613.1	509.7	510.3	529.4	596.7
	V3	656.4	675.4	687.0	706.5	666.3	692.3
Avg. Improvement		602.2	611.2	606.8	614.5	641.1	682.3

The vibration relation refers to the relation between the 'vibration force' and 'no vibration' parameters and is calculated by dividing the 'vibration force' by the 'no vibration'. The correction relation refers to the relation between the 'correction' and 'no vibration' parameters and is calculated by dividing the 'corrected' parameter by the 'no vibration' parameter. The improvement refers to the improvement each scheme has over the PID controller and is calculated by subtracting the correction relation from the vibration relation. The average improvement refers to the improvement obtained by the scheme for all three vibration forces (V1, V2 and V3).

The differences between the simulation and experimental results of table 8.1 are due to variations in the rotational speed of the rotor. In the practical system the rotational speed varied with the application of vibration forces on the rotor. In the simulation model the rotational speed was kept constant. Multiple frequency vibration forces with dominant subsynchronous, rotor synchronous and supersynchronous vibration forces were applied to the system to evaluate scheme 3, therefore the difference in the simulated vibration force (peak-peak) results of this scheme compared to the other two schemes.

From the real-time displacement analysis, correction and identification scheme (discussed in chapter 5) it can be seen that the experimental subsynchronous (shown in figure 5.29) and rotor synchronous (shown in figure 5.30) vibration force results correlated well with the simulated subsynchronous (shown in figure 5.26) and rotor synchronous (shown in figure 5.27) vibration force results during the correction phase. A time delay is noticeable when comparing the experimental supersynchronous vibration force results (shown in figure 5.31) with the simulated results (shown in figure 5.28). The experimental vibration force results do however suffer from noise.

From the real-time current analysis, correction and identification scheme (discussed in chapter 6) it can be seen that the experimental subsynchronous (shown in figure 6.24) and rotor synchronous (shown in figure 6.25) vibration force results correlated well with the simulated subsynchronous (shown in figures 6.21) and rotor synchronous (shown in figures 6.22) vibration forces results, during the correction phase. A time delay is noticeable when comparing the experimental supersynchronous vibration force results (shown in figure 6.26) with the simulated results (shown in figure 6.23). The time delay to minimize the vibration force of the real-time current analysis scheme is smaller than that of the real-time displacement analysis scheme.

From the real-time multiple frequency fault detection, diagnosis and correction scheme (discussed in chapter 7) it can be seen that the experimental subsynchronous (shown in figure 7.21) and rotor synchronous (shown in figure 7.22) vibration force results correlated well with the simulated subsynchronous (shown in figure 7.18) and rotor synchronous (shown in figure 7.19) vibration force results, during the correction phase. A time delay is noticeable when comparing the experimental supersynchronous vibration force results (shown in figure 7.23) with the simulated results (shown in figure 7.20). The real-time multiple frequency scheme has a smaller time delay compared to the real-time current analysis scheme.

From table 8.1 it can be seen that scheme 3 provides the best results for improving subsynchronous vibration forces, scheme 1 the best for rotor synchronous vibration forces and scheme 2 the best for supersynchronous vibration forces. It must be taken into account that single frequency vibration forces were evaluated during the simulation verification section of schemes 1 and 2, but multiple frequency vibration forces were evaluated during the simulation verification section of scheme 3. Scheme 3 provides the best overall result with the best average improvement, followed by scheme 2 and then scheme 1.

The boundaries of the real-time displacement analysis scheme were designed as fixed boundaries, which provided useful results during the fault diagnosis phase. When comparing these fixed boundaries (shown in figure 5.9) with the trained patterns of the real-time current analysis scheme (shown in figure 6.8) and real-time multiple frequency fault detection scheme (shown in figure 7.6), a distinction can be made that these schemes must provide better overall results, which can be seen from the experimental results of these schemes (sections 5.6.2, 6.4.2 and 7.4.2).

All three real-time schemes were able to successfully correct or minimize the vibration forces to a stable operating condition. The real-time multiple frequency fault detection scheme (discussed in section 7.4) showed the best results with the smallest delay, least vibration in the correction phase and closest fit to the normal operating condition.

When comparing the fault identification programs for the three real-time schemes (shown in figures 5.25, 6.18 and 7.15), the fault identification program for the multiple frequency fault detection scheme clearly stands out, since it provides results on multiple frequency vibration forces. This multiple frequency analysis is not possible with the other two real-time schemes, which can cause the user to wrongly interpret the real-time vibration data. The identification subsystem for the last scheme evaluates vibration forces according to ISO vibratory standards, which is an international standard for vibration monitoring.

A comparative evaluation between the different fault detection techniques implemented on the historical fault data of the 250 kW water cooling AMB pump is available in appendix E.

8.3. UNIQUE CONTRIBUTION

The focus of this research is on external faults, since the area of internal faults to the magnetic bearing control system is well established and much research exists. Various schemes exist where off-line diagnosis and identification of internal and external faults are performed on AMB systems, but the area of real-time identification and correction of external faults still needed to be explored. This study therefore proposes three real-time detection, diagnosis, correction and identification schemes for external faults to the magnetic bearing control system of rotational AMB systems. These schemes use the available AMB sensors and actuators to perform condition monitoring and correction, since machine components in industrial applications are not always easily accessible to install condition monitoring equipment.

The last scheme focuses on real-time multiple frequency fault detection, diagnosis, correction and identification of external faults on rotational AMB systems, since more than one fault can occur simultaneously on the AMB system. Analysis of a multiple frequency fault by a single frequency fault scheme causes incorrect identification and correction of the fault.

The three real-time schemes provided knowledge on: 1) the implementation of historical fault data in a fault detection subsystem, 2) the implementation of fault detection techniques in real-time, 3) the real-time correction of vibration forces on the AMB system, 4) the real-time diagnosis and identification of fault features according to a historical fault database and ISO vibration standards and 5) the real-time detection, correction and identification of multiple frequency vibration forces.

Information on articles submitted for publication on each of the three real-time schemes are available in section 1.7. These articles encapsulate the contribution of this thesis. The designs of the three real-time schemes are available in chapters 5, 6 and 7.

8.4. FUTURE RESEARCH

The three real-time schemes only stabilize the rotor with respect to the stator and do not remove the vibration force. When correction forces are applied to the AMB system, to correct the effect of the vibration forces, it may increase the stresses in other critical components e.g. the power amplifiers and system base, which may cause components to be damaged or break down. These stressed components need to be identified by the user as critical or non-critical and the necessary steps must be taken to operate the AMB system under the fault condition or to shut down the system and repair the fault.

A scheme therefore needs to be explored which performs analysis on the complete system and incorporates component stress points (system base, connected machinery, connected components, etc.). Free-body diagrams and mass-spring-damper systems explaining the different fault conditions and different stress points (stressed components) on the AMB system is provided in appendix B.

The complexity of the real-time detection, diagnosis and correctional schemes required a lot of processing time, which caused run-time errors during real-time implementation. This problem was solved by implementing an additional dSPACE® controller. The performance of the three real-time schemes can be improved by using only one dSPACE® 1103 controller board, instead of two dSPACE® 1104 controller boards. The dSPACE® 1103 controller board will be capable of performing the task, without run-time errors. The specifications of the dSPACE® 1104 and dSPACE® 1103 controller boards are available on the CD. The real-time implementation and hardware setup of the dSPACE® controllers for the three schemes is available in sections 5.4, 6.3 and 7.4 and appendix C.

The maximum current capability and bandwidth of the power amplifiers, run-time of the DSP processors and bandwidth of the sensors were the main factors limiting the applicability of the real-time schemes. Since the power amplifiers and sensors were designed and specified for normal operational bandwidth, it was not possible to fully evaluate supersynchronous vibration forces. A scheme can therefore be developed which specifically identifies and corrects supersynchronous vibration forces by also including high frequency bandwidth components.

8.5. CLOSURE

The research performed in this thesis successfully demonstrates the inherent condition monitoring ability of systems with AMBs. Three real-time detection, diagnosis, correction and identification schemes for vibration forces on rotational AMB systems were successfully developed and tested. All three schemes successfully corrected and identified vibration forces on the rotor of the AMB system.

REFERENCES

[1] Aenis M. and Nordmann R., "Fault diagnosis in rotating machinery using active magnetic bearings," *Proc. 8th International Symposium on Magnetic Bearings*, Mito, Japan, pp. 125-132, Aug. 26-28, 2002.

[2] Aenis M., Knopf E., and Nordmann R., "Active magnetic bearings for the identification and fault diagnosis in turbomachinery," *Mechatronics*, vol. 12, 2002.

[3] Ahrens M., Kucera L., and Larsonneur R., "Performance of a magnetically suspended flywheel energy storage device," *IEEE Transactions on Control Systems Technology*, vol. 4, no. 5, pp. 494-502, Sep. 1996.

[4] Allaire P.E. and Maslen E.H., "Introduction to magnetic bearings," Mechanical and Aerospace Engineering Dept., University of Virginia, Charlottesville, 1997.

[5] Alaire P.E. and Knospe C.P., "Short course on magnetic bearings," Alexandria, Virginia, Aug. 19-20, 1997.

[6] Allaire P.E., "First magnetic bearings," Mechanical and Aerospace Engineering Dept., University of Virginia, Charlottesville, no. VA-22901, 1997.

[7] Allaire P.E., Maslen E.H., and Lewis D.W., "Magnetic thrust bearing operation and industrial pump application," Department of Mechanical, Aerospace and Nuclear Engineering, ROMAC Laboratory, Charlottesville, May 1997.

[8] Akansu A.N. and Haddad R.A., *Multiresolution signal decomposition*, Second Edition, Academic Press, 2001.

[9] Baillie D.C. and Mathew J., "A comparison of autoregressive modeling techniques for fault diagnosis of rolling element bearings," *Mechanical Systems and Signal Processing*, no. 10, pp. 1-17, 1996.

[10] Balbahadur A.C., "A thermo-elasto-hydrodynamic model of the Morton effect operating in overhung rotors supported by plain or tilting pad journal bearings," Faculty of the Virginia Polytechnic Institute and State University, Blacksburg, Virginia, Feb. 2001.

[11] Benbouzid M.E.H. and Nejjari H., "A simple fuzzy logic approach for induction motors stator condition monitoring," *International Electric Machines and Drives Conference (IEMDC)*, pp. 634-639, 2001.

[12] Bendat J.S. and Piersol A.G., *Random data, analysis and measurement procedures*, Second Edition, John Wiley & Sons Inc., 1986.

[13] Berry J.E., "How to specify machinery vibration spectral alarm bands," *Journal of Sound and Vibration*, Sep. 1990.

[14] Bishop C.M., *Neural networks for pattern recognition*, Oxford University Press, 1995.

[15] Black H.F., "Interaction of a whirling rotor with a vibrating stator across a clearance annulus," *Journal on Mech. Eng. Science, Trans. IFToMM*, vol. 10, pp. 1-12, 1968.

[16] Blanke M., Kinnaert M., Lunze J., and Staroswiecki M., *Diagnosis and fault-tolerant control*, Springer, p. 571, 2003.

[17] Bonaldo A.V., "Wavelet transform: algorithm based in fast Fourier transform," MSc. thesis, Mechanical Engineering Department, Federal University of Rio de Janeiro, 1993.

[18] Bonato B., Ceravolo R., de Stefano A., and Knaflitz M., "Bilinear time-frequency transformations in the analysis of damaged structures," *Mechanical Systems and Signal Processing*, no. 4, pp. 509-527, 1997.

[19] Brie D., "Spalled bearing vibration signal modelling," *Mechanical Systems and Signal Processing*, vol. 3, no. 14, pp. 353–369, May 2000.

[20] Britcher C., "Comparison of digital controllers used in magnetic suspension systems," *Proceedings of the UVA MAG conference*, 1991.

[21] Bucker H. P., "Comparison of FFT and Prony algorithms for bearing estimation of narrow-band signals in a realist ocean environment," *Journal. Acoust. Soc. Am.*, vol. 61, no. 3, pp. 756-762, 1977.

[22] Caccavale F. and Villani L., "Fault Diagnosis and Fault Tolerance for Mechatronic Systems," *Proc. Workshop at the IEEE Internat. Symposium on Intelligent Control*, Vancouver, Springer, p. 191, 2003.

[23] Chalifoux A. and Baird J., "Reliability centred maintenance (RCM) guide," USACERL Technical Report 99/41, Construction Engineering Research Laboratories, Apr. 1999.

[24] Chiollaz M. and Frave B., "Engine noise characterization with Wigner-Ville time-frequency analysis," *Mechanical Systems and Signal Processing*, vol. 7, no. 5, pp. 375-400, Academic Press, 1993.

[25] Chow M., Magnum M., and Sui O.Y., "A neural network approach to real-time condition monitoring of induction motors," *IEEE Transactions on Industrial Electronics*, vol. 38, no. 6, pp. 448-453, Dec. 1991.

[26] Cioffi J.M. and Kailath T., "Fast recursive-least-squares transversal filters for adaptive filtering," *IEEE Transactions on Acoustic, Speech, and Signal Processing*, vol. 32, no. 2, pp. 304-337, 1984.

[27] Cirstea M.N., Dinu A., and Khor J.G., *Neural and fuzzy logic control of drives and power systems*, Elsevier Science, 2002.

[28] Cohen L., "Time-frequency distributions - a review," *Proceedings of the IEEE*, vol. 77, no. 7, pp. 941-981, 1989.

[29] Cole M.O.T., Keogh P.S., Sahinkaya M.N., and Burrows C.R., "Towards fault-tolerant control of rotor-magnetic bearing systems," *IFAC Journal of Control Engineering Practice*, vol. 12, no. 4, pp. 491-501, 2004.

[30] Cole M.O.T., Keogh P.S., and Burrows C.R., "Predictions on the dynamic behaviour of a rolling element auxiliary bearing for rotor/AMB systems," *Proc. 8th Internat. Symposium on Magnetic Bearings*, Mito, Japan, pp. 501-506, Aug. 26-28, 2002.

[31] Cover T.M. and Thomas J.A., *Elements of information theory*, John Wiley & Sons Inc., 1991.

[32] Crenna F., Michelini R.C., and Rossi G.B., "Measuring vibration patterns for rotor diagnostics," *Proceedings of the Instrumentation and Measurement Technology Conference (IMTC-96)*, pp. 597–602, 1996.

[33] Diez D. and Schweitzer G., "Simulation, test and diagnostics integrated for a safety design of magnetic bearing prototypes," *Proc. IUTAM-Symposium*, ETH Zurich, Springer, pp. 51-62, 1989.

[34] Dorrell D.G., Thomson W.T., and Roach S., "Combined effects of static and dynamic eccentricity on airgap flux waves and the application of current monitoring to detect dynamic eccentricity in 3-phase induction motors," *Seventh International Conference on Electrical Machines and Drives*, pp. 151-155, 1995.

[35] Dolasa A.R., "Computer-aided design software for the undamped two-dimensional static and dynamic analysis of beams and rotors," Faculty of the Virginia Polytechnic Institute and State University, Blacksburg, Virginia, May 1998.

[36] Duda R.O., Stork D.G., and Hart P.E., *Pattern classification*, John Wiley & Sons Inc., ISBN: 0471056693, 2000.

[37] Duyar A., Eldem V., Merrill W., and Guo T.H., "Fault detection and diagnosis in propulsion system: A fault parameter estimation approach," *J. Guidance, Contr., Dynam.*, vol. 17, no. 1, pp. 104-108, 1994.

[38] Edwards S., Lees A.W., and Friswell M.I., "Experimental identification of excitation and support parameters of a flexible rotor-bearing-foundation system from a single run-down." Department of Mechanical Engineering, University of Wales, Swansea, November 1999.

[39] Eren L. and Devaney M.J., "Motor bearing damage detection via Wavelet analysis of the starting current moment," *IEEE Instrumentation and Measurement Technology Conference*, Hungary, Budabest, May 21-23, 2001.

[40] Ewins D.J., *Modal testing: theory and practice*, John Wiley & Sons Inc., 1995.

[41] Flandrin P., "Representation temps-fréquence de sinaux non-stationnaires," Traitement du Sinal, vol. 6, no. 2, pp. 89-101, 1989.

[42] Flandrin P. and Escudié B., "Principe et mise en oeuvre de L'analyse temps-fréquence par transformation de Wigner-Ville," Traitement du Sinal, vol. 2, no. 2, 1985.

[43] Forrester P.D., "Use of the Wigner Ville distribution in helicopter transmission fault detection," *Proceedings of the Australian Symposium on Signal Processing and Applications (ASSPA)*, 1989.

[44] Frank P.M., "Fault diagnosis in dynamic systems using analytical and knowledge-based redundancy – A survey and some new results," *Automatica*, vol. 26, no. 3, pp. 459-474, 1990.

[45] Fukunaga K., *Introduction to statistical pattern recognition*, Second Edition, Academic Press, 1990.

[46] Future Fibre Technologies Pty. Ltd., Machine condition monitoring. [Online]. Available: http://www.fft.com.au/index.htm, [Date of access: March 2005].

[47] Gahler C. and Mohler M., "Multivariable identification of active magnetic bearing systems," *JSME International Journal*, Series C, vol. 40, no. 4, 1997.

[48] Gouws R. and van Schoor G., "The development process of an axial active magnetic bearing," *Proceeding of the Fourteenth South African Universities Power Engineering Conference (SAUPEC'05)*, University of Witwatersrand, Johannesburg, South Africa, Jan. 2005.

[49] Green I., "Real-time monitoring and control of mechanical face seal dynamic behavior," The George W. Woodruff School of Mechanical Engineering, Georgia Institute of Technology, Aug. 2000.

[50] Habetler T.G., "On-line condition monitoring and diagnostics of electric machines," School of Electrical and Computer Engineering, Power Electronics and Motor Diagnostics Laboratory, Georgia Institute of Technology.

[51] Habetler T.G. and Harley R.G., "Diagnostics and intelligent controls in electrical systems," Power Electronics and Motor Diagnostics Laboratory, Georgia Institute of Technology, Feb. 2004.

[52] Hampel R., Wagenknecht M., and Chaker N., *Fuzzy control: Theory and practice*, Berlin: Springer Verlag, Sep. 2000.

[53] Haykin S., *Neural networks: A comprehensive foundation*, Macmillan, 1994.

[54] Hertzog R., Buhler P., Gahler C., and Larsonneur R., "Unbalance compensation using generalized notch filters in the multivariable feedback of magnetic bearings," *IEEE Transactions on Control Systems Technology*, vol. 4, no. 5, pp. 580-586, Sep. 1996.

[55] Ho D. and Randall R.B., "Optimisation of bearing diagnostic techniques using simulated and actual bearing fault signals," *Mechanical Systems and Signal Processing*, vol. 5, no. 14, pp. 763–788, 2000.

[56] Hoffman A.J. and Tollig C.J.A., "Neural network recognition of partial discharge signals," *Proceedings of the Seventh South African Universities Power Engineering Conference*, University of Stellenbosch, South Africa, Jan. 1997.

[57] Hoffman A.J. and van der Merwe N.T., "A comparative evaluation of neural classification techniques for identifying multiple fault conditions," *Proceedings of the 5th WSEAS International Conference on Circuits, Systems, Communications and Computers (CSCC)*, pp. 209–214, Greece, July 2001.

[58] Honkanen T., "Modelling industrial maintenance systems and the effects of automatic condition monitoring," Helsinki University of technology, Feb. 2004.

[59] Hultman A. and Eriksson M.L., The attraction of magnetic bearings. [Online]. Available: http://www.evolution.skf.com/gb/article.asp, [Date of access: March 2005].

[60] Ifeachor E.C. and Jervis B.W., *Digital signal processing: A practical approach*, Addison-Wesley, 1993.

[61] Islam H.M. and Mostafa M.G., "Novel microprocessor based negative phase current relay and meter," *Electrical Power and Energy Systems*, vol. 18, no. 8, pp. 547-552, 1996.

[62] Isaksson J.L., "On the dynamics of a rotor interacting with non-rotating parts," Linkoping University, Thesis no. 426, Sweden, 1994.

[63] Isermann R., "Fault diagnosis of machine via parameter estimation and knowledge processing – Tutorial paper," *Automatica*, vol. 29, no. 4, pp. 815-835, 1993.

[64] ISO 7919-2, *Mechanical vibration — Evaluation of machine vibration by measurements on rotating shafts — Part 2: Land-based steam turbines and generators in excess of 50 MW with normal operating speeds of 1500 r/min, 1800 r/min, 3000 r/min and 3600 r/min*, 2002.

[65] ISO 7919-5, *Mechanical vibration – Evaluation of machine vibration on rotating shafts – Part 5: Machine sets in hydraulic power generating and pumping plants*, 2005.

[66] ISO 9000, *Quality management and quality assurance*, International Organization for Standardization, p. 704, 2003.

[67] ISO 10816-1, *Mechanical vibration – Evaluation of machine vibration by measurements on non-rotating parts – Part 1: General guidelines*, 1995.

[68] ISO 10816-3, *Mechanical vibration – Evaluation of machine vibration by measurements on non-rotating parts – Part 3: Industrial machines with nominal power above 15 kW and nominal speeds between 120 r/min and 15 000 r/min when measured in situ*, 1998.

[69] ISO 11342, *Mechanical vibration – Methods and criteria for the mechanical balancing of flexible rotors*, International Organization for Standardization, 2003.

[70] ISO 14839-1, *Mechanical vibration – Vibration of rotating machinery equipped with active magnetic bearings – Part 1: Vocabulary*, International Organization for Standardization, p. 30, 2002.

[71] ISO/FDIS 14839-2, *Mechanical vibration – Vibration of rotating machinery equipped with active magnetic bearings – Part 2: Evaluation of vibration*, 2004.

[72] Jack L.B. and Nandi A.K., "Fault detection using support vector machines and artificial neural networks, augmented by genetic algorithms," *Mechanical Systems and Signal Processing*, vol. 3, no. 16, pp. 373–390, 2002.

[73] Kasarda M.E.F., "An overview of active magnetic bearing technology and applications," *Shock and Vibration Digest*, vol. 32, no. 2, pp. 91-99, March 2000.

[74] Karasaridis A., Maalej M., and Pantazopoulou S., "Time-frequency analysis of sensor data for detection of structural damage in instrumented structures," *Proceedings of the 13th International Conference on Digital Signal Processing (DSP)*, pp. 817-820, 1997.

[75] Kay S.M., *Fundamentals of statistical signal processing*, Prentice-Hall, 1993.

[76] Keeter B., "Introduction to Weibull," Technical Report, ARMS Reliability Engineers.

[77] Kim S. and Lee C., "Diagnosis of sensor faults in active magnetic bearing system equipped with built-in force transducers," *IEEE/ASME Transactions on Mechatronics*, vol. 4, no. 2, June 1999.

[78] Kirk R.G., "Evaluation of AMB turbomachinery auxiliary bearings," *Transactions ASME, Journal of Vibrations and Acoustics*, vol. 121, pp. 156-161, Apr. 1999.

[79] Kliman G.B. and Premerlani W.J., "Recent development in on-line motor diagnostics," *ICEM conference proceedings*, Istanbul, pp. 471-475, 1998.

[80] Knospe C. and Collins E.G., "Introduction to the special issue on magnetic bearing control," University of Virginia, Charlottesville, 1997.

[81] Kokko V., "Condition monitoring of squirrel-cage motors by axial magnetic flux measurements," Acta Universitatis Ouluensis C179, Oulu, ISBN: 951-42-6937-3, 2003.

[82] Končar N., "Optimisation methodologies for direct inverse neurocontrol," Master's thesis, University of London, 1997.

[83] Korde A., "Online condition monitoring of motors using electrical signature analysis," *Proceedings of the Advances in Condition-Based Plant Maintenance Seminar*, Diagnosis Technologies India Ltd., Mumbai, May 2002.

[84] Kyusung K. and Parlos A.G., "Induction motor fault diagnosis based on neuropredictors and Wavelet signal processing," *IEEE Transactions on Mechatronics*, vol. 7, no. 2, June 2002.

[85] Lang O., Wassermann J., and Springer H., "Adaptive vibration control of a rigid rotor supported by active magnetic bearings," *Proc. of Int. Gas Turbine and Aeroengine Congress and Exposition*, Houston, Texas, 1995.

[86] Lang S.W. and Mcclellan J.H., "Frequency estimation with maximum entropy spectral estimators," *IEEE Transactions on Acoustic, Speech, and Signal Processing*, vol. 28, no. 6, pp. 716-724, 1980.

[87] Larsonneur R., Buehler P., and Richard P., "Active magnetic bearings and motor drive towards integration," *Proc. 8th Internat. Symposium on Magnetic Bearings*, Mito, Japan, pp. 187-192, Aug. 26-28, 2002.

[88] Lindh T., "Condition monitoring of induction machines," Lappeenranta University of Technology, 2003.

[89] Lipovszky G., Sólymovári K., and Varga G., *Vibration testing of machines and their maintenance*, Elsevier Science, 1990.

[90] Loesch F., "Detection and correction of actuator and sensor faults in active magnetic bearing systems," *Proc. 8th Internat. Symposium on Magnetic Bearings*, Mito, Japan, pp. 113-118, Aug. 26-28, 2002.

[91] Mallat S., *A wavelet tour of signal processing*, Second Edition, Elsevier (USA), 1999.

[92] Marple S.L., "Spectral line analysis via fast Prony algorithm," *Proceedings of the IEEE International Conference on Acoustics, Speech and Signal Processing*, Paris, France, pp. 1375-1378, 1982.

[93] Marple S.L., *Digital spectral analysis with applications*, Prentice-Hall Inc., 1987.

[94] Marshall J.T., "A multi-point measurement technique for the enhancement of force measurement with active magnetic bearings," Faculty of the Virginia Polytechnic Institute and State University, Blacksburg, Virginia, May 2001.

[95] Maruthi G.S. and Panduranga K., "Electrical fault detection in three phase squirrel cage induction motor by vibration analysis using MEMS accelerometer," *International Conference on Power Electronics and Drives Systems (PEDS 2005)*, vol. 2, issue 28-01, pp. 838–843, Nov. 2005.

[96] Matsumura F., Namerikawa T., Hagiwara K., and Fujita M., "Application of gain scheduled H∞ robust controllers to a magnetic bearing," *IEEE Transactions on Control Systems Technology*, vol. 4, no. 5, pp. 484-493, Sep. 1996.

[97] McCloskey T., "Guidelines for the use of magnetic bearings in turbomachinery," Technology Insights, San Diego, California, Feb. 1996.

[98] McCormick A.C. and Nandi A.K., "A comparison of artificial neural networks and other statistical methods for rotating machine classification," *Proceedings of the IEE Colloquium on Modelling and Signal Processing for Fault Diagnosis*, vol. 260, pp. 1–6, 1996.

[99] McFadden P.D. and Toozhy M.M., "Application of signal averaging to vibration monitoring of rolling element bearings," Report no. OUEL 2216/99, University of Oxford, Department of Engineering Science, Oxford, 1999.

[100] McFadden P.D. and McFadden P.L., "Application of signal averaging to vibration monitoring of rolling element bearings (I) Introduction and pilot study," Report no. OUEL 2146/97, University of Oxford, Department of Engineering Science, Oxford, 1997.

[101] Mechefske C.K., "Objective machinery fault diagnosis using fuzzy logic," *Mechanical Systems and Signal Processing*, no. 12, pp. 855-862, 1998.

[102] Meng L. and David G., "Pitch detection," University of Regina, March 2004.

[103] Miller H. and Ahrens M., Totally enclosed inline electric motor driven gas compressor. [Online]. Available: http://www.dresser-rand.com [Date of access: Apr. 2005].

[104] MIL-STD-1629A, Military standard - procedures for performing a failure mode, effects and critical analysis. [Online]. Available: http://www.sre.org/pubs/Mil-Std-1629A.pdf, [Date of access: March 2007].

[105] Mitchell J.S., *An introduction to machinery analysis and monitoring*, Pennwell, Second Edition, 1993.

[106] Moss J.C. and Hammond J.K., "A comparison between the modified spectrogram and the pseudo-Wigner-Ville distribution with and without modification," *Mechanical Systems and Signal Processing*, Academic Press, vol. 8, no. 3, pp. 243-258, 1994.

[107] Mueller M.K., "On-line-process monitoring in high speed milling with an active magnetic bearing spindle," Dissertation ETH Zurich, no. 14626, 2002.

[108] Muszynska A., "Rotor-to-stationary part full annular contact modelling," *Proc. 9th Internat. Symposium on Transport Phenomena and Dynamics of Rotating Machinery (ISROMAC)*, Honolulu, Hawaii, Feb. 10-14, 2002.

[109] Newcastle University, Modern flywheel uninterruptible power supplies. [Online]. Available: http://murray.newcastle.edu.au/users/students/2001/c9605166/modern_ups.htm, [Date of access: Apr. 2005].

[110] Newland D.E., *An introduction to random vibrations, spectral & wavelet analysis*, Longman Scientific & Technical, 3rd Edition, 1993.

[111] Nicholas J.C., Gunter E.J., and Allaire P.J., "Effect of residual shaft bow on unbalance response and balancing of a single mass flexible rotor, Part 1 – unbalance response," *Journal of Engineering for Power*, pp. 171-181, 1976.

[112] Nicholas J.C., Gunter E.J., and Allaire P.J., "Effect of residual shaft bow on unbalance response and balancing of a single mass flexible rotor, Part 2 – balancing," *Journal of Engineering for Power*, pp. 182-189, 1976.

[113] Nikolaou N.G. and Antoniadis I.A., "Application of wavelet packets in bearing fault diagnosis," *Proceedings of the 5th WSEAS International Conference on Circuits, Systems, Communications and Computers (CSCC 2001)*, pp. 12–19, Greece, July 2001.

[114] Nixon M.S. and Aguado A.S., *Feature extraction and image processing*, First Edition, Elsevier, 2002.

[115] Norton M.P., *Fundamentals of noise and vibration analysis for engineers*, Cambridge University Press, 1989.

[116] O'Brien J. and Macintyre J., "Wavelets: An alternative to Fourier analysis," Vibration in Fluid Machinery Seminar, Institution of Mechanical Engineer, Nov. 1994.

[117] Ocak H. and Loparo K.A., "A new bearing fault detection and diagnostics schema based on hidden Markov modeling of vibration signal," *Proceedings of the IEEE International Conference on Acoustics, Speech and Signal Processing*, vol. 5, pp. 3141–3144, 2001.

[118] Ohura Y., Ueda K., and Sugita S., "Performance of touchdown bearings for turbo-molecular pumps," *Proc. 8th Internat. Symposium on Magnetic Bearings*, Mito, Japan, pp. 515-520, Aug. 26-28, 2002.

[119] Pan M.C., Sas P., and van Brussel H., "Non-stationary time-frequency analysis for machine condition monitoring," *Proceedings of the IEEE-SP International Symposium on Signal Processing*, pp. 477-480, 1996.

[120] Partanen J., Tuomo L., and Pertti J., "Intelligent applications for the management of electrical systems in industrial plants," *Proceedings of Intelligent System Application to Power Systems (ISAP'99)*, Rio de Janeiro, Brazil, Apr. 1999.

[121] Paya P.A. and Esat I.I., "Artificial neural network based fault diagnostics of rotating machinery using Wavelet-transforms as a preprocessor," *Mechanical Systems and Signal Processing*, no. 11, pp. 751-765, 1997.

[122] Penman J. and Yin C.M., "Feasibility of using unsupervised learning, artificial neural networks for the condition monitoring of electrical machines," *IEE Proceedings on Electric Power Applications*, vol. 141, no. 6, pp. 317-322, Nov. 1994.

[123] Pfleger S., et al., "Data Fusion Applications," Workshop Proceedings, Brussels, 1992.

[124] Poggio A.J. and van Blaricum's M.L., "Evaluation of a processing technique for transient data," *IEEE Transactions on Antennas Propagation*, vol. 26, no. 1, pp. 165-173, 1978.

[125] Pruftechnik Group, Condition monitoring support. [Online]. Available: www.pruftechnik.com/cm/what_cm/what.htm [Date of access: Feb. 2005].

[126] QS9000, One world one quality system. [Online]. Available: http://www.qs-9000.org, [Date of access: March 2007].

[127] Randall R.B., "Bearing diagnostics in helicopter gearboxes", *Proceedings of the Condition Monitoring and Diagnostic Engineering Management (COMADEM) Conference*, pp. 1–11, Manchester, Sep. 2001.

[128] Rao B.K.N., *Handbook of condition monitoring*, First Edition, Elsevier Advanced Technology, 1996.

[129] Rao J.S. and Gupta K., *Introductory course on theory and practice of mechanical vibrations*, Second Edition, New Age International Publishers Ltd., pp. 459, 1984.

[130] Reeves C.W., *The vibration monitoring handbook*, First Edition, Coxmoor Publishing, Oxford, UK.

[131] Reitsma T.W., "Development of long-life auxiliary bearings for critical service turbomachinery and high-speed motors," *Proc. 8th Internat. Symposium on Magnetic Bearings*, Mito, Japan, pp. 507-513, Aug. 26-28, 2002.

[132] Revolve magnetic bearings Inc., Magnetic bearings. [Online]. Available: www.revolve.com /Technology/magbearings.html, [Date of access: March 2005].

[133] Reznik L., *Fuzzy controllers handbook*, First Edition, Elsevier, 1997.

[134] Ribeiro M.P., "Processamento de sinais vibratórios de equipamentos situados a longas distâncias via método de Prony," COPPE/UFRJ, Engenharia mecânica, M.Sc. thesis, 1991.

[135] Ribeiro M.P., "Inaccessible equipment monitoring via vibratory signature analysis utilizing data collected by remote accelerometers," Department of Mechanical Engineering, University of London, Apr. 1999.

[136] Ripley B.D., *Pattern recognition and neural networks*, Cambridge University Press, 1996.

[137] Rundell A.E., Drakunov S.V., and DeCarlo R.A., "A sliding mode observer and controller for stabilization of rotational motion of a vertical shaft magnetic bearing," *IEEE Transactions on Control Systems Technology*, vol. 4, pp. 598-608, Sep. 1996.

[138] Rundell A.E., Drakunov S.V., and DeCarlo R.A., "A sliding mode observer and controller for stabilization of rotational motion of a vertical shaft magnetic bearing," *IEEE Transactions on Control Systems Technology*, vol. 4, pp. 598-608, Sep. 1996.

[139] Sahinkaya M.N., Abulrub A.G., and Keogh P.S., "On the modelling of flexible rotor/magnetic bearing systems when in contact with retainer bearings," *Proc. 9th Internat. Symposium on Magnetic Bearings (ISMB9)*, Kentucky, USA, Aug. 3-6, 2004.

[140] Sahinkaya M.N., Abulrub A.G., and Keogh P.S., "Performance of synchronous controllers for rotor magnetic bearing systems under retainer bearing contact," *Proc. 7th Internat. Conf. on Motion and Vibration Control (ICMVC' 04)*, St. Louis, USA, Aug. 8-11, 2004.

[141] Salles G., Filippetti F., and Tassoni C., "Monitoring of induction motor load by neural network techniques," *IEEE Transactions on Power Electronics*, vol. 15, no. 4, July 2000.

[142] Scherpen J.M.A., "Nonlinear control for magnetic bearings in deployment test rigs: Simulation and experimental results," Faculty of Information Technology & Systems, Dept. of Electrical Engineering, USA, pp. 2613–2618, 1996.

[143] Schoen R.R., Lin B.K., and Habetler T.G., "An unsupervised on-line system for induction motor fault detection using stator current monitoring," Industry Application Society Annual Meeting, *Conference Record of the IEEE*, pp. 103–109, Oct. 1994.

[144] Schweitzer G., Traxler A., and Bleuler H., *Magnetlager, Grundlagen, Eigenschaften und Anwendungen berührungsfreier, elektromagnetischer Lager*, Berlin: Springer Verlag, 1993.

[145] Shi Z., Zha M., and Peng H., "The monitoring system of the PCU for the 10 MW high temperature gas-cooled reactor," *Second International Topical Meeting on High Temperature Reactor Technology*, Beijing, CHINA, Sep. 22-24, 2004.

[146] Shin Y.S. and Jeon J., "Pseudo Wigner-Ville time-frequency distribution and its applications to machinery condition monitoring," *Shock and Vibration*, vol. 1, no. 1, pp. 65-76, 1993.

[147] Shiroshi J., Li Y., Liang S., and Kurfess T., "Bearing condition diagnostics via vibration and acoustic emission measurements," *Mechanical Systems and Signal Processing*, vol. 5, no. 11, pp. 693–705, 1997.

[148] Singh G.R.P., Paul A.K., and Chaterjee A.K., Improving equipment availability and reliability though condition monitoring at cold rolling mill complex of tata steel. [Online]. Available: http://www.reliabilityweb.com, [Date of access: March 2005].

[149] Sinha P.K., "Electromagnetic suspension dynamics and control," *IEE Control Engineering Series*, vol. 30, England, 1987.

[150] Stander C.J., Heyns P.S., and Schoombie W., "Fault detection on gearboxes operating under fluctuating load conditions," *Proceedings of the Condition Monitoring and Diagnostic Engineering Management (COMADEM) Conference*, pp. 537–544, Manchester, Sep. 2001.

[151] Tavner P.J. and Penman J., *Condition monitoring of electric motors*, First Edition, Research Studies Press Ltd., England, ISBN: 0-86380-061-0, 1987.

[152] Taylor J.I., "The vibration analysis handbook," Vibration Consultants, 1994.

[153] Tessier L.P., The development of an auxiliary bearing landing system for a flexible active magnetic bearing supported hydrogen process compressor rotor. From Proceedings: MAG' 97, Alexandria, USA, 1997. [Online]. Available: http://www.revolve.com/Technology/Pdf/dpmt_auxbrg_landing.pdf, [Date of access: March 2005].

[154] Theodoridis S. and Koutroumbas K., *Pattern recognition*, Second Edition, Elsevier (USA), 2003.

[155] Thompson M.T., "Electrodynamic magnetic suspension – models, scaling laws, and experimental results," *IEEE Transactions on Education*, vol. 43, no. 3, Aug. 2000.

[156] Tímár P.L., Fazekas A., and Kiss J., "Noise and vibration of electrical machines," Studies in Electrical and Electronic Engineering 34, Elsevier, Amsterdam, 1989.

[157] Toliyat H., Areffen M., and Parlos A., "A method for dynamic simulation of air-gap eccentricity in induction machines," *IEEE Transactions on Industry Applications*, vol. 32, no. 4, pp. 910-918, Aug. 1996.

[158] Uhrig R.E., "Integration of artificial intelligence systems into a monitoring and diagnostic system for nuclear power plants," *Special Meeting on Instrumentation and Control of the Halden Research Centre*, Lillihammer, 1998.

[159] University of Virginia, Jesse W. Beams 1898–1977. [Online]. Available: www.phys. virginia.edu/History/Beams/beams_and_johnson.jpg, [Date of access: May 2005].

[160] Vaidyanathan P.P., *Multirate systems and filter banks*, Prentice-Hall, 1993.

[161] van der Merwe N.T., "The application of signal processing and artificial intelligence techniques in the condition monitoring of rotating machinery," PhD Dissertation, North-West University, Potchefstroom, 2004.

[162] van Vuuren P.A., "Neuro-fuzzy techniques in pattern recognition," Internal Report, Potchefstroom University for Christian Higher Education, 1998.

[163] Ville J., "Théorie et applications de la notion de signal analytique," *Cables et Transmission*, vol. 2A, pp. 61-74, 1948.

[164] Wang K., *Intelligent condition monitoring and diagnosis systems: A computational intelligence approach*, IOS Press, 2003.

[165] Waukeshu Bearings Corporation, The benefits of magnetic bearings. [Online]. Available: www.magnetic.waukbearing.com/products/magnetic_benefits/magnetic_benefits.html, [Date of access: March 2005].

[166] Yang C. and Knospe C., "Optimal control of a magnetic bearing without bias flux using finite voltage," Department of Mechanical and Aerospace Engineering, University of Virginia.

[167] Yates S.W. and Williams R.D., "A fault tolerant multiprocessor controller for magnetic bearings," *IEE Micro*, Aug. 17, 1988.

[168] Yen G. and Lin K., "Wavelet packet feature extraction for vibration monitoring," *IEEE Transactions on Industrial Electronics*, vol. 47, no. 3, June 2000.

[169] Zeisberger M. and Gawalek W., Losses in magnetic bearings. Materials Science and Engineering, no. B53, pp. 193-197. [Online]. Available: http://www.sciencedirect.com [Date of access: March 2005].

APPENDIX A

PHOTOS OF THE AMB SYSTEMS

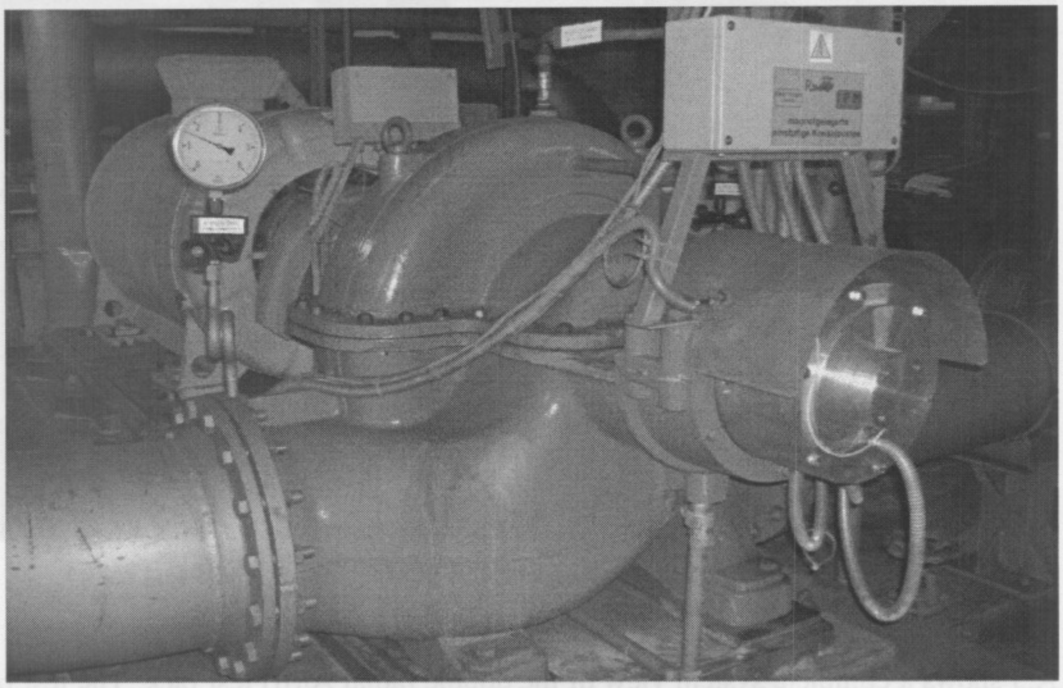

Figure A.1: Complete system view of the 250 kW water cooling AMB pump

Figure A.1 shows a complete system view of the 250 kW water cooling AMB pump. The driven unit can be seen on the left with the pump section on the right. Figure A.2 shows an enlarged view of the AMB pump. In this figure the closure of the AMB pump can be seen.

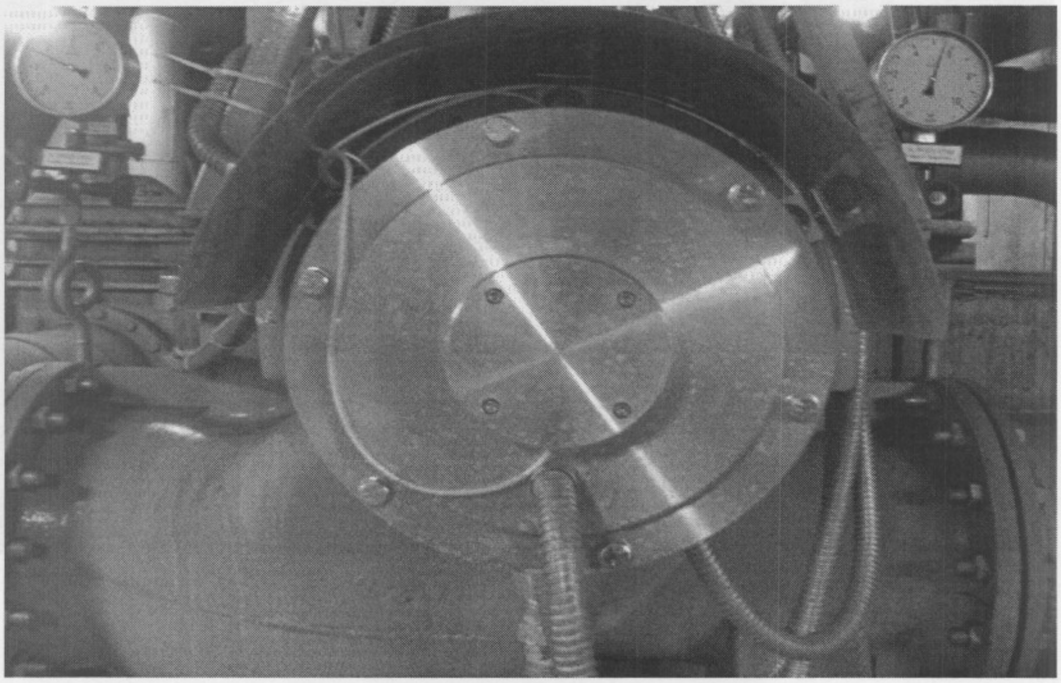

Figure A.2: 250 kW water cooling AMB pump

Figure A.3: Complete system view of the double radial AMB test rack

Figure A.3 shows a complete system view of the double radial AMB test rack. The test rack can be seen on the left with the controllers on the right. Figure A.4 shows an enlarged view of the test rack. In this figure the rotor, magnetic bearings and power amplifier unit is clearly visible.

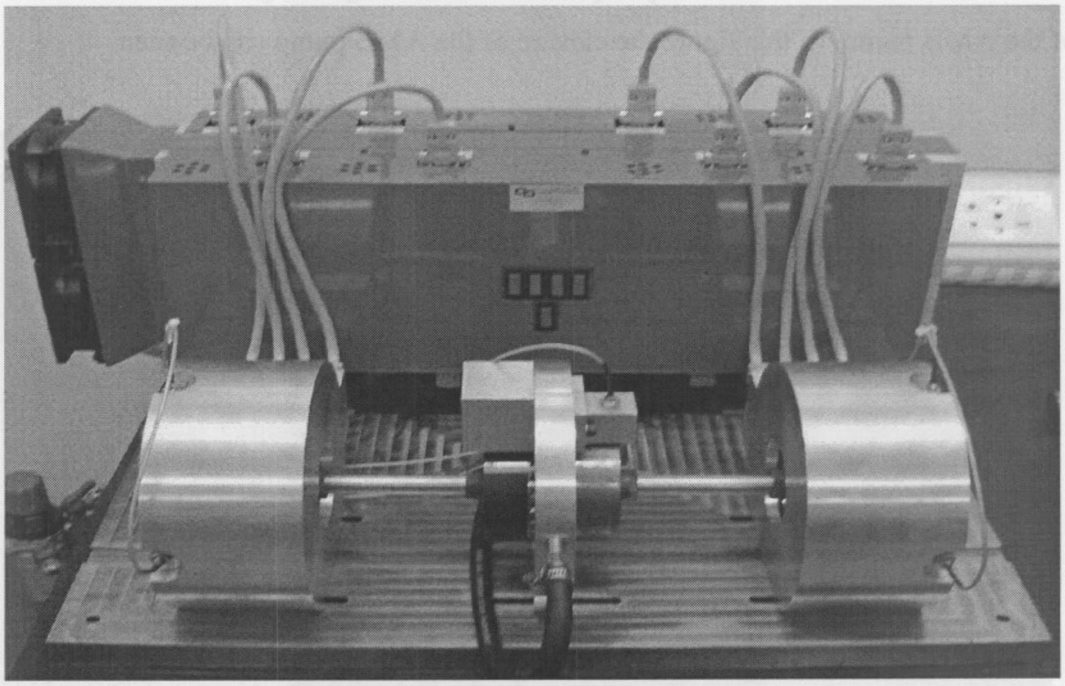

Figure A.4: Double radial AMB test rack

The photos in this section are best viewed in full colour, which is available on the CD.

APPENDIX B

SIMULATION GUI AND BASE CODE

This appendix provides the simulation GUI and the base code that was used to obtain simulation results for the detection, diagnosis and correction schemes. The simulation GUI was written in MATLAB® and interacts directly with Simulink® and the historical fault data obtained from the 250 kW water cooling AMB pump.

This base code for the simulation GUI calculates the displacement, currents and forces of the double radial AMB system. The steady state stiffness, dynamic stiffness and damping are calculated at the end of the code. The base code for the simulation GUI is available on the CD. More detail on the content of the CD is available in appendix G.

B.1. SIMULATION GUI

Figure B.1 shows the main window of the simulation GUI user interface. The main focus of the simulation GUI is to compare simulation results with historical fault data, apply various faults and implement various fault detection techniques on the AMB system.

By selecting the various checkboxes, the GUI opens further options on that selection. The rest of this section explains each of the checkbox options in detail.

The interface in figure B.1 provides six graphs, which can be selected and changed according to the menu options available. This interface provides the option to change the controller gains, apply faults on the AMB system, implement fault detection techniques and upload historical fault data from the database.

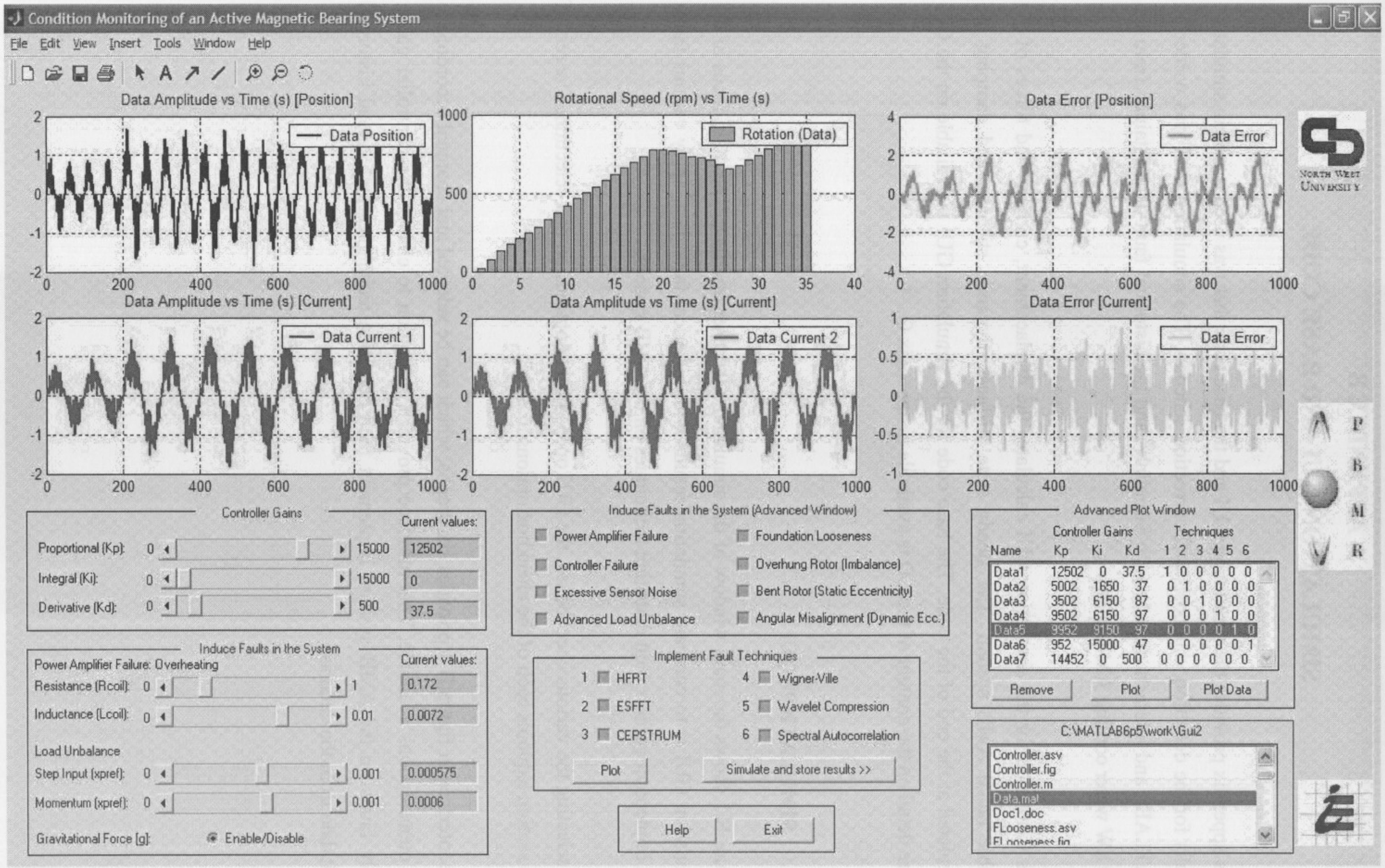

Controller Gains

Current values:

Proportional (Kp): 0 15000 12502

Integral (Ki): 0 15000 0

Derivative (Kd): 0 500 37.5

Induce Faults in the System

Power Amplifier Failure: Overheating

Current values:

Resistance (Rcoil): 0 1 0.172

Inductance (Lcoil): 0 0.01 0.0072

Load Unbalance

Step Input (xpref): 0 0.001 0.000575

Momentum (xpref): 0 0.001 0.0006

Gravitational Force [g]: ● Enable/Disable

Induce Faults in the System (Advanced Window)

☐ Power Amplifier Failure
☐ Controller Failure
☐ Excessive Sensor Noise
☐ Advanced Load Unbalance
☐ Foundation Looseness
☐ Overhung Rotor (Imbalance)
☐ Bent Rotor (Static Eccentricity)
☐ Angular Misalignment (Dynamic Ecc.)

Implement Fault Techniques

1 ☐ HFRT
2 ☐ ESFFT
3 ☐ CEPSTRUM
4 ☐ Wigner-Ville
5 ☐ Wavelet Compression
6 ☐ Spectral Autocorrelation

Advanced Plot Window

	Controller Gains			Techniques					
Name	Kp	Ki	Kd	1	2	3	4	5	6
Data1	12502	0	37.5	1	0	0	0	0	0
Data2	5002	1650	37	0	1	0	0	0	0
Data3	3502	6150	87	0	0	1	0	0	0
Data4	9502	6150	97	0	0	0	1	0	0
Data5	9952	9150	97	0	0	0	0	1	0
Data6	952	15000	47	0	0	0	0	0	1
Data7	14452	0	500	0	0	0	0	0	0

C:\MATLAB6p5\work\Gui2

- Controller.asv
- Controller.fig
- Controller.m
- Data.mat
- Doc1.doc
- FLooseness.asv
- FLooseness.fig

Figure B.1: Simulation GUI user interface

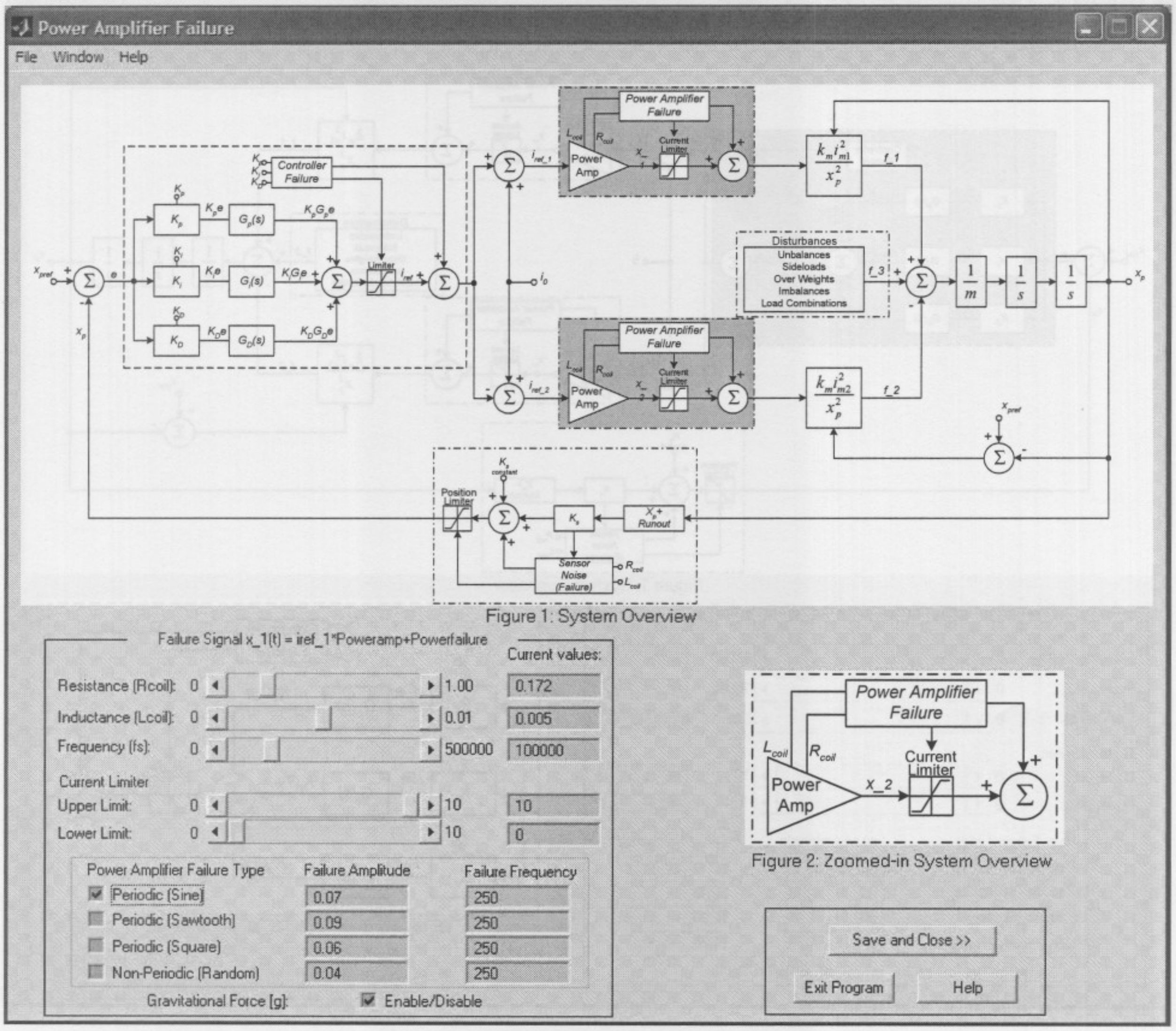

Failure Signal x_1(t) = iref_1*Poweramp+Powerfailure

	Min	Max	Current values:
Resistance (Rcoil):	0	1.00	0.172
Inductance (Lcoil):	0	0.01	0.005
Frequency (fs):	0	500000	100000
Current Limiter			
Upper Limit:	0	10	10
Lower Limit:	0	10	0

Power Amplifier Failure Type	Failure Amplitude	Failure Frequency
☑ Periodic (Sine)	0.07	250
☐ Periodic (Sawtooth)	0.09	250
☐ Periodic (Square)	0.06	250
☐ Non-Periodic (Random)	0.04	250

Gravitational Force [g]: ☑ Enable/Disable

Figure B.2: Power amplifier failure interface

An overview of the simulation model and zoomed in view of the power amplifier failure section is provided in figure B.2. When the power amplifier checkbox (shown in figure B.1) is activated, the power amplifier failure interface is opened.

This interface provides the user with the option to change the resistance of the coil (R_{coil}), inductance of the coil (L_{coil}), switching frequency (f_S) and upper and lower limits of the power amplifier. A power amplifier failure can be induced by adding noise to the output of the power amplifier.

A lot of research already exists on how to increase the reliability of power amplifiers. Most of these research focus on redundant power amplifiers, where additional power amplifiers are installed to increase the reliability. The section on power amplifier failure was therefore only explored and did not become the main focus of this study.

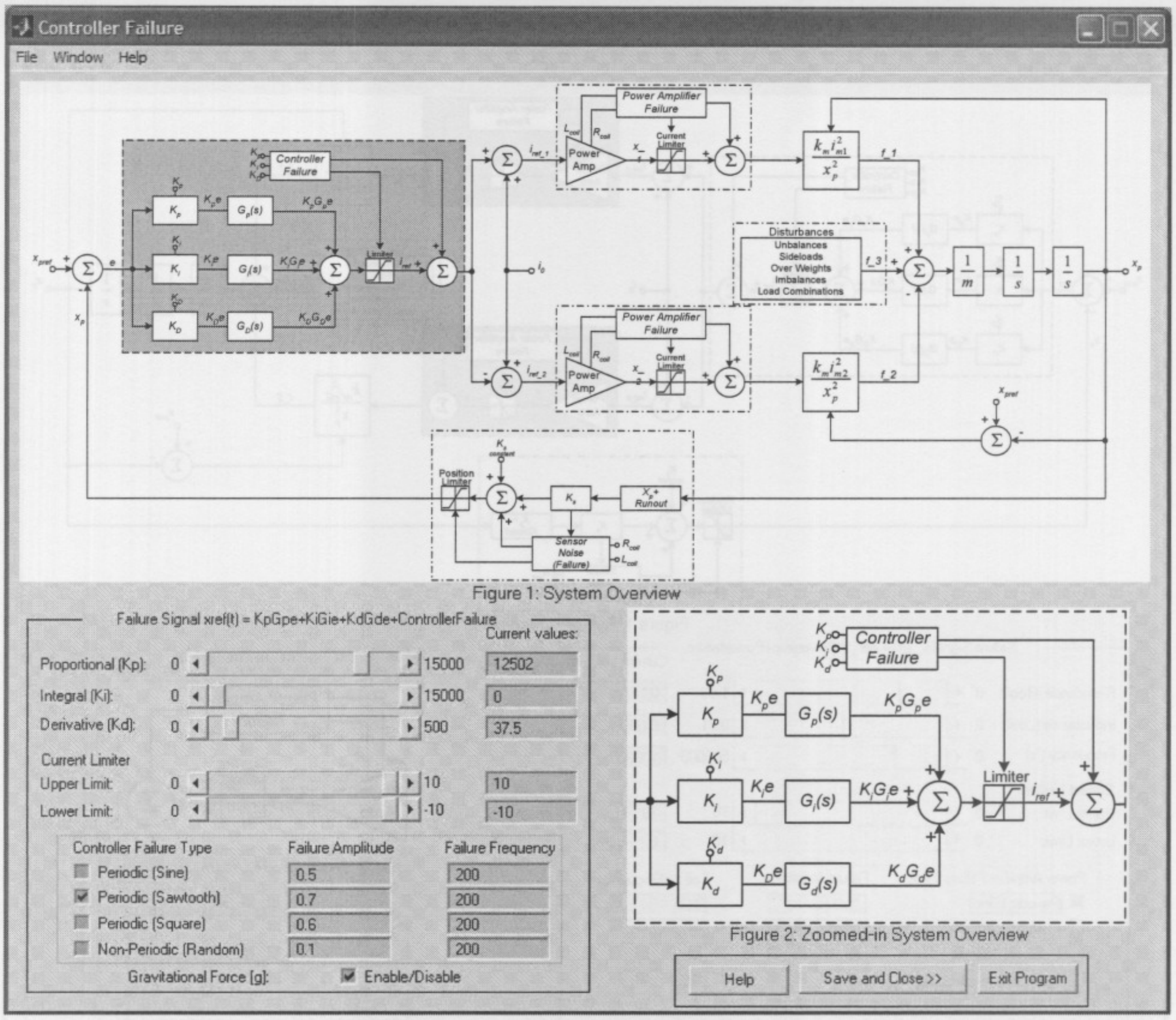

Failure Signal xref(t) = KpGpe+KiGie+KdGde+ControllerFailure

	Min	Max	Current values:
Proportional (Kp):	0	15000	12502
Integral (Ki):	0	15000	0
Derivative (Kd):	0	500	37.5
Current Limiter			
Upper Limit:	0	10	10
Lower Limit:	0	-10	-10

Controller Failure Type	Failure Amplitude	Failure Frequency
☐ Periodic (Sine)	0.5	200
☑ Periodic (Sawtooth)	0.7	200
☐ Periodic (Square)	0.6	200
☐ Non-Periodic (Random)	0.1	200

Gravitational Force [g]: ☑ Enable/Disable

Figure B.3: Controller failure interface

An overview of the simulation model and zoomed in view of the controller failure section is provided in figure B.3. When the controller failure checkbox (shown in figure B.1) is activated, the controller failure interface is opened.

This interface provides the user with real-time access to the controller parameters (k_p, k_i and k_D) and controller current limits. A controller failure can be applied by adding noise to the output of the controller.

Controller failure is mostly associated with failure from external components, like: computer malfunctions, power amplifier malfunctions, sensor malfunctions, temperature growth of critical components and run-time errors of the real-time processor. Controller failures are further described as an ill design of the controlling unit for the specific application. This section was therefore only explored in short and did not become the main focus of the study.

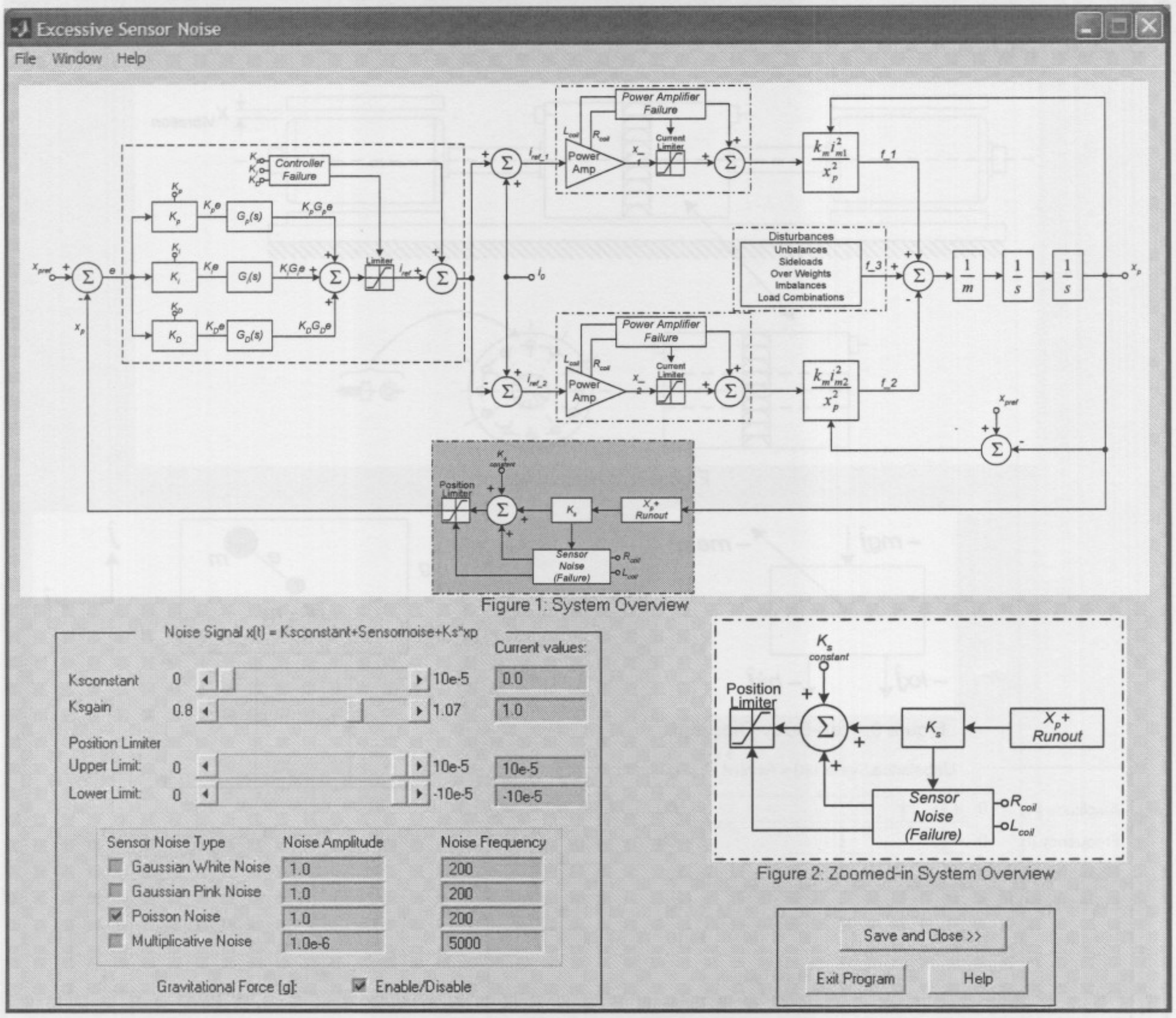

Noise Signal x(t) = Ksconstant+Sensornoise+Ks*xp

			Current values:
Ksconstant	0	10e-5	0.0
Ksgain	0.8	1.07	1.0
Position Limiter			
Upper Limit:	0	10e-5	10e-5
Lower Limit:	0	-10e-5	-10e-5

Sensor Noise Type	Noise Amplitude	Noise Frequency
☐ Gaussian White Noise	1.0	200
☐ Gaussian Pink Noise	1.0	200
☑ Poisson Noise	1.0	200
☐ Multiplicative Noise	1.0e-6	5000

Gravitational Force [g]: ☑ Enable/Disable

Figure B.4: Excessive sensor noise interface

An overview of the simulation model and zoomed in view of the excessive sensor noise section is given by figure B.4. When the excessive sensor noise checkbox (shown in figure B.1) is activated, the excessive sensor noise interface is opened.

This interface provides the user with the option to change the offset ($ks_{constant}$) and gain (ks_{gain}) and upper and lower limits of the sensors. Excessive sensor noise (in the form of Gaussian white noise, Gaussian pink noise, Poisson noise and multiplicative noise) can be applied to the AMB system.

A lot of research already exists on how to increase sensor reliability. Most of these research focus on redundant sensors, where additional sensors are installed to increase the reliability. The section on excessive sensor noise was therefore only for informational purposes and did not become the main focus of this study.

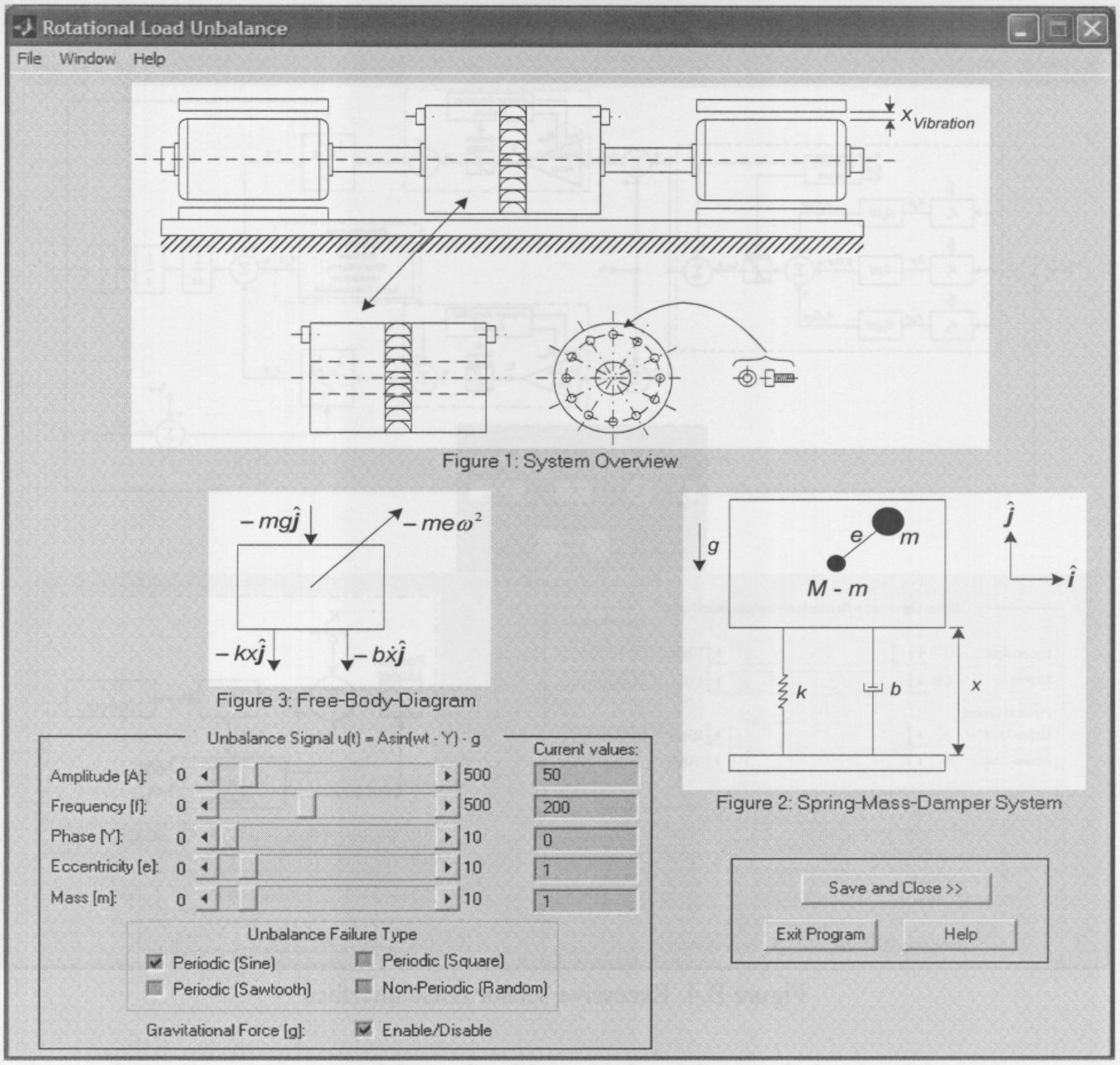

Unbalance Signal u(t) = Asin(wt - Y) · g

Current values:

Amplitude [A]: 0 – 500: 50

Frequency [f]: 0 – 500: 200

Phase [Y]: 0 – 10: 0

Eccentricity [e]: 0 – 10: 1

Mass [m]: 0 – 10: 1

Unbalance Failure Type

☑ Periodic (Sine)
☐ Periodic (Square)
☐ Periodic (Sawtooth)
☐ Non-Periodic (Random)

Gravitational Force [g]: ☑ Enable/Disable

Figure B.5: Rotational load unbalance interface

The rotational load unbalance interface is shown in figure B.5. This interface is opened by activating the advanced load unbalance checkbox (shown in figure B.1). One of the most common of vibration in engineering is rotating unbalance. This is where the rotating machine is not precisely balanced and the rotating out of balance mass causes forces on the engine. We consider the complete engine (including the out of balance mass) to have mass M, and the unbalance mass itself to be m, rotating with eccentricity e.

A real engine unbalance will cause vibration in at least two planes (vertical and rocking), but for this thesis only pure vertical motion is explored. The (vertical) displacement is measured from the equilibrium position, so:

Displacement of non-rotating mass, $$(M - m) = x \tag{B.1}$$

Displacement of rotating mass, $$m = x + e.\sin(\omega t) \tag{B.2}$$

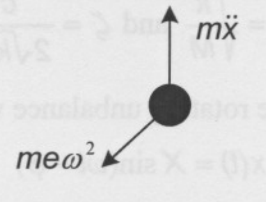

Figure B.6: Free-body diagram for the rotating mass

Figure B.6 provides the free-body diagram for the rotating mass. The resolved upward vertically forces are given (B.3).

$$Tension_{VERTICAL\,COMPONENT} = m\ddot{x} - me\omega^2\sin(\omega t) \tag{B.3}$$

The free-body diagram for the non rotating mass is provided by figure B.5. The resolved upward vertically forces are given by (B.4).

$$Tension_{VERTICAL\,COMPONENT} - kx - c\dot{x} = (M-m)\ddot{x} \tag{B.4}$$

The equation of motion is given by (B.5)

$$-m\ddot{x} + me\omega^2\sin(\omega t) - kx - c\dot{x} = (M-m)\ddot{x}$$

$$M\ddot{x} + c\dot{x} + kx = me\omega^2\sin(\omega t) \tag{B.5}$$

The last equation is essentially the same as for force excitation, replacing the forcing function F_0 with $(me\omega^2)$, which is a function of frequency. We can therefore write the dynamic response of the single degree of freedom with rotating unbalance by comparing the equation of motion with the force excitation case. The response is relative to the product "*me*".

$$\frac{X}{me} = \frac{\omega^2}{M\left\{\left(\omega_n^2 - \omega^2\right) + 2j\zeta\omega\omega_n\right\}} \tag{B.6}$$

The magnitude and phase of this complex function is given by (B.7) and (B.8)

$$\frac{X}{me} = \frac{\omega^2}{M\left\{\left(\omega_n^2 - \omega^2\right)^2 + 4\zeta^2\omega^2\omega_n^2\right\}^{1/2}} \tag{B.7}$$

and

$$\text{phase} = \tan^{-1}\left(\frac{2\zeta\omega\omega_n}{\omega_n^2 - \omega^2}\right) \tag{B.8}$$

Equation (B.5) can be written as follows:

$$\ddot{x} + \frac{c}{M}\dot{x} + \frac{k}{M}x = \frac{m}{M}e\omega^2\sin(\omega t) \tag{B.9}$$

The standard form is given by (B.10)

$$\ddot{x} + 2\zeta\omega_n\dot{x} + \omega_n x = u_0\sin(\omega t) \tag{B.10}$$

where $$\omega_n = \sqrt{\frac{k}{M}} \text{ and } \zeta = \frac{c}{2\sqrt{kM}} \tag{B.11}$$

Equation (B.12) therefore provides the rotating unbalance with respect to the air-gap ($x(t)$).

$$x(t) = X\sin(\omega t - \varphi) \tag{B.12}$$

The parameter φ represents the phase shift of the unbalance force.

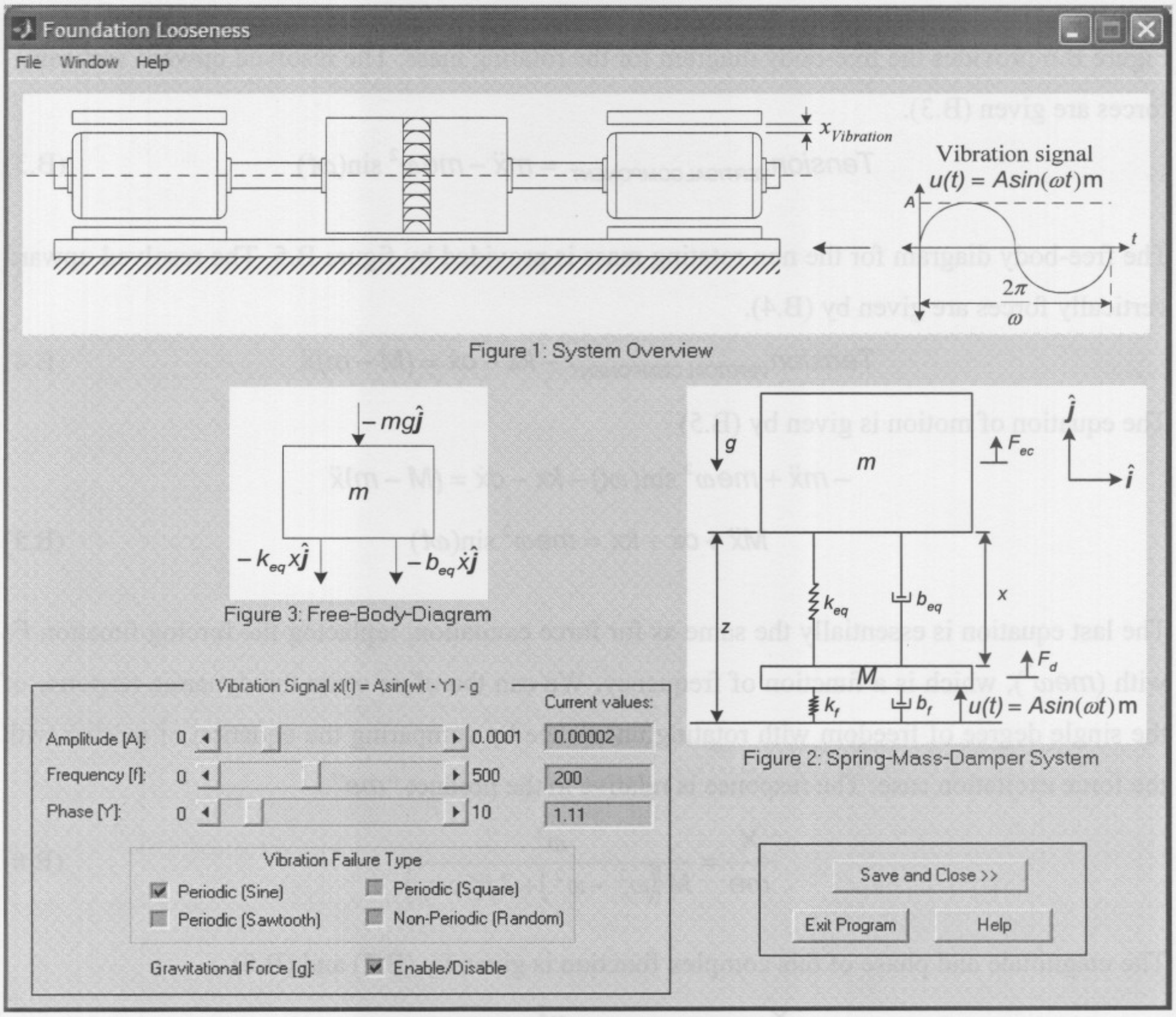

Vibration Signal x(t) = Asin(wt - Y) - g

Current values:

Amplitude [A]: 0 ◂ ▸ 0.0001 0.00002

Frequency [f]: 0 ◂ ▸ 500 200

Phase [Y]: 0 ◂ ▸ 10 1.11

Vibration Failure Type

☑ Periodic (Sine) ☐ Periodic (Square)

☐ Periodic (Sawtooth) ☐ Non-Periodic (Random)

Gravitational Force [g]: ☑ Enable/Disable

Figure B.7: Foundation looseness interface

The spring-mass-damper system and free-body-diagram of the foundation looseness interface is given by figure B.7. The foundation looseness interface is opened by activating the foundation looseness checkbox (shown in figure B.1).

The real-time detection, diagnosis and correction scheme only stabilise the rotor with respect to the stator and do not remove the fault from the AMB system. The force F_d represent the vibration (disturbance) force occurring on the base of the AMB system. This vibration is usually referred to as foundation looseness. The force F_{ec} refers to the correction force applied onto the rotor in order to stabilise it.

When a correction force F_{ec} is applied onto the AMB system, to cancel the effect of F_d, the forces on the parameters k_f and b_f increases. This may cause an increase in the stress of critical components, which may cause components to be damaged or break down. The components need to be identified by the user as critical or non-critical and the necessary steps must be taken to operate the AMB system under the fault condition or to shut down the AMB system and repair the fault.

The following calculations focus on forces acting on the mass m. We define the additional coordinate z, which measures the absolute displacement of the mass with respect to the ground, as:

$$z = x + u(t) \tag{B.13}$$

The free-body-diagram is shows in figure B.7. The only forces acting on the mass arise from the gravitational force, the spring force and the damping force. In terms of the identified coordinates, the acceleration of the mass center is given by (B.14)

$${}^{\mathcal{F}}\boldsymbol{a}_G = \ddot{z}\,\hat{j} = (\ddot{x} + \ddot{u})\,\hat{j} \tag{B.14}$$

with

$$\ddot{u}(t) = -(u_0\omega^2)\sin(\omega t) \tag{B.15}$$

wherefore, the linear momentum balance on the mass yields:

$$\Sigma \boldsymbol{F} = m\,{}^{\mathcal{F}}\boldsymbol{a}_G\,, \tag{B.16}$$

$$(-k_{eq}x - b_{eq}\dot{x} - mg)\,\hat{j} = (m\ddot{x} + m\ddot{u})\,\hat{j} \tag{B.17}$$

Writing this in terms of x, the equation of motion is given by (B.18)

$$m\ddot{x} + b_{eq}\dot{x} + k_{eq}x = -m\ddot{u}(t) - mg$$

$$\ddot{x} + \frac{b_{eq}}{m}\dot{x} + \frac{k_{eq}}{m}x = -\ddot{u}(t) - g \tag{B.18}$$

The standard form is given by (B.19)

$$\ddot{x} + 2\zeta\omega_n\dot{x} + \omega_n^2 x = u_0\omega^2\sin(\omega t) - g \tag{B.19}$$

with

$$\omega_n = \sqrt{\frac{k_{eq}}{m}} \text{ and } \zeta = \frac{b_{eq}}{2\sqrt{km}} \tag{B.20}$$

The amplitude of the forcing is given by (B.21)

$$F = u_0\omega^2 = \frac{1}{2}\omega^2 \tag{B.21}$$

The steady state response of the system therefore becomes:

$$x(t) = A\sin(\omega t - \varphi) - g \tag{B.22}$$

where $x(t)$ is the air-gap and

$$A = u_0\Lambda(r,\zeta) \text{ and } \tan\varphi = \frac{2\zeta r}{1-r^2} \tag{B.23}$$

where $$\Lambda = \frac{r^2}{\sqrt{(1-r^2)^2+(2\zeta r)^2}} \text{ and } r = \frac{\omega}{\omega_n} \tag{B.24}$$

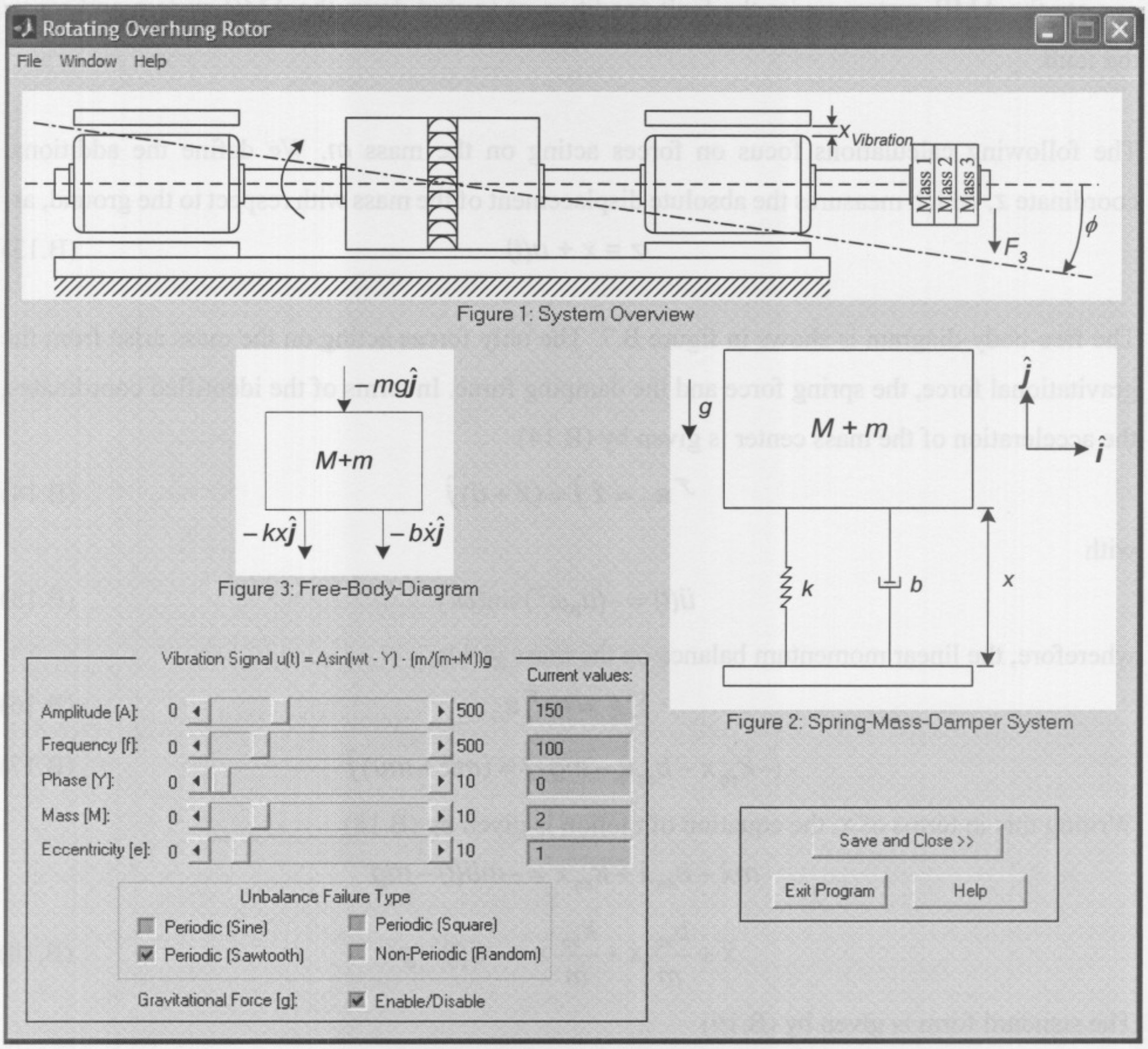

	Min	Max	Current values:
Amplitude [A]:	0	500	150
Frequency [f]:	0	500	100
Phase [Y]:	0	10	0
Mass [M]:	0	10	2
Eccentricity [e]:	0	10	1

Unbalance Failure Type

☐ Periodic (Sine)
☐ Periodic (Square)
☑ Periodic (Sawtooth)
☐ Non-Periodic (Random)

Gravitational Force [g]: ☑ Enable/Disable

Figure B.8: Rotating overhung rotor interface

The spring-mass-damper system and free-body-diagram of the overhung rotor interface is given by figure B.8. The rotating overhung rotor interface is opened by activating the overhung rotor checkbox (shown in figure B.1).

The resolved vertically forces can be written as follow:

$$(-kx - b\dot{x} - mg)\,\hat{j} = (M+m)\ddot{x}\hat{j} \tag{B.25}$$

The equation of motion is given by (B.26)

$$(M+m)\ddot{x} + b\dot{x} + kx = -mg \tag{B.26}$$

This can be written in the standard form as:

$$\ddot{x} + \frac{b}{M+m}\dot{x} + \frac{k}{M+m}x = \frac{-m}{M+m}g \tag{B.27}$$

where

$$\omega_n = \sqrt{\frac{k}{M+m}} \text{ and } \zeta = \frac{b}{2\sqrt{k(M+m)}} \tag{B.28}$$

The air-gap ($x(t)$) function can therefore be written as follows:

$$x(t) = A\sin(\omega t - \varphi) - \frac{m}{M+m}g \tag{B.29}$$

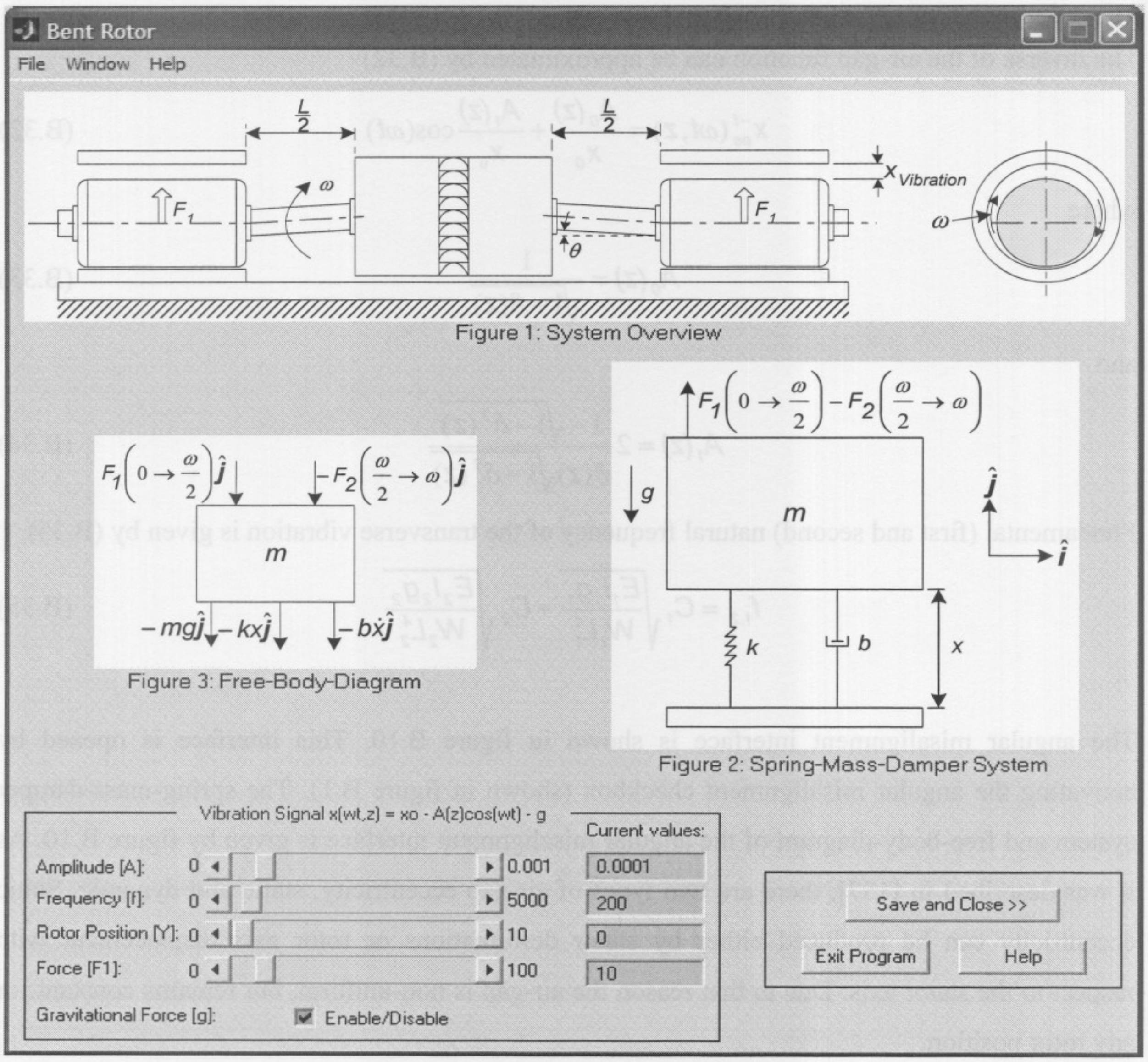

Vibration Signal x(wt,z) = xo - A(z)cos(wt) - g

Current values:

Amplitude [A]: 0 – 0.001: 0.0001

Frequency [f]: 0 – 5000: 200

Rotor Position [Y]: 0 – 10: 0

Force [F1]: 0 – 100: 10

Gravitational Force [g]: ☑ Enable/Disable

Figure B.9: Bent rotor interface

The spring-mass-damper system and free-body-diagram of the bent rotor interface is given by figure B.9. This interface is opened by activating the bent rotor checkbox (shown in figure B.1).

Static eccentricity (caused by the bent rotor interface) can be produced either by stator deformations or rotor axis displacement with respect to the stator axis. If the eccentricity is static, the air-gap function, x_{se}, can be approximated as follows:

$$x_{se}(\omega t, z) = x_0 - \delta(z)\cos(\omega t) \tag{B.30}$$

where $\delta(z)$ is the air-gap variation amplitude, which can vary along the axial length of the motor. The radial air-gap length under no eccentricity condition is given by x_0. As an example, if only one bearing is displaced respect to stator geometric axis, the air-gap variation amplitude can be approximated by (B.31)

$$\delta(z) = \delta_0 + kz \tag{B.31}$$

where δ_0 is the air-gap variation at $z = 0$, and k is a constant.

The inverse of the air-gap function can be approximated by (B.32)

$$x_{es}^{-1}(\omega t, z) = \frac{A_0(z)}{x_0} + \frac{A_1(z)}{x_0}\cos(\omega t) \tag{B.32}$$

where

$$A_0(z) = \frac{1}{\sqrt{1-\delta(z)}} \tag{B.33}$$

and

$$A_1(z) = 2\frac{1-\sqrt{1-\delta^2(z)}}{\delta(z)\sqrt{1-\delta^2(z)}} \tag{B.34}$$

Fundamental (first and second) natural frequency of the transverse vibration is given by (B.35).

$$f_{1,2} = C_1\sqrt{\frac{E_1 I_1 g_1}{W_1 L_1^4}} + C_2\sqrt{\frac{E_2 I_2 g_2}{W_2 L_2^4}} \tag{B.35}$$

The angular misalignment interface is shown in figure B.10. This interface is opened by activating the angular misalignment checkbox (shown in figure B.1). The spring-mass-damper system and free-body-diagram of the angular misalignment interface is given by figure B.10. As it was described in [157], there are two types of air-gap eccentricity, static and dynamic. Static eccentricity can be produced either by stator deformations or rotor axis displacement with respect to the stator axis. Due to that reason the air-gap is non-uniform, but remains constant for any rotor position.

Only the right half is evaluated, since the answer is the same for the other half only 180^0 out of phase. Dynamic eccentricity occurs when the geometric center of the rotor is not at the center of rotation, producing a periodic variation in the air-gap when the rotor turns.

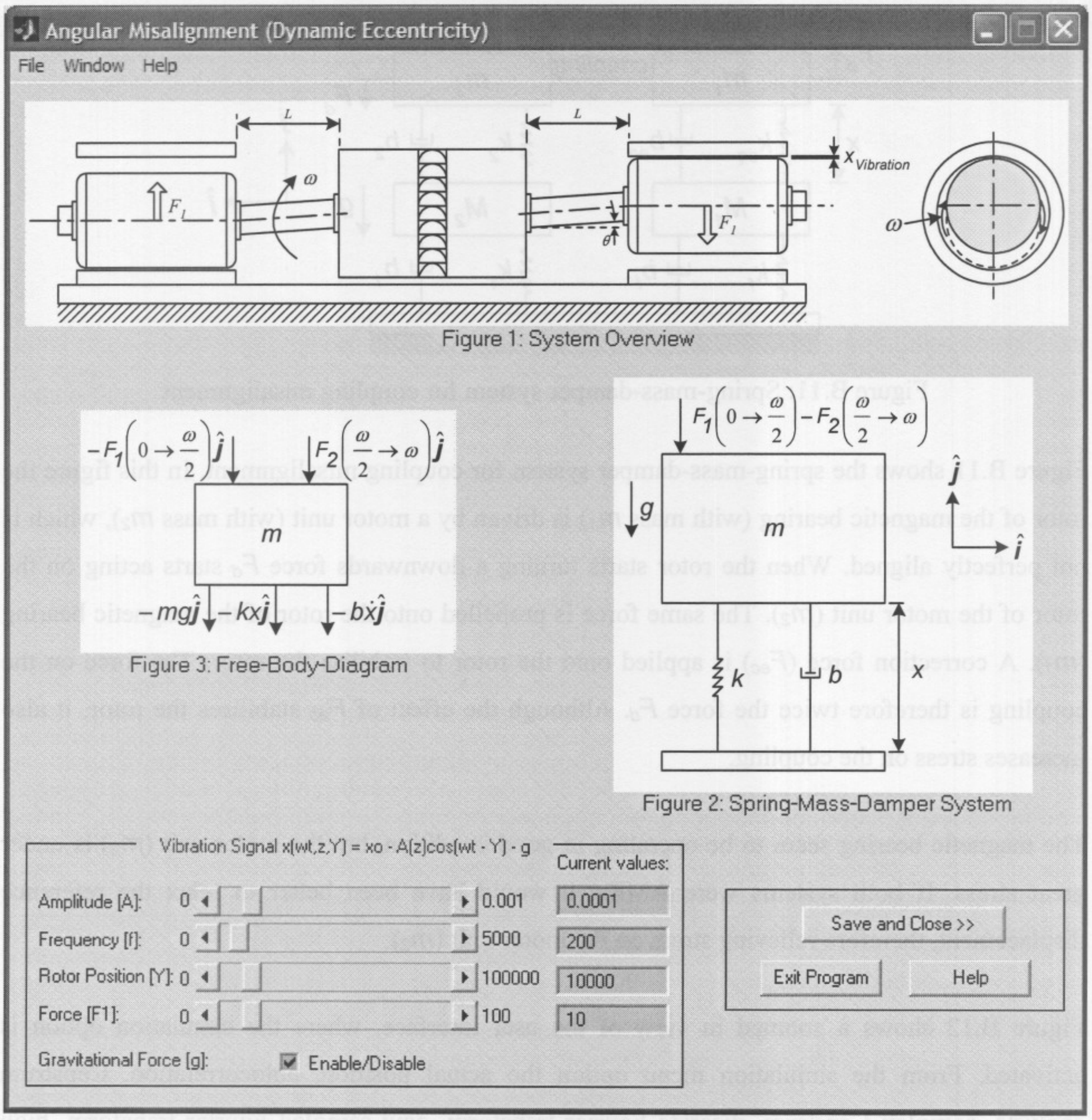

Vibration Signal x(wt,z,Y) = xo - A(z)cos(wt - Y) - g

Amplitude [A]: 0 – 0.001: 0.0001

Frequency [f]: 0 – 5000: 200

Rotor Position [Y]: 0 – 100000: 10000

Force [F1]: 0 – 100: 10

Gravitational Force [g]: ☑ Enable/Disable

Figure B.10: Angular misalignment interface

If the eccentricity is dynamic, the air-gap function, x_{de}, can be approximated as follows:

$$x_{de}(\omega t, z, \varphi) = x_0 - \delta(z)\cos(\omega t - \varphi) \tag{B.36}$$

Fundamental (first and second) natural frequency of the transverse vibration is given by (B.37)

$$f_{1,2} = C_1\sqrt{\frac{E_1 I_1 g_1}{W_1 L_1^4}} + C_2\sqrt{\frac{E_2 I_2 g_2}{W_2 L_2^4}} \tag{B.37}$$

Vibration and misalignment greatly accelerate bearing wear and increase operating temperature.

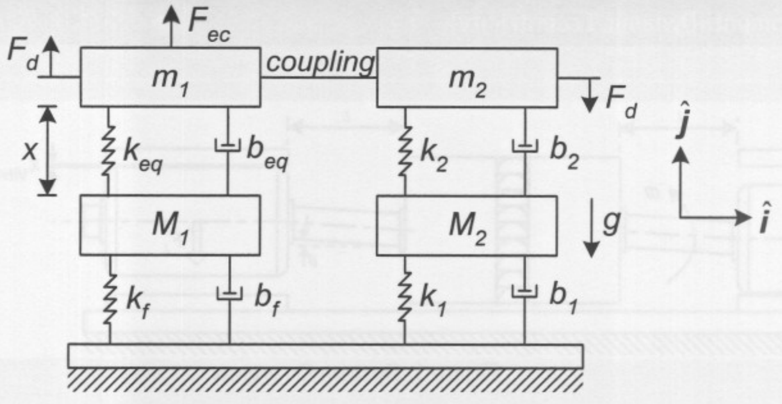

Figure B.11: Spring-mass-damper system for coupling misalignment

Figure B.11 shows the spring-mass-damper system for coupling misalignment. In this figure the rotor of the magnetic bearing (with mass m_1) is driven by a motor unit (with mass m_2), which is not perfectly aligned. When the rotor starts turning a downwards force F_d starts acting on the rotor of the motor unit (m_2). The same force is propelled onto the rotor of the magnetic bearing (m_1). A correction force (F_{ec}) is applied onto the rotor to stabilise the rotor. The force on the coupling is therefore twice the force F_d. Although the effect of F_{ec} stabilises the rotor, it also increases stress on the coupling.

The magnetic bearing seam to be operating in good condition, but the motor unit (m_2) is under great stress. If both systems were AMBs, it would have been better to relax the reference displacement, therefore relieving stress on the motor unit (m_2).

Figure B.12 shows a zoomed in view of the user interface, where the simulation option is activated. From the simulation menu option the actual position, autocorrelation, Cepstrum analysis, complex Cepstrum, discrete Fourier transform, equi-sampled Fourier transform, high frequency resonance technique, histogram decomposition, spectral analysis (magnitude), spectral analysis (phase), spectral correlation density, spectrum analysis, synchronous average, wavelet compression and Wigner-ville distribution can be calculated and displayed. The same variables are calculated and displayed by the simulation (current), real data (position) and real data (current) menu options.

Figure B.13 shows a zoomed in view of the user interface, where the other option is activated. From the other menu option the magnetic flux-density (simulation), rotational speed (real data), force F1 (simulation), force F2 (simulation), position error (simulation), position error (current), current error (simulation), current error (real data), velocity (simulation), velocity (real data), acceleration (simulation) and acceleration (real data) can be calculated and displayed.

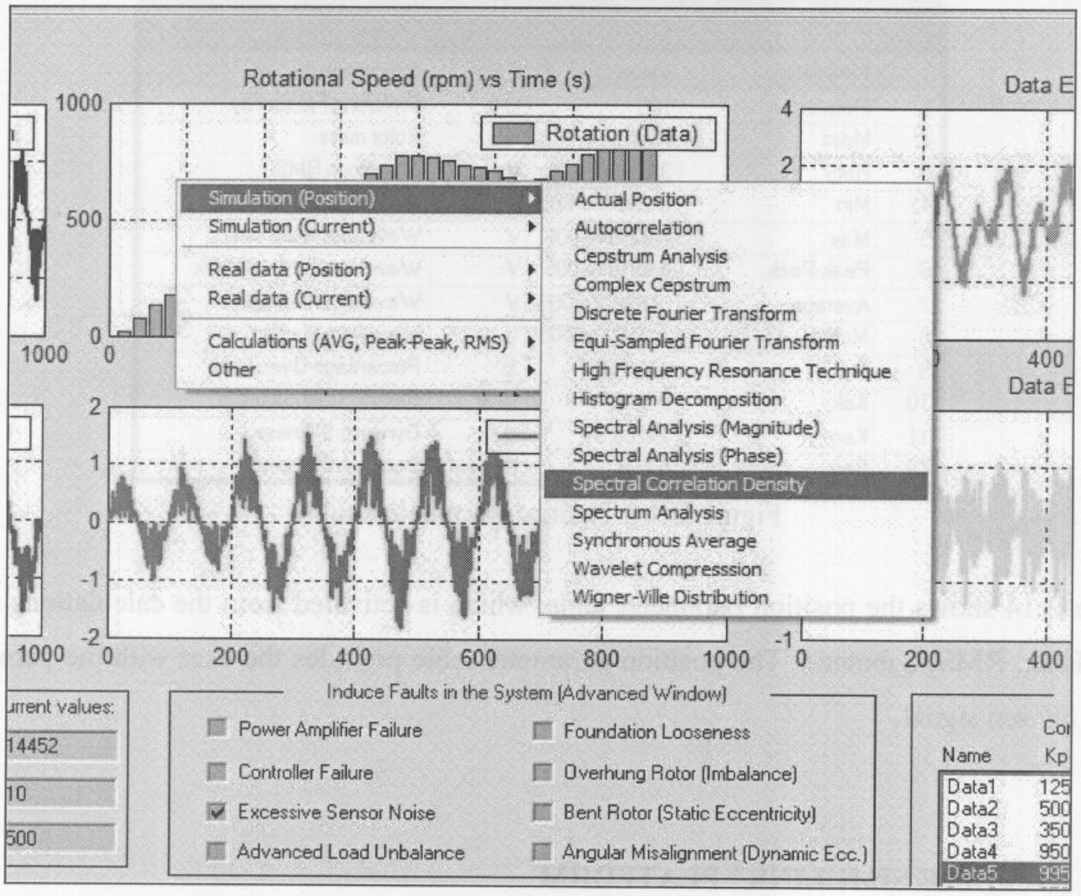

Figure B.12: Zoomed in view of the user interface showing the simulation option

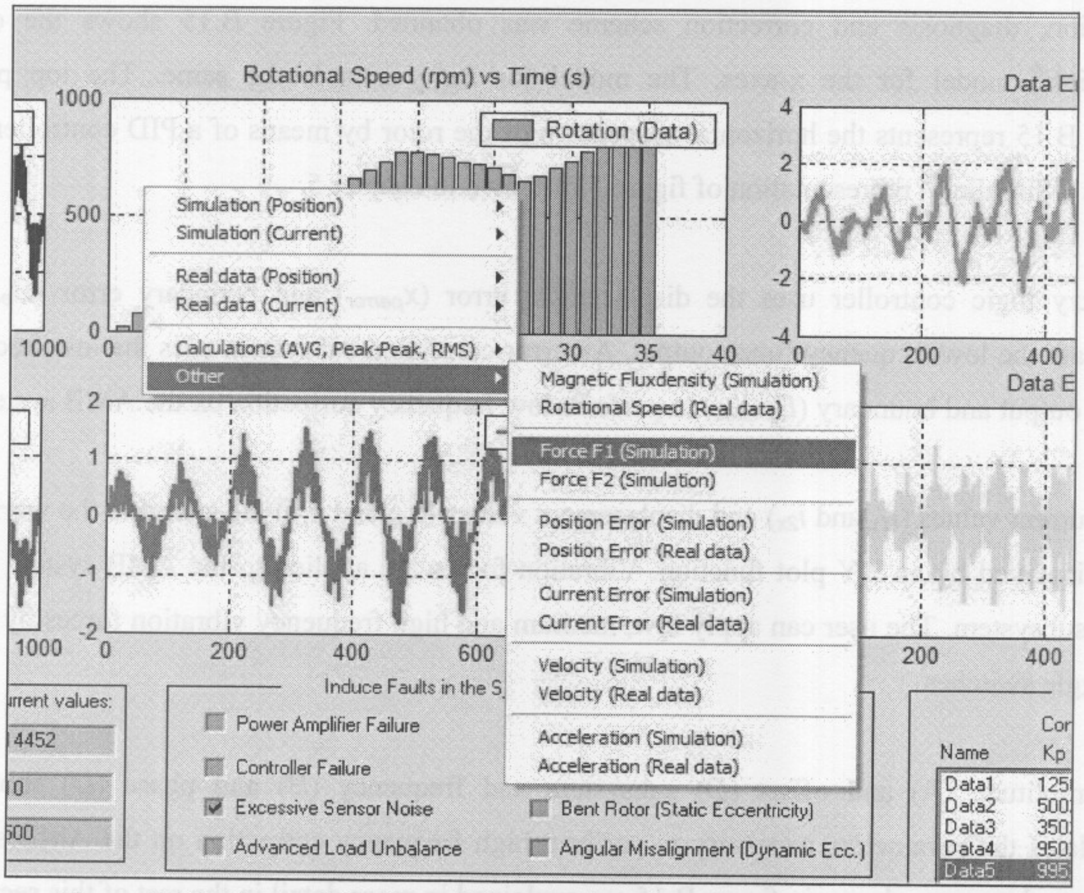

Figure B.13: Zoomed in view of the user interface showing the other option

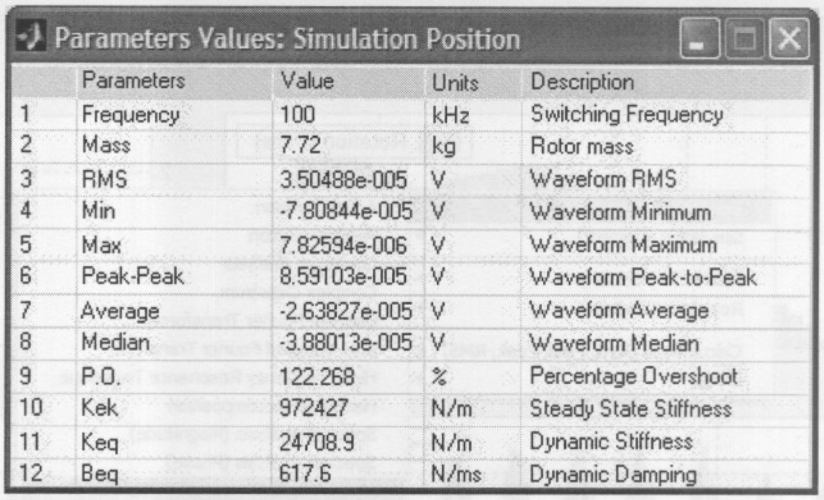

	Parameters	Value	Units	Description
1	Frequency	100	kHz	Switching Frequency
2	Mass	7.72	kg	Rotor mass
3	RMS	3.50488e-005	V	Waveform RMS
4	Min	-7.80844e-005	V	Waveform Minimum
5	Max	7.82594e-006	V	Waveform Maximum
6	Peak-Peak	8.59103e-005	V	Waveform Peak-to-Peak
7	Average	-2.63827e-005	V	Waveform Average
8	Median	-3.88013e-005	V	Waveform Median
9	P.O.	122.268	%	Percentage Overshoot
10	Kek	972427	N/m	Steady State Stiffness
11	Keq	24708.9	N/m	Dynamic Stiffness
12	Beq	617.6	N/ms	Dynamic Damping

Figure B.14: Position parameters table

Figure B.14 shows the position parameter table, which is activated from the calculations (AVG, Peak-Peak, RMS) submenu. The position parameter table provides the user with the parameters of the chosen signal.

B.2. OFFLINE SIMULINK® PLATFORM

This section provides the offline Simulink® platform from where all the simulation results of the detection, diagnosis and correction scheme was obtained. Figure B.15 shows the offline Simulink® model for the x-axes. The model for the y-axes is the same. The top part of figure B.15 represents the horizontal suspension of the rotor by means of a PID controller. This part is a Simulink® representation of figure 5.6, shown in chapter 5.

A fuzzy logic controller uses the displacement error (x_{perror}) and boundary error (B_{error}) to calculate the low frequency fuzzy output. An error correction subsystem uses the low frequency fuzzy output and boundary ($B_{x\text{-}axes}$) to perform low frequency correction on the AMB system.

The current values (i_{1x} and i_{2x}) and displacement values (x_{px} and x_{py}) are stored to the workspace and displayed by an XY plot function. Vibration forces are applied to the AMB system by the error subsystem. The user can apply low, medium and high frequency vibration forces by means of toggle switches.

An amplitude (A) and offset (D) subsystem and frequency (B) and phase (D) subsystem calculates the parameters necessary to perform high frequency correction on the AMB system. All the subsystems shown in figure B.15 are explained in more detail in the rest of this section.

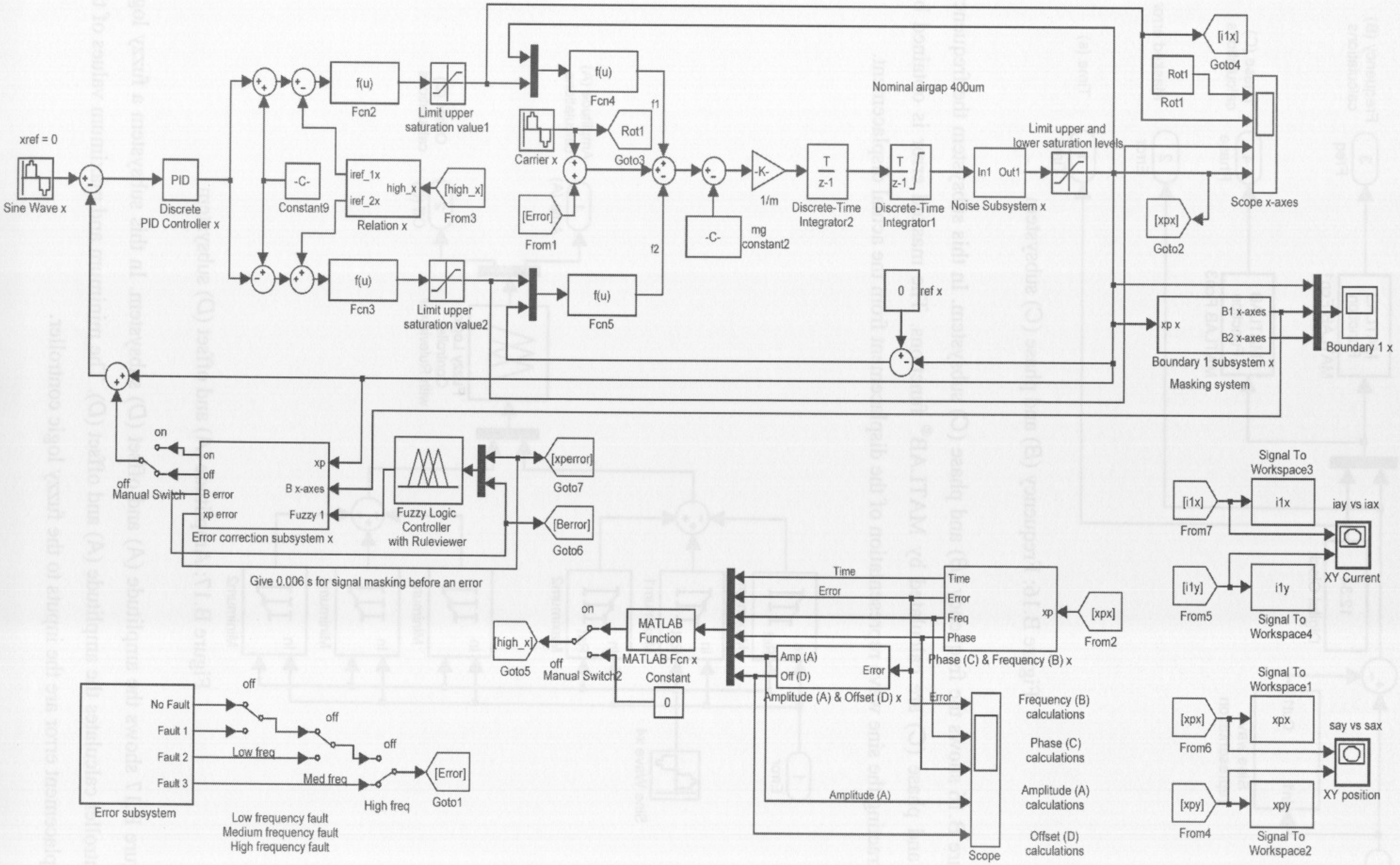

Figure B.15: Offline Simulink® model

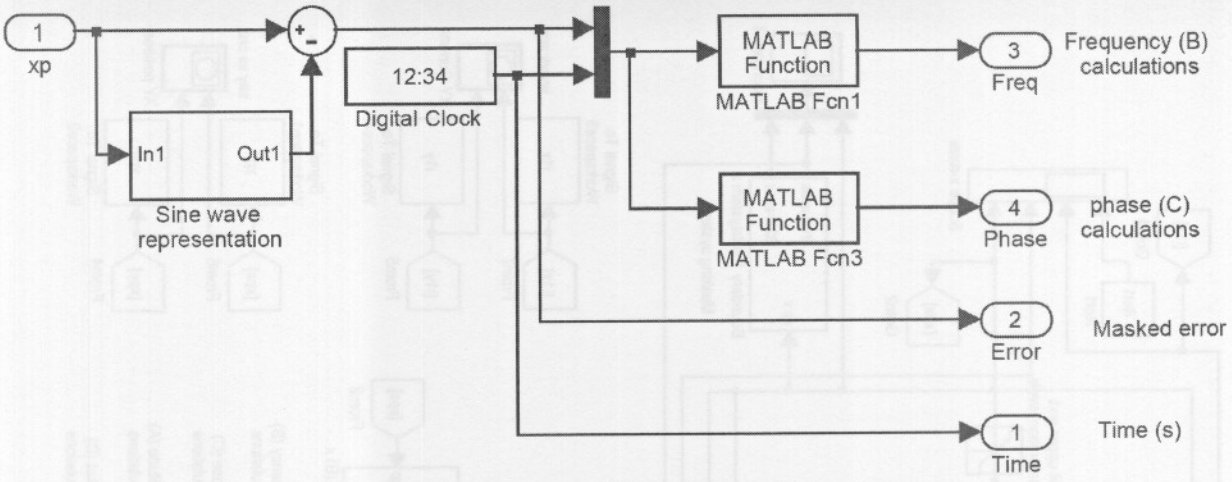

Figure B.16: Frequency (*B*) and phase (*C*) subsystem

Figure B.16 shows the frequency (*B*) and phase (*C*) subsystem. In this subsystem the frequency (*B*) and phase (*C*) are calculated by MATLAB® functions. The masked error is obtained by subtracting the sine wave representation of the displacement from the actual displacement.

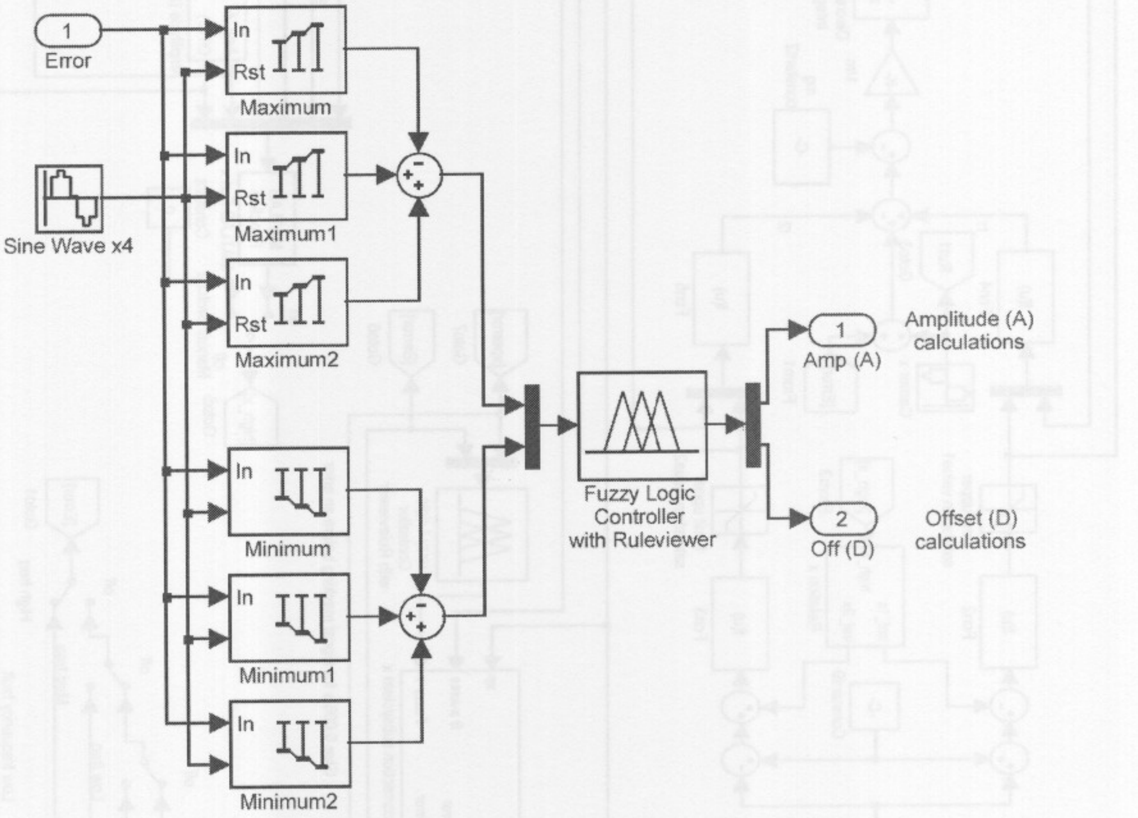

Figure B.17: Amplitude (*A*) and offset (*D*) subsystem

Figure B.17 shows the amplitude (*A*) and offset (*D*) subsystem. In this subsystem a fuzzy logic controller calculates the amplitude (*A*) and offset (*D*). The minimum and maximum values of the displacement error are the inputs to the fuzzy logic controller.

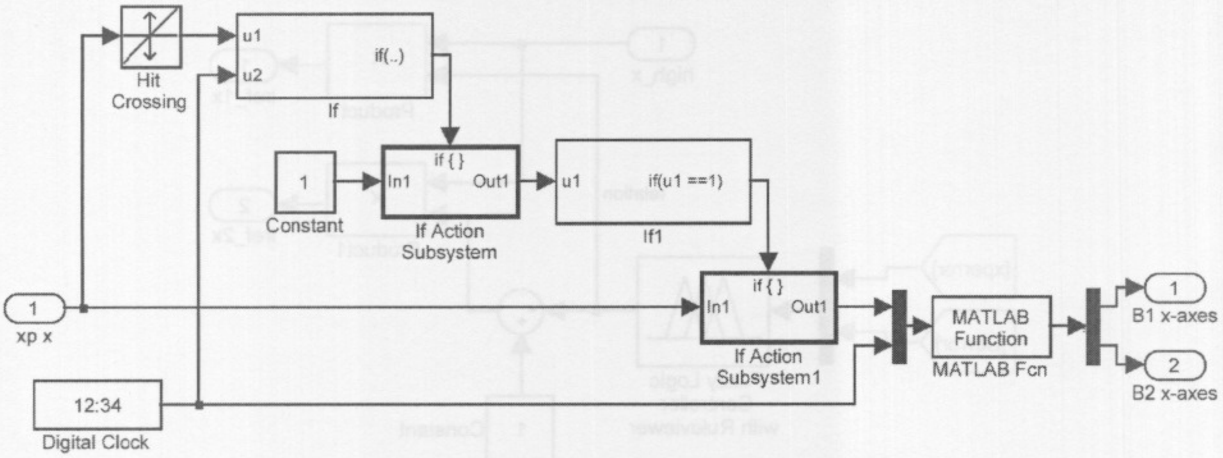

Figure B.18: Boundary subsystem

Figure B.18 shows the boundary subsystem. In this subsystem a MATLAB® function calculates the first and second boundaries ($B1_{x\text{-}axes}$ and $B2_{x\text{-}axes}$). The inputs to the MATLAB® function are the crossing displacement and time.

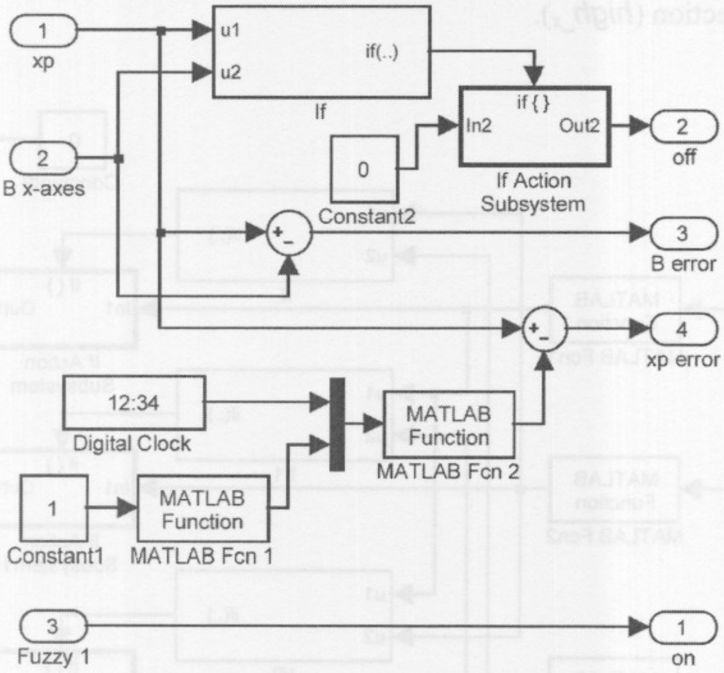

Figure B.19: Error correction subsystem

Figure B.19 shows the error correction subsystem. In this subsystem the boundary error (B_{error}) is calculated by subtracting the boundary ($B_{x\text{-}axes}$) from the actual displacement (x_p). The displacement error is calculated by subtracting the masked displacement from the actual displacement. The masked displacement is calculated by two MATLAB® functions.

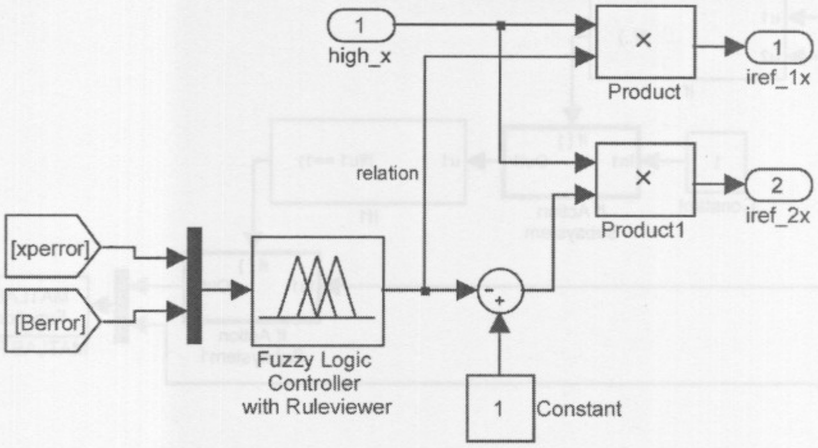

Figure B.20: Relation subsystem

Figure B.20 shows the relation subsystem. In this subsystem the relation current is calculated by a fuzzy logic controller with displacement error and boundary error as inputs. The correctional reference currents (i_{ref_1x} and i_{ref_2x}) are calculated from the product of the relation current and high frequency correction ($high_{\_x}$).

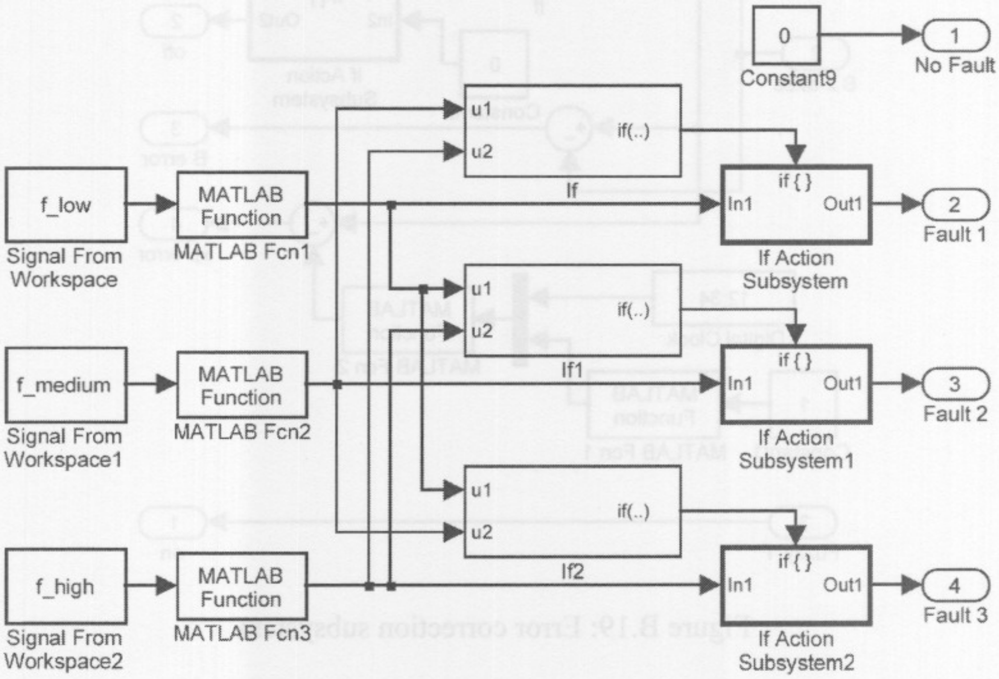

Figure B.21: Error subsystem

Figure B.21 shows the error subsystem. In this subsystem the three vibration forces (*fault1*, *fault2* and *fault3*) are calculated from the three MATLAB® functions. The inputs to the MATLAB® functions come from the workspace.

APPENDIX C

REAL-TIME IMPLEMENTATION AND HARDWARE SETUP

This appendix provides the real-time code that was downloaded onto the dSPACE® 1104 controller board, equipped with a DSP TMS320F240 from Texas Instruments. The real-time code responsible for suspending the rotor, applying vibration forces, performing detection, diagnosis, correction and identification was created in Simulink®. Data acquisition was performed by a user interface created in Controldesk®.

Due to the complexity of the control, detection and correction schemes, the dSPACE® controller was not able to handle all the instructions and real-time errors occurred. This problem was solved by implementing an additional dSPACE® 1104 controller boards, one for each axes of the magnetic bearing. A roller bearing was installed on the right side of the rotor, which increased the sampling time of the DSP, since only one side has to be suspended. More detail on this is available in sections 5.4, 6.3 and 7.3.

C.1. REAL-TIME SIMULINK® DIAGRAM FOR COMPUTER 1

Figure C.1 shows the real-time Simulink® diagram for computer 1. This diagram is responsible to vertically suspend the magnetic bearing and apply vibration forces. The system further detects and corrects vibration forces. This is done by means of a choice subsystem, low correction subsystem and high correction subsystem. The rest of this section explains each of the subsystems in more detail.

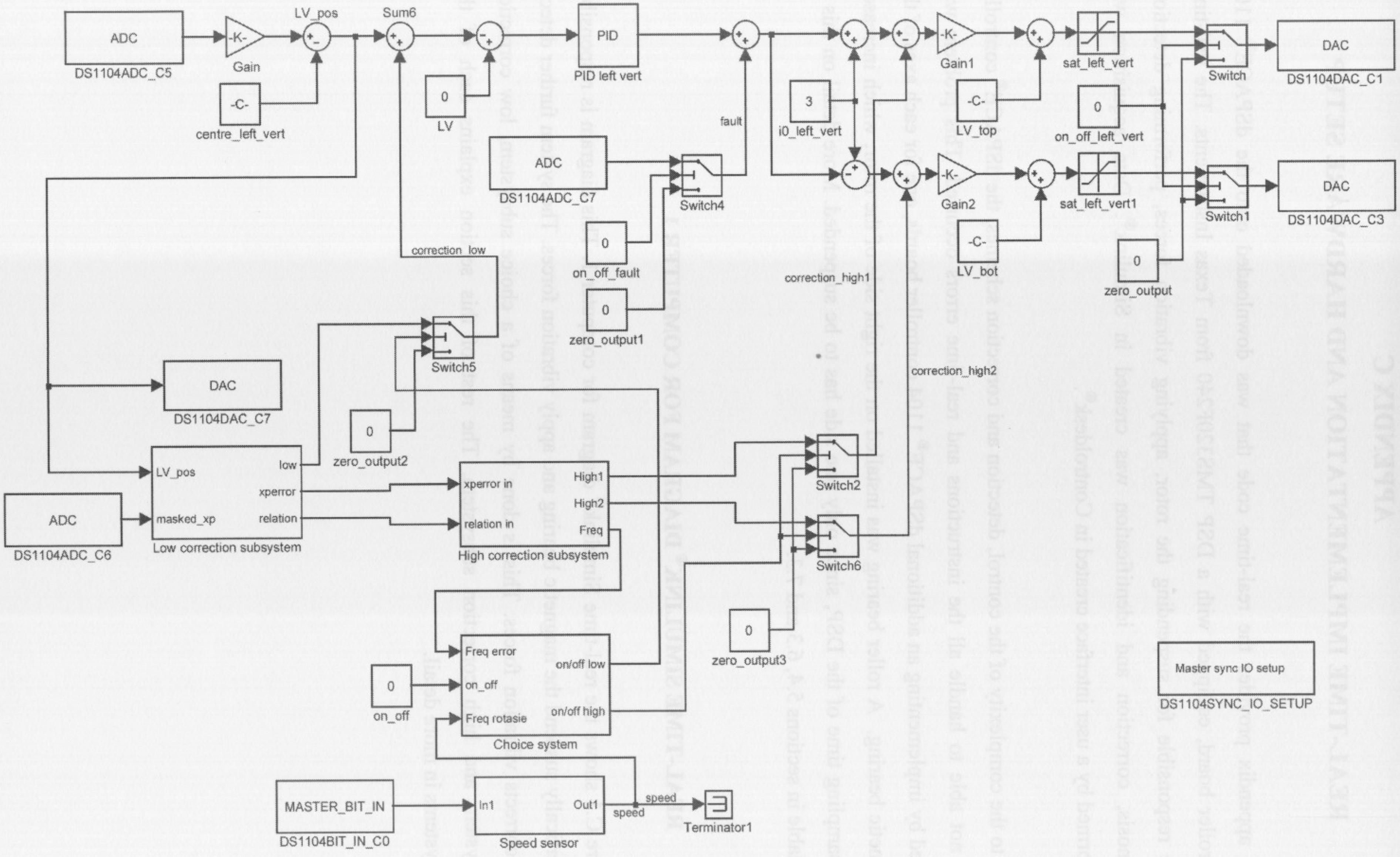

Figure C.1: Real-time Simulink® diagram for computer 1

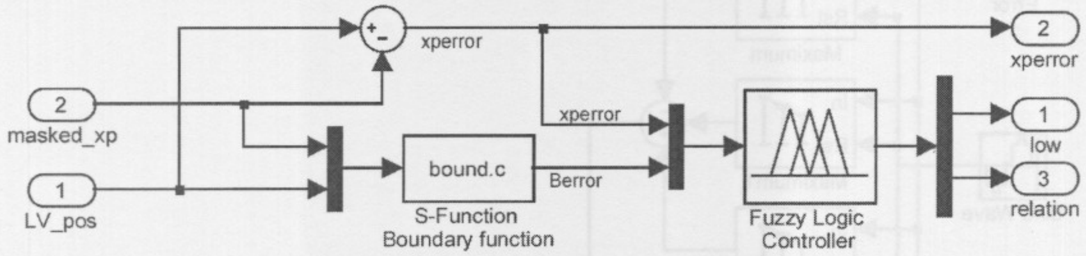

Figure C.2: Low correction subsystem

Figure C.2 shows the low correction subsystem, responsible for correcting low frequency vibration forces. The displacement error (**xperror**) is obtained by subtracting the masked displacement (**masked_xp**) from the left vertical displacement (**LV_pos**). A boundary function calculates the boundary error (**Berror**). A fuzzy logic controller then uses the displacement error and boundary error to calculate the low frequency correction (**low**) and relation current (**relation**).

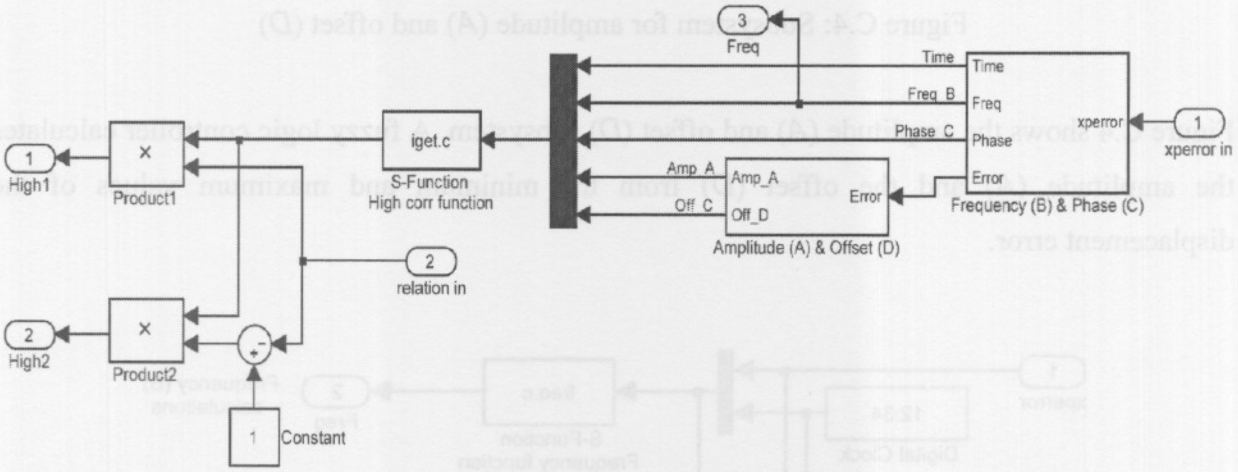

Figure C.3: High correction subsystem

Figure C.3 shows the high correction subsystem, responsible for calculating the high frequency correction current needed to re-stabilise the rotor. A high frequency correction function uses the parameters (*A*, *B*, *C* and *D*) obtained from a frequency (*B*) and phase (*C*) subsystem and an amplitude (*A*) and offset (*D*) subsystem. The high frequency correction currents (**High1** and **High2**) are obtained from the output of the high frequency correction function and relation current.

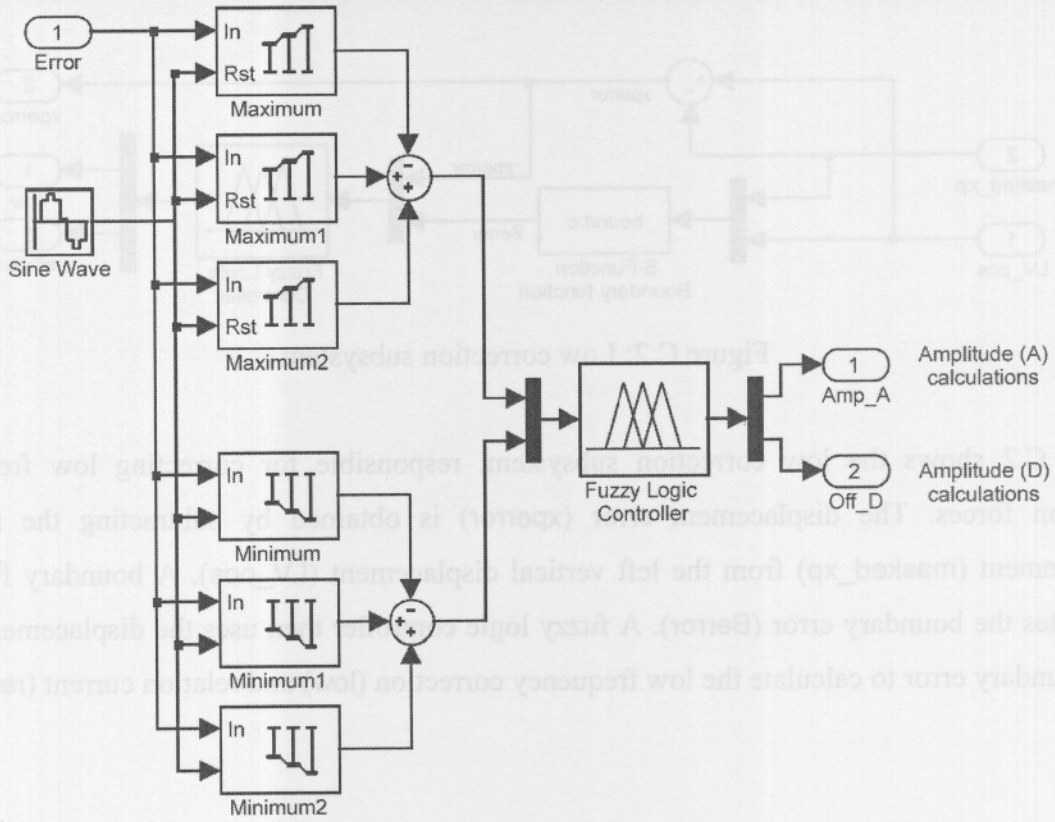

Figure C.4: Subsystem for amplitude (*A*) and offset (*D*)

Figure C.4 shows the amplitude (*A*) and offset (*D*) subsystem. A fuzzy logic controller calculates the amplitude (*A*) and the offset (*D*) from the minimum and maximum values of the displacement error.

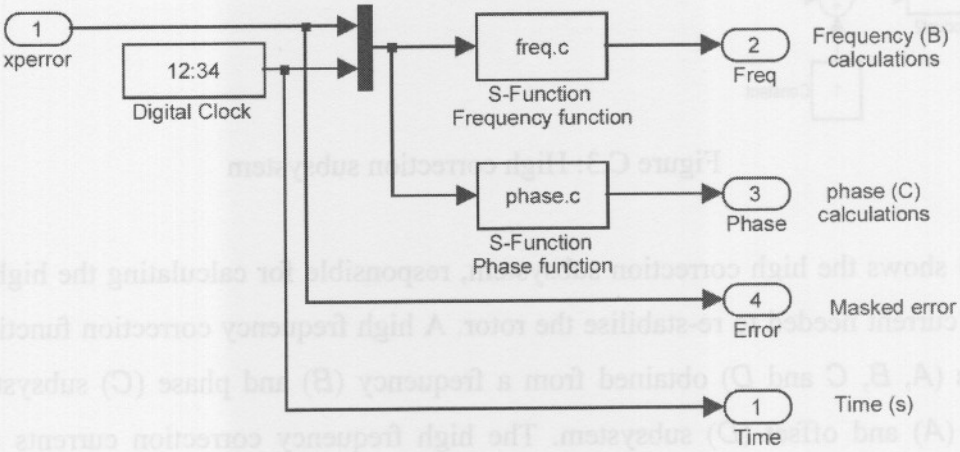

Figure C.5: Subsystem for frequency (*B*) and phase (*C*)

Figure C.5 shows the frequency (*B*) and phase (*C*) subsystem. The frequency and phase is calculated by using S-function blocks, which makes use of the Wigner-Ville distribution and sinusoidal functions to perform calculations.

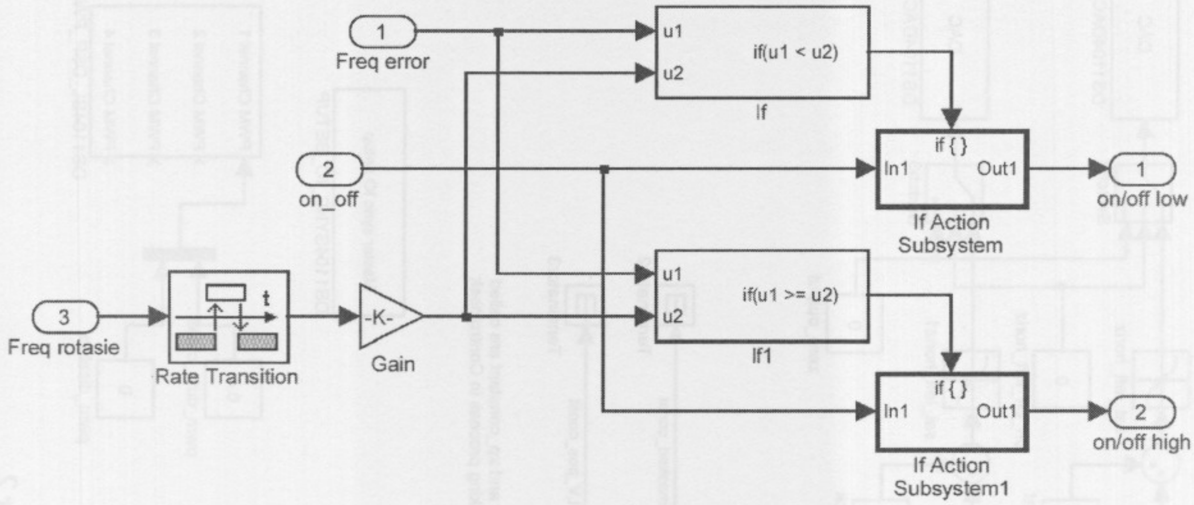

Figure C.6: Choice subsystem

Figure C.6 shows the choice subsystem, responsible for identifying the fault as a low frequency or a high frequency fault. This is done according to the rotational speed of the rotor.

C.2. REAL-TIME SIMULINK® DIAGRAM FOR COMPUTER 2

Figure C.7 shows the real-time Simulink® diagram for computer 2. This diagram was responsible to horizontally suspend the rotor and perform calculations not possible by computer 1. Vibration force calculations and the displacement masking process were performed by this computer. The rest of this section explains the subsystems in more detail.

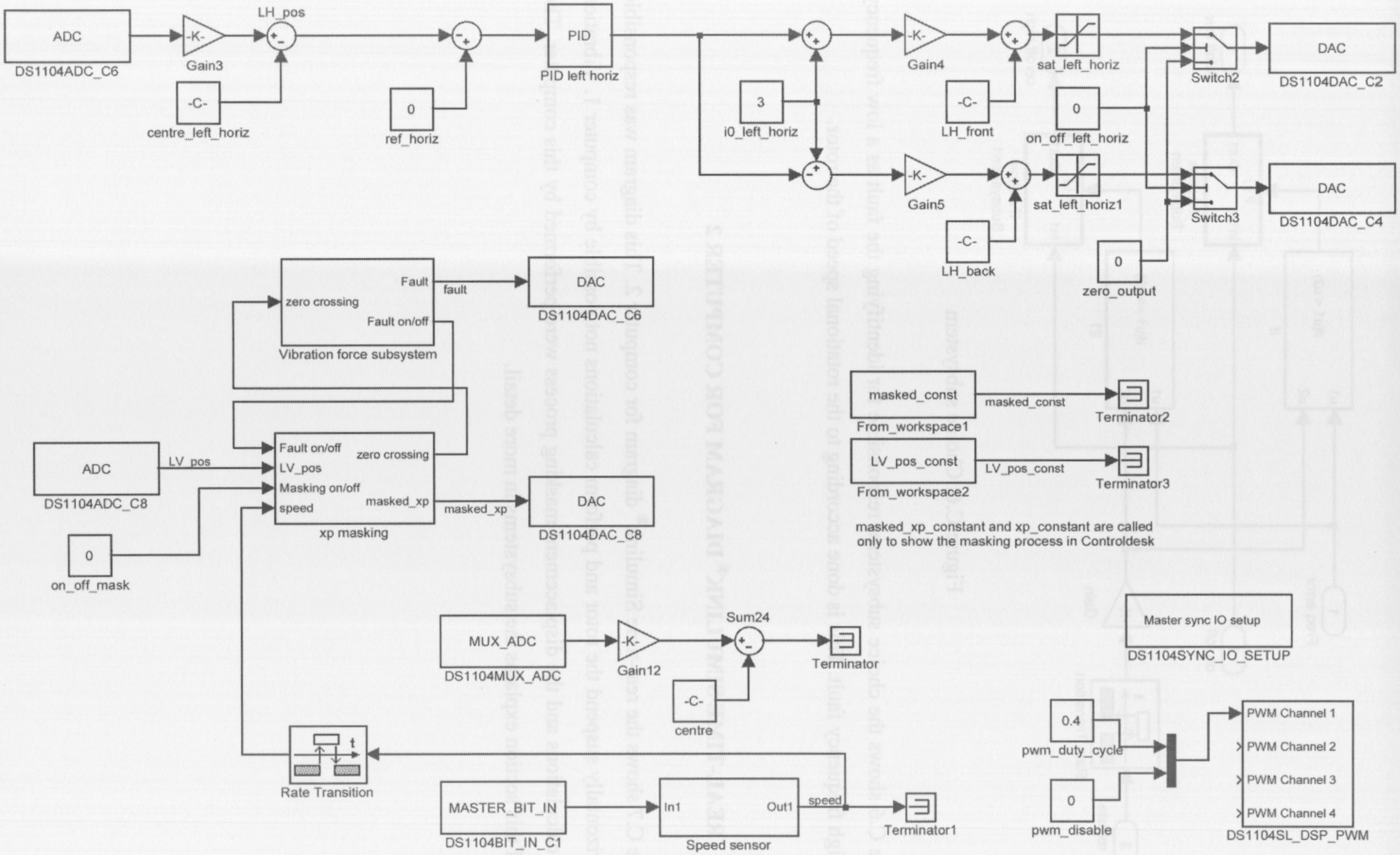

Figure C.7: Real-time Simulink® diagram for computer 2

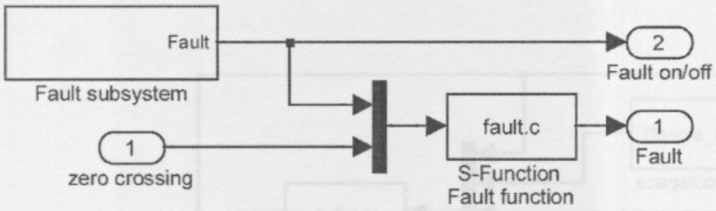

Figure C.8: Vibration force subsystem

Figure C.8 shows the vibration force subsystem. When a fault is activated from the Controldesk® interface, the zero crossing signal goes high (1) and periodically deploys the fault signal on the displacement (x_p).

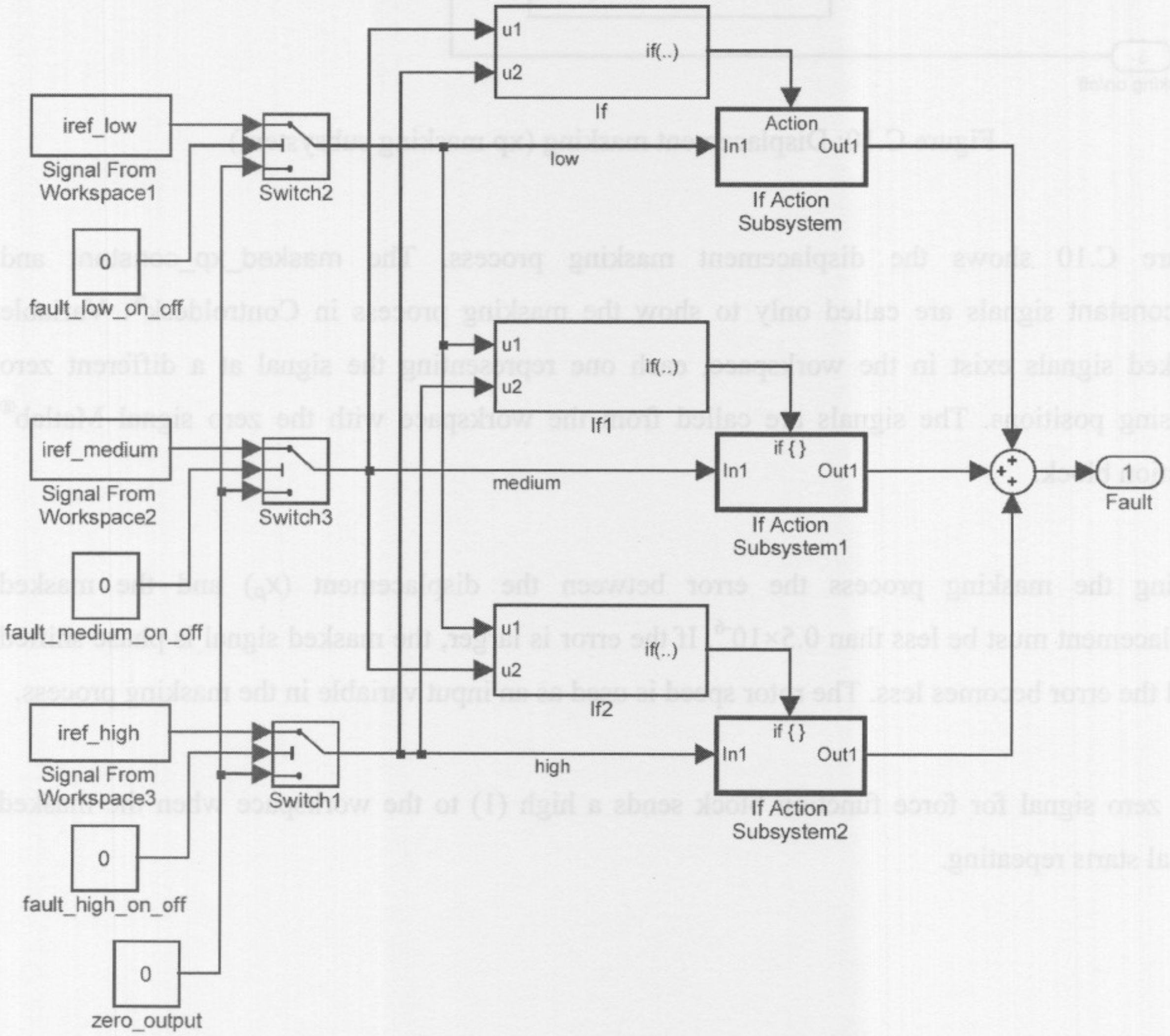

Figure C.9: Fault subsystem

Figure C.9 shows the fault subsystem, responsible for acquiring the fault signal from the workspace and initialisation of the fault.

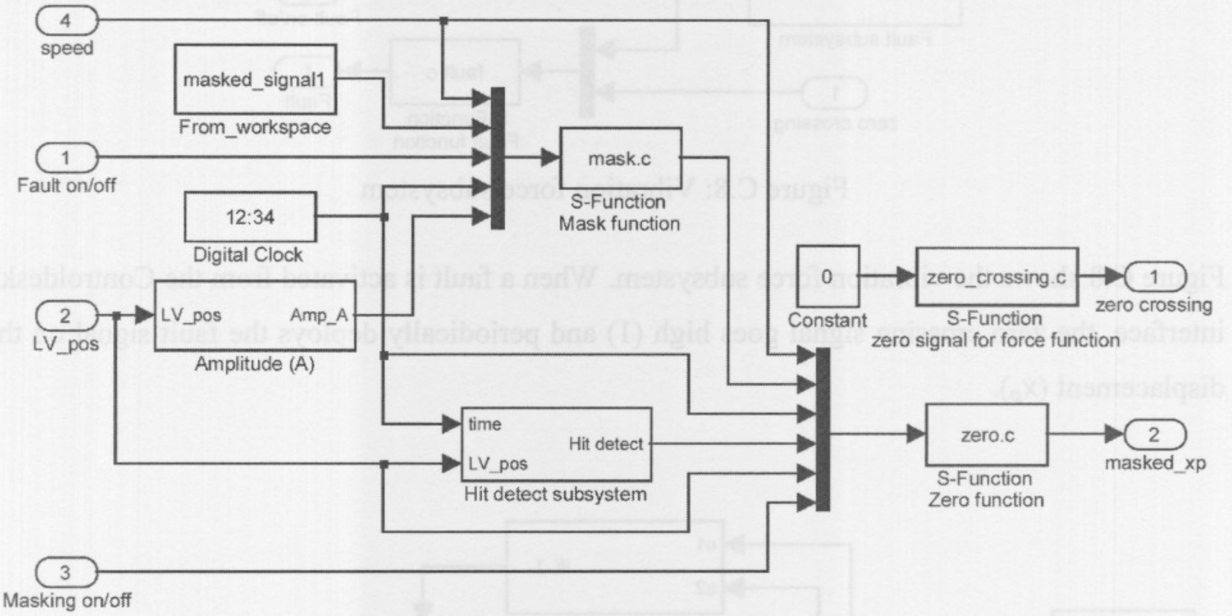

Figure C.10: Displacement masking (xp masking subsystem)

Figure C.10 shows the displacement masking process. The masked_xp_constant and xp_constant signals are called only to show the masking process in Controldesk®. Variable masked signals exist in the workspace, each one representing the signal at a different zero crossing positions. The signals are called from the workspace with the zero signal Matlab® function block.

During the masking process the error between the displacement (x_p) and the masked displacement must be less than 0.5×10^{-6}. If the error is larger, the masked signal is phase shifted until the error becomes less. The rotor speed is used as an input variable in the masking process.

The zero signal for force function block sends a high (1) to the workspace when the masked signal starts repeating.

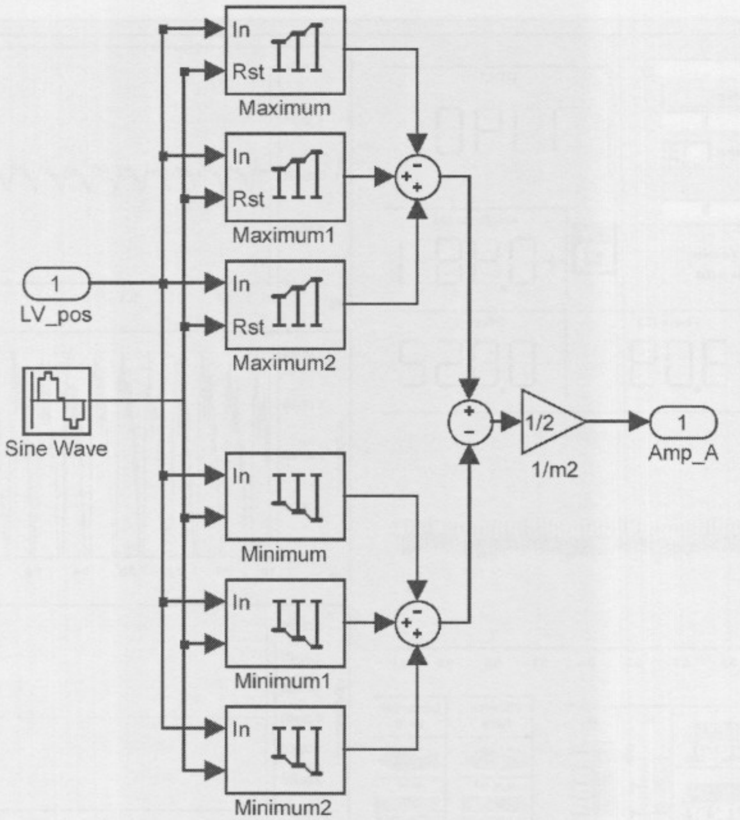

Figure C.11: Subsystem for amplitude (*A*)

Figure C.11 provides the subsystem for amplitude (*A*), which is responsible for calculating the amplitude (*A*) from the minimum and maximum values of the left vertical displacement (LV_pos).

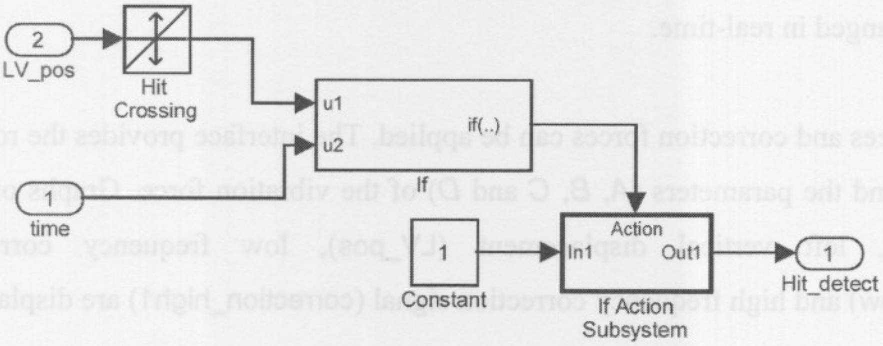

Figure C.12: Hit detect subsystem

Figure C.12 provides the hit detect subsystem, responsible for detecting when the left vertical displacement (LV_pos) performs a zero crossing.

C.3. REAL-TIME CONTROLDESK® INTERFACE FOR COMPUTER 1

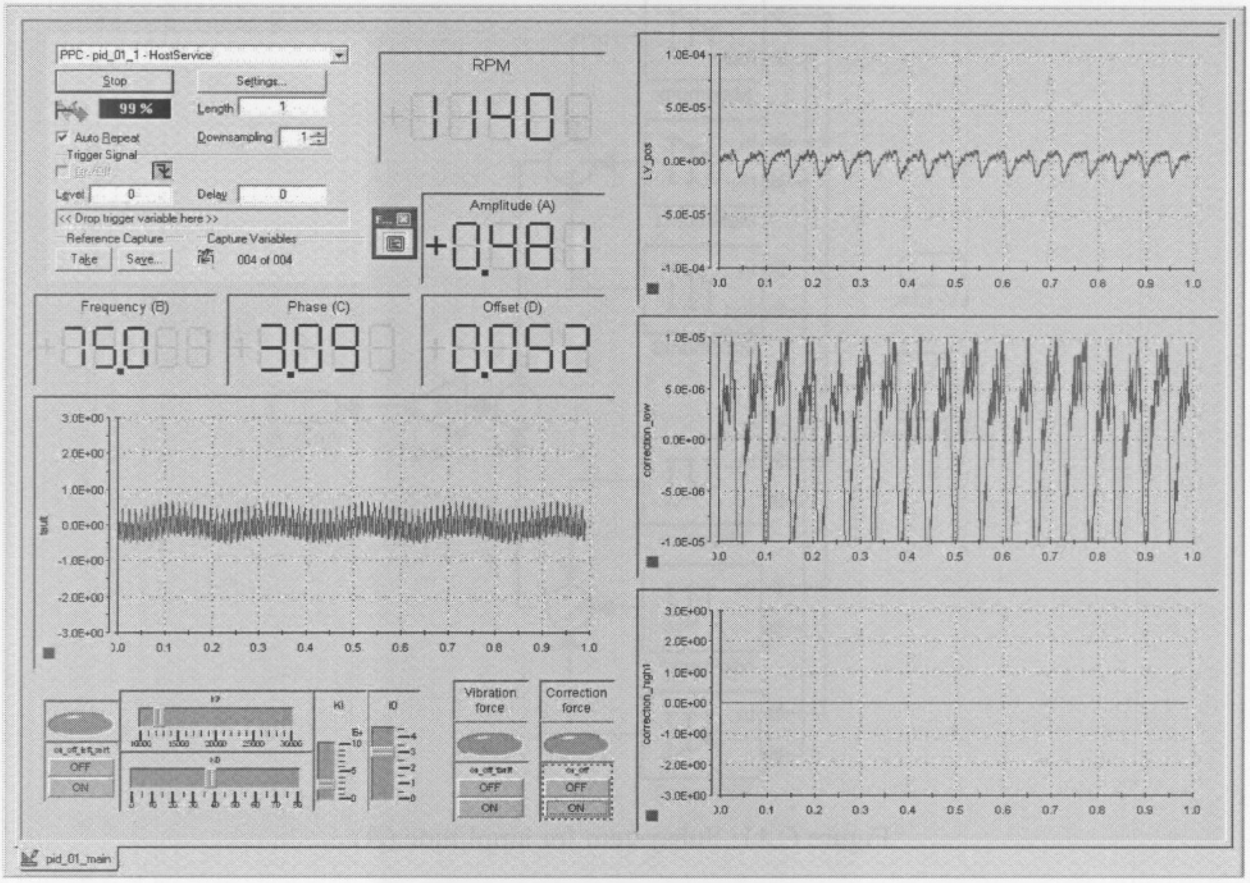

PPC - pid_01_1 - HostService

Length 1

Downsampling 1

☑ Auto Repeat

Level 0

Delay 0

Capture Variables 004 of 004

RPM 1140

Amplitude (A) +0.481

Frequency (B) 75.0

Phase (C) 3.09

Offset (D) 0.052

Figure C.13: Real-time Controldesk® interface for computer 1 with low frequency fault

Figure C.13 shows the real-time Controldesk® interface for computer 1 with low frequency fault. This interface provides the user with real-time access to all commands applicable on the vertical axis of the left magnetic bearing. The controller parameters (k_p, k_i and k_D) and the bias current (i_0) can be changed in real-time.

Vibration forces and correction forces can be applied. The interface provides the rotational speed of the rotor and the parameters (*A*, *B*, *C* and *D*) of the vibration force. Graphs of the vibration force (fault), left vertical displacement (LV_pos), low frequency correction signal (correction_low) and high frequency correction signal (correction_high1) are displayed.

Figure C.14 provides the real-time Controldesk® interface for computer 1 with medium frequency fault. In this figure the vibration force and high frequency signal (correction_high1) is clearly visible. Medium and high frequency faults are corrected by the high frequency correction subsystem. Figure C.15 provides the real-time Controldesk® interface for computer 1 with high frequency fault. In this figure the vibration force (fault) and high frequency correction signal (correction_high1) is clearly visible.

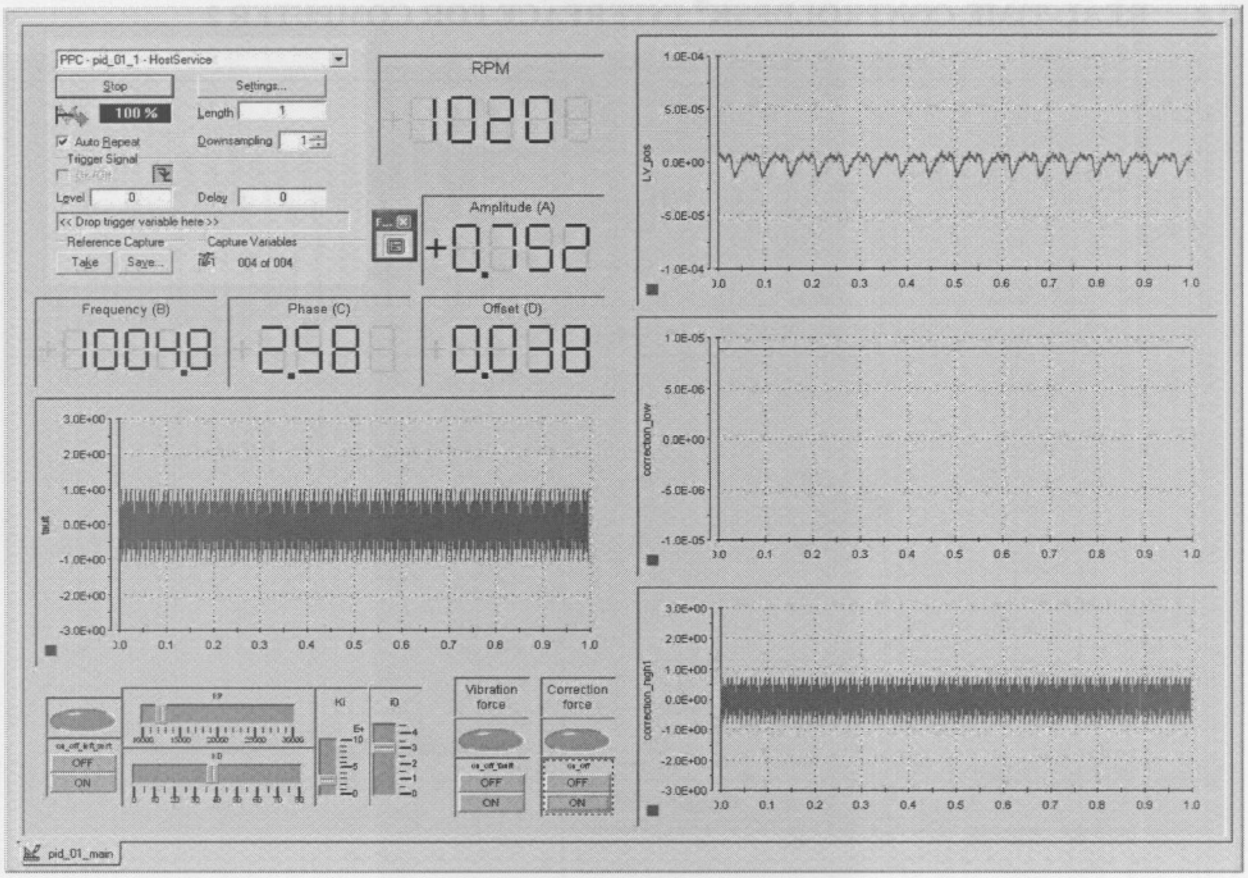

PPC - pid_01_1 - HostService

Length 1

☑ Auto Repeat

Downsampling 1

☐ On/Off

Level 0

Delay 0

Capture Variables 004 of 004

RPM +1020

Amplitude (A) +0.752

Frequency (B) +1004.8

Phase (C) +2.58

Offset (D) +0.038

Figure C.14: Real-time Controldesk® interface for computer 1 with medium frequency fault

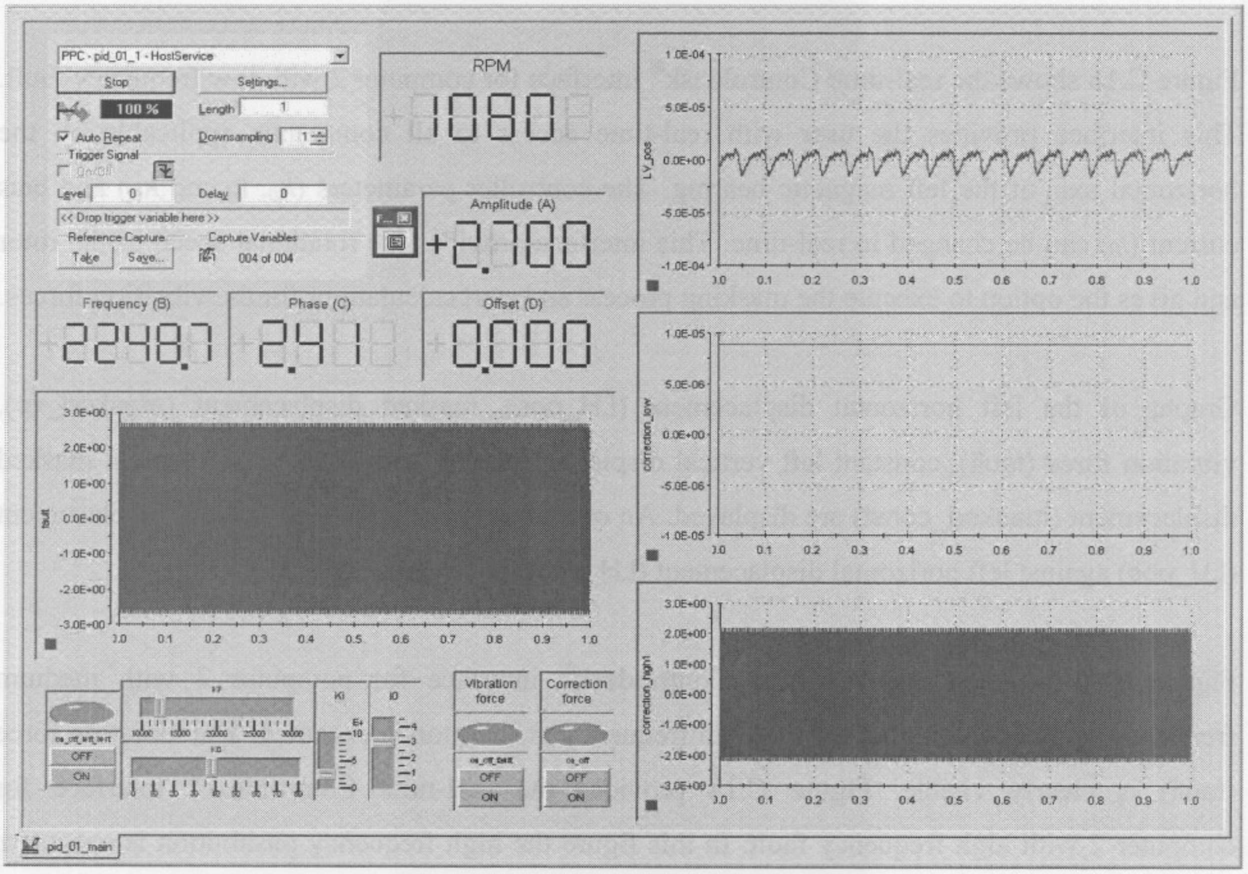

PPC - pid_01_1 - HostService

Length 1

☑ Auto Repeat

Downsampling 1

☐ On/Off

Level 0

Delay 0

Capture Variables 004 of 004

RPM +1080

Amplitude (A) +2.700

Frequency (B) +2248.7

Phase (C) +2.41

Offset (D) +0.000

Figure C.15: Real-time Controldesk® interface for computer 1 with high frequency fault

C.4. REAL-TIME CONTROLDESK® INTERFACE FOR COMPUTER 2

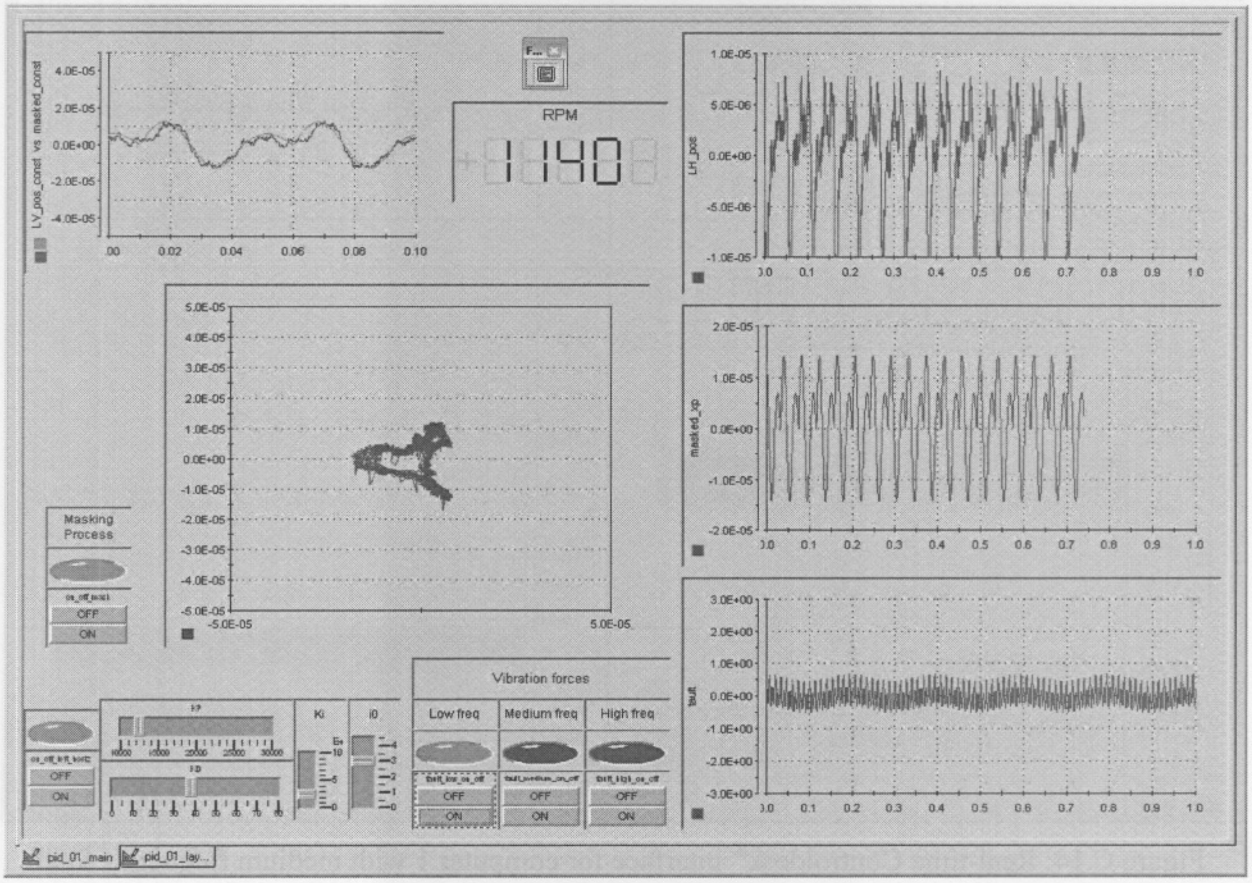

Figure C.16: Real-time Controldesk® interface for computer 2 with low frequency fault

Figure C.16 shows the real-time Controldesk® interface for computer 2 with low frequency fault. This interface provides the user with real-time access to all commands applicable on the horizontal axis of the left magnetic bearing. The controller parameters (k_P, k_i and k_D) and bias current (i_0) can be changed in real-time. This interface provides the rotational speed of the rotor and gives the option to execute the masking process and start calculations for the vibration forces.

Graphs of the left horizontal displacement (LH_pos), masked displacement (masked_xp), vibration force (fault), constant left vertical displacement (LV_pos_const) and constant masked displacement (masked_const) are displayed. An orbital representation (left vertical displacement (LV_pos) against left horizontal displacement (LH_pos)) is also shown.

Figure C.17 provides the real-time Controldesk® interface for computer 2 with medium frequency fault. In this figure the medium frequency pushbutton is executed. The vibration force (fault) is clearly visible. Figure C.18 provides the real-time Controldesk® interface for computer 2 with high frequency fault. In this figure the high frequency pushbutton is executed. The vibration force (fault) signal is clearly visible.

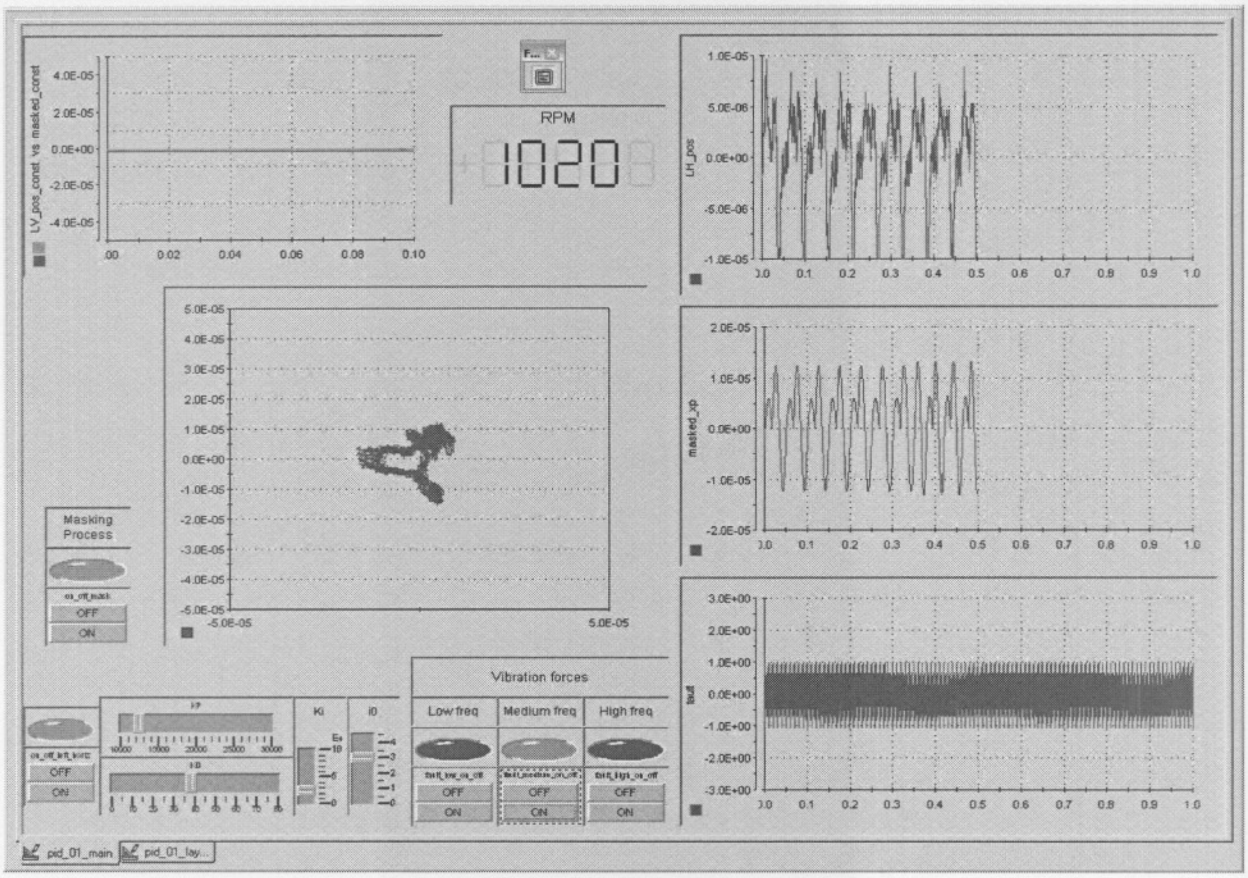

Figure C.17: Real-time Controldesk® interface for computer 2 with medium frequency fault

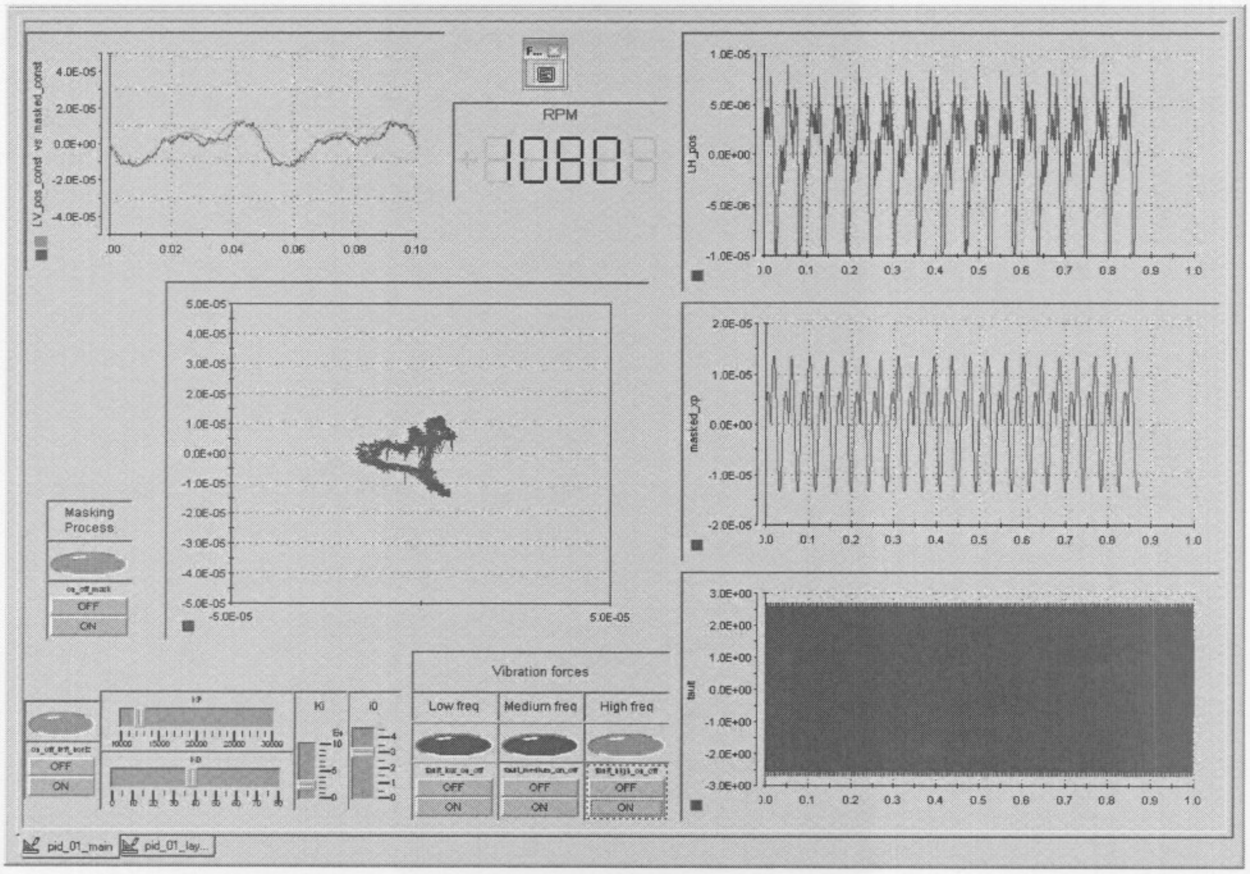

Figure C.18: Real-time Controldesk® interface for computer 2 with high frequency fault

APPENDIX D

CALCULATION OF THE SPRING-MASS-DAMPER CONSTANTS

This appendix focuses on the calculation of the spring-mass-damper constants. Calculation of the constants of the AMB system with one electromagnet will be done first, followed by calculations of the AMB system with both electromagnets.

D.1 AMB SYSTEM WITH ONE ELECTROMAGNET

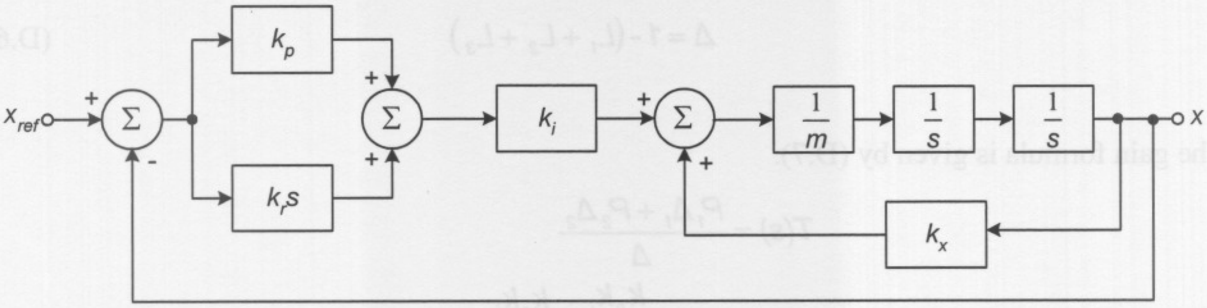

Figure D.1: Block diagram of the AMB system with one electromagnet

Figure D.1 provides the block diagram and figure D.2 the signal flow diagram of the AMB system with one electromagnet. These figures were used to calculate the constants.

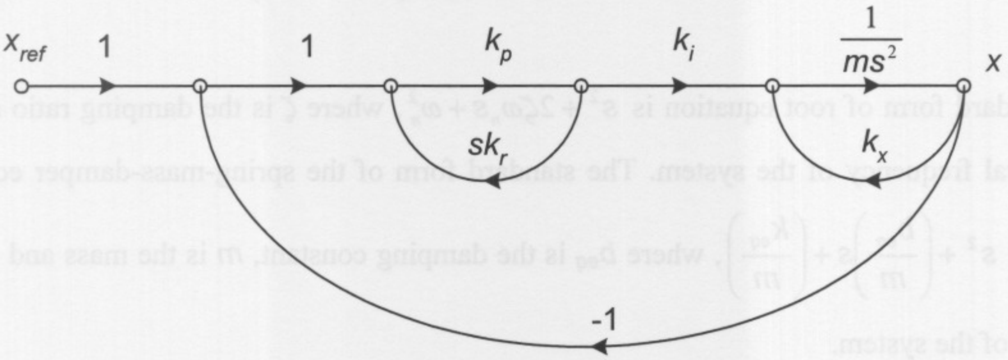

Figure D.2: Signal flow diagram of the AMB system with one electromagnet

The paths and cofactors obtained from figure D.2 are calculated by (D.1) and (D.2).

$$P_1 = \frac{k_p k_i}{ms^2} \qquad \Delta_1 = 1 \tag{D.1}$$

$$P_2 = \frac{k_r k_i}{ms} \qquad \Delta_2 = 1 \tag{D.2}$$

where P_1 and P_2 are the paths and Δ_1 and Δ_2 are the cofactors of the paths.

The loops are calculated by (D.3), (D.4) and (D.5).

$$L_1 = \frac{k_x}{ms^2} \tag{D.3}$$

$$L_2 = -\frac{k_p k_i}{ms^2} \tag{D.4}$$

$$L_3 = -\frac{k_r k_i}{ms} \tag{D.5}$$

The determinant of the graph is given by (D.6).

$$\Delta = 1 - \left(L_1 + L_2 + L_3\right) \tag{D.6}$$

The gain formula is given by (D.7).

$$\begin{aligned} T(s) &= \frac{P_1\Delta_1 + P_2\Delta_2}{\Delta} \\ &= \frac{\dfrac{k_p k_i}{ms^2} + \dfrac{k_r k_i}{ms}}{1 - \dfrac{k_x}{ms^2} + \dfrac{k_p k_i}{ms^2} + \dfrac{k_r k_i}{ms}} \\ &= \frac{\dfrac{k_i}{m}\left(k_r s + k_p\right)}{s^2 + \left(\dfrac{k_r k_i}{m}\right)s + \left(\dfrac{k_p k_i}{m} - \dfrac{k_x}{m}\right)} \end{aligned} \tag{D.7}$$

The standard form of root equation is $s^2 + 2\zeta\omega_n s + \omega_n^2$, where ζ is the damping ratio and ω_n is the natural frequency of the system. The standard form of the spring-mass-damper equation is given by $s^2 + \left(\frac{b_{eq}}{m}\right)s + \left(\frac{k_{eq}}{m}\right)$, where b_{eq} is the damping constant, m is the mass and k_{eq} is the stiffness of the system.

Therefore: $\dfrac{b_{eq}}{m} = \dfrac{k_r k_i}{m} \qquad \therefore b_{eq} = k_r k_i$

and $\dfrac{k_{eq}}{m} = \dfrac{k_p k_i - k_x}{m} \qquad \therefore k_{eq} = k_p k_i - k_x$

Further $\omega_n = \sqrt{\dfrac{k_p k_i - k_x}{m}}$ and $2\zeta\omega_n = \dfrac{k_r k_i}{m} \qquad \therefore \zeta = \dfrac{k_r k_i}{2\omega_n} = \dfrac{k_r k_i \sqrt{m}}{2\sqrt{k_p k_i - k_x}}$

D.2 AMB SYSTEM WITH BOTH ELECTROMAGNETS

Figure D.3 provides the block diagram and figure D.4 the signal flow diagram of the AMB system with both electromagnets. These figures provided the basis for the calculation of the spring-mass-damper constants. The parameter i_0 in figure D.4 represent the bias current.

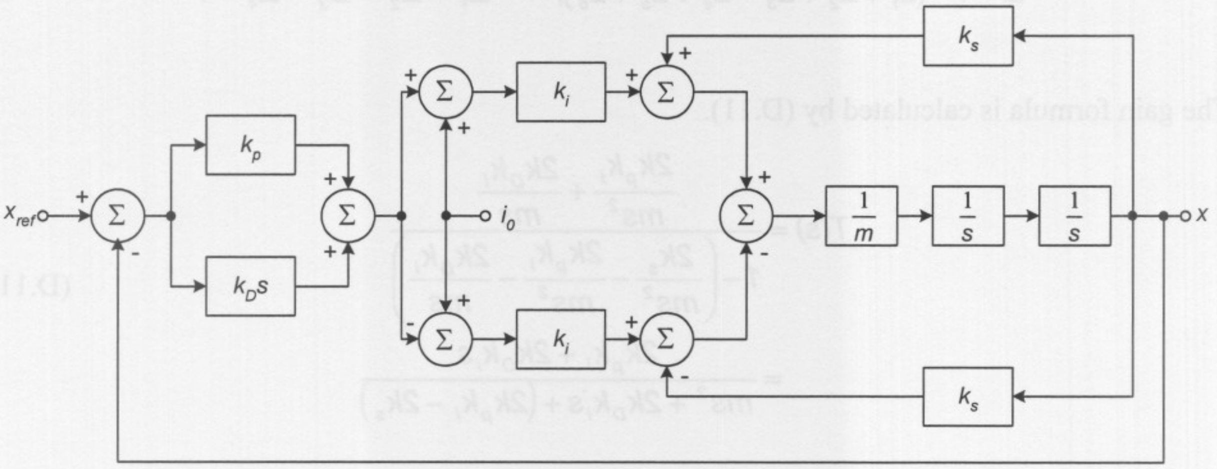

Figure D.3: Block diagram of the AMB system with both electromagnets

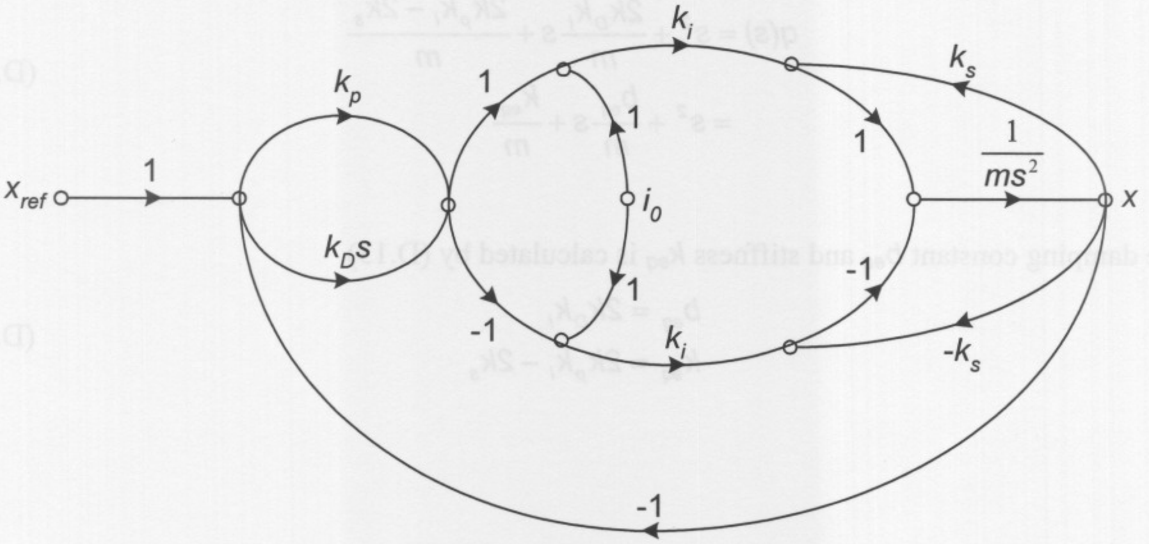

Figure D.4: Signal flow diagram of the AMB system with both electromagnets

The paths and loops obtained from figure D.2 are given by (D.8) and (D.9).

$$P_1 = \frac{k_p k_i}{ms^2},\ P_2 = \frac{k_D s \cdot k_i}{ms^2} = \frac{k_D k_i}{ms},\ P_3 = \frac{k_p k_i}{ms^2},\ P_4 = \frac{k_D s \cdot k_i}{ms^2} = \frac{k_D k_i}{ms} \tag{D.8}$$

$$L_1 = \frac{k_s}{ms^2},\ L_2 = \frac{k_s}{ms^2},\ L_3 = -\frac{k_p k_i}{ms^2},\ L_4 = -\frac{k_D k_i}{ms},\ L_5 = L_3,\ L_6 = L_4 \tag{D.9}$$

The calculation of the gain formula, determinant of the graph and cofactors of the paths is given by (D.10).

$$T(s) = \frac{P_1\Delta_1 + P_2\Delta_2 + P_3\Delta_3 + P_4\Delta_4}{\Delta} \qquad \text{(D.10)}$$
$$\Delta = 1 - (L_1 + L_2 + L_3 + L_4 + L_5 + L_6), \qquad \Delta_1 = \Delta_2 = \Delta_3 = \Delta_4 = 1$$

The gain formula is calculated by (D.11).

$$\begin{aligned} T(s) &= \frac{\dfrac{2k_p k_i}{ms^2} + \dfrac{2k_D k_i}{ms}}{1 - \left(\dfrac{2k_s}{ms^2} - \dfrac{2k_p k_i}{ms^2} - \dfrac{2k_D k_i}{ms}\right)} \\ &= \frac{2k_p k_i + 2k_D k_i s}{ms^2 + 2k_D k_i s + (2k_p k_i - 2k_s)} \end{aligned} \qquad \text{(D.11)}$$

From the root equation and the spring-mass-damper equation constants the following equation can therefore be obtained:

$$\begin{aligned} q(s) &= s^2 + \frac{2k_D k_i}{m}s + \frac{2k_p k_i - 2k_s}{m} \\ &= s^2 + \frac{b_{eq}}{m}s + \frac{k_{eq}}{m} \end{aligned} \qquad \text{(D.12)}$$

The damping constant b_{eq} and stiffness k_{eq} is calculated by (D.13).

$$\begin{aligned} b_{eq} &= 2k_D k_i \\ k_{eq} &= 2k_p k_i - 2k_s \end{aligned} \qquad \text{(D.13)}$$

APPENDIX E

RESULTS ON THE TECHNIQUES FOR FAULT DETECTION

The research presented in this chapter was part of a study completed at the University of Applied Sciences Zittau/Görlitz in Germany in 2006.

Condition monitoring was performed on the 250 kW water cooling AMB pump, situated at the Boxberg power plant in Germany. This was done to obtain fault data. Fault detection techniques were implemented and results were obtained from the historical fault data of the 250 kW water cooling AMB pump.

Techniques were implemented on the three historical fault datasets (subsynchronous, rotor synchronous and supersynchronous vibration force). Results on the three datasets can be found in sections E.1 – E.3, respectively.

The last section of this chapter provides a discussion on the results obtained from the fault detection techniques. In this section amplitude and frequency feature extraction is discussed. The author provides advice on what techniques will provide the best solution for amplitude and frequency features extraction for a specific fault (vibration force).

The purpose of this chapter is to determine which fault detection technique is the best to use for a specific fault (vibration force). All color images in this chapter are available on the CD.

E.1. TECHNIQUES IMPLEMENTED ON HISTORICAL FAULT DATASET 1

This section focuses and analyses one of the subsynchronous vibration force entries in historical fault dataset 1.

E.1.1. OVERVIEW ON HISTORICAL FAULT DATASET 1

Figure E.1 and figure E.2 provides the fundamental part of the displacement and current dataset. In this dataset the displacements and currents are respectively represented as follow: the green line represents the x-axis on the A-side (motor side), the red line the y-axis on the A-side, blue line x-axis on the B-side (non-driven side), the orange line the y-axis on the B-side and the black line represents the z-axis.

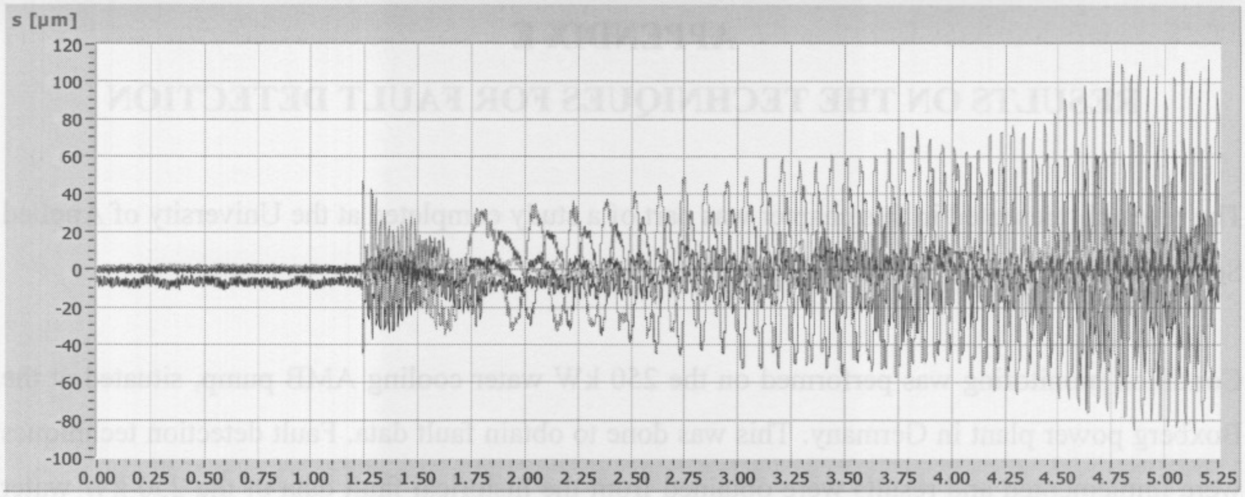

Figure E.1: Fundamental part of the displacement (all axes)

These figures provide the situation from where the fault started up to where the AMB system was shut down due to an excessive amount of vibration.

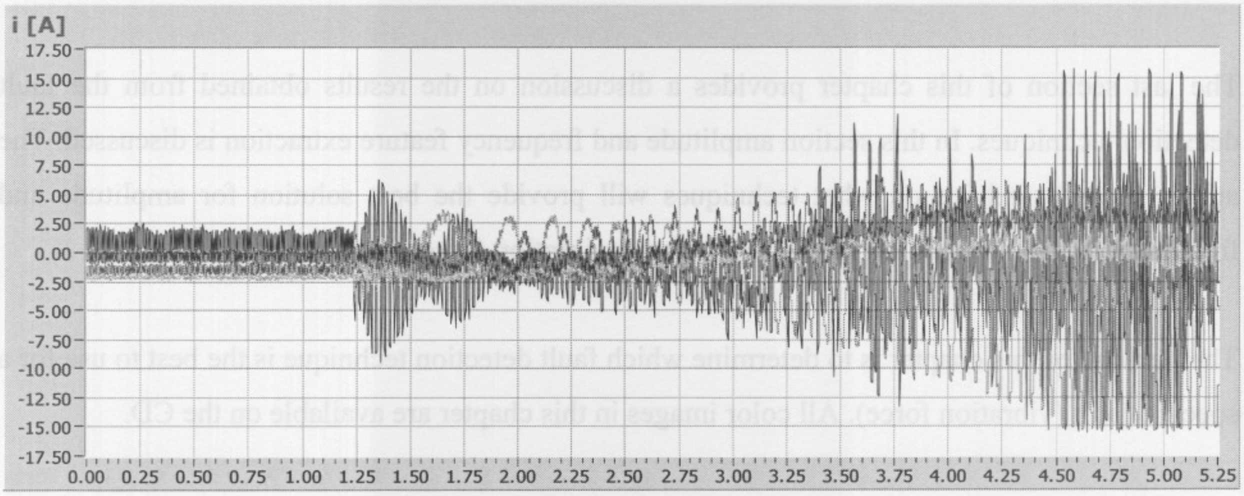

Figure E.2: Fundamental part of the current (all axes)

The most vibration in the data can again be seen on the motor side (A-side), therefore it was decided to concentrate all calculations on this side. Furthermore the increase of the vibration of the current compared to the increase of the vibration of the displacement is almost the same. This can be seen in figure E.3 and figure E.4. The rest of the calculations therefore focus on displacement analysis.

Figure E.3 provides the fundamental displacement before the fault has occurred (first second of the dataset), second phase of the fault (next second of the dataset) and the last phase of the fault (last second of the dataset).

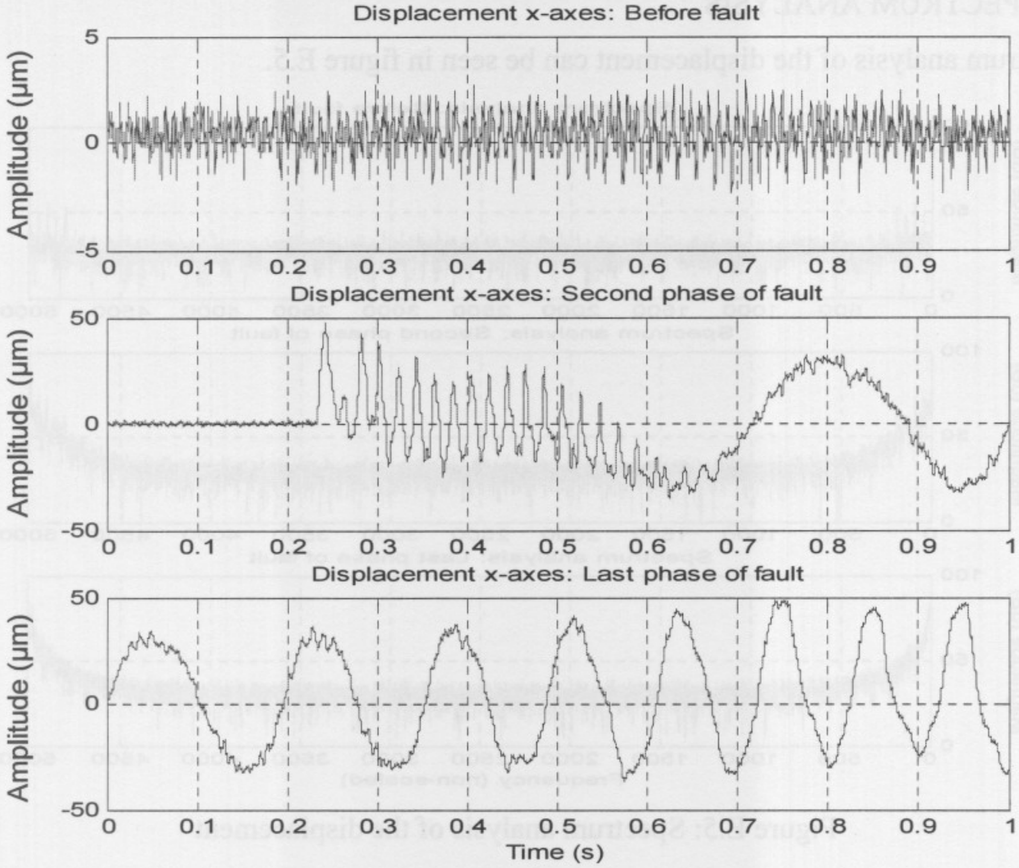

Figure E.3: Displacement x-axis (A-side)

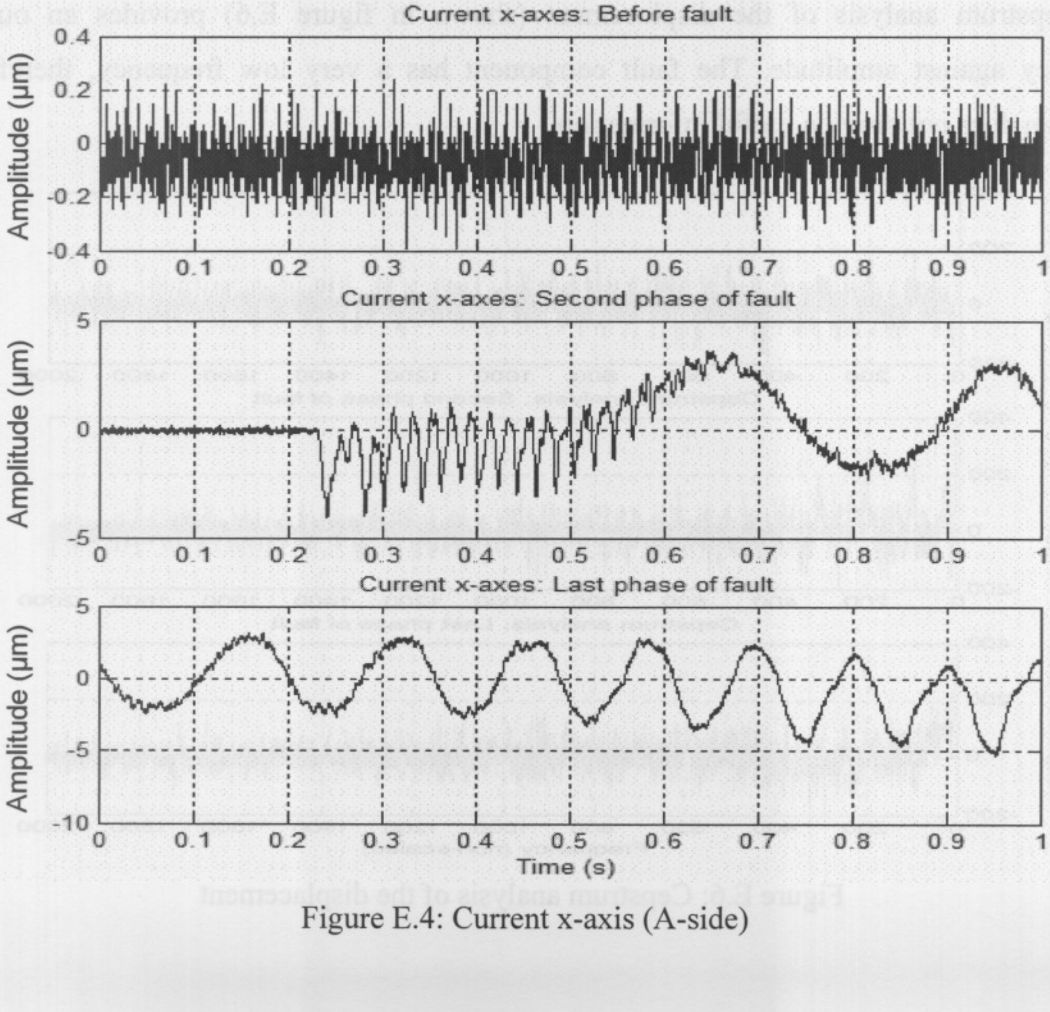

Figure E.4: Current x-axis (A-side)

E.1.2. SPECTRUM ANALYSIS

The spectrum analysis of the displacement can be seen in figure E.5.

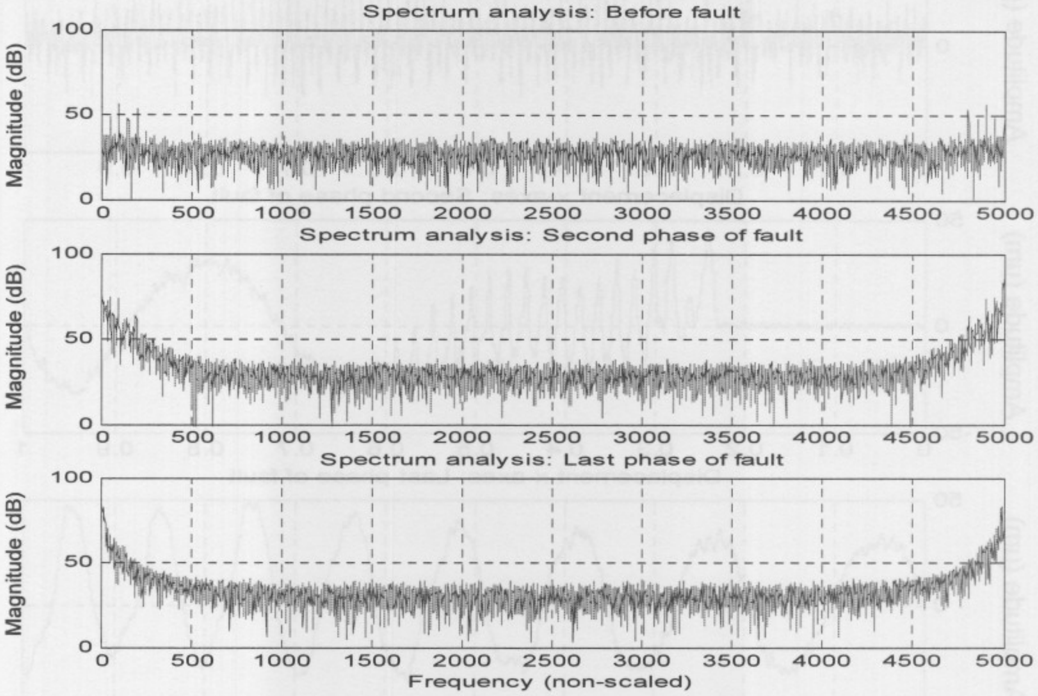

Figure E.5: Spectrum analysis of the displacement

E.1.3. CEPSTRUM ANALYSIS

The Cepstrum analysis of the displacement (shown in figure E.6) provides an output of quefrency against amplitude. The fault component has a very low frequency, therefore the Cepstrum does not provide useful information.

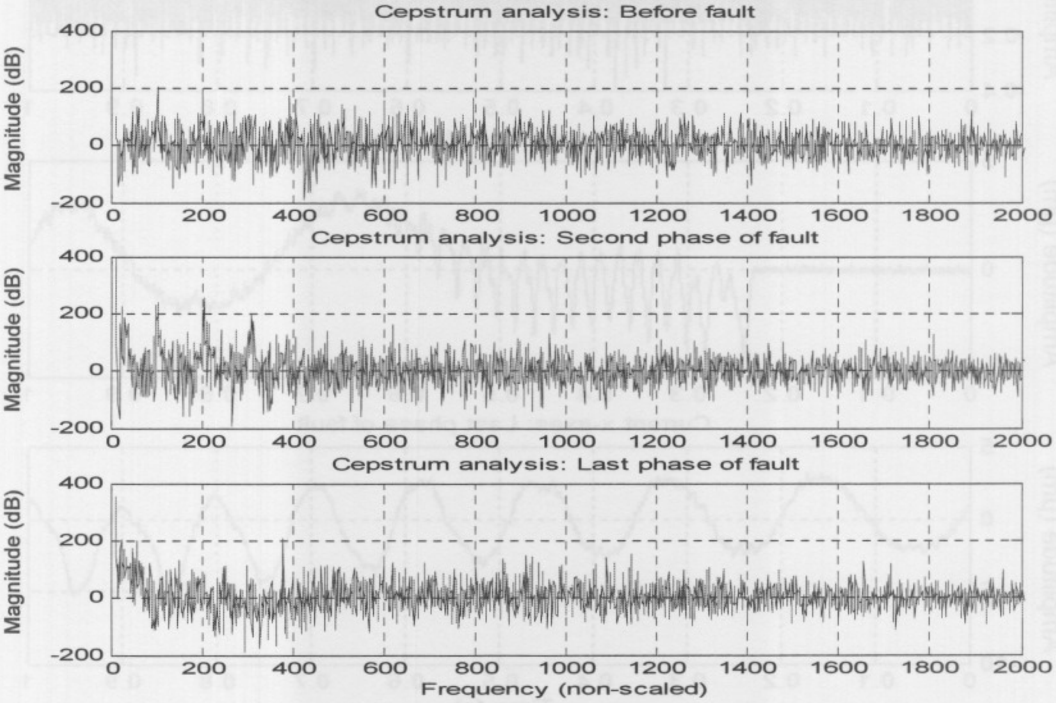

Figure E.6: Cepstrum analysis of the displacement

E.1.4. SYNCHRONOUS AVERAGE

Figure E.7 provides the synchronous average (SA) of the displacement before the fault has occurred, second phase of the fault and the last phase of the fault.

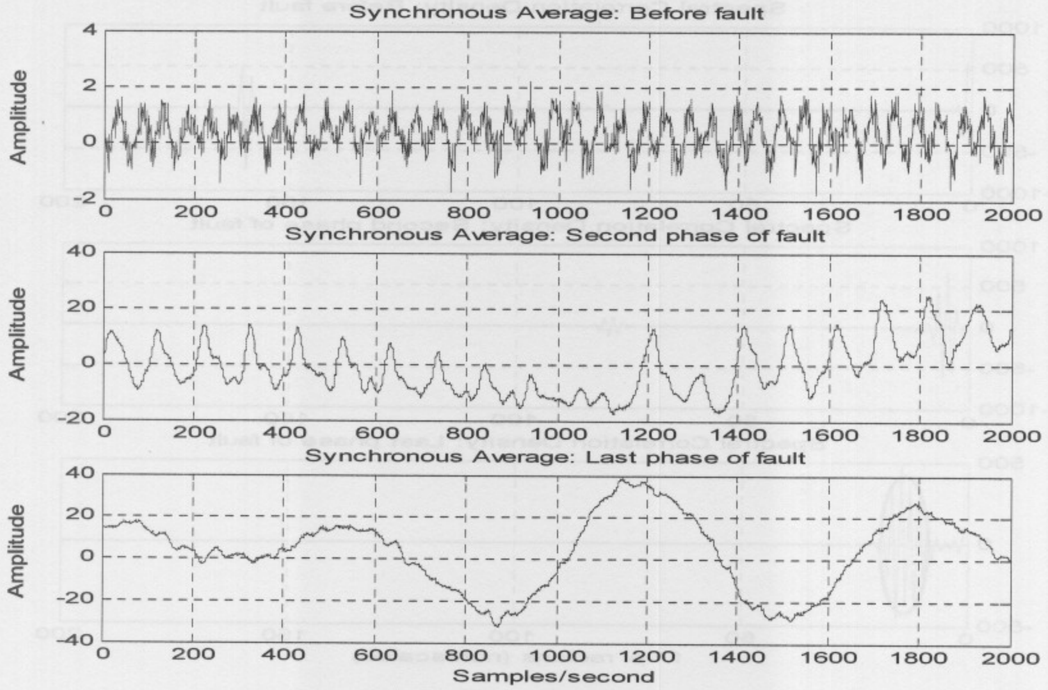

Figure E.7: Synchronous average of the displacement

E.1.5. AUTOCORRELATION

The autocorrelation signal of the displacement before a fault has occurred, second phase of the fault and last phase of the fault can be seen in figure E.8. From this figure it can be seen that the period of the fault increases.

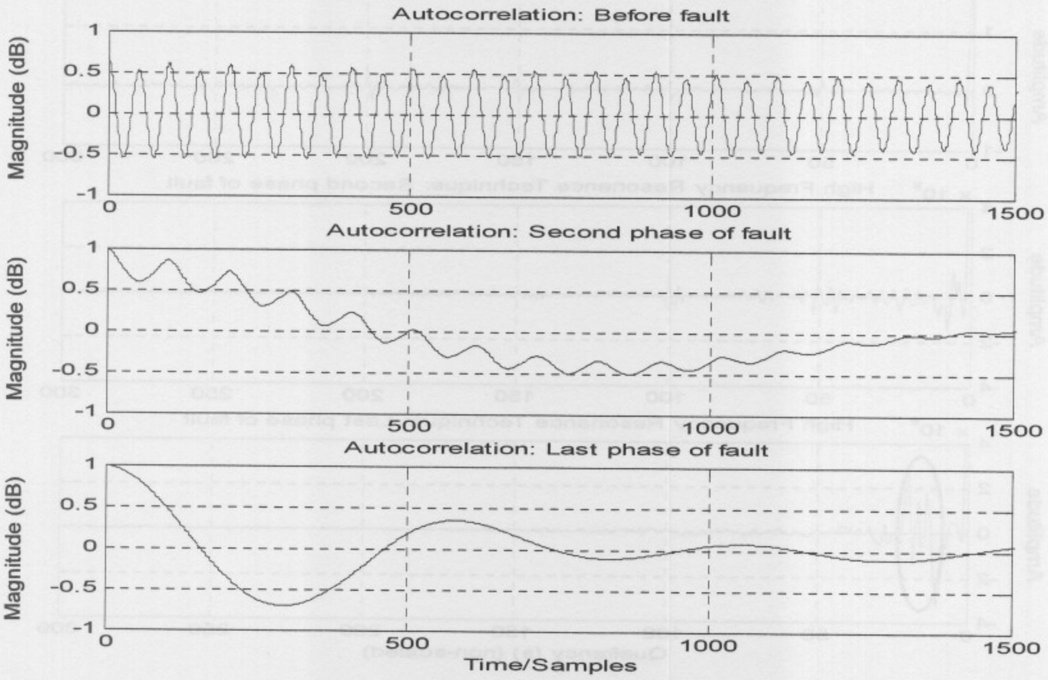

Figure E.8: Autocorrelation of the displacement

E.1.6. SPECTRAL CORRELATION DENSITY FUNCTION

The fault component is clearly visible when the spectral correlation density (SCD) function of the displacement is calculated. This can be seen in figure E.9.

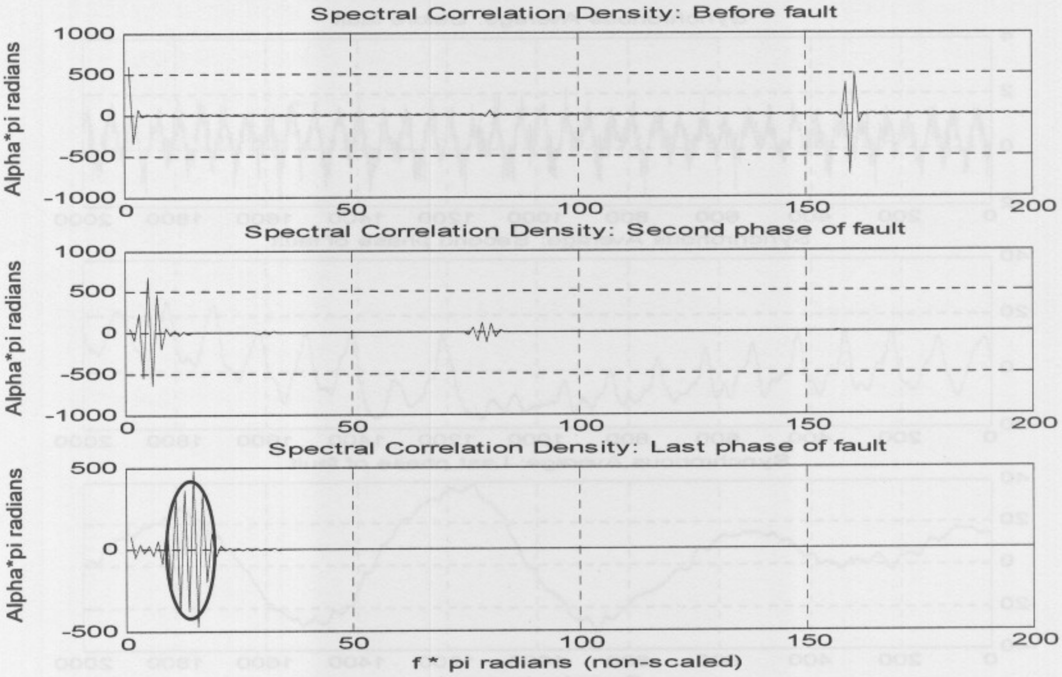

Figure E.9: Spectral correlation density of the displacement

E.1.7. HIGH FREQUENCY RESONANCE TECHNIQUE

Figure E.10 provides the high frequency resonance technique (HFRT) of the displacement. The fault component has been circled.

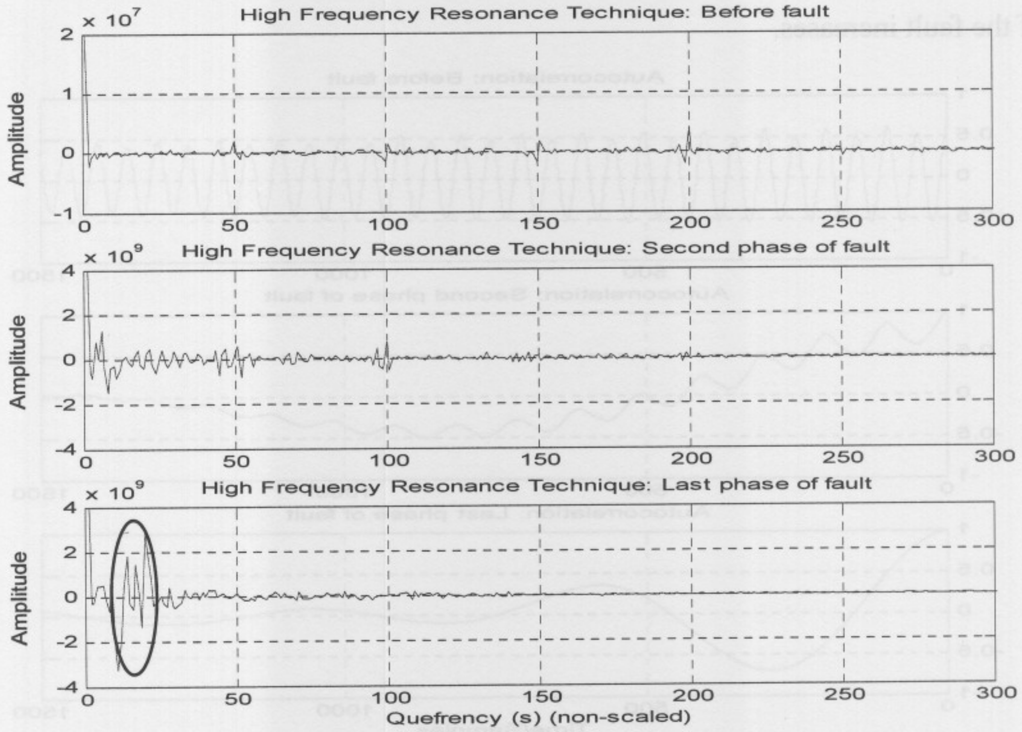

Figure E.10: High frequency resonance technique of the displacement

E.1.8. EQUI-SAMPLED DISCRETE FOURIER TRANSFORM

The equi-sampled discrete Fourier transform (ESDFT) of the displacement can be seen in figure E.11. The fault component has been circled.

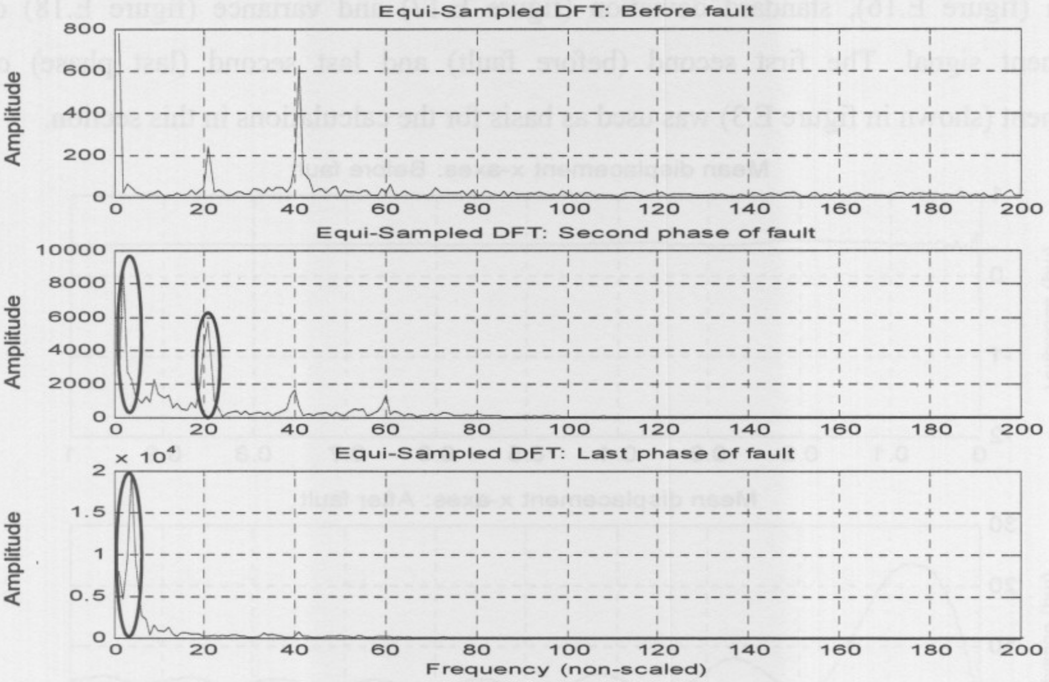

Figure E.11: Equi-sampled discrete Fourier transform of the displacement

E.1.9. WIGNER-VILLE DISTRIBUTION

The WVD of the displacement can be seen in figure E.12. During the second phase of the fault, the vibration signal climbs on the rotational speed frequency of the WVD signal. The period of the subsynchronous vibration force during the last phase of the fault has been marked.

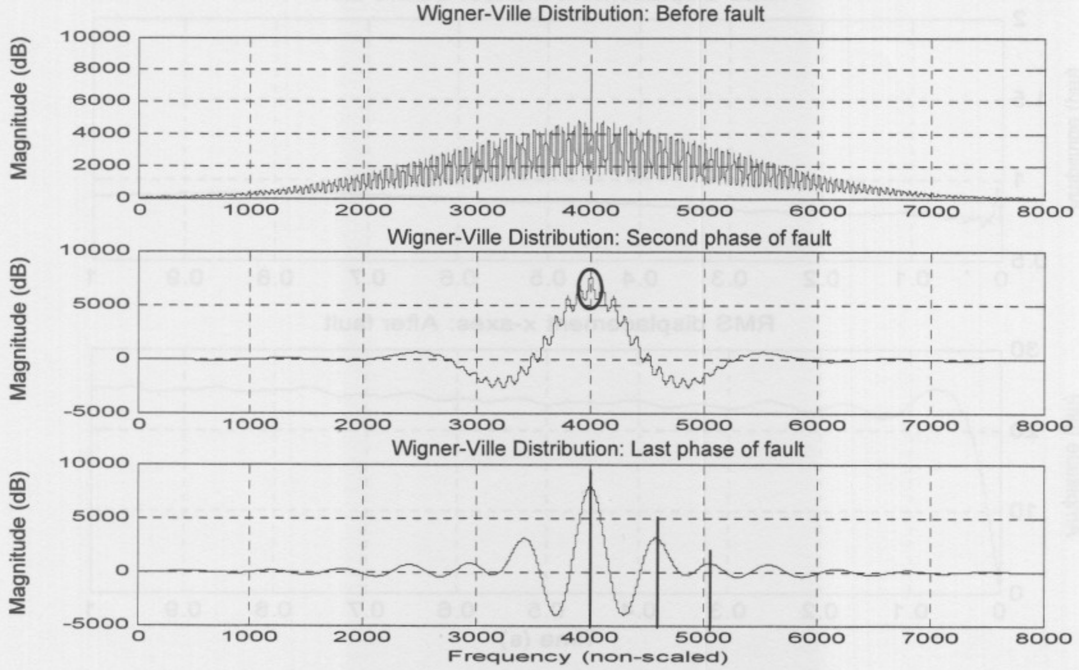

Figure E.12: Wigner-Ville distribution of the displacement

E.1.10. STATISTICAL DIAGNOSIS

This section focuses on vibration diagnosis by means of calculating the continuous mean (shown in figure E.13), continuous RMS (figure E.14), continuous maximum (figure E.15), continuous minimum (figure E.16), standard deviation (figure E.17) and variance (figure E.18) of the displacement signal. The first second (before fault) and last second (last phase) of the displacement (shown in figure E.3) was used as basis for the calculations in this section.

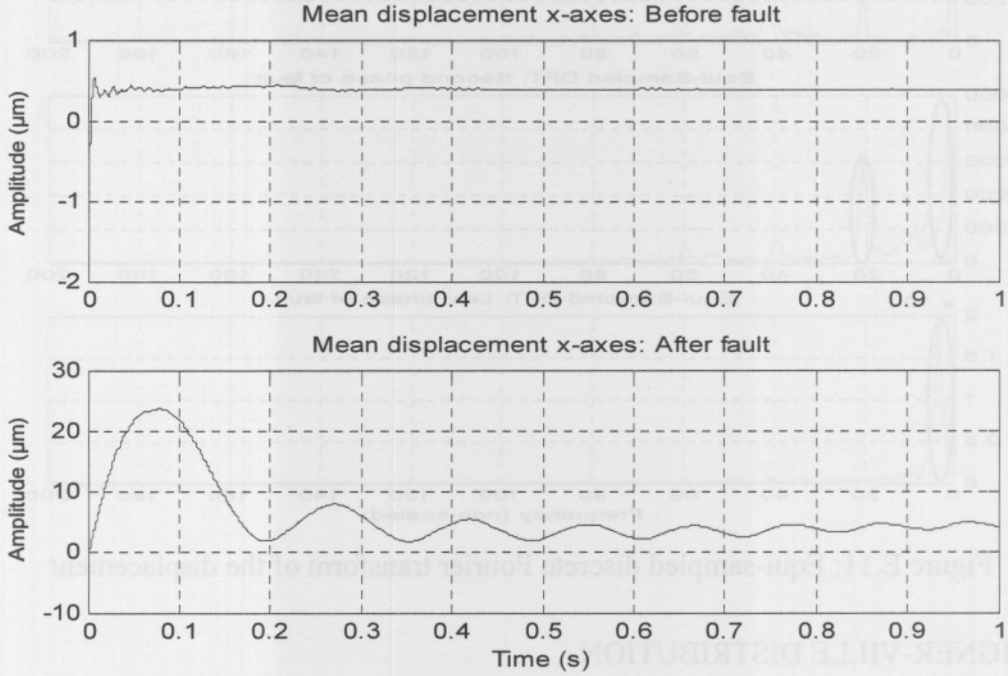

Figure E.13: Continuous mean of the displacement

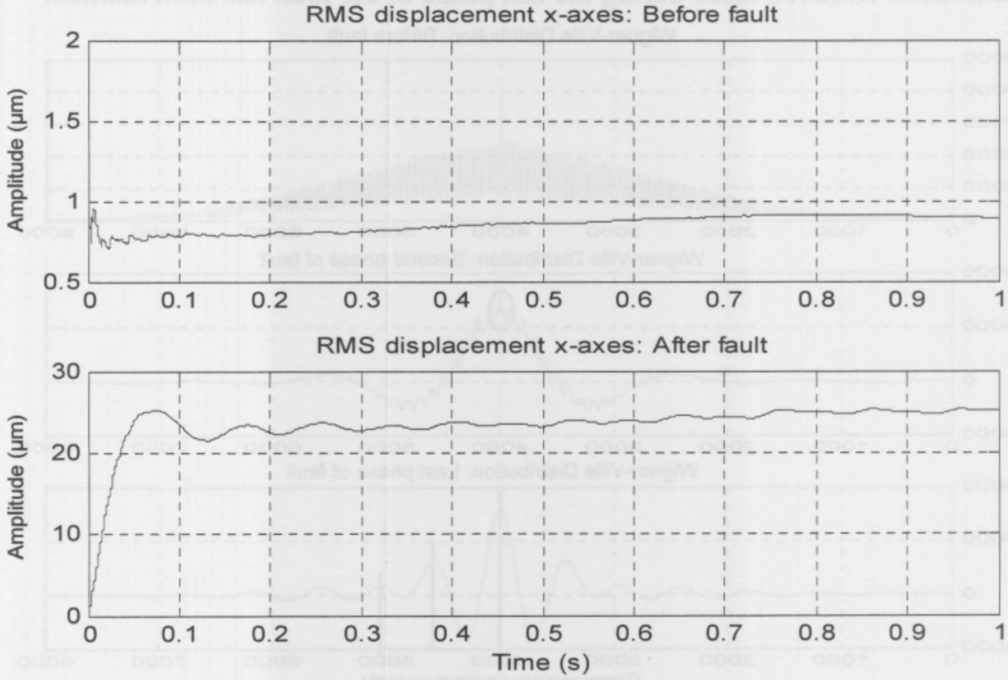

Figure E.14: Continuous RMS of the displacement

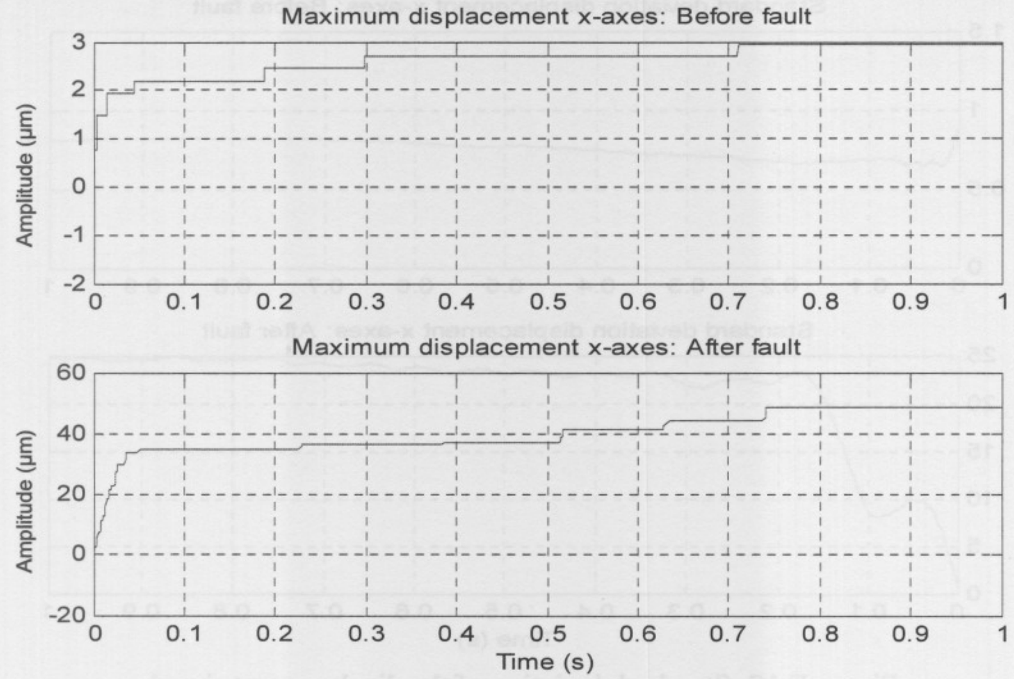

Figure E.15: Continuous maximum of the displacement

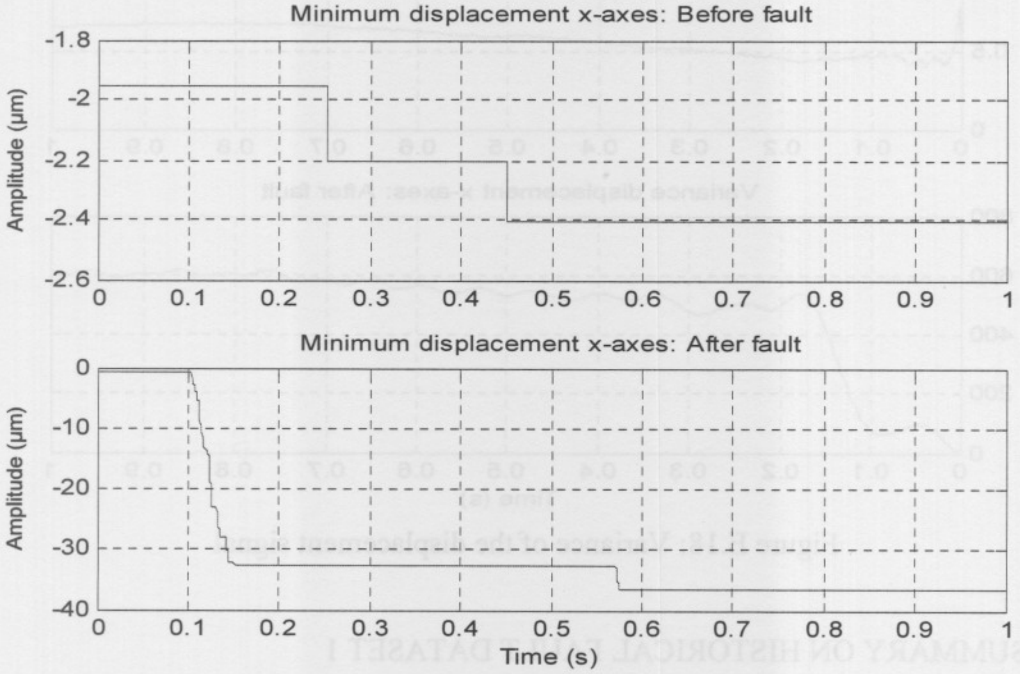

Figure E.16: Continuous minimum of the displacement

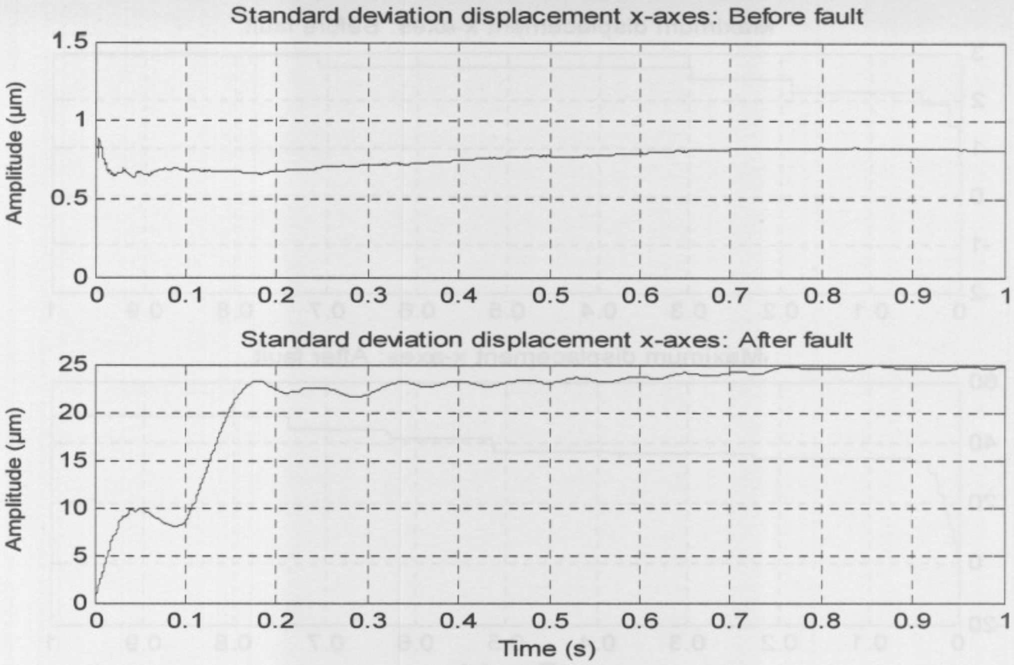

Figure E.17: Standard deviation of the displacement signal

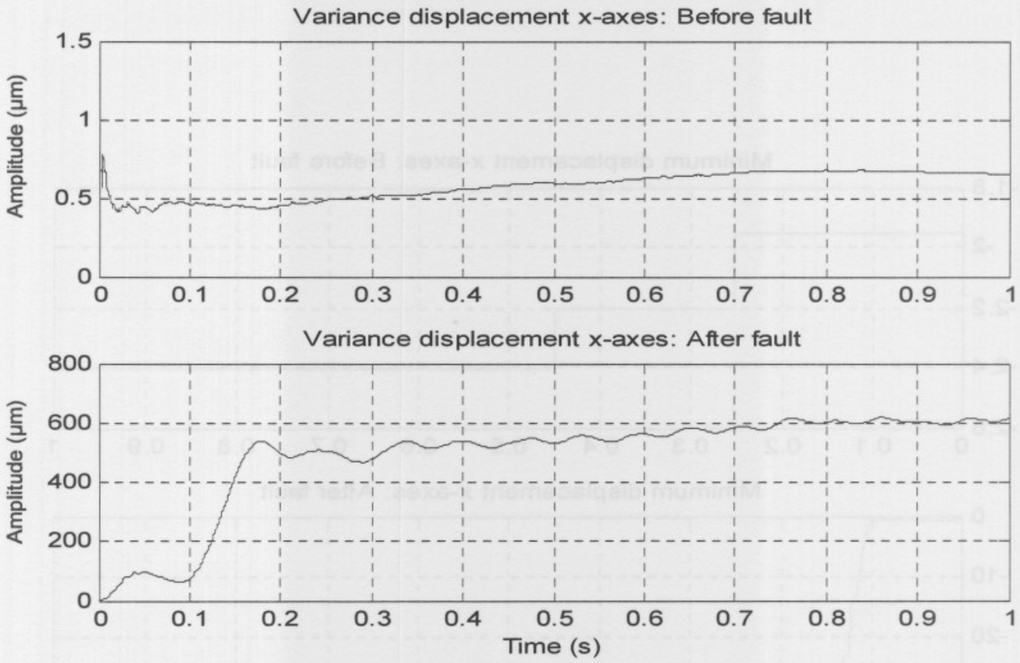

Figure E.18: Variance of the displacement signal

E.1.11. SUMMARY ON HISTORICAL FAULT DATASET 1

By analysing the subsynchronous vibration force data from before the fault (vibration force) occurred and during the last phase of the fault it can be seen that a lower frequency component climbs on the rotational speed frequency and causes vibration in the AMB system. This fault component is clearly visible when the autocorrelation function, ESDFT and WVD of the displacement is calculated over time. The RMS, mean, minimum, maximum, standard deviation and variance provides useful information about the amplitude of the fault.

E.2. TECHNIQUES IMPLEMENTED ON HISTORICAL FAULT DATASET 2

This section focuses and analyses one of the rotor synchronous vibration force entries in the historical fault dataset 2. The entry in this dataset was characterised as load unbalance.

E.2.1. OVERVIEW ON HISTORICAL FAULT DATASET 2

Figure E.19 and figure E.20 provides the fundamental part of the displacement and current dataset. In this dataset the displacements and currents are respectively represented as follow: the green line represents the x-axis on the A-side (motor side), the red line the y-axis on the A-side, blue line x-axis on the B-side (non-driven side), the orange line the y-axis on the B-side and the black line represents the z-axis.

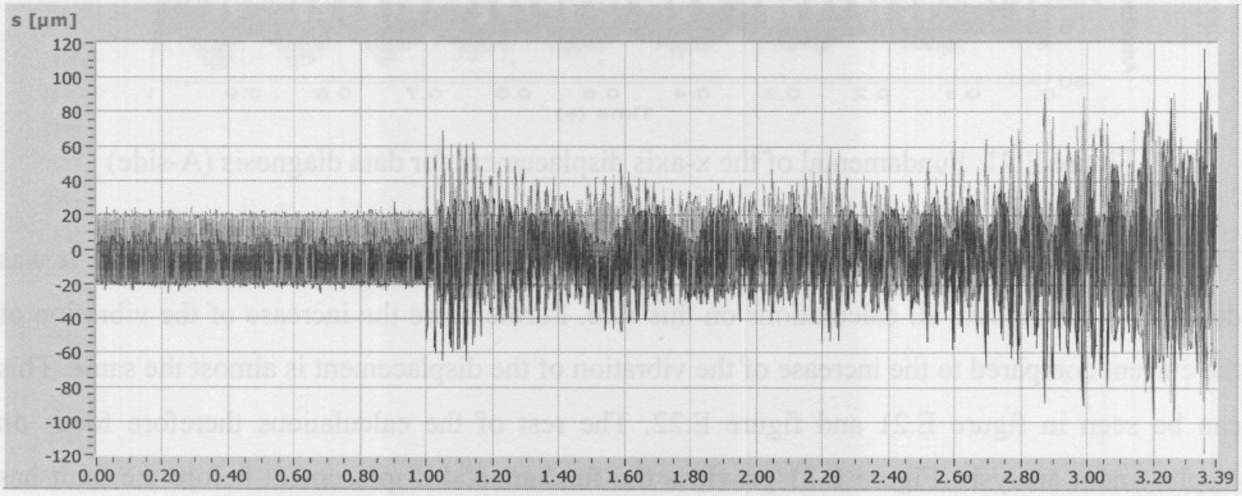

Figure E.19: Fundamental part of the displacement (all axes)

These figures provide the situation from where the fault started up to where the AMB system was shut down due to an excessive amount of vibration.

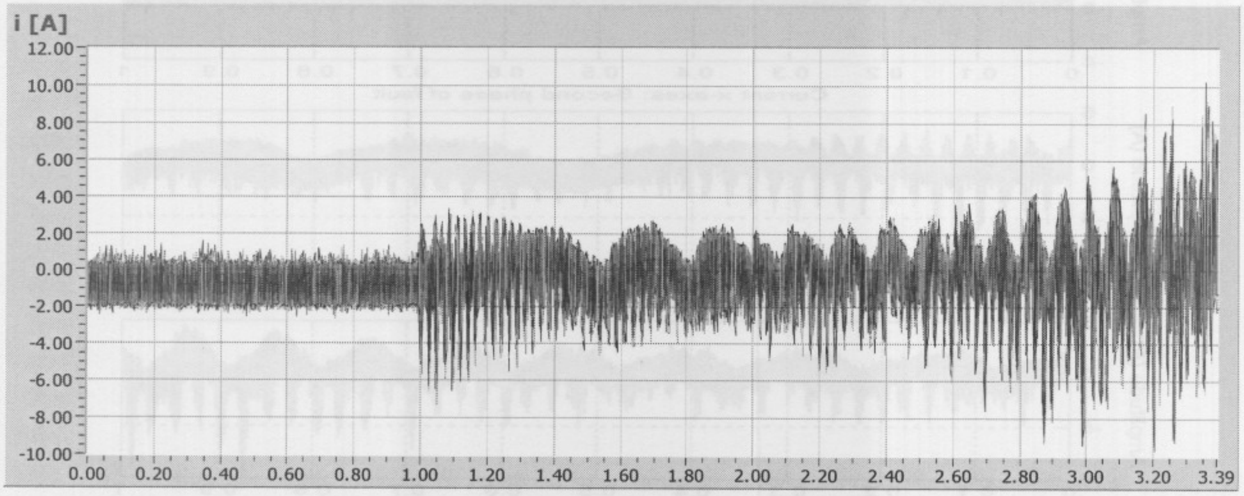

Figure E.20: Fundamental part of the current (all axes)

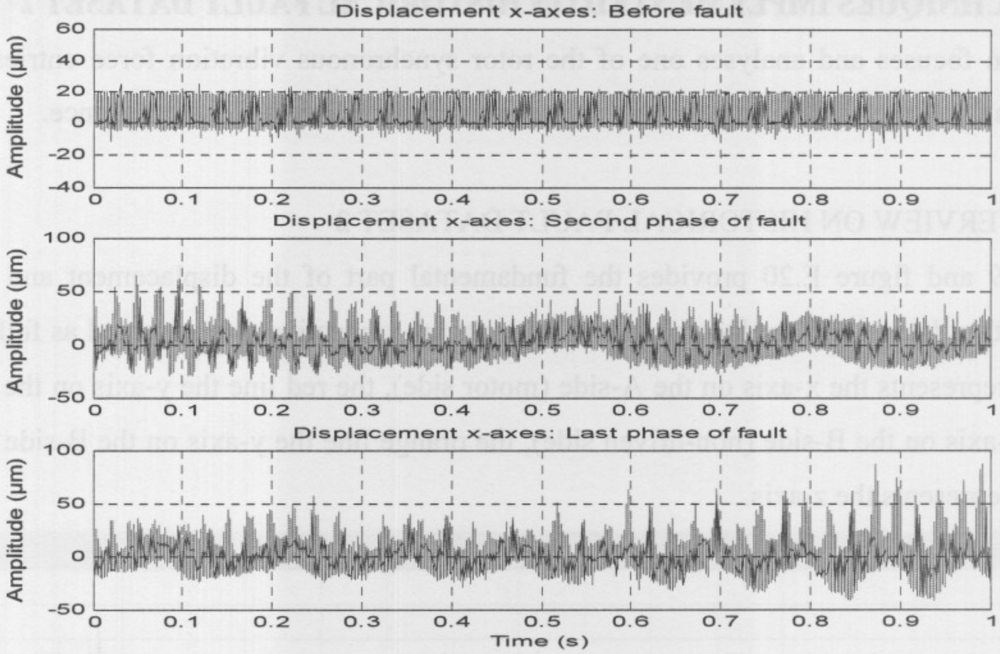

Figure E.21: Fundamental of the x-axis displacement for data diagnosis (A-side)

The most vibration in the data can again be seen on the motor side (A-side), therefore it was decided to concentrate all calculations on this side. Furthermore the increase of the vibration of the current compared to the increase of the vibration of the displacement is almost the same. This can be seen in figure E.21 and figure E.22. The rest of the calculations therefore focus on displacement analysis. Figure E.21 provides the fundamental displacement before the fault has occurred (first second of the dataset), second phase of the fault (next second of the dataset) and the last phase of the fault (last second of the dataset).

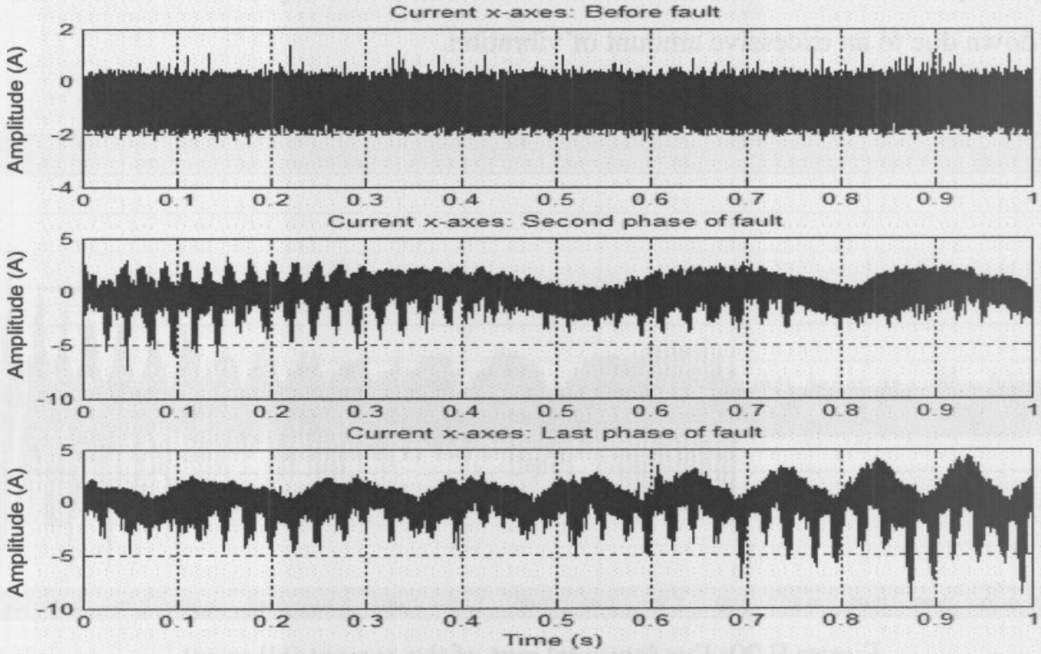

Figure E.22: Current x-axis (A-side)

E.2.2. SPECTRUM ANALYSIS

The spectrum analysis of the displacement before the fault occurred, second phase of the fault and last phase of the fault can be seen in figure E.23.

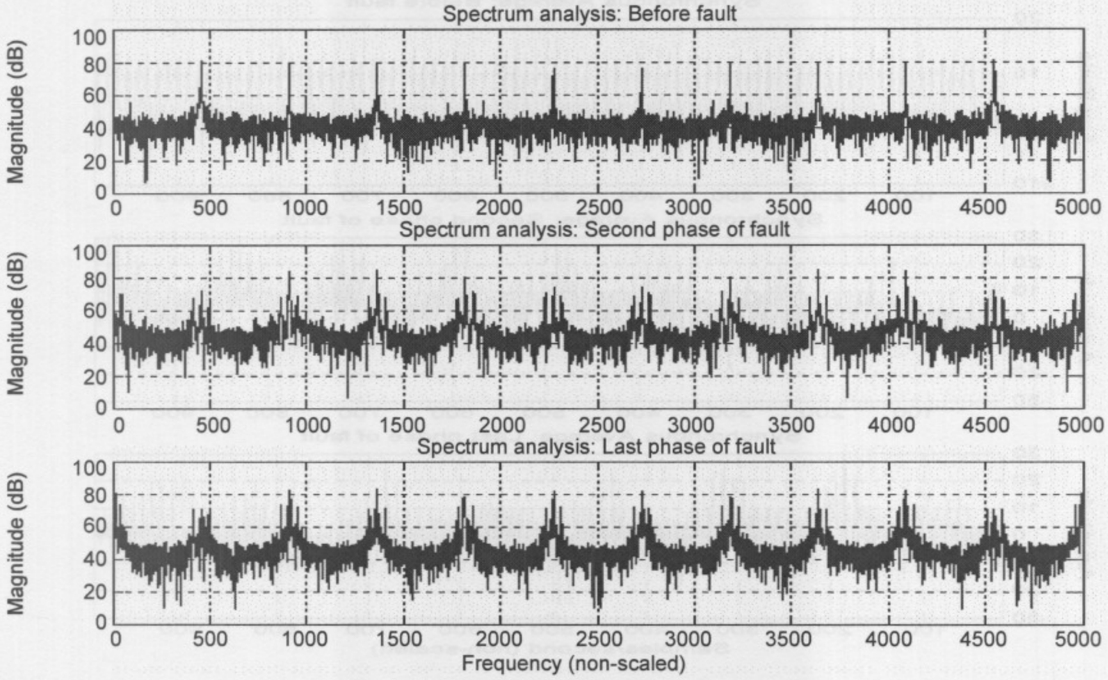

Figure E.23: Spectrum analysis of the displacement

E.2.3. CEPSTRUM ANALYSIS

The Cepstrum analysis of the displacement (shown in figure E.24) provides an output of quefrency against amplitude. The fault component has a low frequency, therefore the Cepstrum does not provide useful information.

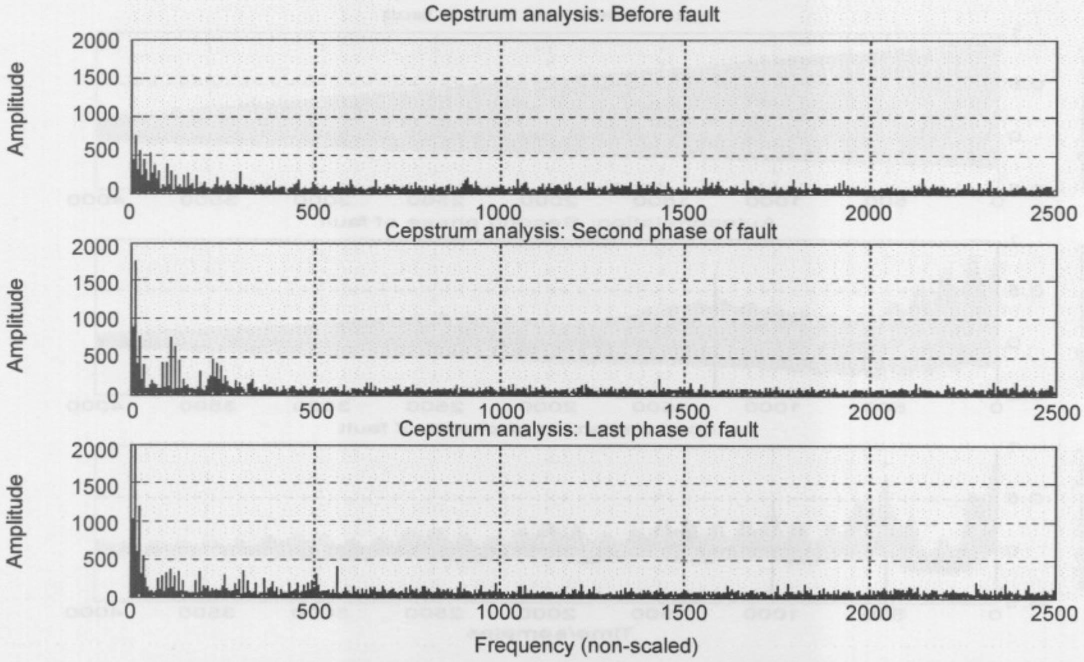

Figure E.24: Cepstrum analysis of the displacement

E.2.4. SYNCHRONOUS AVERAGE

Figure E.25 provides the synchronous average (SA) of the displacement before the fault has occurred, second phase of the fault and the last phase of the fault.

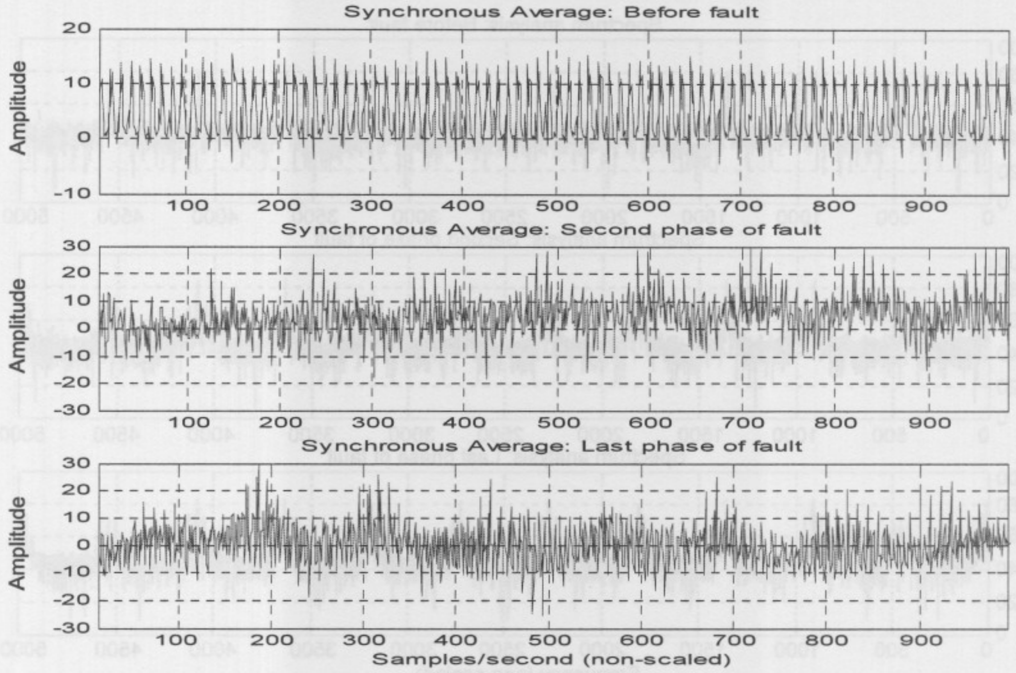

Figure E.25: Synchronous average of the displacement

E.2.5. AUTOCORRELATION

The autocorrelation signal of the displacement before the fault occurred, second phase of the fault and the last phase of the fault can be seen in figure E.26. From this figure it can be seen that the period of the fault decreases from the second phase to the last phase.

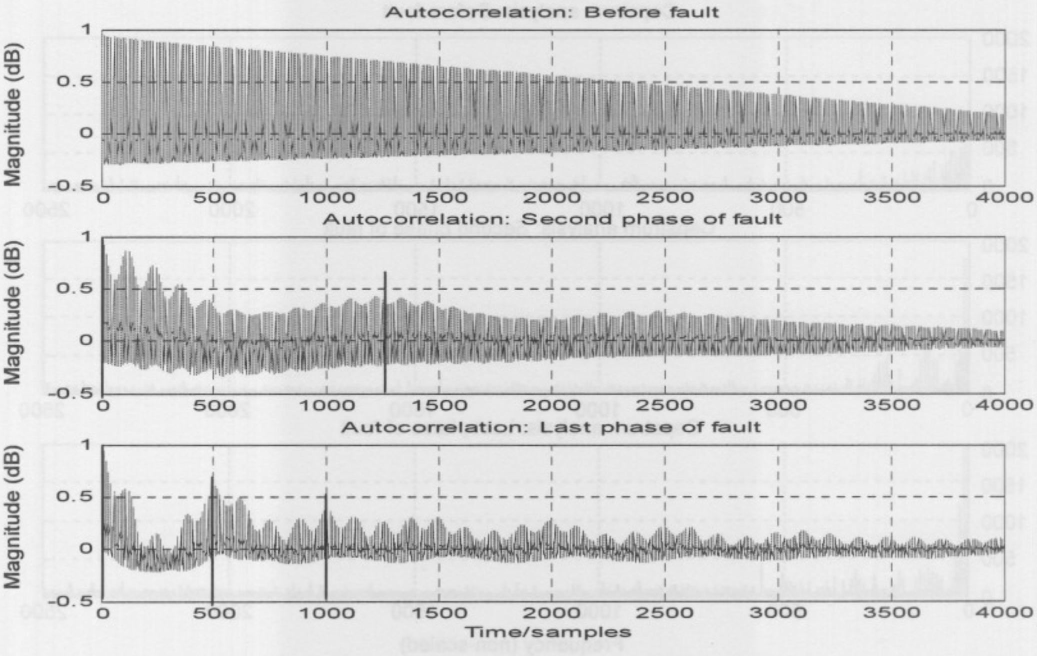

Figure E.26: Autocorrelation of the displacement

E.2.6. SPECTRAL CORRELATION DENSITY FUNCTION

Figure E.27 provides the spectral correlation density (SCD) function of the displacement before the fault occurred, second phase of the fault and the last phase of the fault. The fault component has been circled.

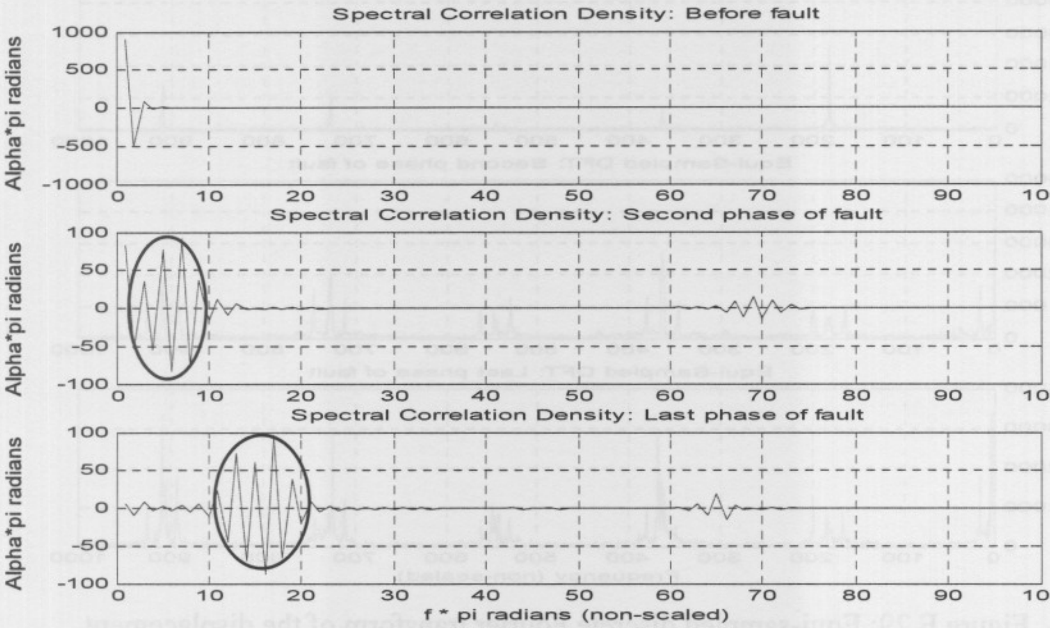

Figure E.27: Spectral correlation density of the displacement

E.2.7. HIGH FREQUENCY RESONANCE TECHNIQUE

Figure E.28 provides the high frequency resonance techniques (HFRT) of the displacement before the fault occurred, second phase of the fault and the last phase of the fault.

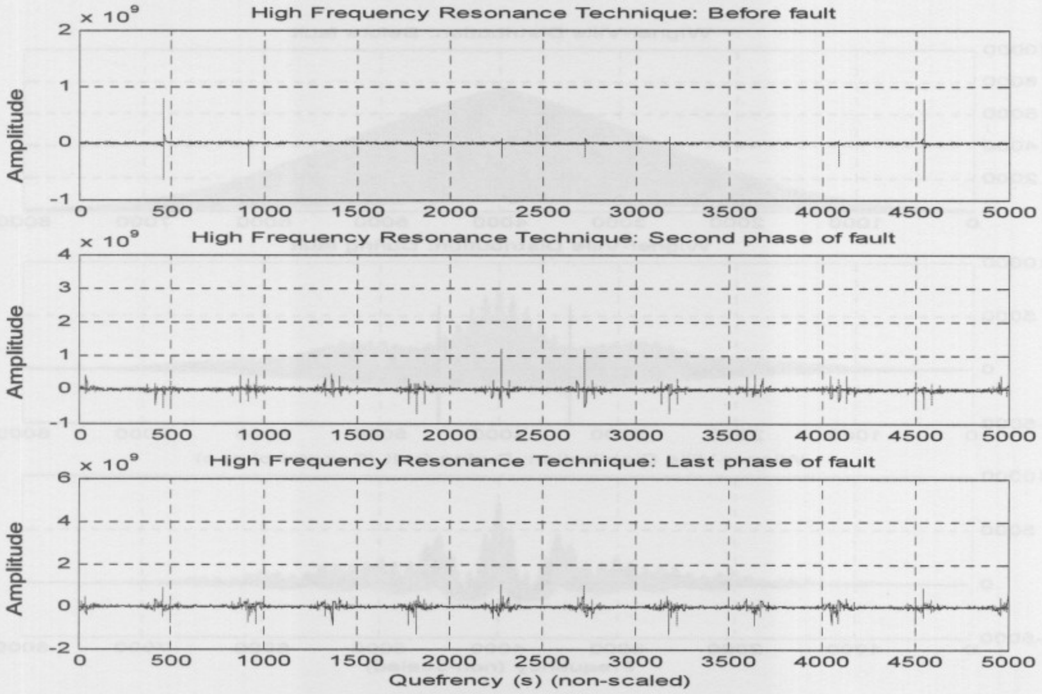

Figure E.28: High frequency resonance technique of the displacement

E.2.8. EQUI-SAMPLED DISCRETE FOURIER TRANSFORM

The equi-sampled discrete Fourier transform (ESDFT) of the displacement before the fault has occurred, second phase of the fault and the last phase of the fault can be seen in figure E.29.

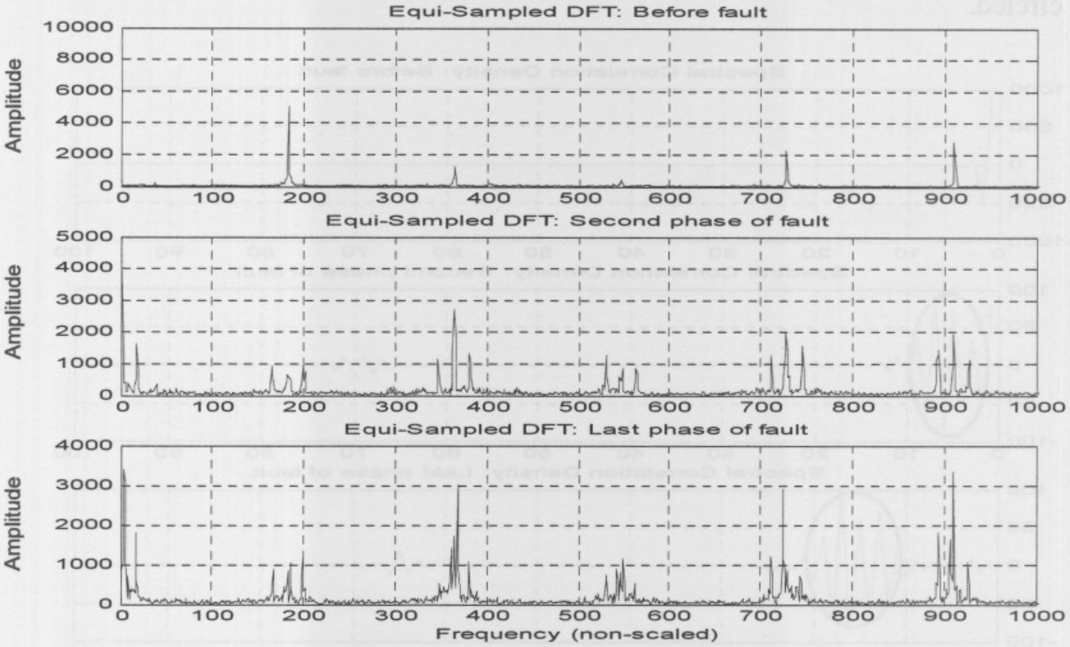

Figure E.29: Equi-sampled discrete Fourier transform of the displacement

E.2.9. WIGNER-VILLE DISTRIBUTION

The Wigner-Ville Distribution (WVD) of the displacement before the fault occurred, second phase of the fault and the last phase of the fault can be seen in figure E.30. The period decreases from the second phase to the last phase. These periods has been marked.

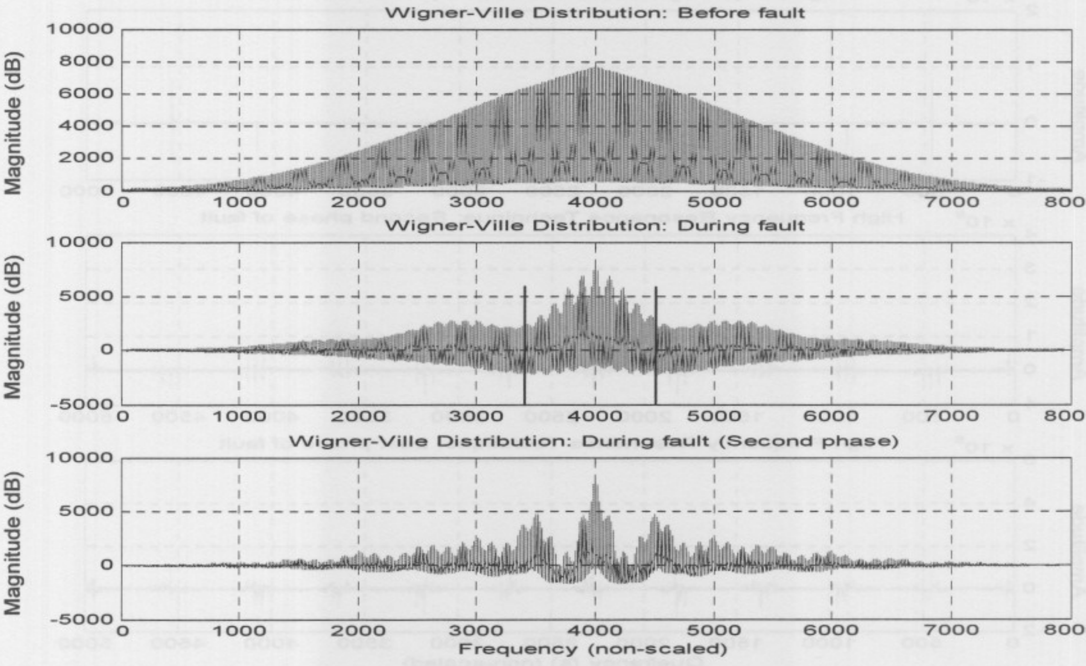

Figure E.30: Wigner-Ville distribution of the displacement

E.2.10. STATISTICAL ANALYSIS

This section focuses on vibration diagnosis by means of calculating the continuous mean (shown in figure E.31), continuous RMS (figure E.32), continuous maximum (figure E.33), continuous minimum (figure E.34), standard deviation (figure E.35) and variance (figure E.36) of the displacement signal. The first second (before fault) and last second (last phase) of the displacement (shown in figure E.21) was used for the calculations in this section.

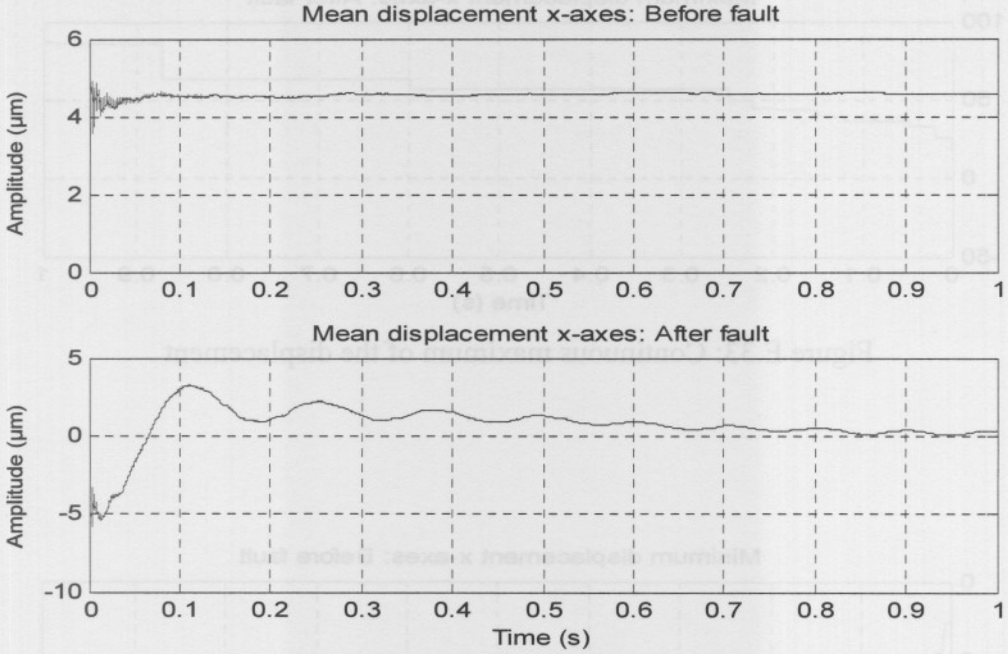
Mean displacement x-axes: Before fault

Mean displacement x-axes: After fault

Figure E.31: Continuous mean of the displacement

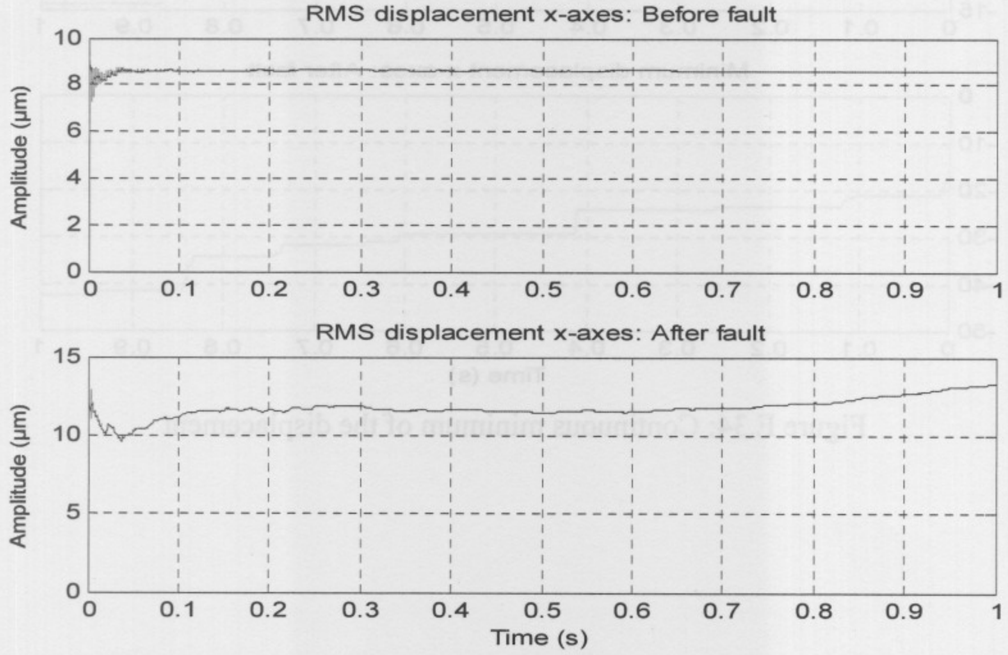
RMS displacement x-axes: Before fault

RMS displacement x-axes: After fault

Figure E.32: Continuous RMS of the displacement

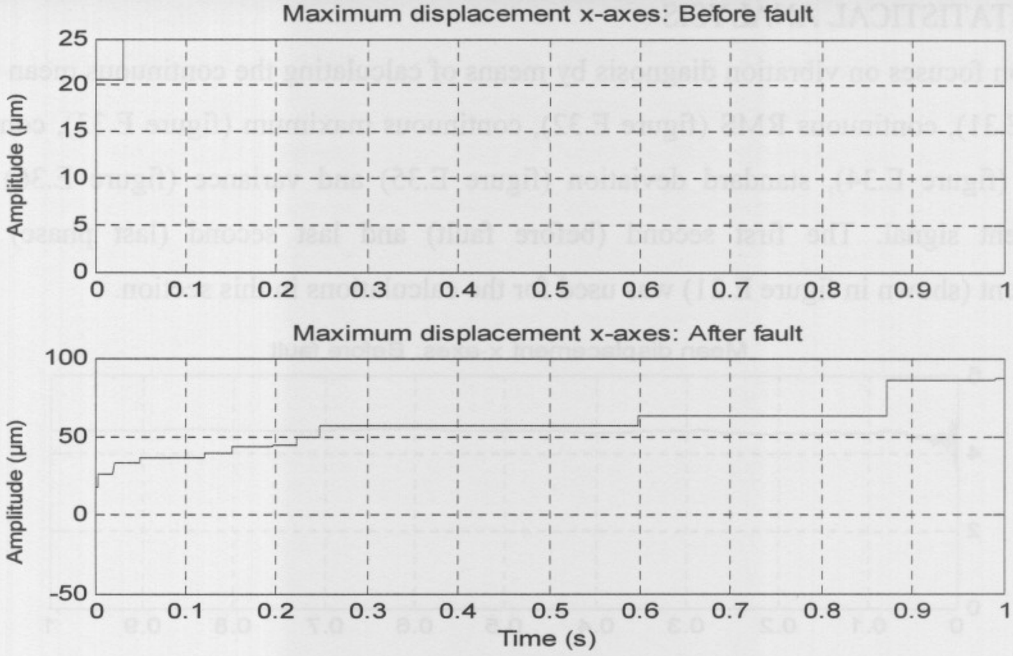

Figure E.33: Continuous maximum of the displacement

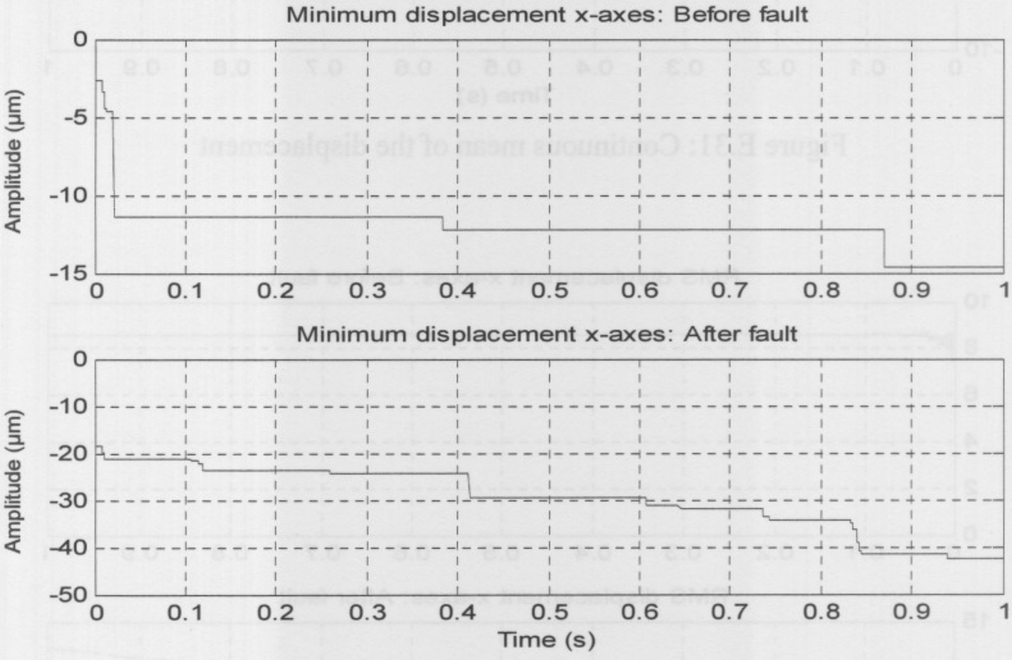

Figure E.34: Continuous minimum of the displacement

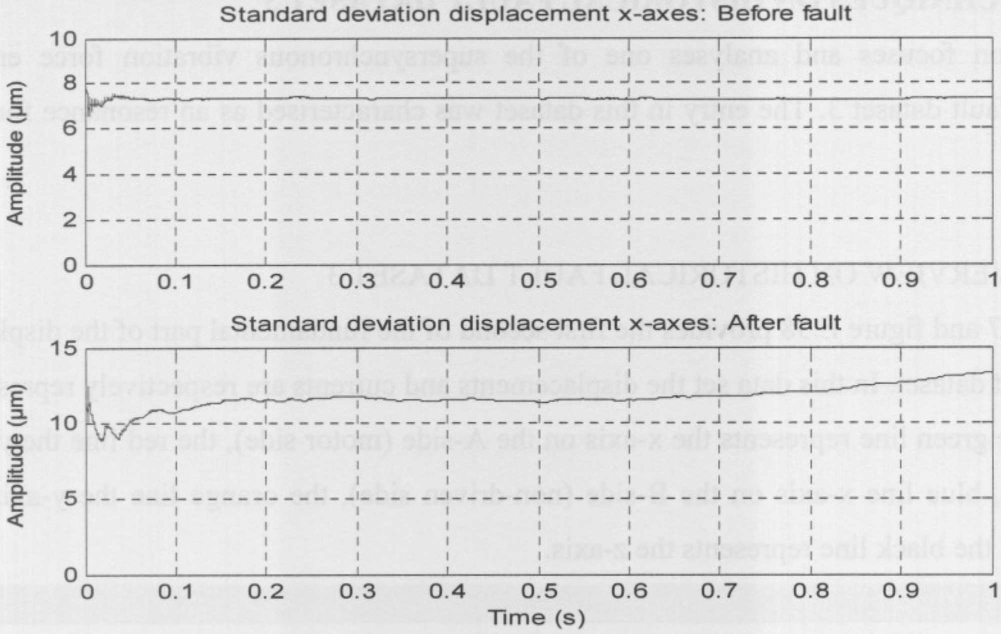

Figure E.35: Standard deviation of the displacement signal

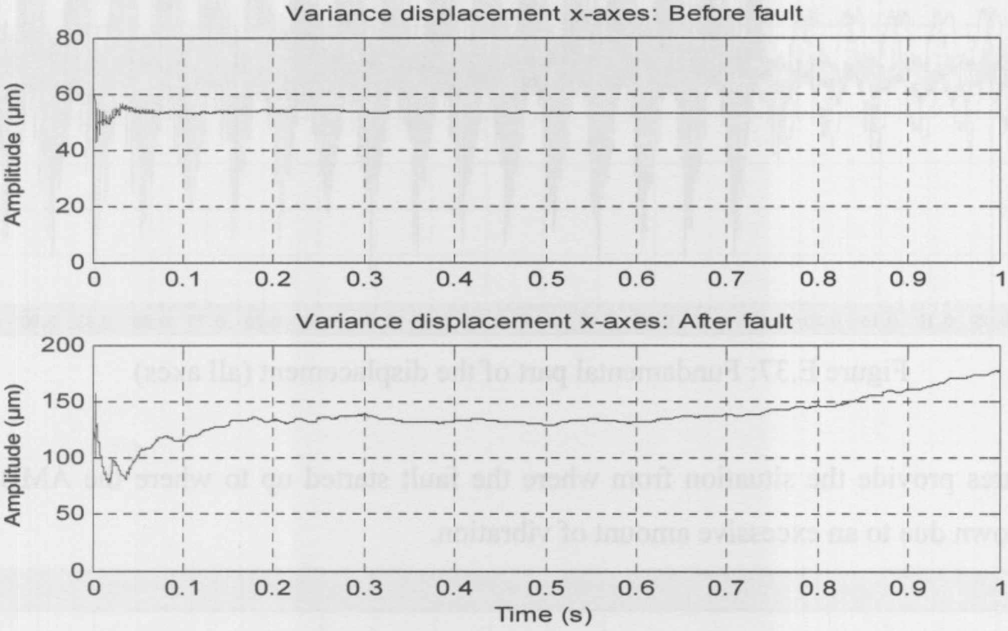

Figure E.36: Variance of the displacement signal

E.2.11. SUMMARY ON HISTORICAL FAULT DATASET 2

By analysing the rotor synchronous vibration force data from before the fault (vibration force) occurred and during the last phase of the fault it can be seen that a lower frequency component climbs on the carrier signal during the second phase and a slightly higher frequency component climbs on during the last phase, which causes a vibration in the system. The fault component is clearly visible when the autocorrelation function, SCD function and WVD of the displacement is calculated over time. The RMS, mean, minimum, maximum, standard deviation and variance provides useful information about the amplitude of the fault (vibration force) over time.

E.3. TECHNIQUES ON HISTORICAL FAULT DATASET 3

This section focuses and analyses one of the supersynchronous vibration force entries in historical fault dataset 3. The entry in this dataset was characterised as an resonance foundation looseness.

E.3.1. OVERVIEW ON HISTORICAL FAULT DATASET 3

Figure E.37 and figure E.38 provides the first second of the fundamental part of the displacement and current dataset. In this data set the displacements and currents are respectively represented as follow: the green line represents the x-axis on the A-side (motor side), the red line the y-axis on the A-side, blue line x-axis on the B-side (non-driven side), the orange line the y-axis on the B-side and the black line represents the z-axis.

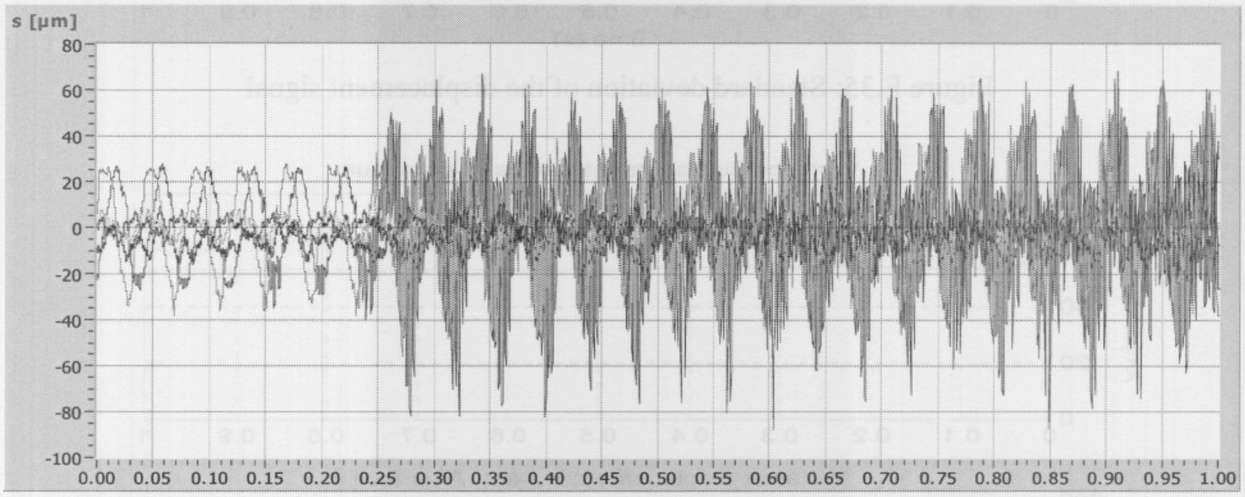

Figure E.37: Fundamental part of the displacement (all axes)

These figures provide the situation from where the fault started up to where the AMB system was shut down due to an excessive amount of vibration.

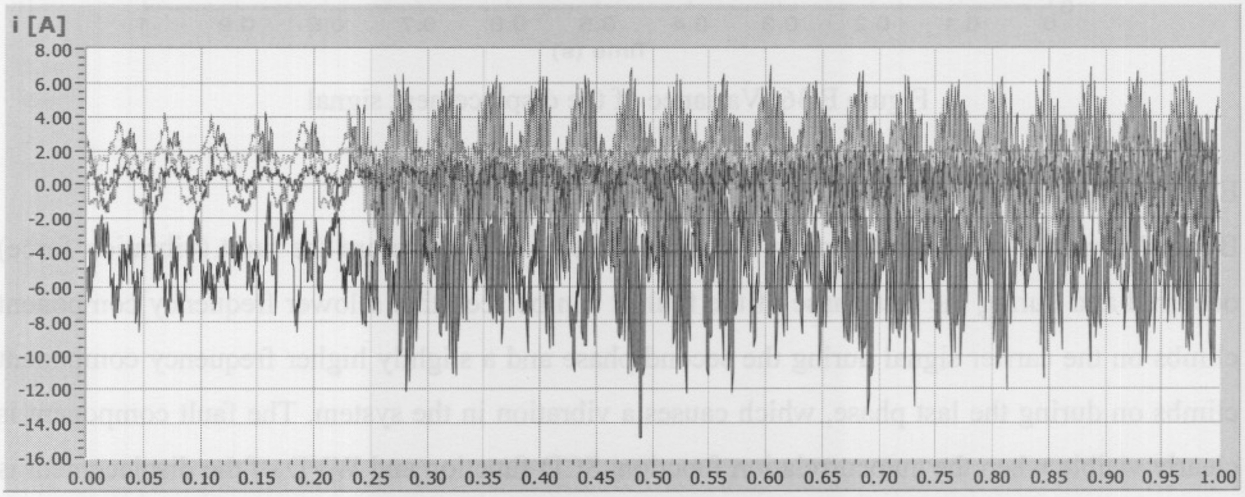

Figure E.38: Fundamental part of the current (all axes)

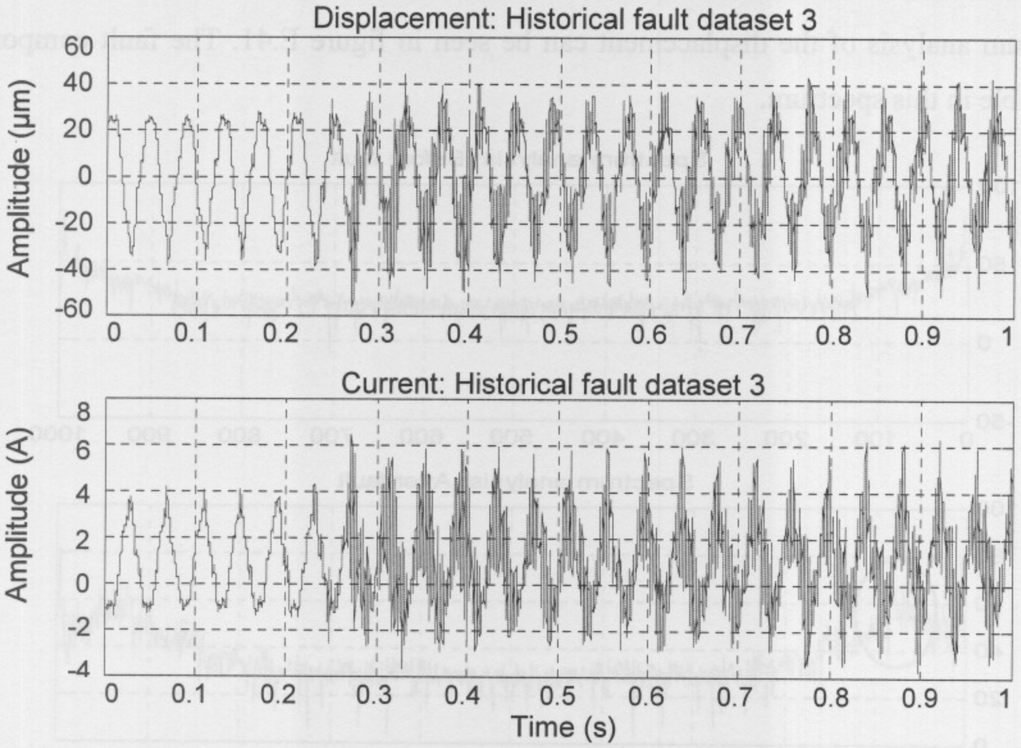

Figure E.39: Fundamental part of the displacement and current x-axis (A-side)

Figure E.39 provides the fundamental part of the displacement and current. Figure E.40 provides the fundamental displacement before the fault has occurred (first 0.2 seconds of the dataset) and after the fault has occurred (next 0.2 seconds of the dataset).

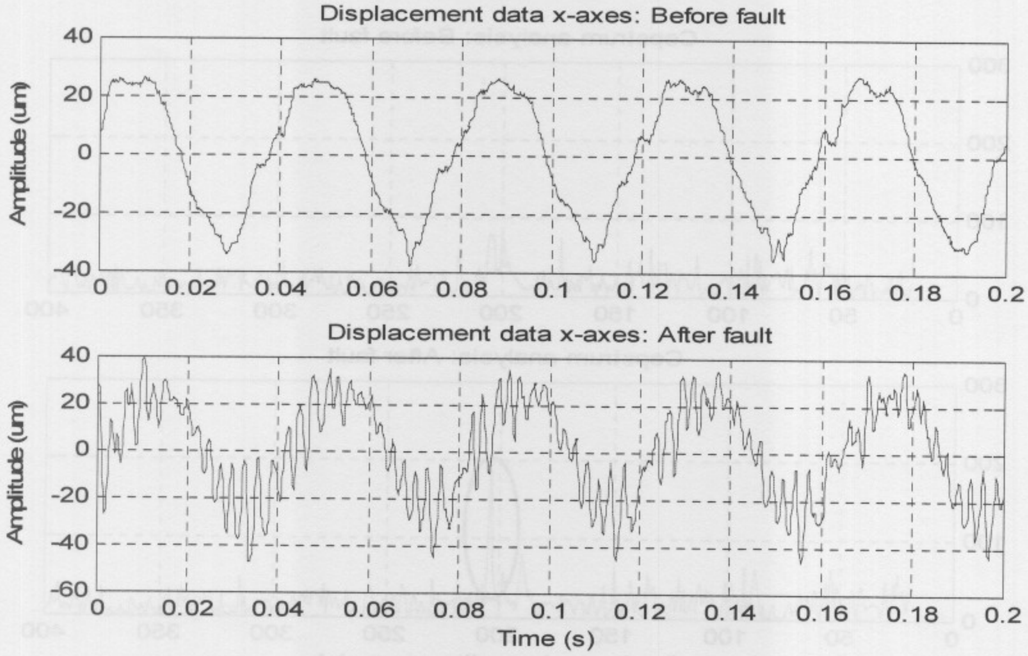

Figure E.40: Fundamental part of the displacement (before and after the fault)

E.3.2. SPECTRUM ANALYSIS

The spectrum analysis of the displacement can be seen in figure E.41. The fault component is clearly visible in this spectrum.

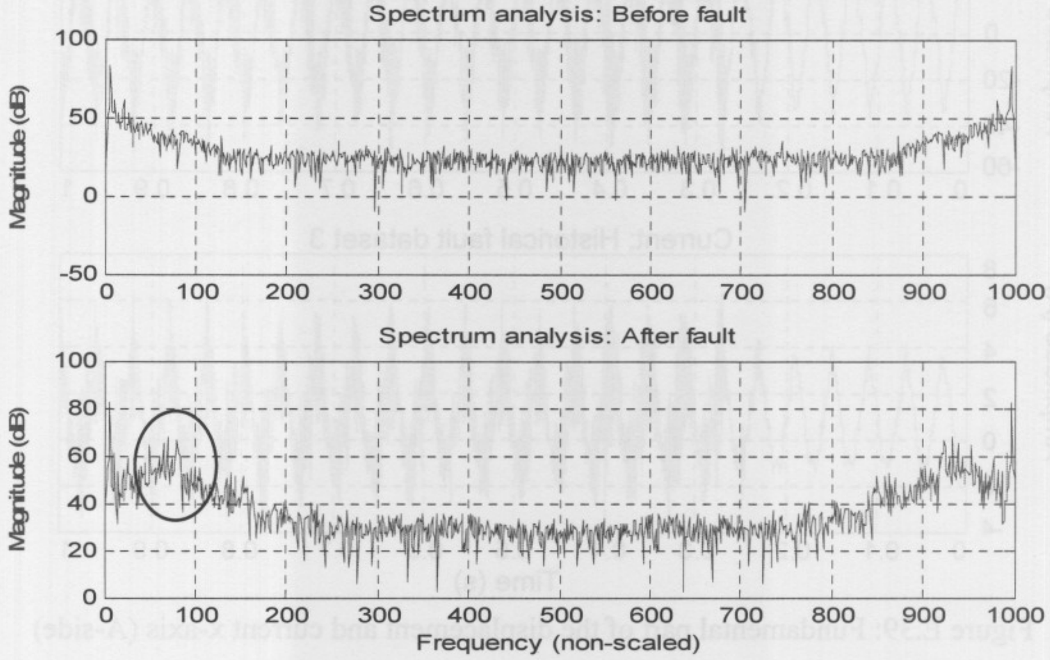

Figure E.41: Spectrum analysis of the displacement

E.3.3. CEPSTRUM ANALYSIS

The Cepstrum analysis of the displacement (as see in figure E.42) provides an output of quefrency against amplitude. The fault component is clearly visible during this analysis.

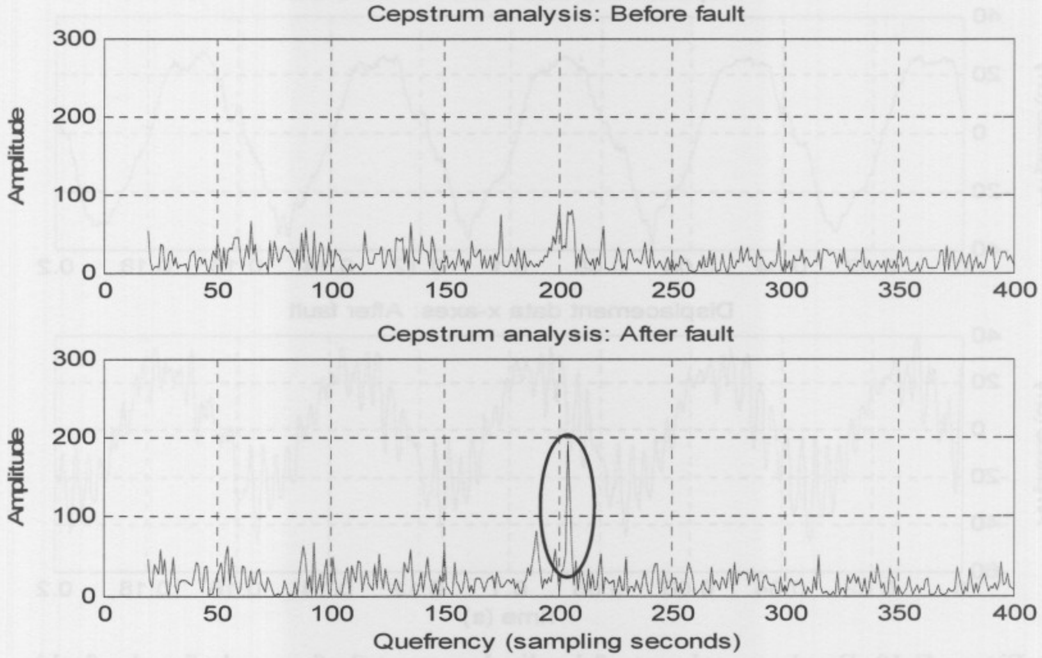

Figure E.42: Cepstrum analysis of the displacement

E.3.4. SYNCHRONOUS AVERAGE

Figure E.43 provide the Synchronous average (SA) of the displacement before and after the fault has occurred.

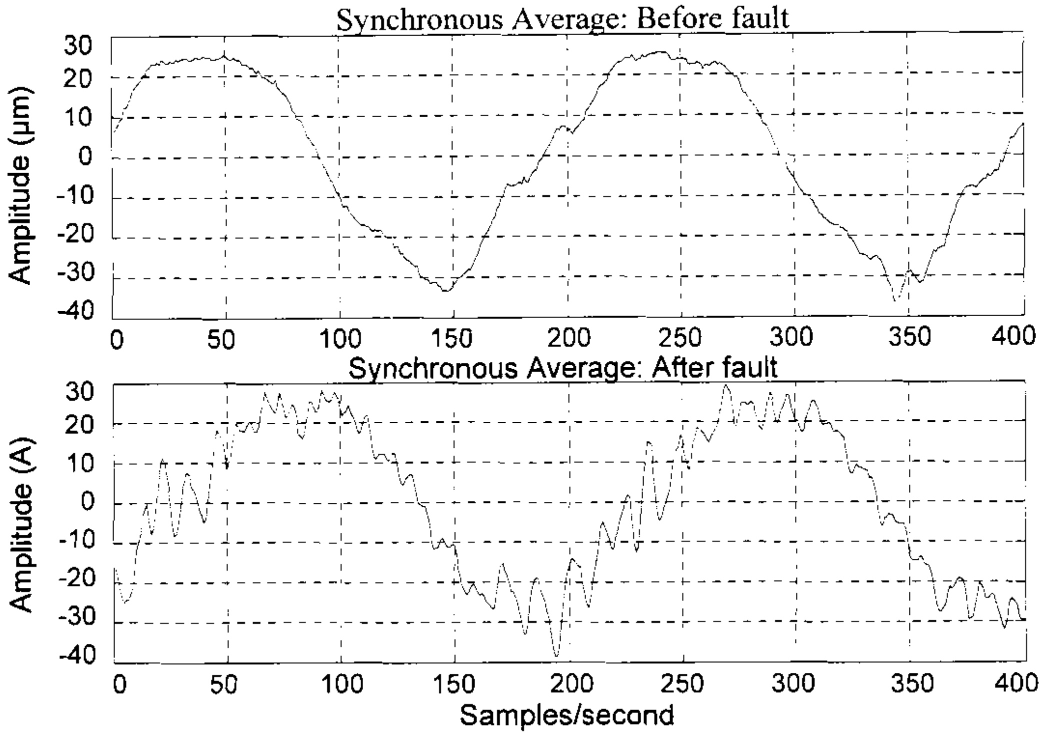

Figure E.43: Synchronous average of the displacement (before and after the fault)

E.3.5. AUTOCORRELATION

The unbiased autocorrelation signal of the displacement before and after the fault has occurred can be seen in figure E.44.

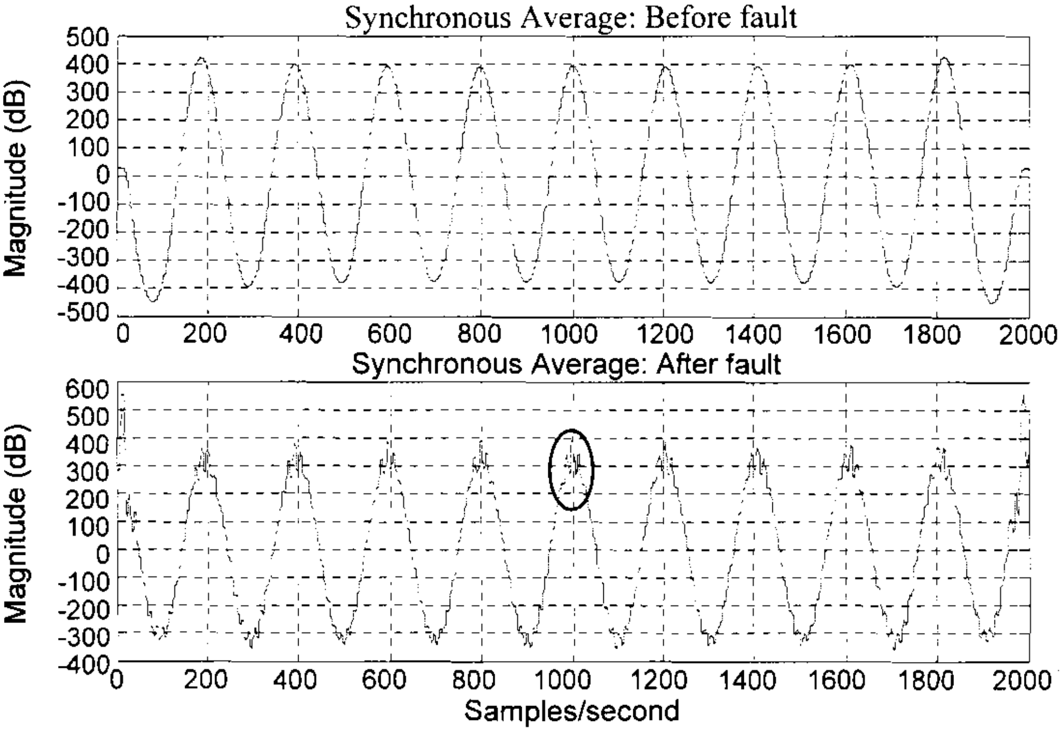

Figure E.44: Autocorrelation (unbiased) of the displacement (before and after the fault)

E.3.6. SPECTRAL CORRELATION DENSITY FUNCTION

The fault component is clearly visible when the spectral correlation density (SCD) function of the displacement is calculated. This can be seen in figure E.45.

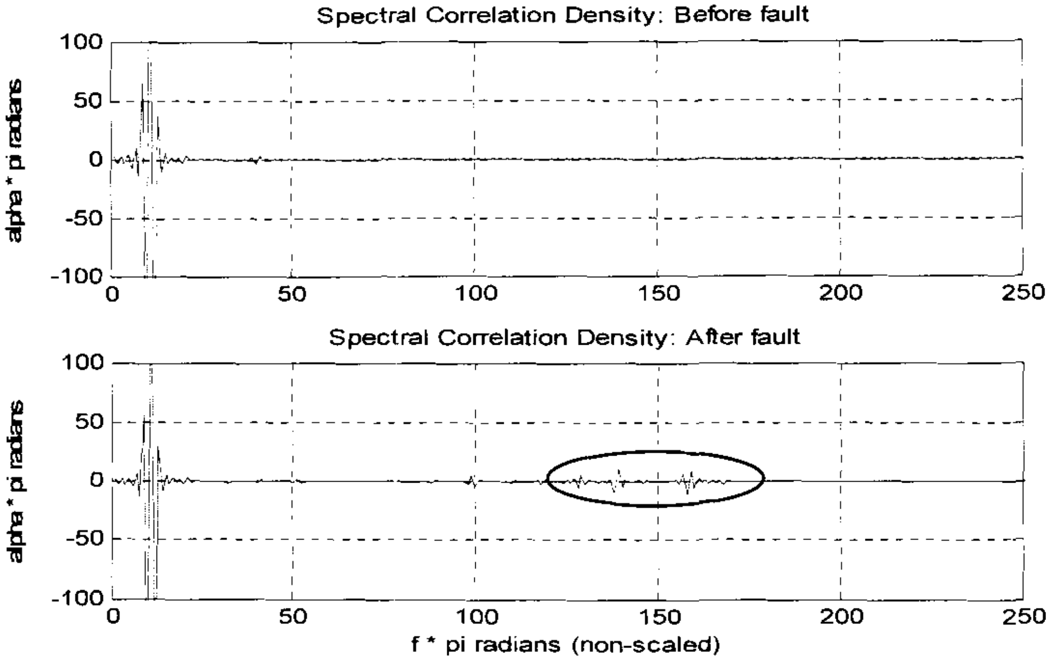

Figure E.45: Spectral correlation density of the displacement

E.3.7. HIGH FREQUENCY RESONANCE TECHNIQUE

Figure E.46 provides the high frequency resonance technique (HFRT) of the displacement.

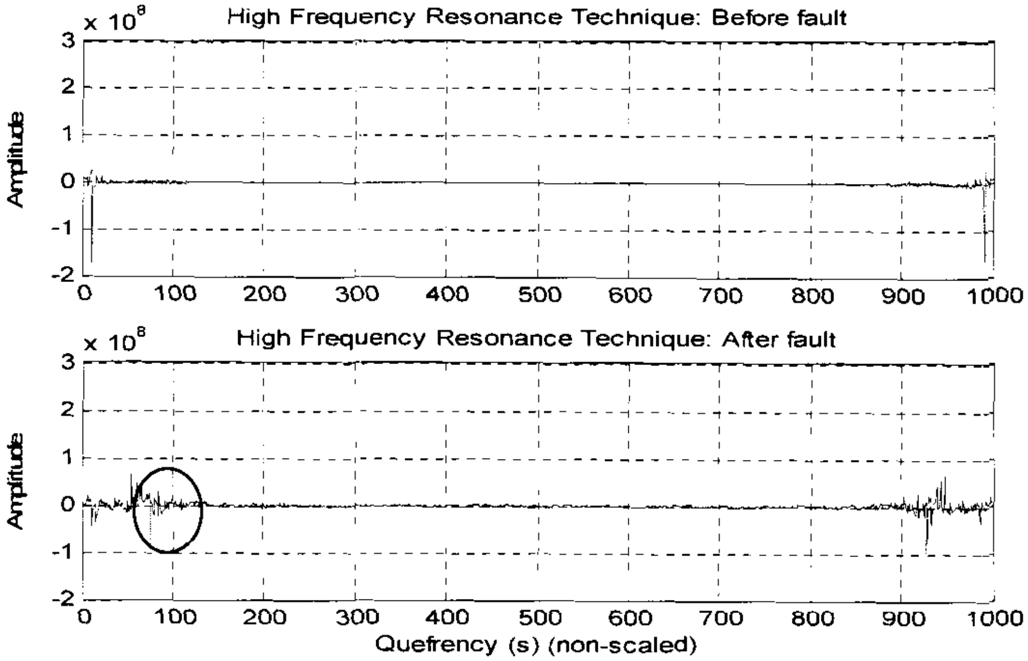

Figure E.46: High frequency resonance technique of the displacement

E.3.8. EQUI-SAMPLED DISCRETE FOURIER TRANSFORM

The equi-sampled discrete Fourier transform (ESDFT) of the displacement can be seen in figure E.47. The fault component has been circled.

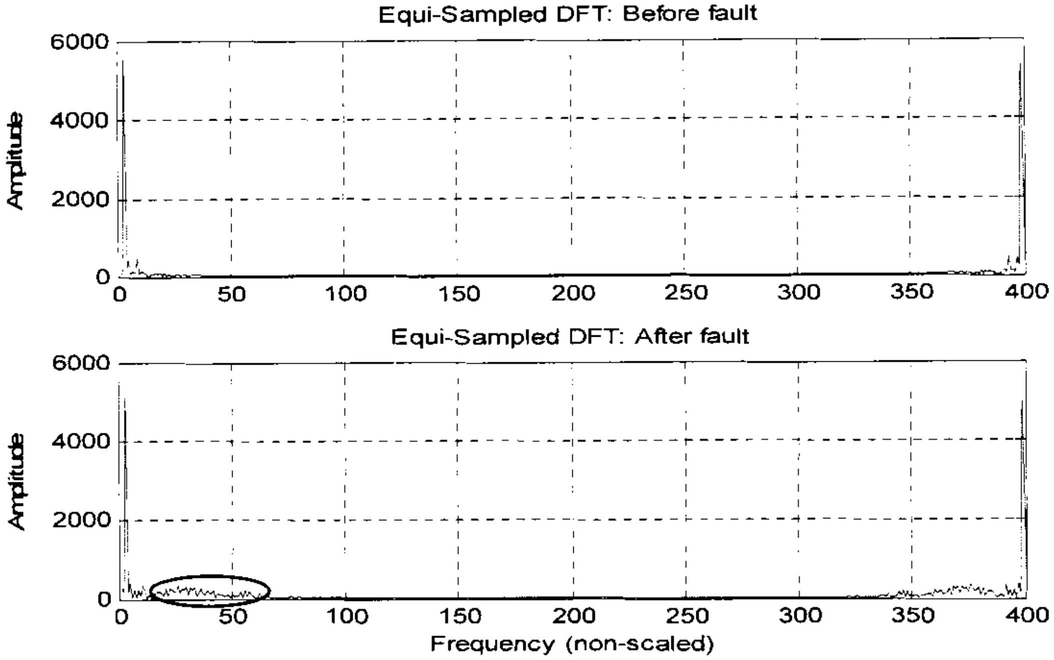

Figure E.47: Equi-sampled discrete Fourier transform of the displacement

E.3.9. WIGNER-VILLE DISTRIBUTION

The Wigner-Ville distribution (WVD) of the displacement can be seen in figure E.48. The vibration signal can be seen on the peaks of the WVD signal.

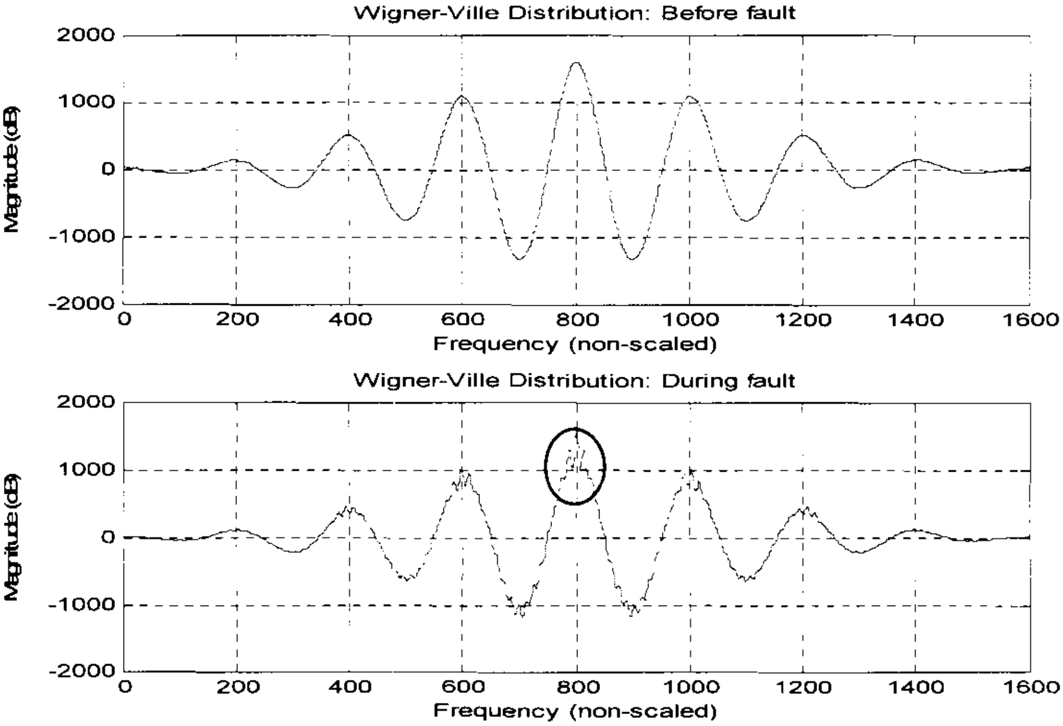

Figure E.48: Wigner-Ville distribution of the displacement

E.3.10. STATISTICAL DIAGNOSIS

This section focuses on vibration diagnosis by means of calculating the continuous mean (shown in figure E.49), continuous RMS (figure E.50), continuous maximum (figure E.51), continuous minimum (figure E.52), standard deviation (figure E.53) and variance (figure E.54) of the displacement signal. The fundamental part of the x-axis displacement for data diagnosis (shown in figure E.40) was used as basis for the calculations in this section.

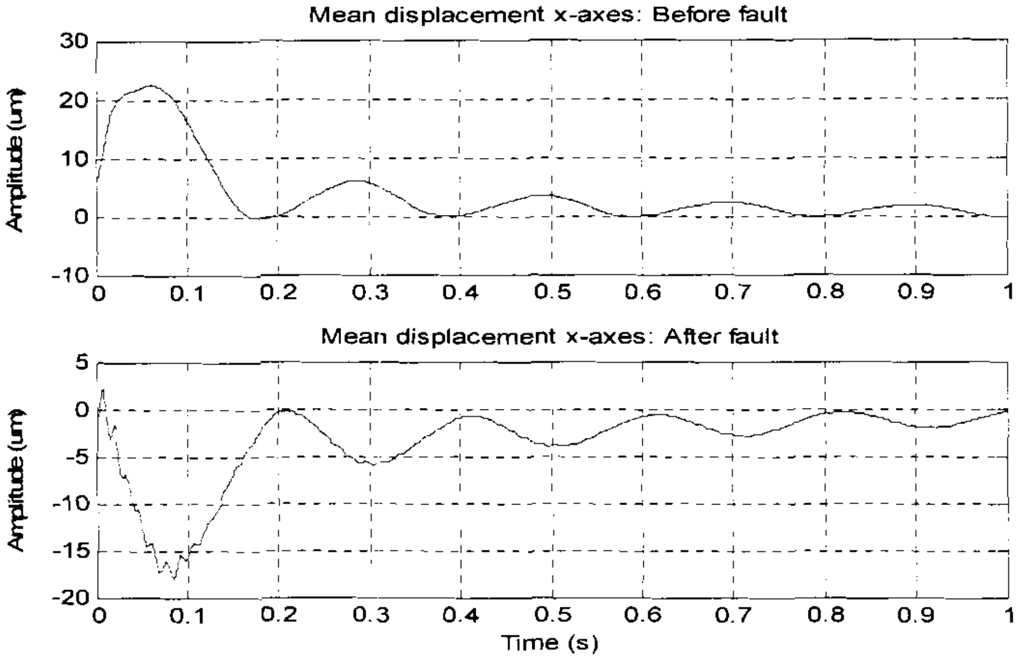

Figure E.49: Continuous mean of the displacement signal

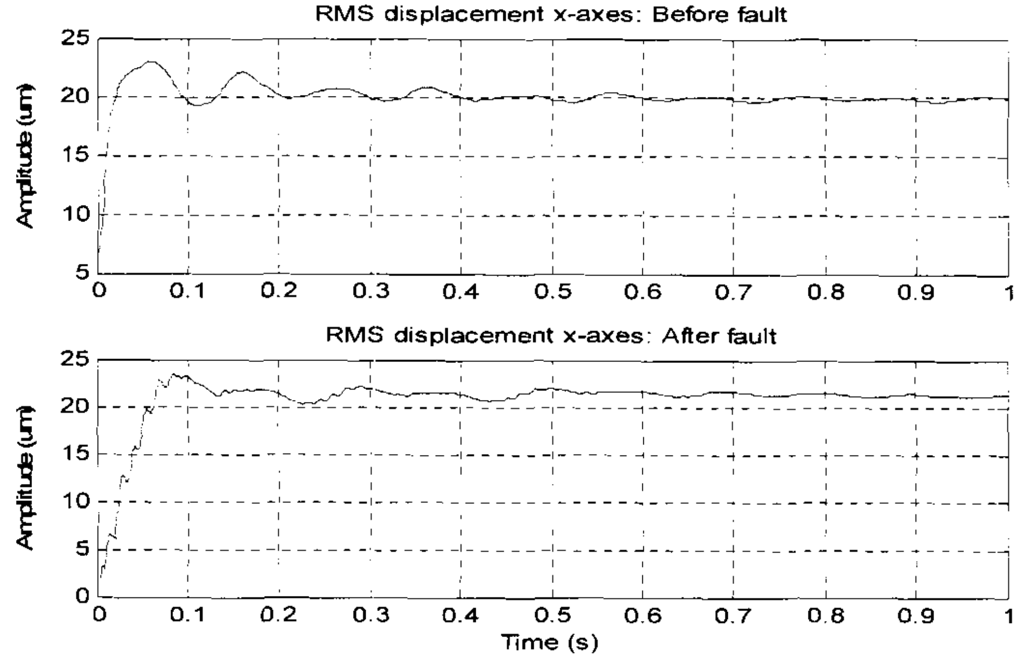

Figure E.50: Continuous RMS of the displacement signal

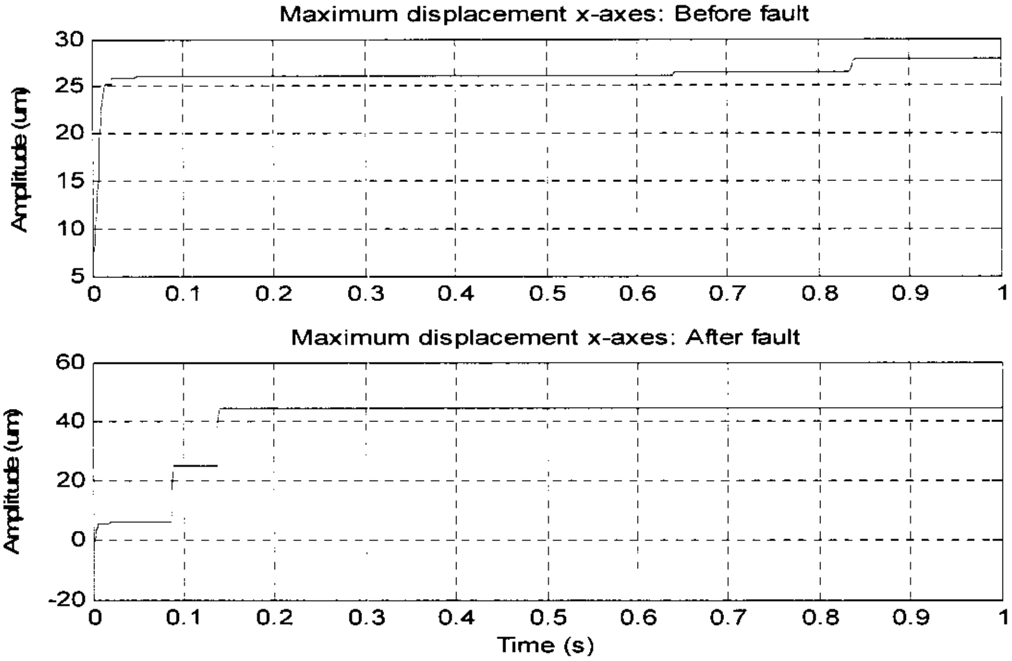

Figure E.51: Continuous maximum of the displacement signal

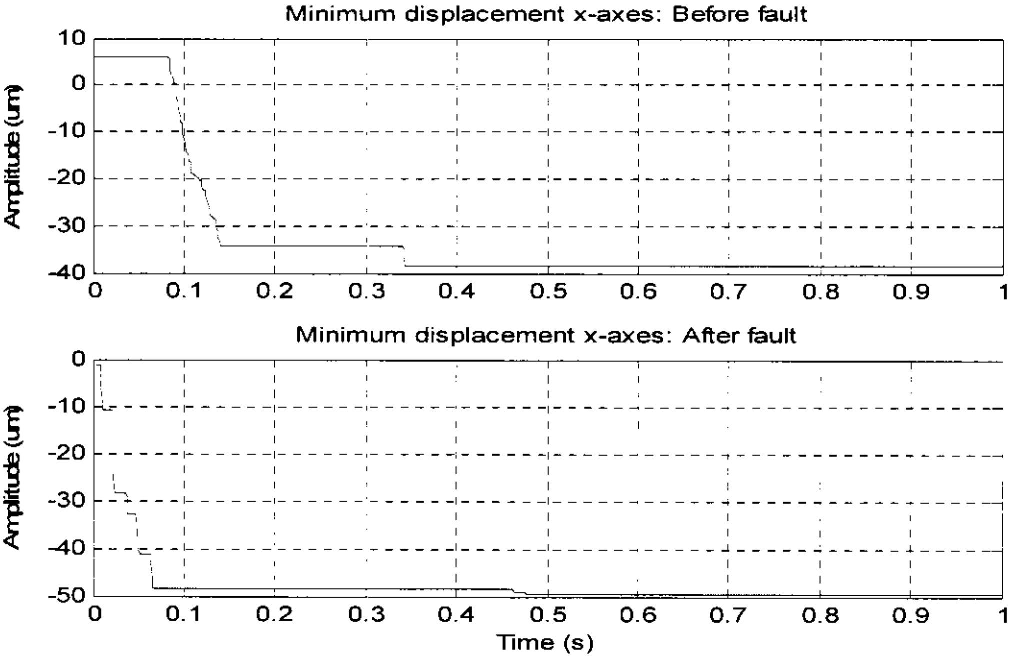

Figure E.52: Continuous minimum of the displacement signal

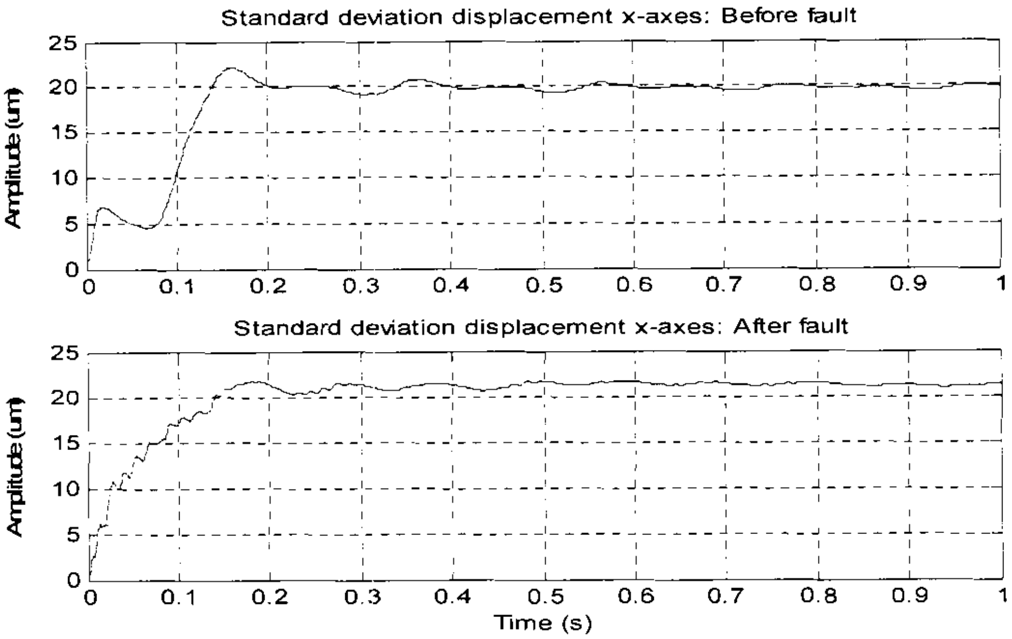

Figure E.53: Standard deviation of the displacement signal

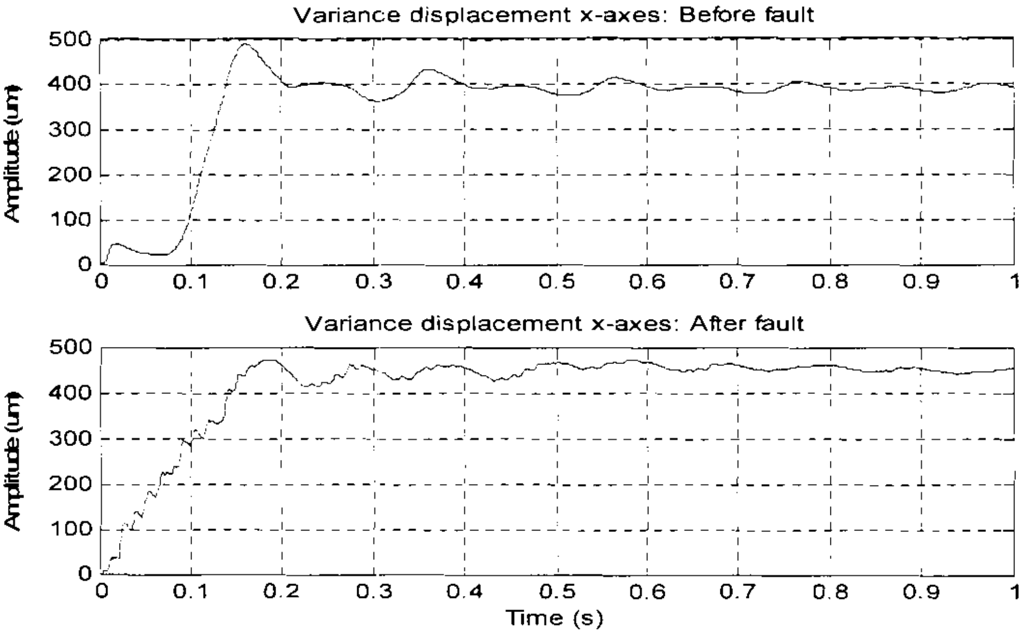

Figure E.54: Variance of the displacement signal

E.3.11. SUMMARY ON HISTORICAL FAULT DATASET 3

By analysing the supersynchronous vibration force data it can be seen that a higher frequency component climbs on the rotational speed frequency and causes a vibration in the AMB system. This fault component is clearly visible with all the techniques used in this section, but the frequency component of the fault is not that easily measurable with all the techniques. The Cepstrum analysis, HFRT and WVD provides precisely measurable frequency features over time. The RMS, mean, minimum, maximum, standard deviation and variance provides useful information about the amplitude of the fault (vibration force) over time.

E.4. DISCUSSION ON RESULTS OBTAINED FROM THE TECHNIQUES

By analysing the historical fault data with different fault detection techniques, it was possible to obtain conclusions and recommendations to which technique is the best to use when a certain fault (vibration force) occurs. From the subsynchronous vibration force data it can be seen that a low frequency fault causes vibration in the AMB system. Measurable frequency components in this data set can be obtained from the autocorrelation function, ESDFT and WVD of the displacement. Amplitude feature extraction is possible with the RMS, mean, minimum, maximum, standard deviation and variance.

From the rotor synchronous vibration force data it can be seen that a medium frequency fault causes vibration in the AMB system. Measurable frequency components in this data set can be obtained from the autocorrelation function, SCD function and WVD of the displacement. The RMS, mean, minimum, maximum, standard deviation and variance of the signal over time provide amplitude features. From the supersynchronous vibration force data it can be seen that a higher frequency fault causes vibration in the AMB system. Measurable frequency components in this data set can be obtained from the Cepstrum analysis, HFRT and WVD. The RMS, mean, minimum, maximum, standard deviation and variance provides useful information about the amplitude of the fault over time.

Table E.1 provides choices of techniques for amplitude and frequency feature extraction. The three historical datasets is compared with the choice of technique for feature extraction. The choice of technique for feature extraction is divided into good, better and measurable, with measurable being the best option for feature extraction of the specific dataset.

Table E.1: Choice of technique for feature extraction

	CHOICE OF TECHNIQUE FOR FEATURE EXTRACTION			
	AMPLITUDE	FREQUENCY		
	MEASURABLE	GOOD	BETTER	MEASURABLE
HISTORICAL FAULT DATASET 1 (SUBSYNCHRONOUS)	RMS, MEAN MIN, MAX STD DEV. VARIANCE	Spectrum Cepstrum HFRT	SA SCD	Autocorrelation ESDFT WVD
HISTORICAL FAULT DATASET 2 (ROTOR SYNCHRONOUS)	RMS, MEAN MIN, MAX STD DEV. VARIANCE	Spectrum SA HFRT	ESDFT Cepstrum	Autocorrelation SCD WVD
HISTORICAL FAULT DATASET 3 (SUPERSYNCHRONOUS)	RMS, MEAN MIN, MAX STD DEV. VARIANCE	SCD ESDFT	Autocorrelation SA Spectrum	Cepstrum HFRT WVD

APPENDIX F

CONDITION MONITORING SUPPLIERS

This appendix provides a list of suppliers on condition monitoring. Table F.1 provides the suppliers on the left side with the corresponding features and websites on the right.

Table F.1: Condition monitoring suppliers

SUPPLIERS	FEATURES AND WEBSITES
Brüel & Kjaer	Provides portable and fixed condition monitoring systems. Extensive system and sensors, together with intelligent trip logic, minimise the false alarms that can lead to costly downtime. http://www.bkvibro.com
Monitran	Provides portable vibration meters and displacement transducers. Vibration monitoring of industrial machinery and robust sensors. http://www.monitran.co.uk/index.htm
Prüftechnik Ltd.	Provides the bearing condition and temperature. Laser shaft alignment system and condition monitoring. http://www.pruftechnik.com/index__.htm
Entek Scientific Corp. USA	The machinery information company. Look into EMONITOR® Odyssey, the new software solution that gives you the complete picture of the health of your plant machinery. Predictive maintenance systems and software http://domino.automation.rockwell.com/applications/gs/REGION/EntekWebST.nsf/pages/Home_Page
VIPAC Engineers Ltd.	Machine condition monitoring, balancing, FEM analysis and torque strain pressure. Testing and design services for machines and structural vibration tests. http://www.vipac.com.au
SKF Condition Monitoring	The SKF condition monitoring product line includes a wide range of instruments that provide the means to ensure proper and optimum maintenance of rotating and reciprocating machinery. Provides vibration monitoring tools. http://www.skfcm.com
Vibro-meter Systems Ltd.	Complete monitoring solutions for gas turbine applications. Provides proximity transducers for vibration and displacement measurement. Accelerometers for reliable, accurate measurement in all types of environments. http://www.sovereign-publications.com/vibro.htm

Spectra Quest Inc.	Provides alignment/balance vibration training. Manufacturing of high quality products for machinery vibration solutions ranging from training to multi-channel measurement systems. http://www.spectraquest.com
IMI Division	Performs condition monitoring. Provides industrial accelerometers, hand-held calibrators and accessories. http://www.imi-sensors.com/industrial
Evam Condition Monitoring	Analysis of vibration forces and spectrum, machine specific evaluation of all parameters and an easy to use software package. http://www.spminstrument.com/solutions/methods/evam.asp
DEI Ltd.	Provides condition monitoring tools and performance analysis for electrical motors. http://www.dei-ltd.co.uk
AV Technology Limited	Maintenance accountants for a large proportion of plant operating cost. Knowledge of machines, through condition monitoring can allow you to reduce periodic maintenance without risk of failure. Provides monitoring techniques and systems within a structured predictive maintenance programme. http://www.avtechnology.co.uk
Beran Instruments	Provides single hardware units for condition monitoring. http://www.beran.co.uk/company.htm
Kistler Instruments Corp.	Provides piezoelectric acceleration measurement equipment, sensors and actuators for industry monitoring tasks. http://www.kistler.com
Dera Systems	Offers expert consultancy on condition monitoring. http://defence-data.com/f2000/pagefa1066.htm
AES Ltd, UK	Machinery health advisors for electrical motors. http://www.aesltd.co.uk
BC Computing Ltd.	Provides predictive maintenance systems and tools. http://www.bccomputinginc.com
IRD Mechanalysis Ltd.	Provides expert systems for condition monitoring. http://www.testpoint.com/IRDMechanalysis.htm
Southhampton Institute, UK	Provides condition monitoring systems and tools. http://www.southampton.liu.edu/academic/cont_studies
ESBI Computing Ltd.	Computerised maintenance management systems. http://www.esbic.ie
Engica Technology Systems Ltd.	Condition monitoring and asset management systems. http://www.engica.com
AEA Technology, UK	Provides corrosion monitoring systems. http://www.aeatechnology.com

Land Infrared, UK	Provides image processing systems and tools for condition monitoring. http://www.landinst.com/infrared/index.htm
Insight Logistics Ltd, UK	Maintenance resource planning and scheduling systems. http://www.insightnl.com/index.shtml
FDS Advanced Systems, UK	Provides maintenance systems for vibration monitoring. http://www.fdsltd.co.uk
Dynamic Logic Ltd.	Maintenance and asset management systems. http://www.dynamiclogic.co.uk
Bentley Nevada, USA	Diagnostics for rotating machinery. http://www.bently.com
Datastream Systems Inc, USA	Maintenance management systems and tools. http://www.datastream.net/English/Default.aspx
SPM Instrument UK Ltd.	The SPM product line addresses four major areas of industrial applications. Provides vibration monitoring, machinery alignment and maintenance instruments. http://www.spminstrument.com
STATUS Technologies Ltd.	MotorStatus is an integrated condition monitoring 'smart sensor' for motors. It is completely self-contained for sensors, analysis, data storage, and power, without the need for expensive data collectors. http://www.statustechnologies.com
Oceana Sensor Technologies	Machine monitoring tools. Embeddable sensors for monitoring the health of rotating machinery. Provides high resolution, low power consuming, piezoceramic accelerometers. http://www.oceanasensor.com
Endevco Corporation	Manufacturing of dynamic instrumentation for vibration http://www.endevco.com
Delta Catalytic Ltd, UK	Provides vibration analysis and tools for rotating machinery.
Cotec Computing services	Provides integrated maintenance management systems and tools.
British Electrical Repairs Ltd.	Provides motor management systems and software for electrical motors.
AGEMA Infrared Systems Ltd.	Thermal analysis and report software for rotating machinery.
Stell Diagnostic Ltd.	Vibration monitoring by radio transmission systems. Provides sensors and beacons designed for harsh environments and explosive zones. Overall levels spectral data collector/analyser and balancers.

APPENDIX G

DATASHEETS, CATALOGS, PHOTOS AND MOVIE CLIPS

This appendix provides a list of datasheets, catalogs, photos and movie clips containing technical detail and additional information about the thesis, which is available on the CD. This thesis is available (in pdf format) on the CD.

G.1. DATASHEETS\CATALOGS

- dSPACE® catalog 2006 (*dSPACE_Catalog_2006.pdf*)
- dSPACE® advanced control education (ACE) kit (*dSPACE_ACE-Kit_2005_en_b202.pdf*)
- Controldesk® real-time interfacing (*ControlDesk_dSPACE_Catalog_2006.pdf*)
- DS1104 R&D controller board specifications (*DS1104_R&D_Controller_Board_dSPACE.pdf*)
- dSPACE® real-time interface (RTI) catalog (*RTI_dSPACE_Catalog_2006-13.pdf*)
- dSPACE® MLIB\MTRACE (*MLIB_MTRACE_dSPACE_Catalog_2006.pdf*)
- dSPACE® compilers (*Compilers_dSPACE_Catalog_2006.pdf*)
- TargetLink for production code generation (*TargetImplementation_dSPACE_Catalog.pdf*)
- dSPACE® targetLink code generation (*TargetLink_dSPACE_Catalog_2006.pdf*)
- dSPACE® real-time interface for multiprocessor systems (RTI-MP) (*RTI_MP_dSPACE.pdf*)

G.2. PHOTOS\SCREENSHOTS

- Complete view of the 250 kW water cooling AMB pump (*pump_complete.jpg*)
- Pump view of the 250 kW water cooling AMB pump (*pump_zoomed.jpg*)
- Complete view of the double radial AMB test rack (*double_complete.jpg*)
- Zoomed view of the double radial AMB test rack (*double_zoomed.jpg*)
- Screenshot of real-time computer 1 with low frequency fault (*comp1_low.jpg*)
- Screenshot of real-time computer 1 with medium frequency fault (*comp1_medium.jgp*)
- Screenshot of real-time computer 1 with high frequency fault (*comp1_high.jgp*)
- Screenshot of real-time computer 2 with low frequency fault (*comp2_low.jpg*)
- Screenshot of real-time computer 2 with medium frequency fault (*comp2_medium.jpg*)
- Screenshot of real-time computer 2 with high frequency fault (*comp2_high.jpg*)

G.3. MOVIE CLIPS

- Double radial AMB test rack with low frequency vibration force (*condition_low.avi*)
- Double radial AMB test rack with medium frequency vibration force (*condition_medium.avi*)
- Double radial AMB test rack with high frequency vibration force (*condition_high.avi*)